USGS
science for a changing world

Prepared in cooperation with the Bureau of Reclamation

Groundwater Discharge by Evapotranspiration, Dixie Valley, West-Central Nevada, March 2009–September 2011

Professional Paper 1805
Version 1.1, April 2015

U.S. Department of the Interior
U.S. Geological Survey

Cover:
Upper left: Eddy-covariance evapotranspiration station at the sparse vegetation site (site 394348118040205). Photograph taken by Amanda Garcia, U.S. Geological Survey, June 3, 2009.

Upper right : Transect measurement tape located near the northwestern playa edge. Photograph taken by Wesley Henson, U.S. Geological Survey, June 17, 2010.

Lower left: Sunrise chamber evaporation measurements at the sparse vegetation evapotranspiration site (site 394348118040205). Photograph taken by Jena Huntington, U.S. Geological Survey, April 11, 2010

Lower right: Soil coring on the playa for water content and stable isotope analyses (site 394559118013705). Photograph taken by Amanda Garcia, U.S. Geological Survey, July 8, 2010.

Groundwater Discharge by Evapotranspiration, Dixie Valley, West-Central Nevada, March 2009–September 2011

By C. Amanda Garcia, Jena M. Huntington, Susan G. Buto, Michael T. Moreo, J. LaRue Smith, and Brian J. Andraski

Prepared in cooperation with the Bureau of Reclamation

Professional Paper 1805
Version 1.1, April 2015

U.S. Department of the Interior
U.S. Geological Survey

U.S. Department of the Interior
SALLY JEWELL, Secretary

U.S. Geological Survey
Suzette M. Kimball, Acting Director

U.S. Geological Survey, Reston, Virginia
First release: 2014
Revised: April 2015 (ver. 1.1)

Suggested citation:
Garcia, C.A., Huntington, J.M., Buto, S.G., Moreo, M.T., Smith, J.L., and Andraski, B.J., 2015, Groundwater discharge by evapotranspiration, Dixie Valley, west-central Nevada, March 2009–September 2011 (ver. 1.1, April 2015): U.S. Geological Survey Professional Paper 1805, 90 p., *http://dx.doi.org/10.3133/pp1805*.

ISSN 2330-7102 (online)

Contents

Contents—Continued

Figures

Figures—Continued

Tables

Conversion Factors, Datums, and Abbreviations and Acronyms

Conversion Factors

SI to Inch/Pound

Multiply	By	To obtain
	Length	
centimeter (cm)	0.3937	inch (in.)
millimeter (mm)	0.03937	inch (in.)
meter (m)	3.281	foot (ft)
kilometer (km)	0.6214	mile (mi)
	Area	
square meter (m^2)	0.0002471	acre
square meter (m^2)	10.76	square foot (ft^2)
hectare (ha)	2.471	acre
square kilometer (km^2)	0.3861	square mile (mi^2)
	Volume	
cubic meter (m^3)	0.0008107	acre-foot (acre-ft)
cubic centimeter (cm^3)	0.06102	cubic inch (in^3)
millions of cubic meters (Mm^3)	811	acre-foot (acre-ft)
	Flow rate, evaporation rate, or transmissivity*	
cubic meter per second (m^3/s)	70.08	acre-foot per day (acre-ft/d)
cubic meter per year (m^3/yr)	0.000811	acre-foot per year (acre-ft/yr)
millions of cubic meters per year (Mm^3/yr)	811	acre-foot per year (acre-ft/yr)
millimeter per day (mm/d)	0.03937	inch per day (in/d)
millimeter per year (mm/yr)	0.03937	inch per year (in/yr)
meter per second (m/s)	283465	foot per day (ft/d)
meter per second (m/s)	2.2369	mile per hour (mi/h)
meter per day (m/d)	3.281	foot per day (ft/d)
meter squared per second (m^2/s)	930049	foot squared per day (ft^2/d)
liter per day (L/d)	0.2642	gallon per day (gal/d)
liter per minute (L/min)	0.2642	gallon per minute (gal/min)
	Pressure	
kilopascal (kPa)	0.145	pound per square inch (lb/in^2)
	Mass flux, density, and water flux	
grams per square meter per second [$(g/m^2)/s$]	0.0002048	pound per square foot per second [$lb/ ft^2)/s$]
grams per millimeter (g/mL)	0.0361	pound per cubic inch (lb/in^3)
grams per cubic meter (g/m^3)	0.00169	pounds per cubic yard (lb/yd^3)
kilograms per cubic meter (kg/m^3)	0.06243	pound per cubic foot (lb/ft^3)
millimeters per year (mm/yr)	0.03937	inch per year (in/yr)
	Heat flux and specific heat	
watt per square meter (W/m^2)	0.0222	calorie per second per square foot [$(cal/s)/ft^2$]
joules per kilogram per kelvin [(J/kg)/K]	0.00024	calorie per gram per degrees Celsius [(cal/g)/°C]
	Electrical conductivity	
milliSiemens per centimeter (mS/cm)	1	millimhos per centimeter (mmhos/cm)
milliSiemens per centimeter (mS/cm)	1	deciSiemens per meter (dS/m)

Conversion Factors, Datums, and Abbreviations and Acronyms

Temperature in degrees Celsius (°C) may be converted to degrees Fahrenheit (°F) as follows:

$$°F = (1.8 \times °C) + 32.$$

Temperature in degrees Celsius may be converted to kelvin (K) as follows:

$$K = °C + 273.15.$$

*Transmissivity: The standard unit for transmissivity is cubic meters per second per square meter times meter of aquifer thickness [$(m^3/s)/m^2$]. In this report, the mathematically reduced form, meters squared per second (m^2/s, is used for convenience).

Concentrations of chemical constituents in water are given either in milligrams per liter (mg/L) or micrograms per liter (µg/L). Concentrations of chemical constituents in soil are given in milligrams per gram (mg/g).

Specific conductance is given in microsiemens per centimeter at 25 degrees Celsius (µS/cm at 25 °C).

Datums

Vertical coordinate information is referenced to the National Geodetic Vertical Datum of 1988 (NAVD 88).

Horizontal coordinate information is referenced to the North American Datum of 1983 (NAD 83).

Elevation, as used in this report, refers to distance above the vertical datum.

Abbreviations and Acronyms

ARVI	Atmospherically Resistant Vegetation Index
bls	below land surface
EBR	energy-balance ratio
ET	evapotranspiration
ET_g	groundwater discharge by evapotranspiration
EVI	Enhanced Vegetation Index
GDA	groundwater discharge area
GIS	geographic information system
Hz	hertz
LEDAPS	Landsat Ecosystem Disturbance Adaptive Processing System
MSAVI	Modified Soil-Adjusted Vegetation Index
NAIP	National Agriculture Imagery Program
NDVI	Normalized Difference Vegetation Index
NSDI	National Spatial Data Infrastructure
PEST	Parameter ESTimation
PRISM	Parameter-elevation Regressions on Independent Slopes Model
PVC	polyvinyl chloride
r^2	coefficient of determination
Reclamation	Bureau of Reclamation
RMS	root-mean-square
SAVI	Soil Adjusted Vegetation Index
TM	Thematic Mapper
TOA	Top of Atmosphere
USGS	U.S. Geological Survey
WISG	World Infrared Standard Group
WY	water year (The 12-month period from October 1, for any given year through September 30, of the following year. A water year is designated by the calendar year in which it ends.)

Groundwater Discharge by Evapotranspiration, Dixie Valley, West-Central Nevada, March 2009–September 2011

By C. Amanda Garcia, Jena M. Huntington, Susan G. Buto, Michael T. Moreo, J. LaRue Smith, and Brian J. Andraski

Abstract

With increasing population growth and land-use change, urban communities in the desert Southwest are progressively looking toward remote basins to supplement existing water supplies. Pending applications by Churchill County for groundwater appropriations from Dixie Valley, Nevada, a primarily undeveloped basin east of the Carson Desert, have prompted a reevaluation of the quantity of naturally discharging groundwater. The objective of this study was to develop a revised, independent estimate of groundwater discharge by evapotranspiration (ET_g) from Dixie Valley using a combination of eddy-covariance evapotranspiration (ET) measurements and multispectral satellite imagery. Mean annual ET_g was estimated during water years 2010 and 2011 at four eddy-covariance sites. Two sites were in phreatophytic shrubland dominated by greasewood, and two sites were on a playa. Estimates of total ET and ET_g were supported with vegetation cover mapping, soil physics considerations, water-level measurements from wells, and isotopic water sourcing analyses to allow partitioning of ET_g into evaporation and transpiration components. Site-based ET_g estimates were scaled to the basin level by combining remotely sensed imagery with field reconnaissance. Enhanced vegetation index and brightness temperature data were compared with mapped vegetation cover to partition Dixie Valley into five discharging ET units and compute basin-scale ET_g. Evapotranspiration units were defined within a delineated groundwater discharge area and were partitioned as (1) playa lake, (2) playa, (3) sparse shrubland, (4) moderate-to-dense shrubland, and (5) grassland.

Groundwater ET is influenced primarily by phreatophytic vegetative cover, salinity of soil and groundwater within the playa, depth to groundwater, solar radiation, and air temperature. The annual groundwater contribution to site-scale ET ranged from 24 to 61 percent of total ET at vegetated sites and 4 to 15 percent of total ET at playa sites. Mean annual ET_g from vegetated sites ranged from 53 millimeters (mm) (0.17 foot [ft], 7.3 percent vegetative cover) to 225 mm (0.74 ft, 24.8 percent vegetative cover). Cumulative liquid-water fluxes in the unsaturated zone indicate that ET_g at vegetated sites was influenced primarily by plant transpiration. Binary mixing analyses of oxygen-18 isotopes in groundwater and shallow soil water indicate that plants predominantly use groundwater throughout the year. Groundwater fractions in greasewood stem water varied seasonally and ranged from 0.63 to 1.0. Mean annual playa ET_g ranged from about 11 mm (0.04 ft) at the inner playa site (near-surface volumetric water content of 37–53 percent) to about 20 mm (0.07 ft) at the outer playa site located within 2 kilometers of the playa edge (near-surface volumetric water content of 25–38 percent), but playa ET_g estimates were within the probable error (plus or minus [±] 20–23 mm; 0.06–0.08 ft). Varying playa ET_g was influenced predominantly by salinity rather than depth to groundwater. Osmotic resistance and physical impediments to ET (such as surface salt crusts and salt precipitate in the soil pore space) increased with increasing salinity toward the playa center, whereas vapor pressure decreased.

Mean annual basin-scale ET_g totaled about 28 million cubic meters (Mm^3) (23,000 acre-feet [acre-ft]), and represents the sum of ET_g from all ET units. Annual groundwater ET from vegetated areas totaled about 26 Mm^3 (21,000 acre-ft), and was dominated by the moderate-to-dense shrubland ET unit (54 percent), followed by sparse shrubland (37 percent) and grassland (9 percent) ET units. Senesced grasses observed in the northern most areas of the moderate-to-dense ET unit likely confounded the vegetation index and led to an overestimate of ET_g for this ET unit. Therefore, mean annual ET_g for moderate-to-dense shrubland presented here is likely an upper bound. Annual groundwater ET from the playa ET unit was 2.2 Mm^3 (1,800 acre-ft), whereas groundwater ET from the playa lake ET unit was 0–0.1 Mm^3 (0–100 acre-ft). Oxygen-18 and deuterium data indicate discharge from the playa center predominantly represents removal of local precipitation-derived recharge. The playa lake estimate, therefore, is considered an upper bound. Mean annual ET_g estimates for Dixie Valley are assumed to represent the pre-development, long-term ET_g rates within the study area.

Introduction

Demand for groundwater resources in the desert Southwest is increasing as a result of population growth and development. Finite water resources in urban areas have led to the initiation of large-scale water importation projects, which commonly require additional appropriations of water from less developed basins. In order to sustain existing (during this study) and increasing water demands in the Fallon urban area of the Carson Desert, Churchill County, Nevada, is considering importing additional water resources from Dixie Valley, a primarily undeveloped basin neighboring the Carson Desert to the east (fig. 1). As a component of the federally appropriated Desert Terminal Lakes Program (Public Law 110-161, Section 208), the Bureau of Reclamation (Reclamation) organized an interagency study team to investigate the groundwater resources in the Dixie Valley flow system. The study team includes the U.S. Geological Survey (USGS), Nevada Department of Water Resources, and staff and representatives of Churchill County (HydroBio Advanced Remote Sensing, Interflow Hydrology, Inc., and Mahannah and Associates, LLC).

Groundwater resource management in semiarid-to-arid environments often requires accurate groundwater budget estimates including groundwater discharge. A primary mechanism for groundwater discharge in closed desert basins is evaporation from bare soil and playas, and transpiration from phreatophytic vegetation (Malek and others, 1990; Nichols, 1993; Moreo and others, 2007). Evaporation and transpiration collectively are referred to as evapotranspiration (ET), the process that transfers water residing at or near the surface of the Earth to the atmosphere. Evapotranspiration is controlled by water availability, energy available at the evaporating surface, and the ease with which water can diffuse into the atmosphere (Shuttleworth, 1993).

The Dixie Valley flow system covers about 6,164 km^2 (2,380 mi^2) (Nevada Division of Water Resources, 2012) and lies within Churchill, Pershing, Lander, and Mineral Counties, Nevada (fig. 1). Dixie Valley, mostly in Churchill County, is the terminus of the flow system, and is hydraulically connected to Pleasant, Jersey, Fairview, Stingaree, Eastgate, and Cowkick Valleys (Cohen and Everett, 1963; Harrill and Hines, 1995). Groundwater in these adjacent valleys or hydrographic areas[1] (HAs) generally flows toward Dixie Valley, where it ultimately discharges naturally through springs, seeps, and by ET from phreatophytic vegetation and playa areas. The largest area of natural discharge in the Dixie Valley flow system is in Dixie Valley.

During the 1960s, the USGS, in cooperation with the State of Nevada, completed a reconnaissance study to evaluate the groundwater resources of the Dixie Valley flow system (Cohen and Everett, 1963). The natural, mean annual discharge from the groundwater reservoir was estimated at about 23 million cubic meters (Mm^3) (19,000 acre-feet [acre-ft]), 87 percent of which was from Dixie and Jersey Valleys. About 81 percent of the total discharge from Dixie and Jersey Valleys was estimated from vegetated areas and 19 percent of discharge was estimated from the Dixie Valley playa. Discharge estimates were based on a combination of general phreatophyte and playa distribution maps and ET rates (Cohen and Everett, 1963). Evapotranspiration rates were determined from previous studies in hydraulically separate basins, which used groundwater-level fluctuations to infer ET rates (White, 1932; Young and Blaney, 1942). Evapotranspiration was assumed to be the primary mechanism for groundwater discharge because spring discharge either was returned to the groundwater reservoir or was consumed by ET.

In the mid-1990s, Harrill and Hines (1995) reevaluated natural annual groundwater discharge from Dixie Valley using a combination of detailed phreatophytic vegetation surveys, static water-level measurements from wells across the flow system, and ET rates reported by previous studies in hydraulically separate basins. The reported ET rates from previous studies were determined from a combination of reconnaissance estimates and analytical hydraulic gradient and micrometeorological measurements for saltgrass, playas, and bare soil (Everett and Rush, 1964; Hines, 1992; Nichols, 1992; Maurer and others, 1994). Rates specific to phreatophytic shrubs were established using measured biomass-to-discharge relations determined from lysimeter measurements made in Winnemucca, Nevada (Robinson and Waananen, 1970). Natural groundwater discharge estimates from ET ranged from 21 to 34 Mm^3 (17,000 to 28,000 acre-ft) (Harrill and Hines, 1995). Vegetated areas contributed about 52–75 percent of the total discharge, whereas the playa was estimated to have contributed the remainder.

Recent applications for groundwater appropriations in Dixie Valley warrant an improved understanding of the groundwater resource including a revised groundwater discharge estimate based on detailed measurements in Dixie Valley. The USGS, in cooperation with Reclamation and Churchill County, estimated groundwater discharge from ET in Dixie Valley during hydrologic water years (WYs) 2010 and 2011 using advancements in ET estimation and remote sensing techniques. High frequency eddy-covariance ET measurements were combined with micrometeorological, plant, unsaturated zone, and water-level measurements to estimate groundwater ET at the site scale. These site-scale estimates were combined with remote sensing data and vegetation surveys to extrapolate estimates to the basin scale.

[1]Formal hydrographic areas in Nevada were delineated systematically by the U.S. Geological Survey and Nevada Division of Water Resources in the late 1960s for scientific and administrative purposes (Cardinalli and others, 1968; Rush, 1968). The official hydrographic-area names, numbers, and geographic boundaries continue to be used in U.S. Geological Survey scientific reports and Nevada Division of Water Resources administrative activities.

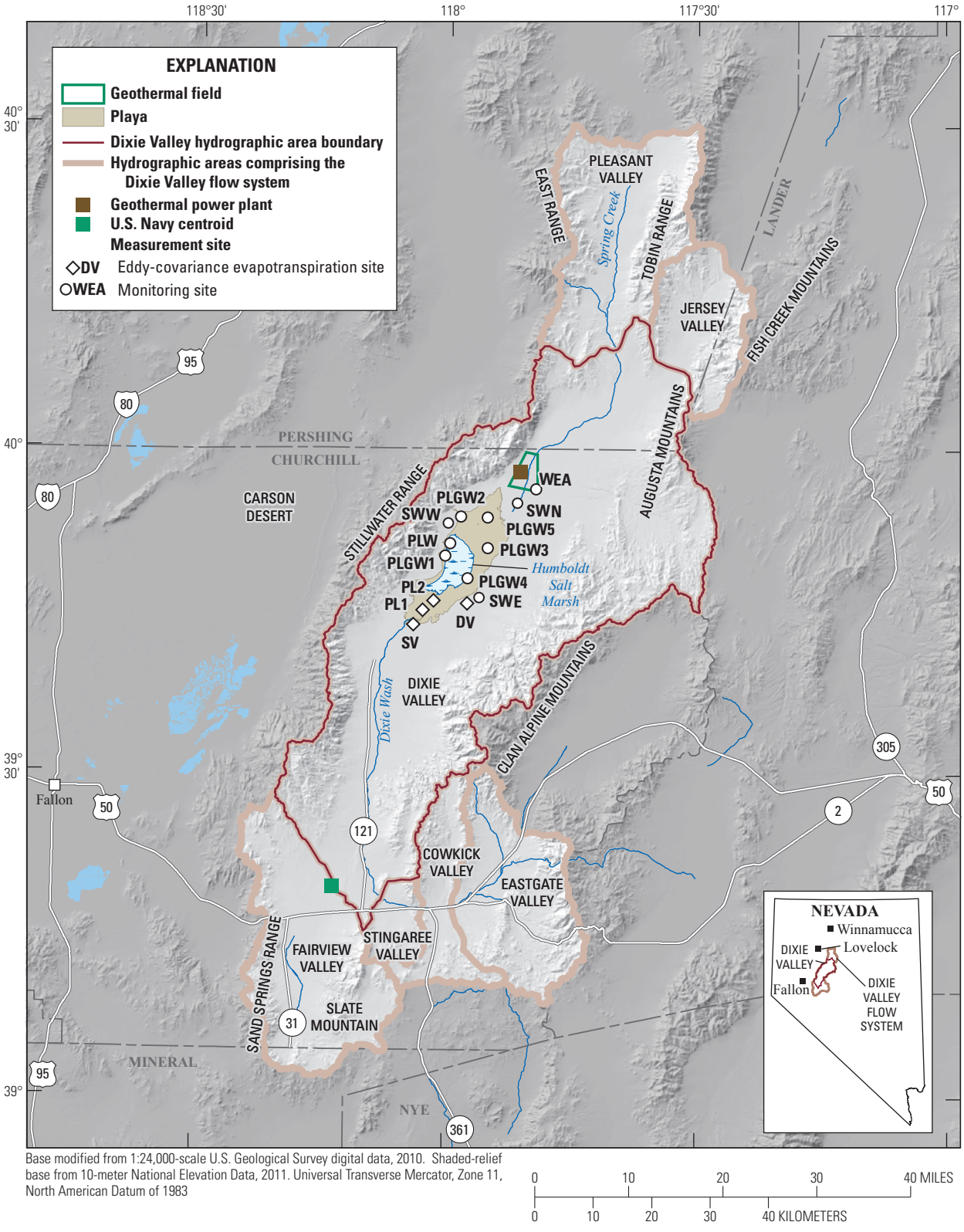

Figure 1. Locations of flow system and evapotranspiration sites including dense vegetation (DV), sparse vegetation (SV), playa 1 (PL1), and playa 2 (PL 2); and monitoring sites including playa-west (PLW), Churchill County weather station (WEA), playa groundwater wells (PLGW1–PLGW5), and north (SWN), east (SWE), and west (SWW) shrubland wells, Dixie Valley, Nevada, 2009–11.

Purpose and Scope

This report describes a refined estimate of groundwater discharge from ET in the Dixie Valley HA. Site-scale groundwater ET rates were estimated using the eddy-covariance method and micrometeorological measurements. Estimates of groundwater ET were supported by vegetation surveys, soil physics, water levels, and water sourcing methods that include ET partitioning and stable isotope analyses of precipitation, groundwater, and plant and soil water. Evapotranspiration and other supporting data were measured and collected at various schedules (continuously, seasonally, or monthly) from March 2009 through September 2011. Groundwater ET was estimated during WYs 2010 and 2011. Site-scale estimates were extrapolated to the basin scale using vegetation and soil characteristics determined from moderate-resolution, multi-spectral satellite imagery. This report describes the procedures used to estimate groundwater ET and presents results of the study. The intensive data collection effort generated much climatic, hydrologic, and ecological data. All relevant data are archived in the USGS National Water Information System or in electronic spreadsheets included with this report. A companion USGS report by Huntington and others (2014) describes the hydrogeologic framework and occurrence, movement, and chemical characterization of groundwater in Dixie Valley.

Description of Study Area

Dixie Valley is an inter-mountain basin located mostly in Churchill County and parts of Pershing County, about 72 km (45 mi) east of Fallon, in west-central Nevada. Dixie Valley, in the Great Basin subsection of the Basin and Range physiographic province, is bounded on the west by the tectonically active Stillwater Range (Okaya and Thompson, 1985) and on the east by the Clan Alpine and Augusta Mountains (Willden and Speed, 1974). Dixie Valley and adjacent basins are HAs that generally coincide with actual topographic basin divides; however, some boundaries are arbitrary and represent divisions with no topographic basis.

General Hydrology

Dixie Valley is characterized topographically as a northeast-trending trough bounded by the Stillwater Range and Clan Alpine and Augusta Mountains (Cohen and Everett, 1963). Valley lowlands become increasingly flat near the playa, the center of which is known as the Humboldt Salt Marsh (fig. 1). The natural groundwater discharge area that is characterized by lowland phreatophytic vegetation and the playa is the focus of this study. The playa, which spans an area of about 17,700 ha (43,700 acres), lies at a minimum elevation of about 1,030 m (3,380 ft) and is the lowest point in the northern two-thirds of Nevada (Cohen and Everett, 1963). The playa evolved from a late Pleistocene lake, often referred to as Lake Dixie, which was isolated hydraulically from Pleistocene Lake Lahontan by surrounding mountains (Thompson and Burke, 1973). Thinly laminated beds of silt and clay that were deposited in the lake cover much of the Dixie Valley floor (Cohen and Everett, 1963).

Climate in the Dixie Valley lowlands is characterized as arid (aridity index between 0.03 and 0.2; Tsakiris and Vangelis, 2005) with hot, dry summers and cold, moist winters. Temperatures on the valley floor range from winter lows less than 0 °C to summer highs that exceed 40 °C; daily temperature fluctuations often exceed 20 °C. Mean annual precipitation measured at the U.S. Navy centroid (1,291 m [4,235 ft] elevation) near the border of Dixie Valley and Fairview Valley (fig. 1) was about 102 mm (4.0 in.) between 2006 and 2011. Mean annual precipitation measured at 32 sites in and adjacent to Dixie Valley during the 19th century ranged from about 127 to 330 mm (5.0 to 13.0 in.) at elevations of about 1,036–2,380 m (3,400–7,800 ft), respectively (Harrill and Hines, 1995). Most annual precipitation occurs as snow during winter and spring in the Stillwater Range and Clan Alpine and Augusta Mountains, with lesser amounts typically falling as rain and snow on the valley floor. Mean annual precipitation ranged from 234 to 444 mm (9.23 to 17.5 in.) in the Stillwater Range and from 298 to 542 mm (11.7 to 21.3 in.) in the Clan Alpine and Augusta Mountains (October 2009–September 2011; Mahannah and Associates, LLC, written commun., 2011). These mean annual precipitation amounts are about 34 (Stillwater Range) and 44 percent (Clan Alpine and Augusta Mountains) higher, respectively, than 30-year mean values determined from the Parameter-elevation Regressions on Independent Slopes Model (PRISM) for 1981–2010 (PRISM Climate Group, 2013). On the playa, mean annual precipitation was 152 mm (6.0 in.) from October 2009 to September 2011 (appendix 1). During summer, infrequent convective storms contribute to about 15 percent of annual precipitation totals.

Surface drainage features in Dixie Valley are composed primarily of intermittent streams fed by spring snowmelt or infrequent, major storms. Predominant streamflow occurs through Dixie Wash, which enters Dixie Valley from Stingaree Valley to the southeast and flows about 64 km (40 mi) northward, ultimately discharging onto the playa (fig. 1). The Dixie Wash also is fed by streams draining the Stillwater Range and Clan Alpine Mountains. Spring Creek flows ephemerally from Pleasant Valley southward into Dixie Valley, receives tributary streamflow from the Stillwater Range, Augusta Mountains, and the northern part of the Clan Alpine Mountains, and eventually discharges onto the playa.

Additional eastern tributaries periodically discharge onto the playa, whereas contributions from western tributaries are minimal. During this study, only a small fraction of stream discharge reached the playa each year (less than 0.6 Mm^3, or less than 500 acre-ft; Interflow Hydrology, Inc., and Mahannah and Associates, LLC, 2013). Most streamflow that originates from the mountain front is lost to infiltration or ET prior to reaching the playa (Cohen and Everett, 1963; Interflow Hydrology, Inc., and Mahannah and Associates, LLC, 2013).

The groundwater-flow system is composed predominantly of unconsolidated younger and older basin-fill deposits that evolved from erosion of surrounding mountain ranges, windblown material, and stream and alluvial fan deposits. Older basin-fill deposits often overlay or are interbedded with Tertiary volcanic materials (Willden and Speed, 1974). Groundwater in Dixie Valley moves from the mountains toward the playa. The shallow basin-fill aquifer system mostly is unconfined, but increasingly becomes confined near the southern edge of the playa as basin-fill deposits gradually interfinger with comparatively impermeable lakebed deposits. Similar to areas adjacent to the playa, interfingering between permeable basin-fill and impermeable lakebed deposits likely occurs along the playa fringe (Huntington and others, 2014). The impermeable clay and permeable basin-fill interface, where most regional groundwater is discharged, is supported by the presence of phreatophytes (plants that rely on groundwater to fulfill a part of their water needs) and many springs. The groundwater potentiometric surface ranges from about 130 m (425 ft) below land surface (bls) to about 9 m (30 ft) above land surface in Dixie Valley, and from about 30 m (98 ft) below land surface to 9 m above land surface in phreatophytic vegetation areas.

Numerous cold and geothermal springs in Dixie Valley discharge in the mountain block along the mountain block-valley interface and on the valley floor where several are adjacent to the playa. Discharge rates and temperatures of valley-floor springs measured during this study range from less than 4 to 1,136 L/min (less than 1 to 300 gal/min), and from 4 to more than 60 °C, respectively (Interflow Hydrology, Inc., and Mahannah and Associates, LLC, 2012; Huntington and others, 2014). Of the 17 valley-floor springs visited from 2009 to 2011, 40 percent were cold (less than 20 °C), 40 percent were warm (20–50 °C), and 20 percent were hot (more than 50 °C). If measured flow is assumed to persist throughout the year, annual spring discharge totals less than 2.5 Mm^3 (2,000 acre-ft) (Interflow Hydrology, Inc., and Mahannah and Associates, LLC, 2012). Nearly 80 percent of the spring discharge was from cold and warm springs and likely discharged from the basin-fill aquifer system. Vegetation surrounding spring discharge areas on the valley floor is composed mostly of thick grasses with some trees and reeds, indicating that most spring discharge is either directly lost to ET or infiltrates the shallow aquifer system where it is subsequently transpired by deep-rooted vegetation.

Groundwater budgets describe the balance or quantify the imbalance between inflow and outflow components of a groundwater flow system. The primary components of the water budget in Dixie Valley, prior to any anthropogenic removal of groundwater, include discharges to the land surface and atmosphere such as spring flow and ET, recharge from the land surface such as infiltration of precipitation and streamflow, and recharge from sub-surface flow across lateral boundaries from upgradient basins. Regional groundwater flow is controlled by hydraulic-head gradients from areas of regional recharge toward areas of regional discharge. Dixie Valley serves as the terminus of the Dixie Valley flow system and is hydraulically connected to six adjacent basins: Pleasant and Jersey Valleys to the north; Fairview Valley to the south; and Stingaree, Cowkick, and Eastgate Valleys to the southeast.

Regional groundwater discharge in Dixie Valley occurs naturally in topographically low areas of the basin where groundwater is at or near the land surface. Natural discharge to and above the land surface under pre-development conditions occurs through springs and seeps, transpiration by phreatophytic vegetation, and by evaporation from soil and open water. Most open water exists as ponds or free-flowing drainages that originate from direct precipitation or spring flow. Evapotranspiration, across a typical discharge area in the Southwest, is inclusive of spring and seep flow. Water discharged from springs and seeps either evaporates or infiltrates downward toward the shallow water table where it potentially evaporates or is transpired by the local phreatophytic vegetation.

Groundwater discharge also occurs through anthropogenically altered areas in the Dixie Valley discharge area. During this study, several artesian wells were flowing in a historical agricultural settlement just south of the playa. During WY 2011, flow rates measured from 36 flowing wells ranged from 2 to about 340 L/min (0.5 to about 90 gal/min), discharging an annual total of about 1.35 Mm^3 (1,100 acre-ft) (Mahannah and Associates, LLC, written commun., 2012). Settlement-established vegetation (cottonwood trees and grasses) and native vegetation near the artesian wells likely caused evapotranspiration of most discharged water. A small amount of this water likely infiltrates back into the shallow subsurface, potentially reaching the water table where it is ultimately discharged by ET.

The general groundwater-flow system near the basin center and playa is conceptualized in figure 2. Although most groundwater is discharged naturally through springs and evapotranspiration from phreatophytic vegetation areas, some regional groundwater also is discharged through playa evaporation because some mixing undoubtedly occurs between fresh basin-fill and playa groundwater. However, transmissivity and chemical contrasts between the two systems that exceed the typical freshwater-saltwater interface in coastal systems indicate that the amount and rate of mixing is marginal in comparison (Huntington and others, 2014). Huntington and others (2014) report that playa transmissivity measurements (9×10-8 m^2/s; 0.1 ft^2/d) are about 10,000 times less than values measured in adjacent wells located just south of the playa, and 100,000 times less than the mean transmissivity of the basin-fill aquifer (9×10-3 m^2/s; 8,700 ft^2/d). Huntington and others (2014) also report that playa total dissolved solids (mean of about 250,000 mg/L) are about 7 times those of seawater (about 35,000 mg/L) and an average of nearly 400 times those of basin-fill aquifer water (640 mg/L). In addition to mixing between basin-fill and playa groundwater, some mixing likely occurs between playa groundwater and the dense brine that accumulates as a precipitation-derived ephemeral pond in the playa center (Humboldt Salt Marsh, fig. 1) during winter and spring (fig. 2; Allison and Barnes, 1985). Dissolution of surface salt crusts in the Humboldt Salt Marsh during pond inundation and accumulation of salts that are carried as run-on from the upgradient playa likely increase the density of pond water above deeper playa groundwater. This density contrast and the pond hydraulic head during winter and spring likely lead to local groundwater recharge and mixing with shallow playa groundwater near the playa center. Huntington and others (2014) noted that playa groundwater density ranges from 1.14 g/mL near the playa edge to 1.21 g/mL in the Humboldt Salt Marsh, indicating that density-controlled convective mixing between the dense brine and playa groundwater is possible (fig. 2). During summer and autumn, when the ephemeral pond has evaporated and the surface is covered with a thickening salt crust, this locally derived recharge water likely discharges slowly through evaporation (fig. 2).

Regional groundwater discharge under natural, pre-development conditions is estimated by determining total ET, minus local, non-groundwater contributions such as precipitation and ephemeral runoff. Total ET equals the volume of water lost to the atmosphere from the discharge area. The amount of water typically subtracted from the estimate of total ET equals the local precipitation or volume of precipitation falling directly on the discharge area. Local precipitation either evaporates or infiltrates downward to the shallow water table where it ultimately is evaporated or is transpired by local phreatophytes. Local precipitation or recharge must be removed from the ET estimate because it is not part of the regional flow system. Precipitation falling outside the discharge area typically is not subtracted because it evaporates, it is transpired by xerophytes, or it recharges the regional groundwater-flow system.

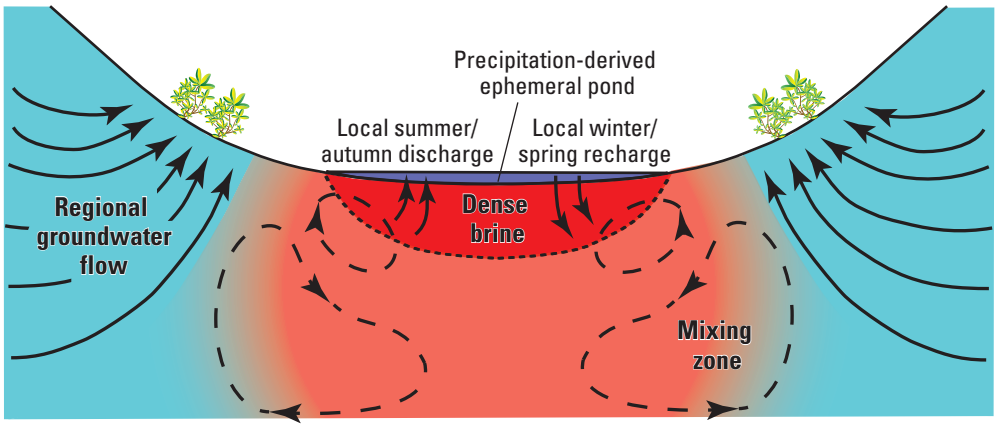

Figure 2. Conceptual diagram showing groundwater flow in and adjacent to the playa, Dixie Valley, Nevada.

Water Use

Groundwater use from the basin-fill aquifer during this study and historically includes agricultural irrigation, livestock watering, domestic supply, and geothermal development. Land use in Dixie Valley includes cattle grazing throughout most of the valley and alfalfa cultivation for seed and feed mostly north of the playa. Currently (2009–11) irrigated agriculture covers about 550 ha (1,360 acres) of Dixie Valley. Considering the Huntington and Allen (2010) net irrigation water requirement for alfalfa in Dixie Valley (1,100 mm/yr; 3.6 ft/yr), irrigation-based agricultural discharge is about 6.1 Mm^3/yr (4,950 acre-ft/yr). With less than 100 residents in Dixie Valley, domestic water use is negligible, and equates to less than 0.03 Mm^3/yr (25 acre-ft/yr) based on the Nevada domestic self-supplied per capita use of 780 L/d (206 gal/d; Kenny and others, 2009).

Historically, agriculture covered more than three times the agricultural landscape delineated in this study, some of which still is influencing the hydrologic balance in Dixie Valley. Numerous artesian wells were drilled by ranchers and farmers in the historical (1940–80s) agricultural settlement south of the playa. Since establishment, many of these wells have intermittently discharged groundwater onto the valley surface. Between 1985 and 1987, the U.S. Navy purchased private land in this settlement area through a congressionally approved buyout of 4,856 ha (12,000 acres) (Misrach, 1990) to use as a supersonic testing ground. This action, in turn, resulted in the dismantling of most settlement homesteads, leaving numerous artesian wells uncapped and flowing during the last 20 or more years. Between 2002 and 2010, the U.S. Navy capped 65 wells, 45 of which were artesian wells (Gary Cottle, U.S. Navy, written commun., 2012). Some wells remain uncapped and continue to discharge onto the land surface. Evaporation of the discharge related to flowing artesian wells likely is similar to the annual discharge measured from 36 uncapped wells in the settlement during 2011 (1.35 Mm^3 [1,100 acre-ft]; Mahanna and Associates, written commun. 2012).

The Dixie Valley geothermal power plant in northwestern Dixie Valley (fig. 1) produces the largest amount of geothermal energy from a single plant in the state of Nevada (Lowell Price, oral commun., Nevada Division of Minerals, 2012). During WYs 2010 and 2011, mean annual geothermal groundwater withdrawals were about 26.4 Mm^3 (21,400 acre-ft), with a mean water temperature of about 160 °C. About 487,000 megawatt hours of energy were produced and about 18.5 Mm^3 (15,000 acre-ft) of the withdrawn geothermal water was reinjected into the geothermal aquifer annually (Nevada Division of Minerals, written commun., 2012). In addition to pumping of the geothermal aquifer, large-scale pumping of the basin-fill aquifer to augment geothermal reservoir pressure began in 1997 (Benoit and others, 2000). The geothermal plant pumps a mean of 2.6 Mm^3/yr (2,100 acre-ft/yr) from the basin-fill aquifer (period of record 2009–11) and re-injects this water above the deeper (150–3,000 m bls [500–9,700 ft bls]) geothermal aquifer (Nevada Division of Minerals, written commun., 2012).

Vegetation

Plant communities in the groundwater discharge area primarily are composed of phreatophytes, or plants that rely on groundwater to fulfill a part of their water needs. Most of these plants also are halophytic and commonly require some salt to reach maximum growth. Phreatophytic shrubs are dominated by greasewood (*Sarcobatus vermiculatus* [Hooker] Torrey) and, to a lesser degree, by big saltbush (*Atriplex lentiformis* [Torr.] S. Watson) and rubber rabbitbrush (*Ericameria nauseosa* [Pall. Ex Pursh]). The understory consists of phreatophytic perennial grasses and forbs such as saltgrass (*Distichlis spicata* [L.] Greene), alkali sacaton (*Sporobolus airoides* [Torr.] Torr.), wild rye (*Leymus cinereus* [Scribn. and Merr.] Á. Löve), seepweed (*Suaeda torreyana* S. Watson), and pickleweed (*Salicornia* L.). Greasewood and rubber rabbitbrush are deciduous shrubs with similar transpiration and phenological patterns such as leaf production in early spring, the highest shoot growth rates in early summer, and senescence in late autumn (Donovan and others, 1996). Big saltbush typically is an evergreen, but can be deciduous under extreme drought conditions. Although phreatophytes typically use groundwater, most species are facultative and will use readily available water sources such as precipitation-derived soil moisture, ditches, irrigated fields (Robinson, 1958), and likely stream channels. In addition to solar radiation, groundwater use by phreatophytes is influenced strongly by air temperature, which controls the length of the growing season and the rate of water use during the growing season (Robinson, 1958).

Saltgrass has been mapped in areas where water-table depths extend to about 4 m bls (13.1 ft bls) (Blaney and others, 1933), whereas greasewood has been mapped where water-table depths extend to 19.0 m bls (62.3 ft bls) (Robinson, 1958; Glancy and Rush, 1968). Although the depth of root penetration often is assumed to be synonymous with depth to the saturated zone or capillary fringe, in areas where the water table or perched water lies at great depth below land surface, plants with deep, extensive roots could obtain their water supply from unsaturated-zone moisture (Robinson, 1958).

Vegetation supported by local spring flow and artesian wells includes small groves of cottonwood (*Populus* L.), desert willow (*Chilopsis linearis*), saltcedar (*Tamarix ramosissima* Ledeb.), and wild rye; areas of open marshland are composed of cattails (*Typha* L.) and likely reeds and bulrush (*Scripus* L.). Adjacent to groundwater discharge areas, vegetation predominantly is xerophytic, indicating the plants obtain water from shallow, precipitation-derived soil moisture. The most common xerophytic shrubs in Dixie Valley include shadscale (*Atriplex confertifolia* [Torr. & Frém.] S. Watson) and Bailey's greasewood (*Sarcobatus Baileyi* Coville).

Groundwater Discharge by Evapotranspiration—Site Scale

Evapotranspiration includes evaporation from dry-to-wet surfaces (open water bodies and soil, rocks, and plant canopies), sublimation from snow or ice, and transpiration by plants (Bossong and others, 2003). Diurnal and seasonal ET rates are affected by soil moisture content, depth to water, solar radiation, air temperature, and plant phenology. In areas dominated by phreatophytic vegetation such as the Great Basin, ET is the primary process by which groundwater is removed under natural or pre-development conditions.

Annual groundwater discharge was computed as annual ET minus local precipitation measurements and ephemeral runoff estimates. Annual ET was estimated at four sites in Dixie Valley using the eddy-covariance method. Precipitation falling directly onto the land surface at the ET sites ultimately is lost by ET; therefore, it was assumed not to contribute to regional groundwater recharge. Because Dixie Valley is characterized as having an arid climate, most if not all precipitation-derived, surface-water flow onto phreatophytic shrubland or playa areas likely did not contribute to regional groundwater recharge or discharge.

Environmental factors affecting ET and groundwater discharge were measured and investigated. These factors included energy-balance fluxes (available energy and turbulent fluxes), soil moisture, vegetation, unsaturated zone hydraulic gradients, and water levels. Groundwater discharge estimates were supported with water sourcing analyses that included stable isotope measurements and partitioned evaporation and transpiration components of total ET.

Surface Energy Budget

The surface energy budget is the balance of incoming and outgoing energy fluxes and constrains the energy available for ET. The land-surface energy budget generally is partitioned into four primary components: (1) net radiation (R_n), (2) latent-heat (λE) flux, (3) sensible-heat (H) flux, and (4) soil-heat flux at land surface (G). This generalized budget assumes negligible energy use by biological processes and limited storage of heat by the plant canopy. Net radiation is the balance resulting from solar and terrestrial radiative energy and is equal to the difference between incoming shortwave and longwave radiation and outgoing shortwave and longwave radiation. Based on the principle of energy conservation, available energy (net radiation occurring on a landscape, less the soil-heat flux) is equal to the turbulent fluxes of λE and H (equation 1):

$$R_n - G = \lambda E + H \quad (1)$$

where all components are in units of watts per square meter (W/m^2).

The latent-heat flux is defined as the energy removed from the landscape in the liquid water-to-water vapor evaporative phase change. The latent heat of vaporization (λ) is the amount of energy needed to evaporate a unit mass of water and varies slightly with air temperature. The resulting E component is the mass flux of water vapor or ET in grams per square meter per second ($[g/m^2]/s$). The ET flux can be converted to a rate of surface discharge by dividing by the density of water. Sensible-heat flux is the heat energy convectively removed from the surface owing to temperature differences between the surface and the atmosphere.

Soil and plants absorb net radiation during the day, which typically causes soil and leaf surfaces to be warmer than the atmosphere (Stannard and others, 2013). This temperature difference between soil and leaf surfaces and the atmosphere drives the daytime sensible-heat flux. During the night, the land and atmosphere temperature difference and vertical gradient reverses and the sensible-heat flux is slightly negative. The moisture difference along with positive net radiation drives the latent heat flux toward the atmosphere.

The soil-heat flux at land surface was computed using the calorimetric method (Fuchs, 1986), defined as the additive flux of that measured at some depth below the land surface (G_{z_m}) using a flux plate and the storage flux estimated in the soil layer above the flux plate (J_s):

$$G = G_{z_m} + J_s;\ J_s = \int_0^{z_m} C_v \frac{dT_s}{dt} dz \quad (2)$$

where

z is depth below land surface (in meters) ranging from 0 at land surface to the depth at which the flux plate is buried (z_m),
C_v is the volumetric heat capacity of the soil, and
T_s is the soil temperature (in kelvin).

Assuming that the contribution from soil air and organic matter to heat capacity is negligible, the volumetric heat capacity of the soil is computed as (Campbell, 1985):

$$C_v = \rho_b c_m + c_w \theta_V \quad (3)$$

where

ρ_b is dry bulk density of the soil, in kilograms per cubic meter (kg/m^3),
c is the specific heat, in joules per kilogram per kelvin ([J/kg]/K) of mineral soil (c_m) and water (c_w), and
θ_v is the volumetric water content, in cubic meter per cubic meter (m^3 water/m^3 soil).

Specific heat of mineral soil and water were assumed constant and assigned values of 840 and 4,180 (J/kg)/K, respectively (Hanks and Ashcroft, 1980).

Eddy-Covariance Method, Data Collection, and Monitoring

The eddy-covariance method measures the one-dimensional net transport of heat, mass, and momentum by eddies between surface and atmospheric boundaries (Foken and others, 2012). Eddies are turbulent air movements caused by wind, surface roughness, and convective heat flow that occur at this boundary (Swinbank, 1951; Campbell and Norman, 1998). The eddy-covariance method relies on high-frequency (10 hertz [Hz] in this study) measurements of fluctuations in vertical wind speed, air temperature, and water-vapor density to measure latent- and sensible-heat fluxes. The latent-heat flux is the product of the latent heat of vaporization and covariance between vertical wind speed and water vapor density (equation 4). The sensible-heat flux is similarly computed, but variations in temperature are considered rather than water vapor. Latent- and sensible-heat fluxes can be approximated as:

$$\lambda E = \lambda \overline{w' \rho'_v} \quad (4)$$

$$H = \rho_a C_p \overline{w' T'_a} \quad (5)$$

where

w' is the instantaneous variation of vertical wind speed from a mean value, in meters per second (m/s),

ρ'_v is the instantaneous variation of water-vapor density from a mean value, in grams per cubic meter (g/m^3),

ρ_a is air density (g/m^3),

C_p is the specific heat of air, in joules per gram per degrees Celsius [(J/g)/°C], and

T'_a is the instantaneous variation in air temperature from a mean value (°C).

The overbars represent averaging across a 30-minute interval.

Site Selection and Description

Four sites were selected and instrumented to measure ET, water levels, and variables affecting ET, and to evaluate groundwater discharge in Dixie Valley (table 1). The study team (USGS, Reclamation, and Churchill County) acknowledged the necessity of an improved understanding of groundwater discharge from the large playa at the center of the basin. Therefore, two ET sites were located in phreatophytic vegetation that mostly characterizes the discharge area and two ET sites were located on the unvegetated playa. One vegetated ET site was in dense vegetation (DV), and the other ET site was in sparse vegetation (SV) (fig. 1). The playa ET sites (playa 1 [PL1] and playa 2 [PL2]) were located in areas characteristic of the various soil regimes and surface properties (fig. 1). Sites also were selected on the basis of year-round accessibility and spatial homogeneity that includes generally flat terrain and uniform vegetative (where applicable) and soil cover.

Seven instrumented monitoring sites, in addition to the ET sites, were installed. A Campbell Scientific, Inc. ET107 weather station (WEA; fig. 1) was installed in an area of sparse shrub cover, and the playa-west (PLW) monitoring site was established near the west edge and lowest point of the playa to periodically monitor evaporation using a hemispherical chamber, stable isotopes, soil-water content, and water levels. The PLW monitoring site was accessible only during late spring through early autumn, when the surface was free of standing water; the site surface typically was submerged by a precipitation-derived ephemeral pond during the remainder of the year. Measurement type and station associations at the PLW site location are as follows: groundwater measurements are associated with USGS stations 395123117594801 and 395123117594802, and soil measurements are associated with USGS stations 395123117594820 and 395123117594822. The five remaining monitoring sites (playa groundwater wells 1–5 [PLGW1–PLGW5]) were used to monitor playa water levels and were equipped with shallow (1.2–1.5 m bls; 3.9–4.9 ft bls) and deep (2.7 m bls; 8.9 ft bls) wells (table 2).

Table 1. Evapotranspiration and monitoring sites, Dixie Valley, Nevada, 2009–11.

[**Site name:** DV, dense vegetation; SV, sparse vegetation; PL1, playa 1; PL2, playa 2; WEA, weather station; PLW, playa-west; PLGW, playa groundwater well; SWN, shrubland well north; SWE, shrubland well east; SWW, shrubland well west. **Abbreviations:** m, meter; NA, not applicable; USGS, U.S. Geological Survey]

Site name	USGS station identification No.	Latitude (decimal degrees)	Longitude (decimal degrees)	Elevation (m)
Evapotranspiration sites				
DV	394545117573605	39.762511	-117.960100	1,045.61
SV	394348118040205	39.730106	-118.067264	1,032.44
PL1	394508118025505	39.752167	-118.048508	1,031.98
PL2	394559118013705	39.766444	-118.026831	1,030.99
Monitoring sites				
WEA	NA	39.939764	-117.823669	1,050.04
PLW	395123117594805	39.856297	-117.996583	1,029.31
PLGW1	395012118001701	39.836683	-118.004786	1,030.65
PLGW2	395348117582301	39.896589	-117.973167	1,031.18
PLGW3	395054117551001	39.848433	-117.919467	1,032.21
PLGW4	394805117573501	39.801431	-117.959744	1,030.66
PLGW5	395345117551301	39.895961	-117.920211	1,032.85
SWN	395503117513601	39.917550	-117.859942	1,037.00
SWE	394618117560601	39.771667	-117.935111	1,044.00
SWW	395310117595001	39.886026	-117.998187	1,061.00

Table 2. Well construction, maximum and minimum water level, and annual water-level change at evapotranspiration and monitoring sites in Dixie Valley, Nevada, 2009–11.

[**Site name:** DV, dense vegetation; SV, sparse vegetation; PL1, playa 1; PL2, playa 2; PLW, playa-west; PLGW, playa groundwater well. **Monitoring sites:** Depth-to-water values represent maximums and minimums determined from periodic field measurements made with a steel tape. Values in confined aquifers represent the potentiometric surface rather than the depth to water below an undisturbed landscape. **Abbreviations:** m, meter; bls, below land surface; USGS, U.S. Geological Survey; –, not available]

Site name	USGS station identification No.	Elevation (m)	Total depth (m bls)	Screened interval (m bls)	Aquifer type	Water year	Maximum depth to water (m bls)	Minimum depth to water (m bls)	Annual water level change (m)
Evapotranspiration sites									
DV	394545117573601	1,045.61	5.8	4.3–5.8	Unconfined	–	–	–	–
	394545117573602	1,045.61	5.9	4.4–5.9	Unconfined	2010	5.5	4.6	0.9
					Confined	2011	5.3	4.6	0.7
SV	394348118040201	1,032.44	7.5	6.0–7.5	Confined	2010	0.7	-0.2	0.9
						2011	0.7	-0.2	0.9
PL1	394508118025503	1,031.98	3.0	1.5–3.0	Confined	2010	1.1	0.2	0.9
						2011	0.9	0.6	0.3
PL2	394559118013701	1,030.99	2.9	1.4–2.9	Confined	2010	0.4	0.2	0.2
						2011	0.5	0.2	0.3
Monitoring sites									
PLW Deep	395123117594801	1,029.31	2.5	1.8–2.4	Confined	2010	0.1	-0.1	0.2
PLW Shallow	395123117594802	1,029.31	0.8	0.3–0.6	Confined	2010	0.2	-0.1	0.3
PLGW1 Deep	395012118001701	1,030.65	2.7	2.1–2.7	Confined	2010	0.7	0.0	0.7
					Confined	2011	0.7	-0.1	0.8
PLGW1 Shallow	395012118001702	1,030.65	1.5	0.9–1.5	Confined	2010	0.6	0.0	0.6
					Confined	2011	0.6	-0.1	0.7
PLGW2 Deep	395348117582301	1,031.18	2.7	1.3–2.5	Confined	2010	0.5	0.2	0.3
					Confined	2011	0.5	0.1	0.4
PLGW2 Shallow	395348117582302	1,031.18	1.2	0.6–1.2	Confined	2010	0.7	0.2	0.5
					Confined	2011	0.4	0.2	0.2
PLGW3 Deep	395054117551001	1,032.21	2.7	1.9–2.7	Confined	2010	0.5	-0.3	0.8
					Confined	2011	0.5	-0.3	0.8
PLGW3 Shallow	395054117551002	1,032.21	1.5	0.9–1.5	Confined	2010	0.4	-0.2	0.6
					Confined	2011	0.4	-0.2	0.6
PLGW4 Deep	394805117573501	1,030.66	2.7	1.2–2.7	Confined	2010	0.5	-0.3	0.8
					Confined	2011	0.8	0.2	0.6
PLGW4 Shallow	394805117573502	1,030.66	1.2	0.6–1.2	Confined	2010	0.7	0.4	0.3
					Confined	2011	1.0	0.3	0.7
PLGW5 Deep	395345117551301	1,032.85	2.7	2.1–2.7	Confined	2011	0.4	0.2	0.2
PLGW5 Shallow	395345117551302	1,032.85	1.3	1.0–1.3	Confined	2011	0.6	0.5	0.1

A combination of National Agriculture Imagery Program (NAIP) high-resolution imagery and field visits were used to identify homogeneous areas of sparse, moderate, and dense vegetative cover. A Normalized Difference Vegetation Index (NDVI) was computed from the 2006 NAIP image and visually compared to color infrared NAIP to identify the presence and relative abundance of vegetation in a pixel. These datasets were used to characterize vegetation quickly at a regional scale and to guide field reconnaissance visits, which were ultimately used to select the final ET sites that adequately characterized the phreatophytic vegetation distribution in the basin.

Dense Vegetation Site

The ET site location with dense vegetation (DV) was established at an elevation of about 1,046 m on March 10, 2009 (tables 1 and 2). This site was characterized by a mean vegetative cover of 24.8 percent during spring and summer months (May 2009–July 2011) (fig. 3*A*), as determined from the line-transect method (Smith, 1974). Summer vegetation was dominated by greasewood (64 percent), with lesser amounts of big saltbush and seepweed (13 and 23 percent, respectively). Mean canopy area and height were 1.6 m^2 and 0.8 m, respectively, for greasewood, and 1.3 m^2 and 0.94 m, respectively, for big saltbush. Surface soils were mapped as the Chuckles (fine-silty, mixed, superactive, mesic Sodic Haplocambids)–Bango (fine-loamy, mixed, superactive, mesic Haplic Natrargids)-association, and were characterized as moderately well-drained to well-drained in the Soil Survey Geographic (SSURGO) database (Soil Survey Staff, Natural Resources Conservation Service, 2011). The soil surface often was dry and cracked, with interspaced salt and biological soil crusts. Biological crusts ranged from 1 to 2.5 cm thick and were much more porous than the underlying soil matrix. The salt-crust concentration varied seasonally, but typically was less saline than that of the SV site, with sodium and chloride concentrations of about 1.27 and 0.11 mg/g, respectively, on August 11, 2009. Near-surface (0–6 cm bls) volumetric water content ranged from about 2 to 35 percent (determined from soil cores, March 2009–September 2011). Subsurface soil predominantly was aeolian silt and clay to 1 m bls, predominantly clayey silt with increasing clay content and salt crystals to about 4 m bls, and clay with silt and fine sand to the water table. The shallow basin-fill aquifer was unconfined with a depth to water ranging from 4.6 to 5.6 m bls (15.1 to 18.3 ft bls) (March 2009–September 2011). Measurement type and station identifier associations for plant and soil measurements made at the ET site location are as follows: plant measurements are associated with USGS station numbers 394545117573610 and 394545117573611, and soil measurements are associated with USGS station numbers 394545117573620 through 394545117573667.

Sparse Vegetation Site

The ET site location with sparse vegetation (SV) was established at an elevation of about 1,032 m on March 3, 2009 (tables 1 and 2). This site was characterized by a mean vegetative cover of 7.3 percent during spring and summer months (May 2009–July 2011), as determined from the line-transect method (Smith, 1974) (fig. 3*B*). Summer vegetation was dominated by greasewood (87 percent), with lesser amounts of seepweed (9 percent), and big saltbush (4 percent). Mean canopy area and height of individual greasewood shrubs were 1.2 m^2 and 0.7 m, respectively. Surface soils were mapped as the Chuckles (fine-silty, mixed, superactive, mesic Sodic Haplocambids)–Playas (fine, smectitic, mesic Typic Aquisalids)–Slaw (fine-silty, mixed, superactive, calcareous, mesic Typic Torrifluvents) association, and were characterized as poorly to moderately well drained in the SSURGO database (Soil Survey Staff, Natural Resources Conservation Service, 2011). Physical characteristics of surface soils included cracked, salt-crusted soil beneath and adjacent to plant canopies and dry, hard, and often cracked alkali flat (crust about 0.5–1.5 cm thick) within plant interspace areas. The soil crust was composed of about 36 mg/g of sodium and 38 mg/g of chloride, on August 10, 2009. Near-surface (0–6 cm bls) volumetric water content ranged from about 5 to 31 percent (determined from soil cores, March 2009–September 2011). Subsurface soil predominantly was silt, with increasing clay content to a depth of 1.2 m bls. Below the 1.2-m depth, the soil was composed of lakebed sediments characterized by 0.2 m of moist blue-green clay, followed by black, hydrogen-sulfide (H_2S) rich moist clay to the saturated zone. The depth to the saturated zone was about 5.2 m bls (17 ft bls); however, because the shallow basin-fill aquifer is confined by about 1 m of clay, measured water levels in the site observation well (table 2) ranged from about -0.2 to 0.8 m bls (-0.6 to 2.5 ft bls) (March 2009–September 2011). Measurement type and station identifier associations for plant and soil measurements made at the ET site location are as follows: plant measurements are associated with USGS stations 394348118040210 and 394348118040211, and soil measurements are associated with USGS stations 394348118040220 through 394348118040262.

Playa 1 Site

Playa 1 (PL1) was the driest of the two playa ET site locations, was established at an elevation of about 1,032 m on March 5, 2009, and was about 2 km northeast from the southwestern playa edge (figs. 1 and 4*A*; tables 1 and 2). Playa surface soils were mapped as the playas (fine, smectitic, mesic Typic Aquisalids) association in the SSURGO database (Soil Survey Staff, Natural Resources Conservation Service, 2011).

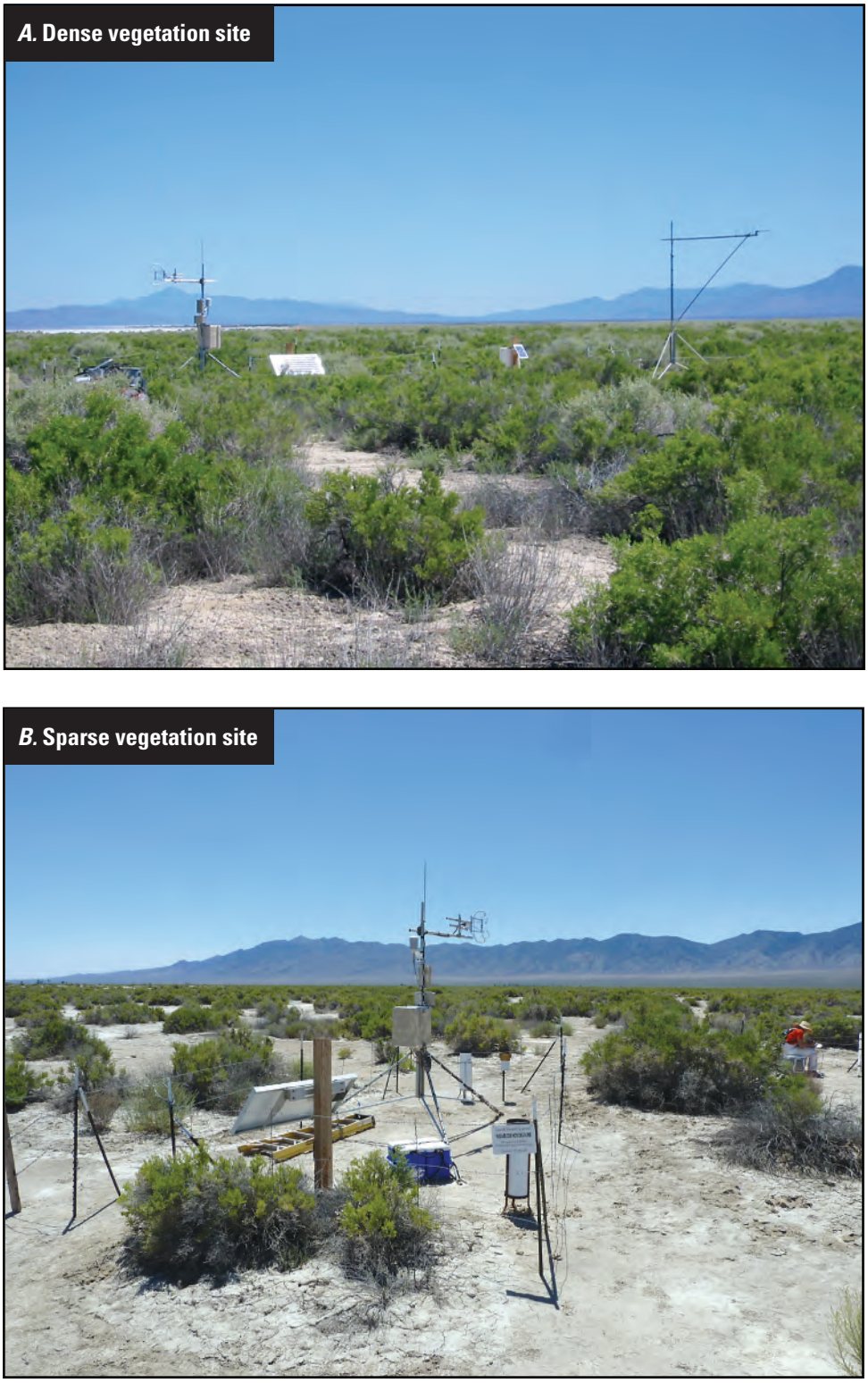

Figure 3. Vegetated evapotranspiration sites, Dixie Valley, Nevada. Photograph (*A*) taken by Jena M. Huntington, U.S. Geological Survey, June 23, 2009; photograph (*B*) taken by C. Amanda Garcia, U.S. Geological Survey, July 6, 2010.

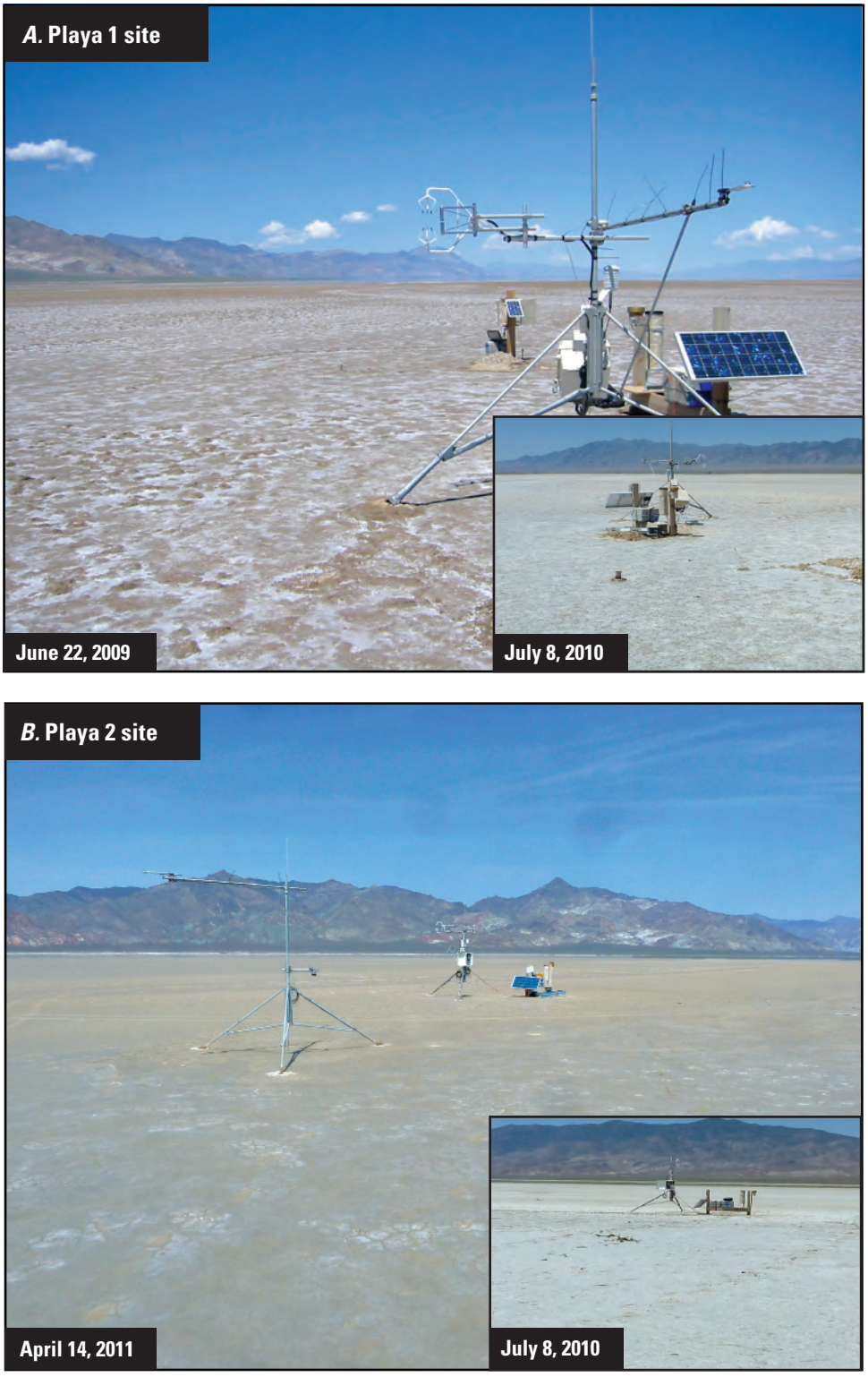

Figure 4. Playa evapotranspiration sites, Dixie Valley, Nevada, 2009–11. Photographs taken by (*A*) Jena M. Huntington, (*A*-inset) C. Justin Mayers, (*B*) C. Amanda Garcia, and (*B*-inset) Michael A. Barrenchea, U.S. Geological Survey.

The playa surface was characterized as dry-to-moist silty clay with interspersed humic, salt-crusted (about 1–1.5 cm thick) mounds (less than 7 cm thick). The humic mounds often were cracked and dry within, whereas the interspaced flat clay surface typically was moist below a thin salt crust when present. The soil crust was much more saline than the soil crust at the vegetated sites, with sodium and chloride concentrations of about 68 and 94 mg/g, respectively, on August 12, 2009. Near-surface (0–6 cm bls) volumetric water content ranged from about 25 to 38 percent (determined from soil cores, March 2009–September 2011). Subsurface soil predominantly was silty, moldable clay to 1.8 m bls, followed by greenish-brown clay from 1.8 to 2.3 m bls, and black anaerobic clay below 2.3 m bls. Depth to the saturated zone was about 1.2 m bls (4 ft bls), and the confined water table ranged from 0.2 to 1.2 m bls (0.7 to 4 ft bls) (March 2009–September 2011). Soil measurements made at the ET site location are associated with USGS stations 394508118025520 through 394508118025552.

Playa 2 Site

Playa 2 (PL2) was the wetter of two playa ET site locations, was established at an elevation of about 1,031 m on March 3, 2009, and was about 4.5 km northeast of the southwestern playa edge (figs. 1 and 4*B*; tables 1 and 2). The playa surface was characterized as moist silty clay with a thin salt crust (less than 3 mm thick) and thin cracks; cracks greatly increase in width and depth (by as much as 1.5 and 3 cm, respectively) when anthropogenically disturbed areas dry out after large precipitation events. The soil crust at this site was the most saline of the four sites, with sodium and chloride concentrations of about 125 and 193 mg/g, respectively, on August 12, 2009. Near-surface (0–6 cm bls) volumetric water content ranged from about 37 to 53 percent (determined from soil cores, March 2009–September 2011). Subsurface soil predominantly was moist, moldable, and cohesive clay from the land surface to more than 3 m bls. A thin, vesicular hardpan was present between about 0.8 and 0.9 m bls. Depth to the saturated zone was about 0.76 m bls (2.5 ft bls), and the shallow, confined water table ranged from 0.01 to 0.6 m bls (0.04 to 1.9 ft bls) (March 2009–September 2011). Soil measurements made at the ET site location are associated with USGS stations 394559118013720 through 394559118013749.

Instrumentation and Site Maintenance

Eddy-covariance sites were equipped with identical data recording and sensor arrays. Eddy-covariance instruments and net radiometers were installed on 3-m steel tripods. Tripods set on the playa were secured by fastening and burying 20-by-28-cm plastic boards to the tripod feet. The boards were anchored into the playa using 0.6-m steel pipes and were buried with playa material. Sites also were equipped with aboveground tipping bucket and volumetric precipitation gages and belowground energy-flux sensors, heat-dissipation probes, and monitoring wells equipped with pressure transducers. Most sensors were powered with a combination of 10- and 64-watt (W) solar panels and multiple deep-cycle marine batteries.

Available energy was measured at each site with a Kipp and Zonen CNR2 net radiometer (net longwave and shortwave), two self-calibrating Huskeflux HFP01SC heat flux plates, 8 Campbell Scientific, Inc. TCAV averaging soil temperature probes, and a Campbell Scientific, Inc. CS616 water content reflectometer. Heat flux plates were installed at 8-cm bls, with replicate temperature probes placed at 2 and 6 cm bls. The water content reflectometer was installed horizontally, and integrated measurements between two horizontal rods at 2 and 6 cm bls. Flux plate, temperature, and water content sensor spatial locations were selected so that the mean degree of shading from vegetation approximated the degree of shading across each site.

High-frequency (10-Hz) fluctuations of water-vapor density were obtained using a Campbell Scientific, Inc. KH20 krypton hygrometer. High frequency (10-Hz) wind-speed vectors and sonic temperature measurements were obtained with a Campbell Scientific, Inc. CSAT 3 three-dimensional sonic anemometer. Absolute water vapor density was measured with a Campbell Scientific, Inc. HMP45C temperature and relative humidity probe. These data allow calculation of latent- and sensible-heat fluxes by the eddy-covariance method. A Campbell Scientific, Inc. CR3000 electronic datalogger received sensor readings 10 times per second and computed means, variances, and covariances every 30 minutes. The hygrometer and sonic anemometer were positioned 10 cm apart.

Precipitation was measured at each site with a National Weather Service-approved standard 20.3-cm (8-in.) diameter NovaLynx volumetric rain gage. A Campbell Scientific, Inc. TE525 tipping bucket rain gage was co-located with each volumetric rain gage to monitor the timing and intensity of rainfall. Installation heights of all aboveground sensors are shown in table 3. Volumetric gage orifice inlets were equipped with stainless steel 20–40 mesh screens to prevent insects and other debris from altering volumetric measurements within collection tubes.

Volumetric water-content measurements were collected with a neutron probe at vegetated sites throughout the period of record and through November 2009 and February 2010 at the PL1 and PL2 sites, respectively. Replicate polyvinyl chloride (PVC) access tubes were installed to 5 m bls at the DV site, 4 m bls at the SV site, 1.2 m bls at the PL1 site, and 0.6 m bls at the PL2 site. Measurements were made at 15 and 25 cm bls, and continued at 25-cm increments from 25 cm bls to the access tube base. Access tubes on the playa frequently cracked and filled with water as the playa sediments expanded and contracted. Therefore, after winter 2010, quarterly

Table 3. Aboveground sensor heights at evapotranspiration sites, Dixie Valley, Nevada, 2009–11.

[**Site name:** DV, dense vegetation; SV, sparse vegetation; PL1, playa 1; PL2, playa 2. All units are height above land surface in meters. **Abbreviation:** USGS, U.S. Geological Survey]

Site name	Sensor				
	CSAT 3 3D sonic anemometer	KH2O krypton hygrometer	CNR2 net radiometer	Tipping bucket rain gage	Bulk storage rain gage
DV	2.72	2.72	3.24	0.79	0.82
SV	2.72	2.71	2.79	0.79	0.86
PL1	1.91	1.91	1.96	1.19	1.15
PL2	2.72	2.72	2.74	1.26	1.22

water-content profiles at the playa sites were measured using soil cores collected with a 15-cm long sampler with a 5-cm inner diameter from the following depths: 0–0.15, 0.3–0.45, and 0.6–0.75 m bls. These depths correspond with intervals between soil cores sampled for stable isotope analyses (see section, "Water Sourcing").

Matric potentials were measured in this study to investigate unsaturated zone hydraulic gradients and water movement. Matric potential was monitored at each site with a series of Campbell Scientific, Inc. Model 229 heat dissipation matric water potential sensors, installed in shallow (≤0.6 m bls) trenches and boreholes (≥0.9 m bls). Heat-dissipation-sensor calibrations were made according to procedures developed by Flint and others (2002) that measure soil matric potential and soil temperature. Replicate shallow probes were installed horizontally and perpendicular to trench walls at 0.3 and 0.6 m bls. Additional replicate probes were installed at 0.15 m bls at the playa sites. Deeper probes were installed vertically in boreholes at depths of 1.2, 2.4, and 3.7 m bls at the SV site and 1.2, 2.4, 3.7, and 4.9 m bls at the DV site. At the PL1 site, replicate probes were installed in a borehole at 0.9 m bls; at the PL2 site, individual probes were installed at 1.2 and 1.8 m bls.

During instrumentation, soil cores and bulk soil samples were collected for measurements of physical, chemical, and hydrologic properties (appendix 2). Standard laboratory measurements of bulk density, pH, electrical conductivity (determined from a soil paste), volumetric water content, saturated hydraulic conductivity, and moisture retention characteristics (five-point tension analysis), were made. Textural (hydrometer) and salt characterization analyses were done for surface soil samples. Moisture retention and hydraulic conductivity measurements were used to compute van Genuchten (1980) parameters, unsaturated hydraulic conductivity, and, ultimately, liquid-water fluxes between heat dissipation sensors in the unsaturated zone (equations shown in appendix 2).

Instruments were checked and evaluated monthly, and repaired or replaced as necessary. The net radiometer and sonic anemometer were checked for proper horizontal level and adjusted if necessary, and the net radiometer and krypton hygrometer were cleaned with distilled water. Solar panels and precipitation gage orifices were cleaned of dust and debris and batteries routinely were refilled with distilled water. Precipitation accumulated in the volumetric rain gage was measured and recorded. Accumulated precipitation was sampled quarterly for analysis of stable isotopes, and collection tubes were drained, wiped dry, and refilled with a 0.5-in. layer of mineral oil to prevent evaporative losses of the subsequently collected precipitation. Care was taken to ensure that mineral oil did not contact the inner walls of the collection tubes during filling.

Data Correction, Filtering, and Gap-Filling Procedures

Available energy, eddy-covariance, and other site-specific data were processed to reduce systematic errors, and data gaps were identified to develop a continuous dataset of 30-minute fluxes. Raw shortwave and longwave radiation measurements at each site were corrected to a single Hukseflux NR01 four-component net radiation sensor to compensate for instrument variability among sensors. Volumetric water content measurements made with a Campbell Scientific, Inc. CS616 water content reflectometer and neutron probes were calibrated using field-measured soil cores. Raw latent- and sensible-heat flux data were corrected to compensate for limitations in eddy-covariance theory and equipment design (see section, "Turbulent Fluxes"). Data were filtered to identify poor-quality data. Gap-filling procedures differed with the variability, length and timing of the gap, and followed existing ET techniques (Moreo and others, 2007; Shoemaker and others, 2011) and a new multivariate regression technique (Halford and others, 2012). Precipitation measurements were corrected for wind related undercatch.

Net Radiation

Net radiation data from the four Dixie Valley ET stations were corrected to a single reference instrument. A Hukseflux NR01 four-component net radiation sensor was used as the reference standard in this study to which four Kipp and Zonen CNR2 two-component radiometers were compared and adjusted. The NR01 was installed at the same height as and at a horizontal distance of about 0.5 m from the CNR2 sensor. Site comparisons between CNR2 and NR01 measurements were based on filtered data that excluded periods during and just after precipitation events. Negative net-shortwave radiation data were removed from the dataset and calibration analysis to avoid an erroneous bias. To document calibration drift, all radiometers were calibrated before field installations by the manufacturer and after sensors were removed from the field. Calibration drifts were applied to measurements prior to comparing NR01 and CNR2 sensors. The NR01 calibration drift was assumed to be linear, and calibration factors determined before and after field installations were interpolated in time and applied to the entire dataset. The calibration drift was negligible for shortwave sensors and was within 2 percent for longwave sensors. Additionally, the analysis accounted for adjustments to the standard (NR01) sensor calibration owing to calibration method. Hukseflux NR01 longwave net radiation sensors are calibrated using a blackbody source indoors that is traceable to the ITS-90 International Temperature Scale, whereas Kipp and Zonen CNR2 longwave net radiation sensors are calibrated to a clear nighttime sky using a reference pyrgeometer traceable to the World Infrared Standard Group (WISG). (Shortwave calibrations are internationally standardized and, therefore, do not differ between sensors evaluated in this study.) Discrepancies between calibration methods and resulting measurements are attributable partly to the lack of international longwave standards. To normalize the blackbody calibration to the outdoor WISG-traceable calibration, Hukseflux recommends a 6.5–8.5 percent adjustment to the incoming longwave calibration factor (Robert Dolce, HukseфluxUSA, written commun., 2012). Considering that the WISG is an internationally accepted reference, NR01 calibration factors were adjusted using the mean of the manufacturer-recommended range (7.5 percent) prior to correcting CNR2 measurements. The CNR2 manufacturer calibration drift measured after field installation was assumed to occur during the first year of deployment as a result of moisture equilibration with the native environment. Therefore, CNR2 calibrations applied to the first year of data were based on linearly interpolated (in time) calibration factors determined before and after field installation, and the calibration factor determined after field installation was applied directly to the remaining dataset. The CNR2 shortwave calibration factors drifted by 5 percent or less among all sites, whereas the longwave calibration factors drifted by 5–9 percent.

Scaling caused by precipitation and debris on the surface of pyrgeometers used to measure incoming longwave radiation can cause notable error in net radiation measurements. This error occurs because pyrgeometer windows are flat, and upward-facing windows provide a surface that permits water droplets and debris to settle. Downward-facing pyrgeometer windows are mostly unaffected because they do not get wet. Similarly, upward- and downward-facing pyranometer windows, which receive shortwave radiation, are hemispherical domes that are less prone to water and debris accumulation. Brotzge and Duchon (2000) noted that water droplets on pyranometers and pyrgeometers could cause spurious values immediately following rainfall; therefore, reliable measurements can be expected only when all moisture has evaporated. They also noted that, in drier regions, dust or residual debris remaining after precipitation or dew evaporation can alter surface albedo and absorption properties. Precipitation was observed to cause spurious net longwave values in this study, as in Brotzge and Duchon (2000). Additionally, residual debris on upward-facing pyrgeometers after the evaporation of precipitation occasionally led to a notable positive bias in net-longwave measurements that persisted for several weeks. This bias was shown from a comparison between CNR2 and NR01 measurements made at the DV site during intermittent precipitation events. Because the net longwave budget is upward (negative), a positive bias means that the measurement is less negative. This implies that dirt on the upward-facing pyrgeometer windows increases the measured incoming longwave radiation. Shortwave measurements during the study appeared unaffected by precipitation or debris.

Scaling of upward-facing pyrgeometers was identified by comparing net-longwave radiation values between vegetated sites and playa sites throughout the study period. The relation between net-longwave measurements from PL1 and PL2 sites appeared consistent within a given season prior to and following precipitation events, indicating that scaling effects on sensor output either was minimal or occurred simultaneously at both sites. Vegetated sites, however, showed evidence of scaling effects on longwave radiation measurements. The DV site showed less negative net-longwave magnitudes relative to the SV site during summer 2011 after precipitation, deposition of avian fecal matter, or accumulation of dust. The latter two factors were identified during monthly sensor cleaning. A distinct change in the diurnal signature of net-longwave radiation following sensor cleaning indicated that the pyrgeometer was scaled previously. Apparent scaling effects at the DV site persisted from June 19, 2011 to July 11, 2011, and from August 8, 2011 to August 16, 2011. The SV site also showed obvious scaling effects from July 29, 2009 to August 10, 2009. Data collected during these periods were filtered from the dataset. Consistent diurnal patterns in net-shortwave radiation at all sites during the period of record and cleaner pyranometer windows (with

respect to pyrgeometer windows) observed during field visits indicate that dust and debris scaling over pyranometers was minimal and had little effect on sensor output.

In addition to spurious values caused by precipitation and observed sensor scaling, data also were filtered during periods when sensors were cleaned and serviced, and when data logger programs were revised. Data gaps typically spanned 2 hours or less and were filled using linear interpolation. At the PL1 site, the data logger malfunctioned during most of August 2010, causing complete loss of all data. Gaps in net radiation and soil-heat flux were filled using ordinary least squares regression with PL2 site data (coefficients of determination [r^2] = 0.99 and 0.94, respectively).

Volumetric Water Content

Near-surface water content measurements made with the CS616 probe at the vegetated sites were calibrated against volumetric water content measurements in cubic centimeters per cubic centimeter (cm^3/cm^3) determined from soil samples collected periodically near the CS616 probes. Shallow burial of the CS616 instrument control box (1–7 cm bls) resulted in thermal loading measured as diurnal fluctuations in water content (averaging about 1 percent at the DV site and 3 percent at the SV site). Therefore, 30-minute measurement means were computed across 24-hour intervals (from midnight to midnight), the 24-hour mean was assigned to the 12:00 p.m. 30-minute measurement interval and these values were linearly interpolated from day to day to compute a continuous 30-minute dataset. The change in soil temperature and soil-water content measured above each heat flux plate was converted to heat flux and added to the mean soil-heat flux measured across the plate (equation 2). Calibration equations were based on mean daily measurements and had coefficients of determination (r^2) of 0.83 at the DV site and 0.92 at the SV site. Water content measurements made at playa sites using the CS616 probe were skewed because of sensor instability in saline soils where electrical conductivity exceeds 5 mS/cm. Therefore, periodically collected soil samples used to measure gravimetric water content were interpolated between measurements to develop a continuous dataset covering the period of record. Volumetric water content was computed by multiplying gravimetric water content by the mean bulk density determined from all periodic measurements.

Neutron probe profile measurements made in PVC access tubes were calibrated for neutron attenuation using soil cores collected during instrumentation. Neutron-probe water content measurements were made immediately following access tube installation and used to develop individual calibration equations for each tube. Additional shallow neutron-probe and soil-core measurements were collected throughout the study period and used to refine calibration equations. Separate calibration equations were based on count ratios calculated for measurements at (1) depths of 0.15 m bls, and (2) depths greater than 0.15 m bls. Calibration equations at vegetated sites had r^2 values of greater than 0.82 at depths below 0.15 m bls, and between 0.58 and 0.9 at 0.15 m bls. Calibration equations at playa sites poorly described the variation in water content, with r^2 values averaging 0.56 because playa soil was consistently moist and volumetric water content values used for calibration equations narrowly ranged from about 0.3 to 0.52 m^3/m^3.

Turbulent Fluxes

High-frequency (10-Hz) latent- and sensible-heat fluxes were processed and corrected using the program EdiRe (Clement, 1999) to improve flux measurements. Data spikes occasionally occur in response to electronic and physical noise. Spikes in the datasets representing more than six times the standard deviation for a given 30-minute averaging period were removed and replaced with the running mean. Coordinate rotation of the three-dimensional wind components was applied to account for imperfect leveling of the CSAT 3 anemometer so that its horizontal axis was perpendicular to the mean wind streamline. This was done using the planar fit method where the mean angle of the horizontal plane is equal to zero (Gash and Dolman, 2003; Lee and others, 2004). Frequency response errors resulting from flux losses or attenuation at high (fast) and low (slow) frequencies also were corrected (Moore, 1986; Massman, 2000). Frequency response corrections include: (1) sensor separation to compensate for the separation between the CSAT 3 anemometer and krypton hygrometer, and inability of the vertical wind speed and scalar sensors to sample in the same volume; (2) path-length averaging to account for the flux loss caused by averaging over a path rather than at a point; and (3) low-pass filtering to account for the loss of flux resulting from a finite sampling duration and insufficiently long averaging period to record all low frequencies (large eddies). Additional corrections to the latent heat flux include the Webb, Pearman, and Leuning (WPL)-correction (Webb and others, 1980) to account for variations in air density resulting from fluctuating temperature (thermal expansion) and humidity (vapor dilution), and the krypton hygrometer oxygen-sensitivity correction (Tanner and Greene, 1989). The sonic temperature also was corrected for measurement errors caused by deflection of the sound path and variations in air density prior to computing the sensible-heat flux (Schotanus and others, 1983).

High-frequency data have occasional spikes arising from electronic and physical noise. Water accumulation on the hygrometer represents a large part of the physical noise. Wet hygrometer windows arising from precipitation, dew, or frost and snow often can cause a substantial decrease in the millivolt output. Data were considered poor and were rejected when this phenomenon occurred.

Additional data filtering included establishing upper and lower bounds of 700 and -150 W/m^2 for sensible-heat fluxes, 700 and -50 W/m^2 for latent-heat fluxes when net radiation was greater than 5 W/m^2, and 50 and -50 W/m^2 for latent-heat fluxes when net radiation was less than 5 W/m^2. Upper filtering bounds for sensible- and latent-(daytime) heat fluxes and the lower bound for sensible-heat fluxes were based on guidelines from the AmeriFlux data archive (Law and others, 2005). Remaining filtering bounds were based on evaluation of each site-specific dataset. The sonic anemometer was much less sensitive to interference from precipitation, yet occasional bad data were flagged and discarded. Spikes in morning λE values that periodically occurred during dry summer days highlighted the potential for dew formation on the playa.

Dew formation on the playa surface and potential contributions to evaporation measurements were investigated during mid-July through September 2011 at site PL2. In arid environments, dew can be an important part of the water balance (Malek and others, 1999; Moro and others, 2007). Thorburn and others (1992) observed the presence of condensation at night on playas with high surface salinity. Although a relative humidity near 100 percent typically is necessary to form dew on playa surfaces, salt accumulation can greatly reduce the relative humidity at which the vapor pressure reaches saturation and dew forms. As in Moro and others (2007), Campbell Scientific, Inc. LWS-L leaf-wetness sensors that measure the dielectric constant just above the sensor surface were used to identify the presence of dew. These sensors output a signal that is proportional to the amount of water or ice on the sensor surface. Leaf-wetness sensors were installed on the soil surface and on the sensor tripod at about 0.3 m above land surface. The surface of wetness sensors is manufactured to mimic a leaf surface; therefore, thermal and water vapor absorption properties likely differ somewhat from the silty saline playa surface. Agam and Berliner (2006) noted that in arid environments during the dry season, manufactured surfaces often indicate the formation of dew, whereas bare soil more commonly absorbs water vapor. Although the addition of salt on bare soil playas reduces the saturation vapor pressure necessary to promote dew formation, the addition of salt and increased osmotic potential likely would enhance water vapor absorption relative to dew formation.

Data gaps arising from discarded poor-quality data or sensor malfunction were filled using estimated values based on the time of day, seasonal variability, and gap length. Gap-filling techniques include linear interpolation, ordinary least-squares regression, multivariate regression, and substituting values from a previous or subsequent day with similar meteorological conditions. Gaps of 2 hours or less were interpolated for all sensors using previous and subsequent measurements. Air temperature (HMP45C) data gaps of more than 2 hours were filled using ordinary least squares regressions with sonic temperature output from the CSAT 3 anemometer where available, followed by regressions with air temperature measured at the nearest site using the HMP45C temperature and relative humidity probe.

Gaps in latent- and sensible-heat flux data of more than 2 hours were filled using the following methods. Nighttime gaps (net radiation less than 5 W/m^2) in the latent heat flux were set equal to zero unless they followed or preceded a gap in daytime data. Gaps resulting from precipitation on the krypton hygrometer or CSAT 3 anemometer, or hygrometer scaling from a mix of precipitation and blowing dust often lasted from several hours up to several weeks. When sufficient data either before or after the gap were available, these gaps were filled using a multivariate regression between turbulent fluxes and micrometeorological data. When micrometeorological data surrounding the gap were limited, fluxes were set equal to another field site flux where flux magnitudes and trends were similar before and after the data gap. When data from alternate sites were limited and the gap was limited to less than 24 hours, the flux was set equal to fluxes from a previous or subsequent day where micrometeorological trends were similar. During winter when snow was present and data antecedent or subsequent to the latent heat flux data gap were limited or when sufficient daytime data were available to establish a trend in the 30-minute flux, daytime data were interpolated between gaps and nighttime data were set equal to zero.

The multivariate regression technique applied to fill data gaps uses an approach similar to neural networks (Papale and Valentini, 2003), where the complex relation between micrometeorological variables driving the flux of interest can be simulated and used for flux approximation. Fluxes are approximated by summing multiple micrometeorological component fluctuations during a period prior or subsequent to the data gap, minimizing the difference between measured and approximated fluxes (here after referred to as simulated fluxes) and projecting this fit across the data gap. This technique was applied using the Microsoft® Excel program SeriesSEE (Halford and others, 2012), where micrometeorological fluctuations were used to simulate turbulent fluxes.

A simulated flux (*SF*) at time, *t*, is described as (Halford and others, 2012):

$$SF(t) = C_0 + \sum_{i=1}^{n} MC(t)_i \qquad (6)$$

where

C_0 is a constant equal to the summation of all y-intercepts (or offsets) from each component (W/m^2),

n is the number of components, and

MC_i is the ith micrometeorological component in units of the simulated flux.

Component units are converted to simulated flux units using an amplitude multiplier described in equation 9. Micrometeorological components are created from measured time series such as net radiation, soil-heat flux, sensible-heat flux, air temperature, latent- or sensible-heat fluxes from an alternate site, precipitation, and the latent-heat flux computed from the Priestley-Taylor model (Priestley and Taylor, 1972). The Priestly-Taylor model is described as

$$\lambda E = \alpha \frac{\Delta}{\Delta + \gamma}\left(R_n - G\right) \tag{7}$$

where

- α is an empirically determined dimensionless coefficient that was allowed to vary during the fitting process,
- Δ is the slope of the saturation vapor pressure-temperature curve (kPa °C–1) and γ is the psychrometric constant (kPa °C–1; pressure-corrected for site elevation). Air temperature (T_a in degrees Celsius) was used to compute the second term on the right side of equation 7 using a polynomial regression equation fit to data from Shuttleworth (1993, table 4.2.1) with the psychrometric constant:

$$\frac{\Delta}{\Delta + \gamma} = -0.00015T_a^2 + 0.017T_a + 0.430 \tag{8}$$

Micrometeorological components other than precipitation were transformed using multiple, moving averages to represent different signal frequencies. The moving-average transform was applied to the ith MC at time, t, with

$$MC\left(t\right)_i = a_i V_i\left(t + \phi_i\right) \tag{9}$$

where

- a_i is the amplitude multiplier of the ith component in units of the simulated flux divided by units of the ith component,
- ϕ_i is the phase-shift of the ith component [t, time], and
- $V_i(t+\phi_i)$ is the value of the moving average of ith component at time $t+\phi_i$ in units of ith component.

A meteorological component that was transformed with a moving average is adjusted automatically for optimal flux simulation by changing amplitude (a) and phase (ϕ) in equation 9. Raw input series were added as meteorological components by assigning a moving average interval of 0 days (for example, no averaging).

Precipitation pulses were transformed into decay curves using a gamma function to imitate a latent-heat flux response (Halford and others, 2012). The gamma function was adapted from a model that simulates recharge to the water table from precipitation (O'Reilly, 2004). Transformations of precipitation pulses were attenuated or intensified, and prolonged or condensed depending on the season, available energy, and soil-water content.

Parameters used to transform micrometeorological components were calibrated automatically using Parameter ESTimation (PEST) software (Doherty, 2010). Differences between simulated and measured fluxes were minimized using PEST, and a root-mean-square (RMS) error was provided to evaluate the fit and to compare with measured values.

Precipitation

Prior to analyzing the catch of precipitation gages, wind-related undercatch was quantified at the height of the gage. Point measurements of precipitation can have deficiencies in catch as a result of wind (Larson and Peck, 1974; Yang and others, 1996; Nešpor and Sevruk, 1999). Wind-related errors increase with wind speed and are related to turbulence near the gage, which acts as an obstacle to the wind stream. Based on several previous studies, Larson and Peck (1974) surmised that a 10 percent deficiency at 4.47 m/s (10 mi/h) could be expected for unshielded liquid precipitation. The relation between measurement deficiency and wind speed for liquid precipitation is nearly linear for these studies. Using an unshielded National Weather Service 20.3-cm (8-in.) bulk precipitation gage similar to the one used in this study, Yang and others (1996) measured a 14 percent deficiency at 4.47 m/s for liquid precipitation, and discovered an exponential relation between undercatch deficiency and wind speed. Yang and others (1996) also established linear and exponential relations for mixed and solid (snow) precipitation, respectively. Wind-related undercatch corrections were applied using the following equations (Yang and others, 1996):

$$R_{solid} = exp\left(4.606 - 0.157U^{1.28}\right) \tag{10}$$

$$R_{mixed} = 100.77 - 8.34U \tag{11}$$

$$R_{liquid} = exp\left(4.605 - 0.062U^{0.58}\right) \tag{12}$$

$$P_t = \frac{P_m}{R} \times 100 \tag{13}$$

where

- R is the percentage of precipitation measured for liquid, mixed, and solid precipitation;
- U is the mean daily wind speed at the height of the precipitation gage (m/s);
- P_t is total daily precipitation (mm); and
- P_m is measured daily precipitation (mm).

Temperature bounds used to characterize mixed and solid precipitation range from 3 to -2 °C and less than -2 °C, respectively (Yang and others, 1996).

Wind speed decreases with decreasing height above the plant canopy or playa surface; therefore, measurements made at the height of the CSAT 3 anemometer on the instrument tripod were considered insufficient to use directly for undercatch corrections. Continuous, CSAT 3 anemometer wind-speed measurements were made from heights ranging from 1.91 to 2.72 m, whereas volumetric precipitation was measured at heights ranging from 0.82 to 1.22 m (table 3). Therefore, an additional CSAT 3 anemometer was rotated from site to site and deployed at the mean height of the volumetric and tipping-bucket precipitation gages for month-long intervals to (1) develop ordinary least squares regressions between the 30-minute mean wind speed measurements at the two heights, and (2) adjust CSAT 3 anemometer measurements to the height of the precipitation collector.

Regressions represented wind speeds ranging from 0.1 to 15 m/s, and, therefore, were considered adequate to characterize the complete period of record at most sites. Coefficients of determination describing regressions at the SV, PL1, and PL2 sites were reasonable and greater than 0.92, but the r^2 value determined at the DV site was only 0.62. Therefore, the DV site relation between measurement heights was reevaluated using a multivariate regression as described in equation 6, where wind speed at the height of the precipitation gage was simulated using wind speed measured by the CSAT 3 anemometer. The multivariate regression was a substantial improvement with respect to the ordinary least squares regression with an $r^2=0.96$. Therefore, the multivariate regression was used to adjust continuous CSAT 3 anemometer wind speed to the height of the precipitation collector at the DV site. Remarkably, undercatch corrections at the DV site using multivariate and ordinary least squares regressions resulted in water-year precipitation measurements that were within 1 percent of each other.

Gaps in the tipping bucket precipitation measurements made during a 30-minute interval were filled and corrected to match monthly volumetric measurements prior to applying wind-related undercatch corrections. During the start of the measurement period, gaps in the tipping bucket precipitation gage data at the PL2 site were filled using an ordinary least squares regression with the PL1 site ($r^2=0.77$) in order to capture precipitation timing and wind speed. The regression omitted data where precipitation was measured at one site and not the other. The same relation was used to fill gaps in data at the PL1 site during August 2010 when the datalogger malfunctioned. Volumetric-gage corrections to tipping bucket measurements increased values by 10 percent at the DV site, 15 percent at the SV site, 34 percent at the PL1 site, and 38 percent at the PL2 site during the period of record. Wind-related undercatch corrections increased volumetric-corrected tipping bucket measurements by about 7 percent at vegetated sites and about 15 percent on the playa during the period of record.

Snowfall measurement errors were assumed to minimally affect water-year precipitation measurements. Snowfall typically accumulates in the gage orifice (while temperatures remain below freezing) and is not measured by the tipping bucket gage until it melts. Measurement of this precipitation at a later time and altered wind speed could bias estimates high or low. Similarly, if snowfall exceeds a few inches before melting, it can overtop tipping bucket or volumetric gages and avoid measurement, biasing measurements low. Although snowfall occurred during the study, most precipitation measured at the four ET sites fell as rainfall; therefore, snowfall measurement errors were assumed to minimally affect cumulative water-year measurements.

Source Area of Measurements

Source areas for turbulent flux and available-energy measurements represent the areas from which the measured fluxes originate. The source area for eddy-covariance turbulent-flux measurements is the dynamic upwind land-surface area contributing to measured water vapor and heat fluxes, whereas source areas for available-energy measurements are constant and depend on instrument placement. Thus, turbulent-flux source areas typically are larger and more variable than available-energy source areas.

Turbulent-flux source areas depend on atmospheric stability, surface roughness, and sensor height. Sensors were mounted high enough to capture the well-mixed surface layer above the canopy or playa surface during unstable daytime conditions, but not so high that the source area during stable nighttime conditions extended beyond the homogeneous surface of interest. Source areas were derived from a dispersion model (Schuepp and others, 1990) assuming mildly unstable atmospheric conditions. The Obokuv length input variable was computed as the difference between the zero displacement height and sensor height, where the zero displacement height is about 66 percent of the canopy height. These areas were confirmed with a crosswind-integrated and crosswind-distributed source area (Kormann and Meixner, 2001) computed with the EdiRe processing program that apportions relative flux contributions within the source area. Turbulent-flux sensors were placed at least 2 m above the canopy and at least 1.5 m above the playa surface to avoid measuring recirculating flow caused by turbulence at the edge of the canopy or playa surface. Roughness lengths characterizing surface roughness ranged from 0.001 m at the playa sites to 0.1 m at the DV site (Stull, 1988), and increased with increasing canopy height and cover. Zero-plane displacement heights, where the logarithmic wind profile approaches zero near the canopy top, ranged from 0.001 m at the playa sites to 0.55 m at the DV site.

Source areas for eddy-covariance measurements decreased with increasing canopy cover at vegetated sites and with lower instrument heights at the playa sites. Source areas computed using the Schuepp and others (1990) dispersion model indicate that as much as 90 percent of the turbulent flux originated from upwind distances of 160 to 240 m at the DV and SV sites, respectively, and from about 360 to 550 m at the PL1 and PL2 sites, respectively (fig. 5). The relative flux contribution peaked a short distance (from 8 m at the DV site to 29 m at the PL2 site) upwind of the sensors and decreased asymptotically thereafter. Differences in source areas at playa sites represent differences in deployment heights of turbulent flux sensors (1.91- and 2.72-m heights at PL1 and PL2 sites, respectively).

Alternative source areas determined using the Kormann and Meixner (2001) approach support estimates made using Schuepp and others (1990) and are summarized in appendix 3. At the DV and SV sites, more than 90 percent of the turbulent flux occurred within 200 m of instrument tripods (on average) between February and October of each year. At the PL1 site, more than 90 percent of the turbulent flux typically occurred within 300 m of the sensors between February and October, whereas at the PL2 site, flux percentages ranged from 82 to 91 percent. These differences among playa sites likely represent variable sensor deployment heights. Measured turbulent fluxes at all sites predominantly were from a northwest (315 degrees) to northeast (45 degrees) source area during cooler months (October–March), and from a southwest (225 degrees) to northwest source area during warmer months (April–September). Wind direction seldom occurred from the east within the 30-degree window (75–105 degrees) behind the instrument tripod, suggesting that the presence of the tripod as an aerodynamic obstacle did not substantively affect airflow near the eddy-covariance sensors (appendix 3).

Source areas for available-energy measurements are small relative to turbulent-flux measurements. The downward-facing sensors of net radiometers measure across a cosine-weighted circular area with a radius about 3 times the sensor height, representing 90 percent of the measured flux. Sensors in vegetated areas were high enough to record variability in canopy height and cover. Net radiometer source areas extended radially from nearly 20 m at the PL1 site to about 30 m at the DV site. Source areas for ground-heat-flux measurements are small and represent less than a 0.3-m diameter circle surrounding the sensor.

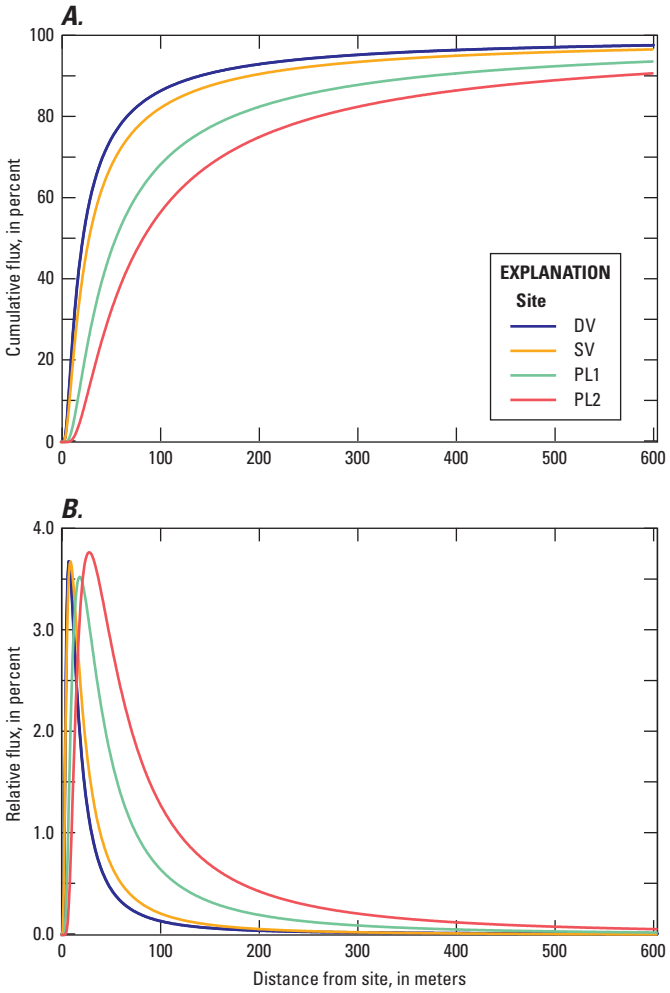

Figure 5. Source area contribution to (*A*) cumulative flux and (*B*) relative measured turbulent flux with distance from dense vegetation (DV), sparse vegetation (SV), playa 1 (PL1), and playa 2 (PL2) evapotranspiration sites, Dixie Valley, Nevada.

Energy-Balance Closure

The conservation of energy equation or energy balance at the land surface relates sensible- and latent-heat fluxes to available energy (equation 1). Storage of heat in the biomass and air, and the energy consumed by photosynthesis are assumed to be negligible. The left side of equation 1 represents available energy ($R_n - G$) measured with net radiometers, soil-heat-flux plates, temperature probes, and water content probes, whereas the right side of equation 1 represents the turbulent flux ($\lambda E+H$) measured with eddy covariance (Wilson and others, 2002). The systematic accuracy of eddy covariance estimates or energy balance is determined by comparing the left and right sides of equation 1 within the limits of measurement accuracy.

The fundamental criterion of the conservation of energy is that the energy balance is satisfied and available energy is equal to the turbulent flux. This concept commonly is referred to as energy-balance closure. Energy-balance closure often is evaluated using the energy-balance ratio (EBR), or ratio of the turbulent flux to available energy:

$$EBR = \frac{\lambda E + H}{R_n - G} \quad (14)$$

However, many studies have determined that turbulent fluxes are systematically underestimated with respect to available energy (by as much as 30 percent) despite many corrections to high-frequency, eddy-covariance data (Twine and others, 2000; Wilson and others, 2002; Foken and others, 2006; Mauder and others, 2007). This lack of closure is apparent because the eddy-covariance system measures latent- and sensible-heat fluxes independently, whereas many other turbulent-flux measurement and estimation techniques force closure by computing latent- and sensible-heat fluxes as a residual to the energy budget. Resolving the energy balance by adjusting latent-heat energy, sensible-heat energy, or both against independently measured available energy is an active area of research, and there is currently no consensus on whether eddy-covariance latent- and sensible-heat fluxes should be increased empirically to fit the available energy and force closure. Nevertheless, Foken and others (2012) recommend that as a first approximation, the energy balance can be closed according to the eddy-covariance measured Bowen ratio if the system is assumed to represent equally small and large eddies. The Bowen (1926) ratio (β) is defined as the ratio of sensible- to latent-heat flux, and can be combined with equation 1 and rearranged to solve for energy-balance corrected latent heat (λE_c) and sensible-heat fluxes (H_c):

$$\lambda E_c = \frac{R_n - G}{1 + \beta} \tag{15}$$

$$H_c = \beta \lambda E_c \tag{16}$$

Leuning and others (2012) argue that 30-minute turbulent-flux measurements systematically underestimate the available energy at most eddy-covariance sites because of phase lags caused by incorrect estimates of energy storage in air, biomass, and soil below the measurement height. In bare soil or areas with sparse vegetative cover, soil-heat flux measurements using the calorimetric method (used in this study) can produce large errors because the change in soil moisture and temperature with depth above the heat flux plate is difficult to estimate accurately (Leuning and others, 2012). Additionally, large spatial and temporal variability often exists within a measurement site. Errors in soil-heat storage estimates for bare soil or sparse vegetation areas can range from 10–200 W/m^2 (Heusinkveld and others, 2004). Considering that the energy stored in the air, biomass, and soil during the morning is released in the late afternoon and evening, Leuning and others (2012) suggest that evaluation of the energy balance on a daily rather than shorter-term basis can reduce the effects of soil-heat-flux measurement inaccuracies. After correcting for these phase lags, they conclude that the remaining imbalance may be explained by advective flux divergence that can move energy either toward or away from eddy-covariance sensors.

Foken and others (2012) and Finnigan and others (2003) propose that the lack of balance at many eddy-covariance sites is not related to errors in the method, but instead is related to atmospheric conditions that cannot be measured using the eddy-covariance method. When airflow contacts major landscape heterogeneities, large eddies are formed and a secondary atmospheric circulation pattern is developed; therefore, these secondary circulation patterns are not uniformly distributed across an area and often are not measured within a typical half-hour, turbulent-flux averaging period. Mauder and Foken (2006) showed that longer-term averaging of turbulent fluxes (as much as 17 hours) could be used to improve the energy balance.

The effect of longer-term averaging of the turbulent flux on the energy balance was evaluated in this study during autumn 2010 (September–November) and spring 2011 (March–June) at each site. Turbulent flux averaging intervals of 30 minutes and 1, 2, 3, and 4 hours were investigated. Averaging intervals of greater than 4 hours were not considered as they were expected to violate the assumed statistical stationarity of velocity, sonic temperature, and vapor density within the averaging period. Energy-balance closure was evaluated using the energy-balance ratio (equation 14). The evaluation was based on seasonal summations of the turbulent flux and available energy. Evaluations were limited to filtered, non-gap-filled data.

Longer-term averaging of turbulent fluxes produced inconsistent results with respect to the energy balance. Longer-term averaging intervals, evaluated with equation 16, increased the energy-balance ratio by as much as 12 percent in autumn and as much as 5 percent in spring with respect to a 30-minute averaging interval, but the ideal averaging interval was not consistent between sites or seasons. For example, at the SV site, the 30-minute averaging interval produced the greatest energy-balance ratio during autumn (0.72), whereas the 3-hour interval produced the greatest ratio during spring (0.83). This lack of a discernible pattern of closure with varying averaging intervals could be a result of the short (seasonal) analysis period or could indicate that larger eddies minimally contribute to the total turbulent flux in this field setting. Minimal contribution from large eddies is supported by large aperture scintillometer data measured between PL1 and PL2 sites by the Desert Research Institute (Justin Huntington, oral commun., 2012), where scintillometer and eddy-covariance sensible-heat flux measurements were similar.

The 30-minute averaging interval was used for this study as was done in similar groundwater studies where eddy-covariance fluxes were used. The energy imbalance was evaluated during individual WYs 2010 and 2011, and during the period of record using the energy-balance ratio (equation 14) and the ordinary least squares regression of the turbulent flux compared to available energy. The energy-balance ratio was evaluated using mean 30-minute turbulent flux and available energy components (equation 14), averaged over

the respective water year. This annual energy-balance ratio is considered more accurate than short-term energy-balance ratios. For example, during sunrise and sunset, or during overcast winter periods, if the energy-balance ratio is small, and the latent- and sensible-heat fluxes are of similar magnitude and opposite in sign, the resulting Bowen-ratio corrected latent- and sensible-heat values could be erroneously high (by orders of magnitude) (Stannard and others, 2013). This random noise in the system can be removed by averaging across longer periods, such as during the entire water year to produce more reliable energy-balance ratios. Although ET computed using this approach might be slightly overestimated or underestimated at times as compared to ET computed using shorter-term energy-balance ratios, the study-period averages are identical.

Daily mean turbulent flux and available-energy measurements were used for regressions to avoid potential inaccuracies in soil-heat-flux estimates (Leuning and others, 2012). Analyses included only days in which 48 good (non-gap-filled) 30-minute measurements were made (that is, no data gaps were present) to remove potential daytime or nighttime bias.

Vegetation, Soil Physics, and Groundwater Monitoring

Vegetation and soil characteristics were monitored during site visits to capture both slowly and rapidly changing variables. Photographs were taken monthly to document the greenness and vigor of vegetation, and the color and presence or absence of moisture, salt precipitate, and salt and biological soil crusts on the soil surface. Vegetation surveys were conducted using the line-transect method (Smith, 1974) during the spring, summer, and autumn to document plant-species dominance and to measure canopy height, major and minor canopy axes, percentage of canopy cover, and dead vegetation on the land surface. Surveys summarized measurements from four 100-m transects extending north, west, south, and east from a point near each eddy-covariance instrument tripod. Canopy height was estimated as the mean plant height measured across all transects. The length of the vertical projection of green (active) plant canopies overlying line transects was used to compute percent canopy cover. Bare soil cover included gaps between plants and within plant canopies. Percentage of canopy cover was computed as the ratio of the sum of individual measured canopy lengths across all transects to the total transect length (400 m), and is assumed to apply to the whole plant community on an areal basis. Canopy cover was computed using canopy lengths from phreatophytes only.

Volumetric water-content profiles were monitored quarterly at each site using a neutron probe. Changes in water content were evaluated using one-way analysis of variance procedures (PROC GLM; SAS Institute, Inc., 2001). Mean values (n=2 measurement tubes) were compared using Fisher's least significant difference test (Steel and Torrie, 1980). Water storage is analogous to a depth of water held within the soil profile. In this study, water storage was used as a water budget variable and is reported as a length of water (for example, centimeters of water).

In addition to measuring the amount of water in the soil, the amount of water available for soil-water movement and plant uptake also was characterized. The forces acting on a soil can be so tight that the water therein is essentially immobile. Depending on the soil conditions, two soils with similar water content might differ greatly in their ability to transmit water (Jury and Horton, 2004). In unsaturated soils, water availability is controlled by the water potential, which is composed of matric potential or suction pressure, gravitational potential, and osmotic or solute potential. The primary driving force for liquid soil water flow is the hydraulic head (H), or summation of matric (h) and gravitational potential (z). Osmotic potential generally does not influence liquid soil water flow because soils contain open pores (Evett, 2007).

Matric potential and temperature were monitored continuously with heat dissipation sensors installed in vertical unsaturated zone profiles at each site to determine hydraulic and thermal gradients, to compute unsaturated-zone fluxes of liquid water generated by these gradients, and to determine whether groundwater contributes to bare-soil evaporation. The probe measurement range is between 0.01 and -2.5 MPa (-1.02 to -255.25 m of water). Above this range, measurements cannot be made because the soil matrix is at or near saturation (Reece, 1996).

Unsaturated zone fluxes of isothermal and thermal liquid water were estimated using field data collected during the study (appendix 2). Unsaturated zone water movement is controlled by the soil-water content and soil hydraulic properties. In unsaturated soils, the liquid water phase is bounded partially by solid surfaces and the air-water interface. Therefore, as the water content decreases, the transport pathway for liquid water movement becomes more constrained. The isothermal liquid-water flux (q_{Li}) is described by Darcy's law (Philip and de Vries, 1957):

$$q_{Li} = -K_{Li}\frac{dH}{dz} = -K_{Li}\left(\frac{dh}{dz}+1\right) \qquad (17)$$

where

K_{Li} is unsaturated isothermal liquid hydraulic conductivity (m/s) calculated as the geometric mean for the two depths in the interval,

H is the hydraulic head in unsaturated soil ($h+z$),

h is the matric potential (m),

z is depth (m), and ($dh/dz+1$) is the hydraulic gradient (appendix 2).

The thermal, or temperature driven liquid-water flux (q_{LT}) is defined as (Noborio and others, 1996):

$$q_{LT} = -K_{LT}\frac{dT}{dz} \quad (18)$$

where

K_{LT} is the unsaturated thermal liquid conductivity calculated as the geometric mean for the two depths in the interval (m/s),
T is the temperature (K), and
dT/dz is the thermal gradient.

Matric potential and temperature were measured continuously at each site with heat dissipation sensors. Isothermal unsaturated hydraulic conductivity was computed as a function of continuously measured matric potential, and saturated hydraulic conductivity and van Genuchten soil water retention parameters determined from laboratory tension analyses (Mualem, 1976; van Genuchten, 1980). Because K_{Li} is a function of matric potential, it varies proportionally with water availability. Thermal hydraulic conductivity is a function of K_{Li} and was defined using Noborio and others (1996). Hydraulic conductivity equations are available in appendix 2.

Vapor fluxes were not computed because of the possible influence of osmotic potential. Although differences in osmotic potential generally do not influence the liquid soil-water flux (Evett, 2007), in soils with large variations in salt concentration across depth, such as those measured during this study, osmotic potential can be as effective as matric potentials in driving vapor flow (Campbell, 1985). Because continuous osmotic potential measurements were unavailable, vapor fluxes were not computed.

Water levels in shallow (less than 8 m deep; 25 ft deep) observation wells (tables 1 and 2) at ET stations were measured at 30-minute intervals using vented transducers. Water levels in these wells and other selected monitoring sites also were measured periodically using a steel tape (table 2). Water-level data are available in the USGS National Water Information System (U.S. Geological Survey, 2014).

Evapotranspiration

Environmental variables affecting energy-balance fluxes and daily and annual ET estimates were evaluated to estimate groundwater ET at each of four ET sites in Dixie Valley. Evapotranspiration and groundwater discharge are controlled by variables and processes that extend throughout the atmosphere-to-groundwater continuum. Therefore, the spatio-temporal variability of environmental variables, in combination with energy-balance fluxes, was investigated to understand the factors controlling ET and groundwater discharge. Evapotranspiration was evaluated on a daily and annual basis and used in combination with precipitation to estimate groundwater ET at each site.

Environmental Variables Affecting Evapotranspiration

Environmental variables are discussed in order from the atmosphere to the water table.

Precipitation and Air Temperature

Measured precipitation on the valley floor varied spatially among sites and temporally among water years. Precipitation consistently decreased with proximity to the playa and increased from WY 2010 to 2011 at all sites by an average of about 35 percent. Corrected water-year precipitation totals ranged from 127 mm (5.0 in.) at the PL2 site in WY 2010 to 218 mm (8.6 in.) at the DV site in WY 2011 (table 4). The large temporal difference was primarily a result of autumn (October–November) precipitation, which increased by more than 10 times on average from WY 2010 to 2011 (fig. 6). Winter (December–February) precipitation decreased, summer (June–September) precipitation slightly increased, and spring precipitation remained relatively similar from WY 2010 to 2011.

Precipitation corrections for wind-related undercatch increased measurements by about 7 percent at vegetated sites and about 15 percent on the playa during the period of record. Lower undercatch corrections at vegetated sites likely were due to wind speed reduction by the canopy.

Table 4. Annual precipitation measured at evapotranspiration sites, Dixie Valley, Nevada, water years 2010–11.

[**Site name:** DV, dense vegetation; SV, sparse vegetation; PL1, playa 1; PL2, playa 2. **Precipitation:** Corrected for wind-related undercatch, in millimeters (mm)]

Site name	Water year	Precipitation (mm)
DV	2010	156
	2011	218
SV	2010	140
	2011	187
PL1	2010	134
	2011	172
PL2	2010	127
	2011	175

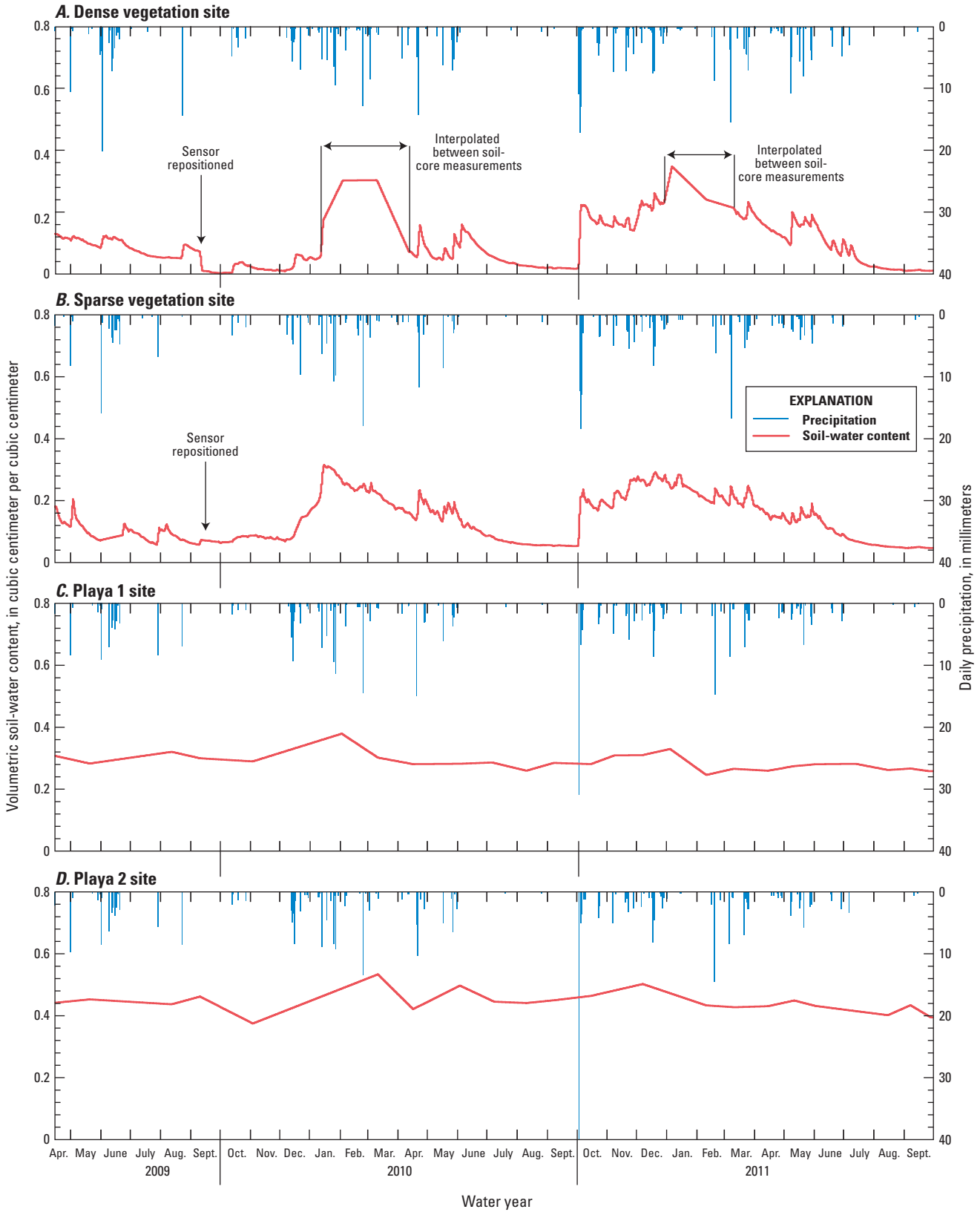

Figure 6. Continuously measured precipitation and near-surface (2–6 centimeters below land surface) soil-water content at vegetated evapotranspiration (ET) sites, and continuously measured precipitation and interpolated (between monthly measurements) near surface soil-water content at playa ET sites, Dixie Valley, Nevada, April 2009–September 2011.

Precipitation collector orifices were positioned just above the vegetation canopy, where wind is greatly reduced. On the playa, however, the wind profile approaches zero just above the land surface; therefore, wind speeds at the collector were slightly less than measurements made from the instrument tripods. In addition to profile effects, wind speeds measured on the instrument tripods increased as surface roughness decreased from site to site. Wind speeds at the DV site were slightly lower on average than at the SV site, whereas wind speeds on the playa were much greater than in vegetated areas and increased from sites PL1 to PL2.

Annual precipitation measurements were compared with the 30-year mean (1981–2011) determined from Western Regional Climate Center datasets for northwest Nevada and for Lovelock and Winnemucca, Nevada (Western Regional Climate Center, 2012). Lovelock is about 45 km northeast of Dixie Valley and Winnemucca is about 90 km north of Dixie Valley. Precipitation data for northwest Nevada indicate that the WY 2010 total was 0.9 times the 30-year mean (212 mm, October through September), whereas WY 2011 was about 1.26 times the 30-year mean. Local data from Lovelock and Winnemucca indicate that annual precipitation was nearly equal to the 30-year mean (149 and 208 mm, respectively) in WY 2010 and was 1.1 and 1.7 times the 30-year mean in WY 2011, respectively. If precipitation patterns in Winnemucca, Lovelock, and northwest Nevada at large are similar to patterns in Dixie Valley, then these results indicate that annual precipitation measurements made in Dixie Valley during WY 2010 likely are similar to the long-term mean for the valley, whereas measurements made during WY 2011 likely are greater than (by about 30 percent) the long-term mean.

Mean daily air temperature at vegetated sites was 10.7 and 12.1 °C during WYs 2010 and 2011, respectively. Average temperatures at playa sites were about 1.2 °C greater than mean temperatures at vegetated sites. Mean temperatures during the warmest (July) and coldest (December) months were 27.6 and -3.9 °C, respectively, at vegetated sites, and 29.1 and -3.2 °C, respectively, at playa sites.

The warmth of the growing season can greatly affect greasewood ET rates (Robinson and Waananen, 1970). The warmth of the growing season for vegetated sites was analyzed on a monthly (May–August) basis and compared between water years using degree days (table 5). Degree days are computed as mean daily temperatures above a base of 0 °C; therefore, a mean temperature of 20 °C for 1 day equates to 20 degree-days (Robinson and Waananen, 1970). Evaluations were based on the sum of degree days within a month. Degree-day analyses indicate that May and August were cooler during WY 2010 than during 2011, with degree-day differences of 19 and 49 °C at the DV site, respectively, and of 26 and 53 °C at the SV, respectively. During June and July, WY 2010 was warmer than WY 2011, with degree-day differences of 49 and 31 °C at the DV site, respectively and of 53 and 30 °C at the SV site, respectively.

Table 5. Growing season warmth at dense and sparse vegetation evapotranspiration sites, Dixie Valley, Nevada , May 1–August 31, 2010–11.

[**Site name:** DV, dense vegetation; SV, sparse vegetation. **Degree days per month:** Computed as mean daily temperatures above a base of 0 degrees Celsius (°C); therefore, a mean temperature of 20 °C for 1 day equates to 20 degree days (Robinson and Waananen, 1970); water-year differences are computed monthly as degree days in 2011 less degree days in 2010]

Site name	Water year	Degree days per month (°C)			
		May	June	July	August
DV	2010	414	647	886	730
	2011	433	598	855	779
	Difference	19	-49	-31	49
SV	2010	426	664	907	744
	2011	452	611	877	797
	Difference	26	-53	-30	53

Vegetation and Surface Characteristics

Vegetation cover and soil characteristics varied seasonally with species phenology and precipitation patterns. Greasewood leaves typically began to sprout in April, became stressed by September, and senesced during October–November. Differences in senescence patterns were observed between the two vegetated sites; greasewood at the DV site typically would drop leaves 1–2 weeks earlier than greasewood at the SV site.

During spring through summer, the mean canopy cover for all phreatophytes was about 24.8 and 7.3 percent at the DV and SV sites, respectively (table 6). Phreatophytic shrubs dominated the plant community by about 77 percent at the DV site and 91 percent at the SV site during summer months. Total canopy cover during spring and summer increased overall from 2009 to 2010 and from 2010 to 2011 at both sites. Inter-annual variations seem to be associated with increasing forb cover from year to year in addition to changes in shrub cover. Between 2009 and 2011, canopy cover of seepweed, the predominant forb, increased during summer months from 3.9 to 9.4 percent at the DV site and from 0.5 to 2.0 percent at the SV site. Variations in mean (spring-summer) shrub cover from year to year likely represent varying dates of measurement during a season and (or) varying phenological responses to changing temperatures and soil moisture. Smaller variations could result from measurement errors, such as multiple personnel making measurements and a wind-blown transect tape during a measurement. Variability in summer shrub cover at the DV site was within the measurement noise (coefficient of variation = 10 percent), whereas summer shrub cover variability at the SV site was above the noise (coefficient of variation = 23 percent) indicating that an actual change in canopy cover likely occurred.

Table 6. Canopy cover of phreatophytes measured at dense and sparse vegetation evapotranspiration sites, Dixie Valley, Nevada, 2009–11.

[**Canopy cover of phreatophytes:** Total canopy cover for all four transects divided by the total transect length (400 meters); canopy cover was estimated from additive measurements of the vertical projection of green (active) plant canopies overlying line transects. **Shrub:** Phreatophytic shrubs are composed of greasewood and big saltbush. **Forb:** Seepweed is the predominant phreatophytic forb; phenological cycle of seepweed typically begins during mid-to-late June]

Measurement date	Canopy cover of phreatophytes (percent)					
	Dense vegetation site			Sparse vegetation site		
	Total	Shrub	Forb	Total	Shrub	Forb
May 18–19, 2009	21.5	20.9	0.6	5.5	5.1	0.4
August 10–11, 2009	22.6	18.6	3.9	6.9	6.3	0.5
November 2–5, 2009	3.6	3.5	0.1	3.8	3.7	0.1
April 14–15, 2010	20.1	20.1	0	5.1	5.1	0
June 14, 2010	31.2	24.6	6.6	9.1	8.6	0.5
October 13–14, 2010	9.4	9.4	0	6.7	6.4	0.3
April 12–13, 2011	23.3	23.3	0	4.8	4.8	0
July 11–12, 2011	30.3	20.9	9.4	12.2	10.2	2.0
September 26–27, 2011	23.7	12.8	10.9	9.6	6.8	2.8
Mean growing season (April–August)	24.8	21.4	3.4	7.3	6.7	0.6

Soil color and appearance of salt varied with seasonal precipitation. At the vegetated sites, soil color darkened with increased soil moisture. At the DV site, biological soil crusts were present and active during prolonged periods of high soil-water content in early spring and immediately following summer precipitation. During the spring following drying of accumulated winter moisture, thin salt crusts appeared at both sites, creating a mottled tan and white soil surface.

The soil surface color at the PL1 site varied greatly during winter and remained mostly constant during summer, whereas the surface color at the PL2 site varied seasonally, but remained mostly constant during a season. During winter, the PL1 surface varied from dark immediately following precipitation to mostly white after surface soils dried, whereas the PL2 surface typically was dark. During summer, the surfaces at both playa sites typically were covered with a thin salt crust that would dissolve periodically with sporadic precipitation events.

Near-Surface Soil-Water Content and Electrical Conductivity

Near-surface (0–15-cm depth) volumetric soil-water content remained mostly constant at the playa sites and varied seasonally at the vegetated sites (fig. 6). Water content typically ranged between 0.25 and 0.35 cm^3/cm^3 at the PL1 site and between 0.4 and 0.5 cm^3/cm^3 at the PL2 site. The highest water content at playa sites corresponded with winter precipitation, and the lowest water content corresponded with late summer–early autumn seasons. Minimal change in playa water content corresponds with the textural classification of soil at both playa sites as a low-permeability clay loam, a thin evaporation-limiting salt crust, and a shallow water table. Water content at the vegetated sites increased to maximum values of more than 0.3 cm^3/cm^3 following winter precipitation and by late summer decreased to minimum values of about 0.01–0.02 cm^3/cm^3 at the DV site and 0.05 cm^3/cm^3 at the SV site (fig. 6). Although near-surface water content increased in response to precipitation at both sites, the rate of soil drying appeared more rapid at the DV site. Differences in minimum water content and soil-drying rates following precipitation likely represent differences in near-surface soil characteristics. Textural analyses show that near-surface soils at the DV and SV sites are characterized as silt loam and silty clay loam, respectively. The increased clay content at the SV site likely reduced soil permeability and increased moisture retention in comparison to the DV site.

Electrical conductivity of near-surface (0–15-cm bls) soil water mostly varied with water content and decreased with increasing distance from the playa center (figs. 6 and 7). Electrical conductivity of soil water was determined from soil-paste methods similar to those noted in the U.S. Department of Agriculture, Agriculture Handbook (U.S. Salinity Laboratory Staff, 1954). During the period of record, the mean near-surface electrical conductivity was 24.2 ± 10.5 mS/cm at the DV site, 38.6 ± 12.6 mS/cm at the SV site, 68.9 ± 11.4 mS/cm at the PL1 site, and 88.4 ± 7.5 mS/cm at the PL2 site.

Electrical conductivity of shallow (45–60-cm depth) soil water was similar to that of near-surface soil water (fig. 7), whereas electrical conductivity of groundwater (data not shown) was much greater than soil water at playa sites and less than soil water at vegetated sites. Mean shallow soil water values were 72.7 ± 14.7 and 87.6 ± 4.3 mS/cm at the PL1 and PL2 sites, respectively, and 27.2 ± 4.1 and 31.3 ± 4.9 mS/cm at the DV and SV sites, respectively. Groundwater electrical conductivities at the PL1 site were more than twice conductivities of near-surface soil-water electrical conductivities, with a mean value of 167 ± 24.7 mS/cm. At the PL2 site, mean groundwater electrical conductivity was greater than 200 mS/cm. Electrical conductivity of groundwater beneath vegetated sites was less than 1 mS/cm.

Soil Physics

Measurements of soil physics were made to evaluate unsaturated-zone water content, availability, and movement. Measurements, trends, and gradients in unsaturated water content and water storage, soil temperature, and hydraulic head (matric potential plus gravitational potential) were analyzed. Soil temperature and hydraulic head gradients were combined to compute unsaturated-zone liquid-water fluxes.

Water Content and Water Storage Trends

Seasonal variations in water content with depth at the DV site were limited to the shallow (above 0.75 m bls) and deep (below 2.50 m bls) unsaturated zone, with minimal change between these two depths (fig. 8). Periodic water-content and storage-profile measurements were made with a neutron probe. Uncertainty associated with neutron probe measurements (represented as the standard deviation between replicate measurements at a given depth and a measurement period) was less than 0.02 cm^3/cm^3 above 2.25 m bls, and typically less than 0.03 cm^3/cm^3 below 2.25 m bls. Variations in shallow-water content from 0.03 to 0.31 cm^3/cm^3 occurred within the upper 0.75 m bls. Deeper water content measured between 2.75 and 5 m bls ranged from 0.28 to 0.44 cm^3/cm^3. Variations of as much as 0.04 cm^3/cm^3 were measured at a given depth for this deeper interval, but these changes typically were within the measurement uncertainty. Water storage within shallow and deep intervals averaged 12.5 ± 2.5 cm (0–0.75 m bls) and 80.8 ± 2.4 cm (2.75–5.00 m bls), respectively. Variations at and above 0.75 m bls reflect precipitation, evaporation, and shallow root-water uptake, whereas variations below 2.75 m bls reflect variations in the capillary fringe corresponding to water table (4.6–5.5 m bls) and regional recharge fluctuations, and deep root-water uptake. Minimal variation in water content (less than 0.02 cm^3/cm^3) between 0.75 and 2.5 m bls indicates that notable percolation of precipitation and shallow root-water uptake typically is limited to the upper 0.75 m of soil. This is supported by hydraulic head measurements discussed in the section, "Soil Temperature and Hydraulic Head Trends."

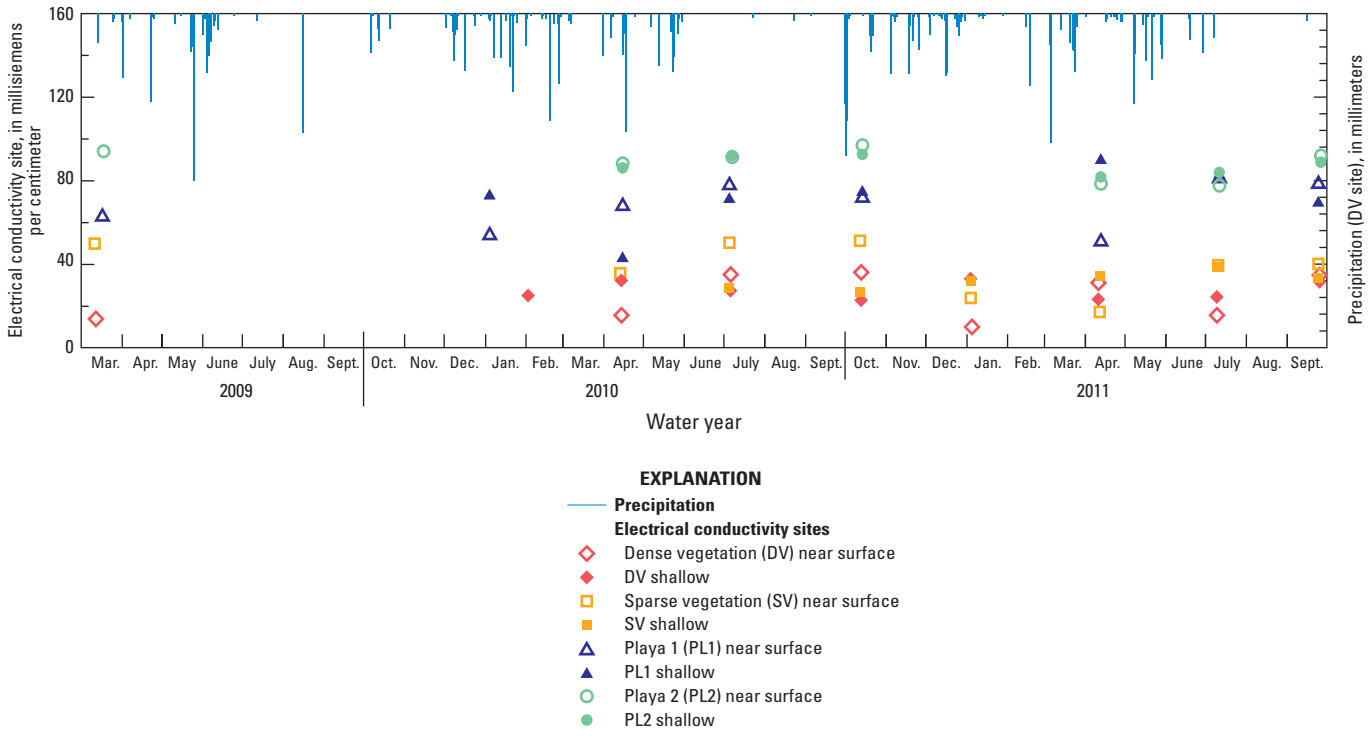

Figure 7. Periodic measurements of near-surface (0–15-centimeters below land surface) and shallow (45–60-centimeters below land surface) soil-water electrical conductivity and precipitation at evapotranspiration sites, Dixie Valley, Nevada, March 2009–September 2011.

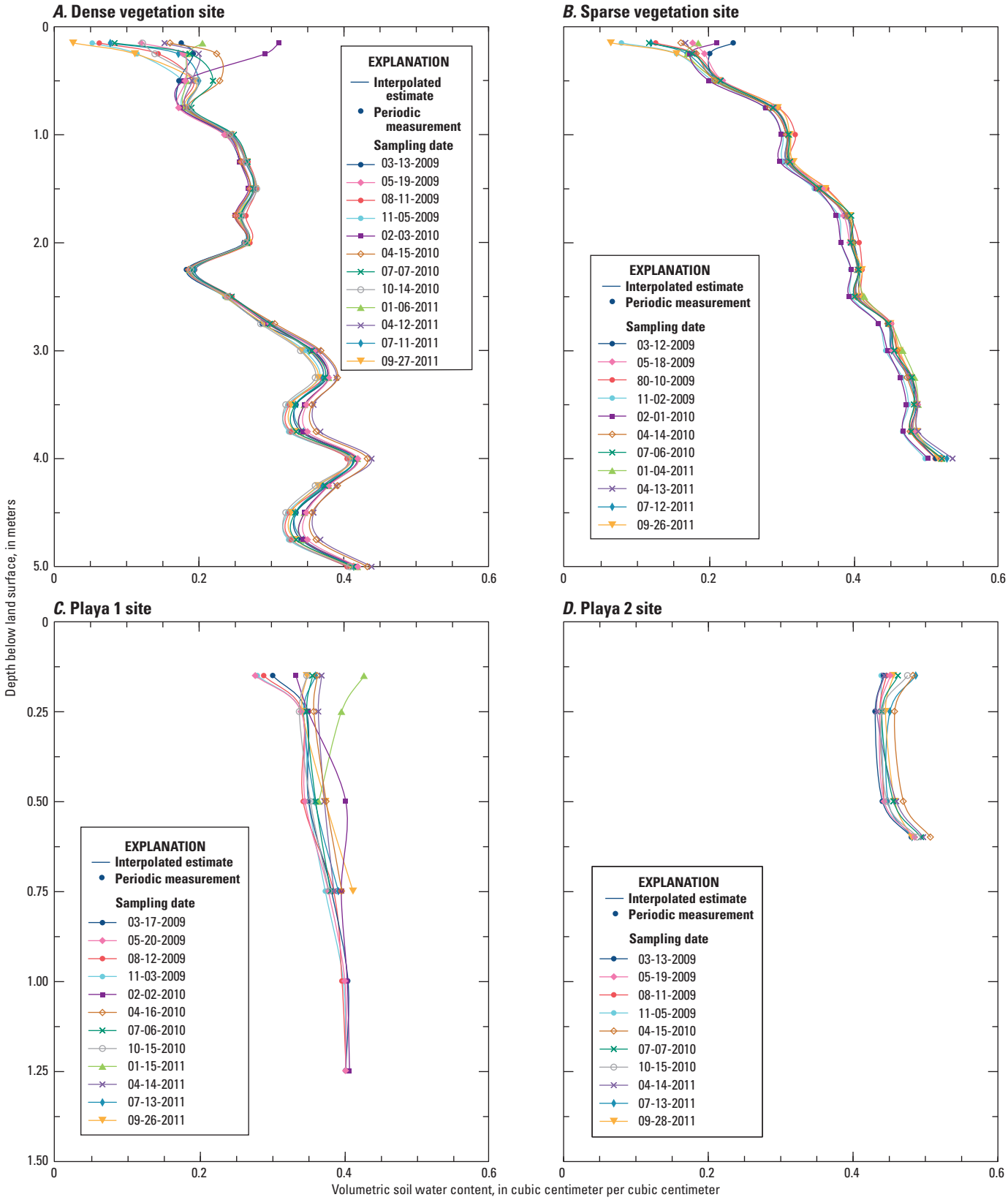

Figure 8. Periodic measurements and interpolated estimates of unsaturated-zone water-content profiles at evapotranspiration sites, Dixie Valley, Nevada; March 2009–September 2011.

Water content variations at the SV site occurred primarily at and above 0.5 m bls (fig. 8). Water content above 0.5 m bls ranged from 0.06 to 0.23 cm^3/cm^3, with variations of as much as 0.17 cm^3/cm^3 at 0.15 m bls and 0.02 cm^3/cm^3 at 0.5 m bls. These variations consistently were greater than the average measurement uncertainty of 0.01 cm^3/cm^3 for these depths. Water storage between 0 and 0.5-m bls averaged 8.5 ± 1.4 cm. At 0.75 m bls, seasonal changes were almost as small (less than 0.02 cm^3/cm^3) as the measurement uncertainty (0.01 cm^3/cm^3), indicating that precipitation percolation, evaporative extinction, and shallow root-water uptake were limited to less than 0.5-m depths. Between 1 and 4 m bls, water content ranged from about 0.3 to 0.54 cm^3/cm^3, with seasonal variations at a given depth of 0.01–0.03 cm^3/cm^3 above the measurement uncertainty (less than 0.01 to 0.03 cm^3/cm^3). Similar to the water content at the DV site, these variations represent pressure fluctuations in the saturated zone (5.2 m bls) resulting from deep root-water uptake and regional recharge patterns.

At the PL1 site, soil-water content at and above 0.75 m bls (0.28–0.43 cm^3/cm^3) was measured throughout the study period; below 0.75 m bls, measurements ceased following February 2010 when PVC access tubes cracked as a result of playa expansion and contraction. Water-content profiles varied seasonally between land surface and 0.75 m bls, with maximum variations ranging from 0.06 cm^3/cm^3 at 0.25 m bls to 0.15 cm^3/cm^3 at 0.15 m bls. Measurement uncertainty for the upper 0.75 m bls was within 0.01 cm^3/cm^3. Below 0.75 m bls, water content was nearly constant, with a range of 0.48 to 0.51 cm^3/cm^3 and variations within 0.02 cm^3/cm^3 (uncertainty within 0.01 cm^3/cm^3). Greater water content at the PL1 site during February 2010 (0.50 m bls) and January 2011 (0.25 m bls) likely represents percolation of snowmelt from snow that fell during the previous months. Minimal variation below the 0.75-m depth from March 2009 to February 2010 indicates soil-water content is affected minimally by pressure variations in the saturated zone (1.2 m bls).

At the PL2 site, water content remained mostly constant at all measured depths (within 4 percent), with less water content between 0.25 and 0.50 m bls and more water content above and below that depth range. More water content below 0.50 m bls might represent textural differences in soil composition or pressure variations within the saturated zone (0.75 m bls). At 0.15 m bls, slightly higher water content could result from textural differences at the respective depths, or a physical (salt crust) and chemical salt barrier that causes upward moving water to accumulate near the soil surface (addition of salt reduces vapor pressure and evaporation). Water storage in the upper 0.75 m of soil at the PL1 and PL2 sites averaged 26.6 ± 1.3 cm and 34.6 ± 0.7 cm of water, respectively.

Replicate (n=2) locations for measuring soil-water content enabled the statistical testing of the effect of seasonality on soil-water content at each depth and site. Soil-water content data were log-normally distributed; therefore, a logarithmic transformation was applied to the data before statistical analyses were made. The analysis of variation ($p>F<0.05$) showed that the seasonality effect was significant at the SV site at 0.15 and 0.25 m bls; at the DV site at and above 0.75 m bls, and at 4 and 5 m bls; at the PL1 site at 0.15, 0.25, and 0.75 m bls; and at the PL2 site at 0.15 m bls. All other depths analyzed showed no significant water content changes from season to season.

For depths where seasonality was significant, Fisher's least significant difference tests ($p<0.05$) were used to evaluate if changes between water years were significant and needed to be considered in annual groundwater ET estimates. This was done by comparing the mean water content determined from replicate measurements at each site and depth during the start and end of each water year. Despite seasonal differences, mean water content at the start and end of each water year was statistically similar at the SV, PL1, and PL2 sites at all depths, and at the DV site at all depths except 0.15 and 0.75 m bls. Water-year differences in mean shallow water content at the DV site (0.15 and 0.75 m bls) represent residual soil moisture derived from precipitation that might or might not have occurred during the respective water years. Water-content profiles describing the start and end of the water year were measured on November 5, 2009, October 14, 2010, and September 27, 2011. Higher water content during October 2010 likely represents the 41 mm (1.6 in.) of precipitation that fell between October 3 and 7, 2010 rather than the residual water content at the end of WY 2010. Comparisons between water content measurements made from soil cores (collected at 0.02–0.06 m bls) on September 7 and October 14, 2010 support this assumption and show an increase from 0.03 to 0.17 cm^3/cm^3 at this depth interval. Therefore, mean water content changes between water years were considered insignificant at all sites and were not considered in annual groundwater ET estimates.

Soil Temperature and Hydraulic Head Trends

Soil temperature and hydraulic head trends were evaluated to investigate thermal and hydraulic gradients in the unsaturated zone and to improve the understanding of unsaturated zone water availability and movement. Soil temperatures at all sites varied seasonally throughout the unsaturated zone and provided seasonally changing gradients for thermally generated waterflow (fig. 9). At the vegetated sites, soil temperatures at the shallowest depth (0.3 m bls) varied seasonally between 0 and 28 °C. Soil temperatures at playa sites measured at 0.3 m bls trended to similar minimums, but reached much greater maximums (averaging about 36 °C) during summer months. Similarly, soil temperatures measured on the playa at depths of greater than 0.3 m bls were about 5 °C greater than temperatures measured at vegetated sites.

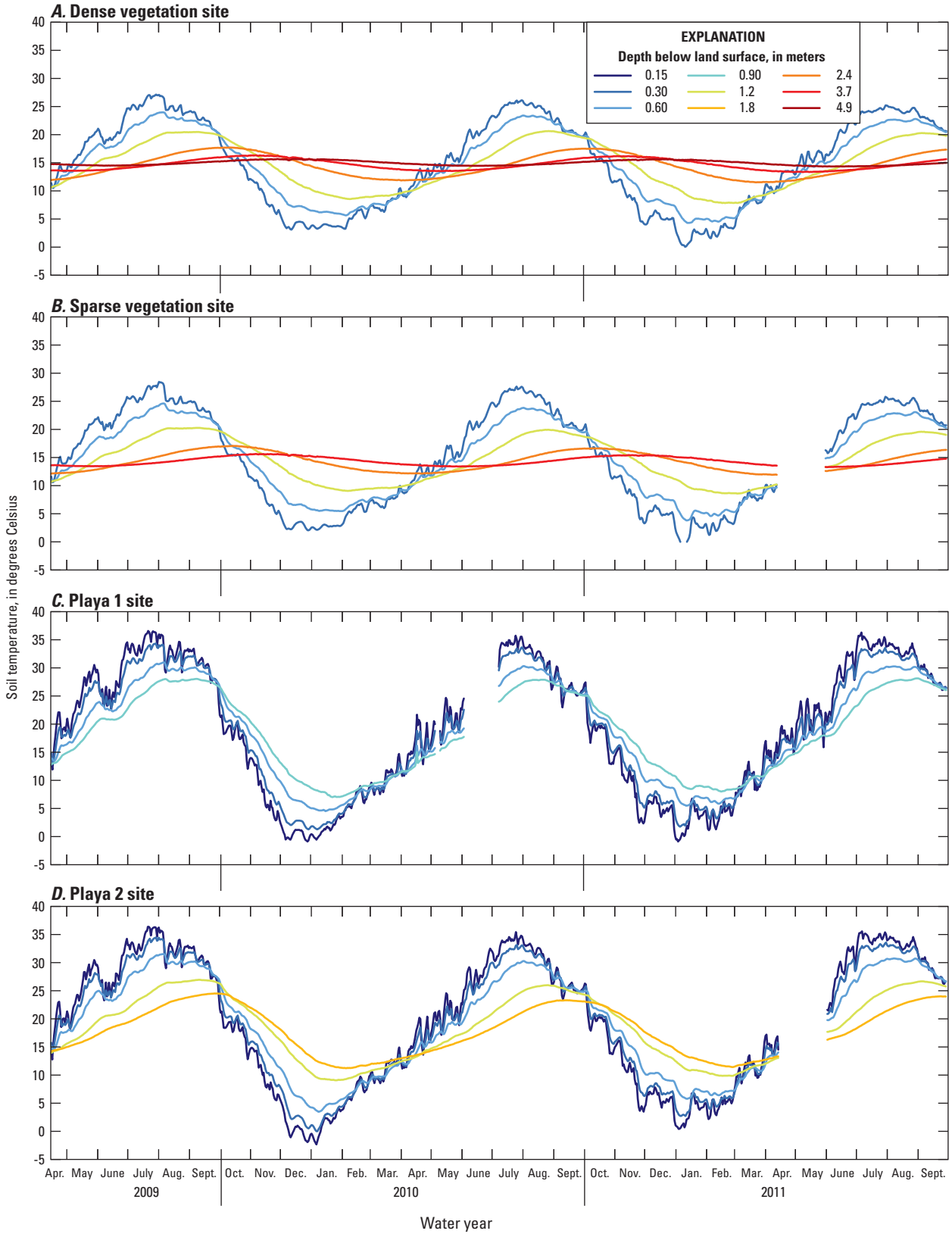

Figure 9. Continuously measured unsaturated-zone temperature profiles at evapotranspiration sites, Dixie Valley, Nevada, April 2009–September 2011.

Thermal gradients between 0.15 and 0.3 m bls at the playa sites and between 0.3 and 0.6 m bls at all sites typically were upward between October and April, and downward thereafter, representing seasonal heat losses and gains (fig. 9). At depths greater than these, gradient-direction reversals occurred later, and temperature differences between sensors were smaller. Thermal gradients between the greatest depths measured at vegetated sites (2.4 and 3.7 m bls at SV, and 3.7 and 4.9 m bls at DV) were least in magnitude and were downward between July and December and upward thereafter. These deeper gradients likely are influenced by a combination of time-shifted and depth-attenuated air temperature gradients.

Continuous unsaturated hydraulic head ($H=h+z$, or matric potential plus gravitational potential) for the DV and SV sites is shown in figure 10. Matric potential is equivalent to suction pressure, and, therefore, is zero at saturation and less than zero (negative) at less than saturation. A gravitational potential of zero was assumed at land surface; therefore, gravitational potential decreased with increasing depth below land surface. For the PL1 site, soil measurement locations (0.15, 0.3, 0.61, and 0.9 m bls) were near saturation and measurements exceeded or hovered near the upper limit (-1.02 m of water) of the sensor measurement range (from -1.02 to -255 m of water) throughout the study period (not shown in figure 10). For the PL2 site, matric potentials exceeded the sensor measurement range for the entire study period; therefore, playa data were not considered reliable. Hydraulic heads at the SV site were analyzed at depths of 0.3 and 0.6 m bls only through WY 2010 because because animal burrowing near shallow sensors beginning in late spring 2010 provided a fast pathway for liquid water percolation to measurement depths of 0.3 and 0.6 m bls by October 2010. Hydraulic heads at greater depths are shown only through mid-April 2011 because of an excitation module (a device that applies a constant current to heat dissipation sensor heating elements) malfunction. Hydraulic heads measured from 0.3 to 3.7 m bls at the DV site ranged from about -18 to -3.2 m; at the SV site they ranged from -130 to -12 m (fig. 10). For the SV site, the gravitational component (-0.3 to -3.7 m) of the hydraulic head was relatively small compared to the matric component; at and below 2.4 m bls at the DV site, gravitational contributions ranged from 30 to more than 50 percent of the hydraulic head.

Shallow (0.3 m bls) hydraulic heads at both vegetated sites typically increased sharply following winter snowmelt and decreased gradually thereafter as moisture either was removed by ET or percolated downward. For example, as snow melted during late January and early February 2010, hydraulic heads increased by more than 1.5 m/d at both sites, and decreased at rates of less than 0.04 m/d during the 2 months that followed. Hydraulic heads measured at 0.6 m bls also increased in response to the 2010 snowmelt, but the response was greater at the DV site than it was at the SV site. During the remainder of the study period, the hydraulic heads at 0.6 m bls showed smaller seasonal variations.

Hydraulic head measured at 1.2 m bls and below varied seasonally at both vegetated sites. Hydraulic heads at the DV site varied seasonally by as much as 0.7 m at 1.2 and 2.4 m bls and as much as 1.2 m at 3.7 m bls. Head variations at 3.7 m bls likely represent the rising and falling water table. Heads at the SV site also varied seasonally and gradually increased during the study period at depths greater than 1.2 m bls. The large increase in total head between April and August 2009 at 1.2 m bls (nearly 70 m overall) likely was the result of the sensor equilibrating with the soil matrix. This is evident by the mostly constant trend during the remainder of the study period at the SV site. At depths greater than 1.2 m bls, increasing hydraulic head trends (by 40–60 m) throughout the study could be actual, or could indicate that after more than 2.5 years of in-place measurements, the sensors had not yet reached equilibrium with the soil matrix. Laboratory soil-water tension analyses and drillers' logs indicate that soil clay content increases with increasing depth at the SV site. Near the 3.7-m-bls measurement depth, hard blue-green clay was observed during drilling, and tension analyses indicated that the saturated water content of this clay was more than 90 percent. Sharp contrasts between hydraulic properties characterizing the porous matrix of the heat-dissipation sensor (which is similar to fine-grained sand) and the native low-permeability clay material could be hindering moisture movement from native soil to the sensor.

Gradients in hydraulic head at vegetated sites varied seasonally at 0.6 m bls and above, in response to precipitation percolation, and generally were constant below 0.6 m bls. Hydraulic heads between 0.3 and 0.6 m bls typically provided a downward (negative) driving force for isothermal flow following winter precipitation and an upward (positive) gradient for flow during the remainder of the year as shallow soil dried through evaporation (fig. 10). At the DV site, hydraulic head gradients between 0.6 and 1.2 m bls predominantly were upward, but varied seasonally following winter precipitation. Between 1.2 and 2.4 m bls, hydraulic head gradients at the DV site provided a downward driving force for isothermal flow throughout the study period. Although the difference between hydraulic heads at 1.2 and 2.4 m bls is small, it is about 6 times the measurement resolution of heat-dissipation sensors (0.1 m of water) on average. At the SV site, hydraulic head gradients between 0.6 and 1.2 m bls consistently were downward. At depths greater than 1.2 m bls, hydraulic head gradient interpretations at the SV site are flawed because sensors likely had not equilibrated with the soil matrix. Despite this observation, the increasing equilibration trend is similar at 2.4 and 3.7 m bls; therefore, the measured downward driving force for isothermal flow between these depths could be valid.

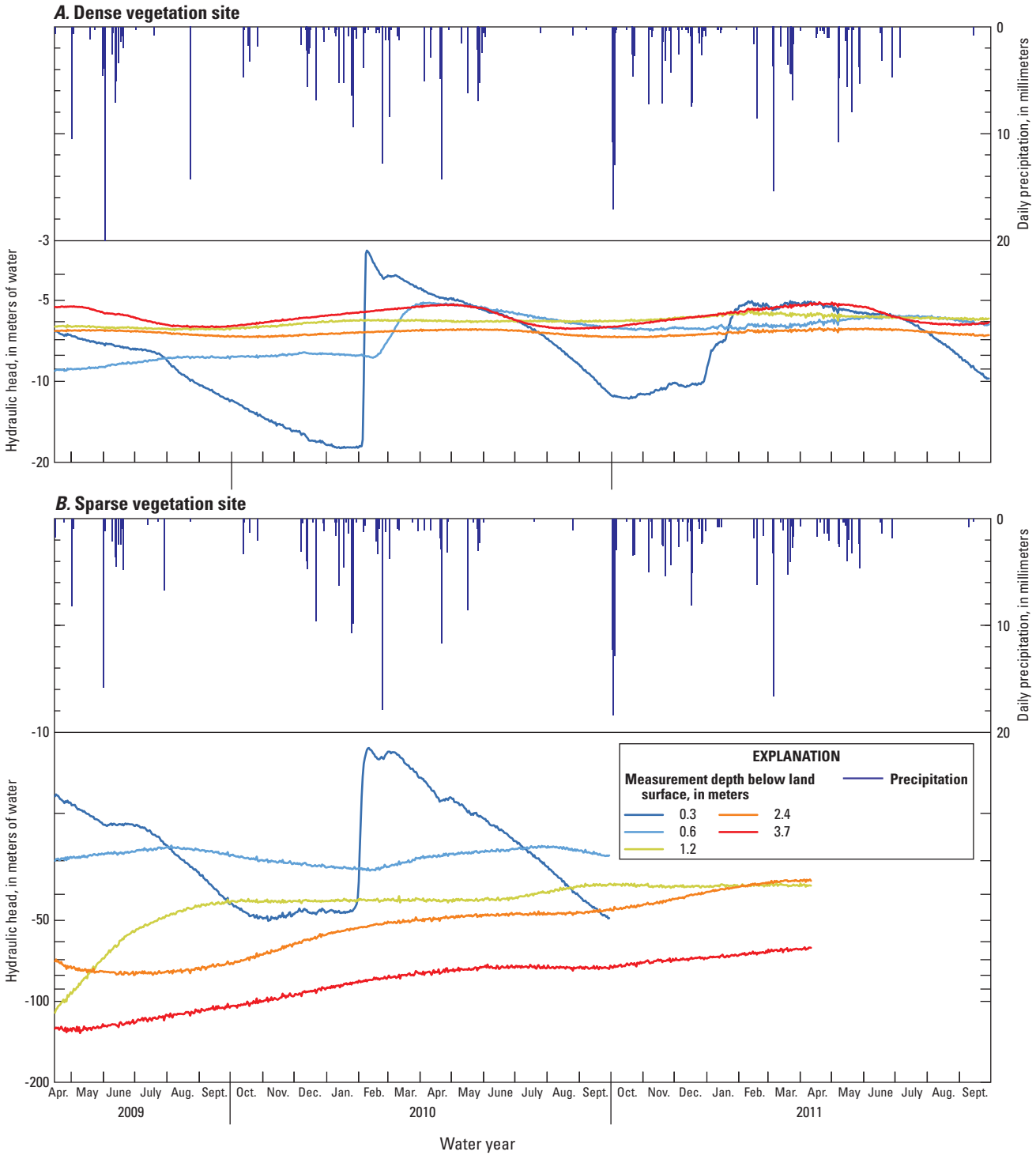

Figure 10. Continuously measured unsaturated-zone hydraulic head (matric plus gravitational potential) profiles and daily precipitation at vegetated evapotranspiration sites, Dixie Valley, Nevada, April 2009–September 2011. Zero head is equal to water at atmospheric pressure at the local land surface.

Liquid-Water Fluxes

Like hydraulic head and thermal gradients, fluxes of total liquid water (isothermal and thermal liquid water) varied with depth and between sites (fig. 11). Fluxes were computed hourly by multiplying the hydraulic head gradient with depth by the unsaturated hydraulic conductivity (appendix table 2*B*), and then summing the product over the day (fig. 11) and water year (table 7). Because unsaturated-zone hydraulic conductivity is a function of water availability, water movement typically decreases with decreasing water availability as transport pathways become more constrained.

Total liquid-water fluxes at the DV site varied seasonally from upward (positive) to downward (negative) within the depth intervals of 0.3–0.6 and 0.6–1.2 m bls. These direction reversals indicate precipitation occasionally percolated below 0.6 m bls, some of which subsequently was removed as shallow soils dried through evapotranspiration. The total liquid-water flux within the depth interval of 1.2–2.4 m bls was consistently downward, whereas the total liquid-water flux within the interval of 2.4–3.7 m bls was consistently upward (positive). Opposing fluxes above and below 2.4 m bls likely highlight the occurrence of deep root-water uptake and denote the upper bound of the capillary fringe above the water table. A lack of upward movement within the depth interval of 1.2–2.4 m bls also indicates that groundwater discharge by evaporation does not occur at this site. These data are supported by water-content data (fig. 8), which show a lack of change in moisture at the depth of 2.4 m bls relative to more shallow and deep locations. This indicates that moisture above about 2.4 m bls is supplied primarily by precipitation and temperature fluctuations, whereas moisture below about 2.4 m bls is supplied by a fluctuating water table and capillary fringe.

Total liquid-water fluxes at the SV site varied seasonally from upward (positive) to downward (negative) within the depth interval of 0.3–0.6 m bls and were consistently downward (negative) within the interval of 0.6–1.2 m bls (fig. 11). A lack of sensor equilibration precluded flux computations below 1.2 m bls. Like fluxes within the same depth interval at the DV site, fluxes within the interval of 0.3–0.6 m bls at the SV site represent downward movement of water during cool, wet months and upward movement of water during warm, dry months. Although hydraulic heads at 0.6 m bls did not show a sharp increase in response to precipitation, a consistently downward (negative) flux within the depth interval of 0.6–1.2 m bls indicates that not all precipitation derived soil moisture that percolated to 0.6 m bls was removed by shallow ET. Some of this residual moisture continued moving downward toward 1.2 m bls. Additionally, a consistent downward flux through the soil matrix within the depth interval of 0.6–1.2 m bls indicates that groundwater discharge by evaporation also did not occur at this site. This is because a downward flux within this depth interval would preclude any upward-moving groundwater from reaching the soil surface through soil waterflow.

Cumulative total liquid-water fluxes (isothermal+thermal liquid) for WYs 2010 and 2011 at the DV site were upward in the depth intervals of 0.3–0.6, 0.6–1.2, and 2.4–3.7 m bls, and downward in the interval of 1.2–2.4 m bls (table 7). Upward fluxes at the DV site ranged from 1.99 mm/yr (WY 2010; interval of 2.4–3.7 m bls) to 37.6 mm/yr (WY 2011; interval of 0.3–0.6-m bls), whereas the downward flux ranged from -0.67 to -1.03 mm/yr (WYs 2010 and 2011, respectively). A consistent and cumulative downward flux within the interval of 1.2–2.4 m bls and upward flux within the depth interval of 2.4–3.7 m bls indicate that a zero-flux plane exists near 2.4 m bls during the water years analyzed. A zero-flux plane marks the position where the vertical water flux is zero and separates movement of soil water above and below the horizontal plane (Kutílek and Nielsen, 1994). Following similar trends in unsaturated-zone water content, the zero-flux plane highlights the presence of a bimodal system where the shallow unsaturated zone is controlled by atmospheric processes (ET and precipitation) and the deep unsaturated zone is controlled by transpiration, groundwater fluctuations, and regional recharge patterns.

Cumulative total liquid-water fluxes at the SV site were downward at all depths for WY 2010 and at least one order of magnitude lower than respective DV fluxes (table 7). Water year 2011 totals were not determined because shallow measurements were compromised because of animal burrowing. Cumulative downward total liquid-water fluxes ranged from -0.056 (interval of 0.6–1.2 m bls) to -0.58 mm/yr (interval of 0.3–0.6 m bls). Downward percolation of residual precipitation below 0.6 m bls (as much as 0.056 mm) is assumed to be removed completely by deep root-water uptake prior to reaching the saturated zone.

Reduced fluxes at the SV site, compared to the DV site, were expected as total heads, head gradients, and unsaturated hydraulic conductivities derived from matric potentials (data not shown) were much lower. The physical cause for lower head gradients and hydraulic conductivities at the SV site likely is the difference in soil texture and resulting canopy cover. The SV site predominantly is composed of fine silt, whereas the DV site is a mix of fine silt and loam. The mix of silt and loam at the DV site allows for more liquid drainage and overall water movement compared to the SV site (Soil Survey Staff, Natural Resources Conservation Service, 2011), which, in turn, supports a relatively dense vegetation canopy (table 6). Greater water movement at the DV site with respect to the SV site also is supported by comparisons between water-content profiles and hydraulic heads at vegetated sites. For example, water content at 1.2 m bls is similar at both vegetated sites: about 0.25 cm^3/cm^3 at the DV site and about 0.30 cm^3/cm^3 at the SV site (fig. 8). Hydraulic heads depicting water availability at 1.2 m bls, however, vary by one order of magnitude between sites, averaging about -7 m of water at the DV site and about -40 m of water at the SV site (fig. 10). This large variation occurs because soils at the SV site are less permeable than soils at the DV site; therefore, less water is available for movement at the SV site.

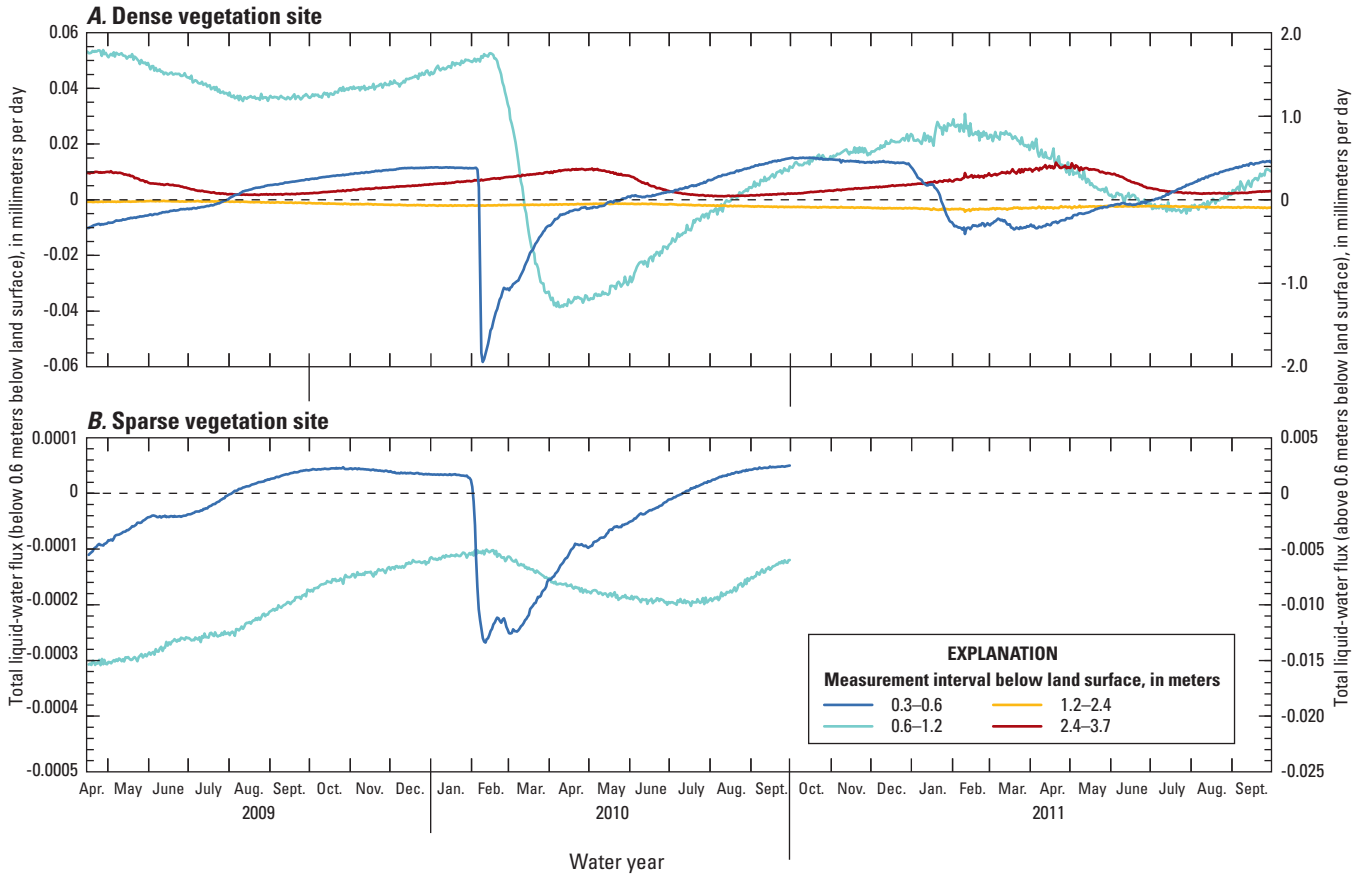

Figure 11. Continuously measured liquid-water fluxes in the unsaturated zone at vegetated evapotranspiration sites, Dixie Valley, Nevada, April 2009–September 2011.

Table 7. Cumulative vertical unsaturated-zone liquid-water flux measured at vegetated evapotranspiration sites, Dixie Valley, Nevada, water years 2010–11.

[**Site name:** DV, dense vegetation; SV, sparse vegetation. **Cumulative vertical flux:** q_{Li}, isothermal liquid-water flux; q_{LT}, thermal liquid-water flux; q_L, total liquid-water flux; positive fluxes indicate upward liquid-water movement and negative indicate downward movement. **Abbreviations:** m, meter; bls, below land surface; mm/yr, millimeter per year; <, less than; –, data not available]

Site name	Depth interval (m bls)	Cumulative vertical flux (mm/yr)					
		Water year 2010			Water year 2011		
		q_{Li}	q_{LT}	q_L	q_{Li}	q_{LT}	q_L
DV	0.3–0.6	15.2	-0.035	15.2	37.6	-0.012	37.6
	0.6–1.2	3.57	-0.0005	3.57	4.43	0.0016	4.43
	1.2–2.4	-0.680	0.0003	-0.670	-1.03	0.0004	-1.03
	2.4–3.7	1.99	0.0005	1.99	2.21	0.0005	2.21
SV	0.3–0.6	-0.581	-0.0001	-0.580	–[1]	–[1]	–[1]
	0.6–1.2	-0.056	<0.0001	-0.056	–[1]	–[1]	–[1]

[1]Animal burrowing near the sensors beginning in late spring 2010 provided a fast track for precipitation percolation. Adjacent water content measurements indicated no change, whereas liquid-water fluxes increased substantially following precipitation beginning in October 2010.

Liquid-water fluxes at vegetated sites primarily were generated by isothermal liquid water flow. Thermal liquid-water fluxes were small and ranged from three to four orders of magnitude less than isothermal liquid-water fluxes at the DV site, and were three or more orders of magnitude less than isothermal fluxes at the SV site.

A zero-flux plane at the DV site and a consistently downward total liquid-water flux within the interval of 0.6–1.2 m bls at the SV site indicates that groundwater discharge (ET_g) through bare-soil evaporation did not occur during the study period. These results are supported by water-content profiles at the DV site, which show a bimodal system where the upper unsaturated zone is controlled by atmospheric processes and the lower zone is controlled by water-table fluctuations and deep root-water uptake. The absence of water-content change between depths of 1 and 2.5 m bls indicates that root-water uptake and soil-water movement within these intervals likely is minimal. The absence of groundwater discharge through evaporation at the SV site also is supported by increasing clay content with depth, which induces a confined aquifer state. Soil coring and drilling at the SV site revealed 0.2 m of blue-green clay beneath the depth of 1.2 m bls, followed by black anaerobic clay to the saturated zone. Although not measured with heat dissipation sensors because of a lack of equilibration, any potential upward movement of groundwater through this thick clay sequence likely is removed by deep root-water uptake prior to reaching shallower depths. Therefore, bare soil evaporation at both sites seems to remove only precipitation-derived, shallow soil moisture.

Water-Level Fluctuations

Water levels fluctuated annually at all sites in response to discharge and recharge patterns, weather patterns, or both (fig. 12). Water levels declined by about 0.9 m at vegetated sites between the start and end of each growing season (table 2). Declining water levels or the groundwater depression that forms during the growing season beneath areas covered by phreatophytic vegetation indicates that local discharge exceeds recharge. The seasonal drawdown of water levels is an approximate indicator of annual groundwater discharge through ET. The maximum depth to water at vegetated sites corresponds with the onset of canopy stress in late summer. The period of gradual water-table recovery after phreatophytes go dormant indicates that recharge exceeds discharge. This seasonal recovery of the drawdown depression is a result of lateral groundwater movement from adjacent areas of aquifer storage. Aquifer storage is replenished with regional recharge. Seasonal water level drawdown and recovery beneath vegetated areas highlights the complementary relation between regional groundwater discharge and recharge.

Diurnal fluctuations of about 0.03 m were measured at vegetated sites. At the DV site, fluctuations of this magnitude persisted throughout the year and resulted from a combination of barometric pressure and groundwater withdrawal by phreatophytes during the growing season (fig. 12). Although unconfined, the apparent barometric signal in the water-level record at the DV site likely is a result of the non-uniform loading of the pressure signal or "lag" through the low-permeability unsaturated zone, which is characterized by clayey silt sediments. Diurnal fluctuations at the SV site persisted only during the growing season and represented plant transpiration. Although confined, the absence of an apparent barometric signal in the SV water-level record likely is a result of the deformable, moist clay confining layer that also responds to loading of the pressure signal.

The annual maximum depth to water during late summer of each year remained mostly constant from year to year at the SV site (within 0.03 m), but decreased in 2011 at the DV site (from 5.5 m bls in 2010 to 5.3 m bls in 2011) (table 2, fig. 12). This decrease at the DV site might represent a change in mountain-block recharge during WY 2011, differences in aquifer storage properties between confined and unconfined parts of the aquifer, or both. Mountain-block precipitation measured in the Clan Alpine Mountains along eastern Dixie Valley during WY 2011 was an average of 1.5 times that measured in WYs 2009 and 2010 (Mahannah and Associates, LLC, written commun., 2012). Increased mountain-block precipitation likely steepened hydraulic gradients between regional recharge and discharge areas in eastern Dixie Valley, which potentially led to higher water levels at the higher elevation DV site (13 m higher with respect to the SV site) located in eastern Dixie Valley.

Depth to water at playa ET sites varied by an average of about 0.5 m during the water year (table 2), with maximum depths typically occurring during the winter and minimum depths occurring during the summer (fig. 12). These trends likely are more representative of surface forcing than regional recharge patterns because seasonal fluctuations are out of phase with respect to vegetated sites. Water levels measured in three shallow monitoring wells and five deep monitoring wells at playa monitoring sites (fig. 1, appendix 4) show similar phase trends and indicate fluctuations of as much as 0.8 m between summer and winter measurements. In areas with shallow water tables, thermal expansion of trapped air in the soil above the water table during the warmer months can cause water levels in wells to rise (Turk, 1975). Similarly, reduction of surface tension at higher temperatures can "release" unsaturated-zone water, which, in turn, can cause a rise in the water table (Turk, 1975; Tyler and others, 2006). Additionally, thermal expansion or swelling of clay sediments during the warmer months can reduce pore space and cause water levels to rise. Measurements from a snow-depth sensor deployed at the PL2 site indicated that the playa surface rises and falls seasonally (data not shown) with increasing and decreasing air and soil temperature and water level.

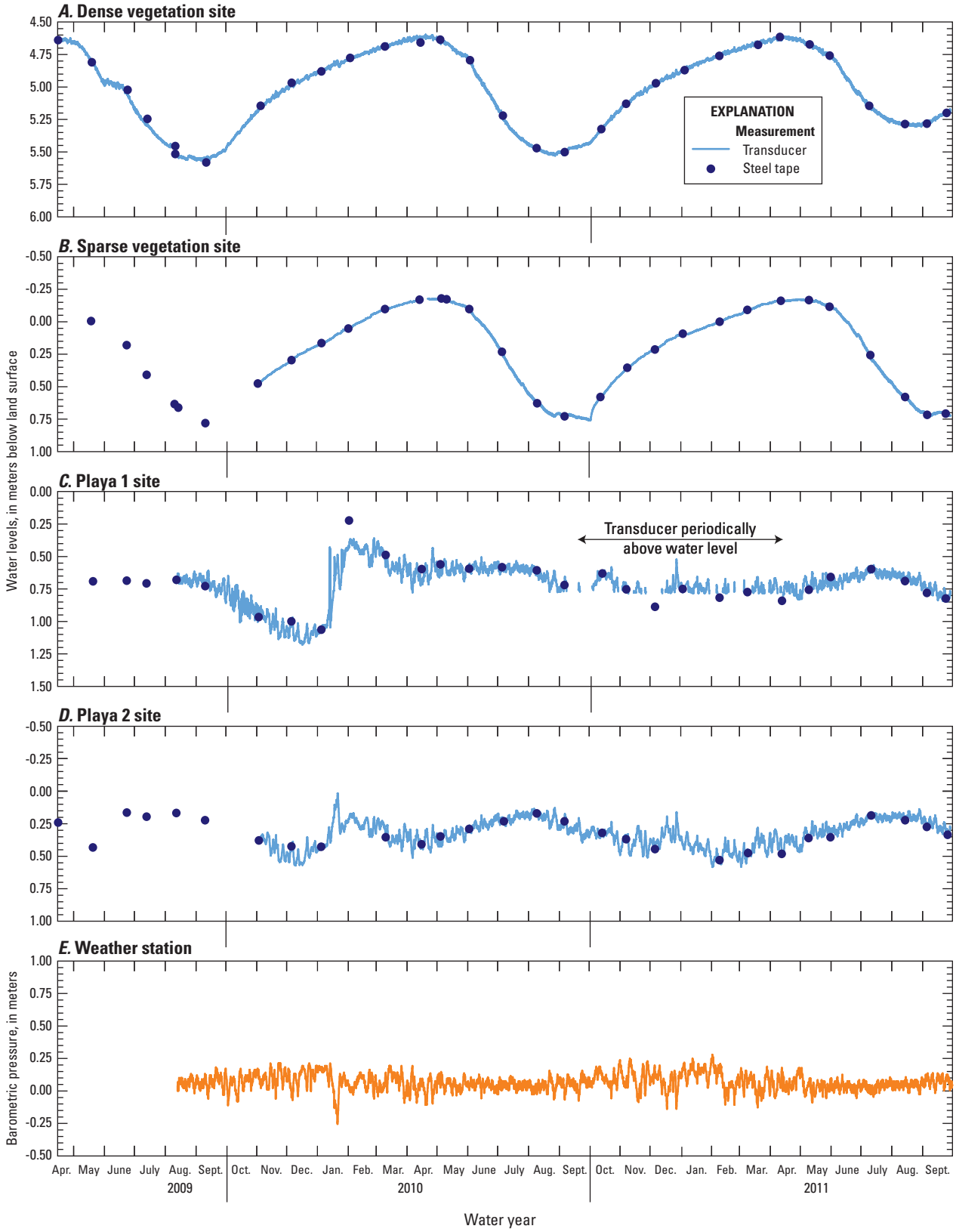

Figure 12. Water levels measured in wells at evapotranspiration sites and barometric pressure measured at the weather station monitoring site, Dixie Valley, Nevada, April 2009–September 2011. Water levels represent depth to the potentiometric surface rather than the saturated zone in confined aquifers.

Finally, salt crusts on the playa surface that limit evaporation also can reduce the amount of atmospheric water demand (that is, potential ET) on subsurface soils, which effectively causes a rise in the water table (Tyler and others, 2006). The magnitude of water table rise will largely be dependent on the water content and effective specific yield of the overlying unsaturated clay sediments. If the capillary fringe intersects the land surface and is near saturation, only small changes in the water content will cause large changes in the water table elevation (Gillham, 1984).

In addition to seasonal trends, playa groundwater fluctuations of as much as about 0.4 m during several days occurred in response to barometric pressure (fig. 12*E*). Large barometric signals in the water-level record, as measured with a vented transducer, indicate that the playa permeability is low and that the playa water table (within 1 m bls) and the atmosphere are poorly connected. In contrast, barometric signals in the water-level record at vegetated sites, where the atmosphere and aquifer are well connected, were about one order of magnitude smaller than signals at the playa sites.

Water levels at the PL1 site during January 2010 rose substantially following snowmelt and subsequent melting, and never fully declined to November–December 2010 levels during the remainder of the study period. This increase of greater than 0.5 m cannot be explained fully by barometric pressure alone, and might indicate downward percolation of snowmelt toward the water table that occurred as bypass flow along the observation well casing. This hypothesis is supported by diluted stable isotope signatures discussed in the section, "Groundwater Evapotranspiration Partitioning."

Opposing phase trends between shallow and deep wells at PLGW5 and PLGW2 monitoring sites (near the eastern and western edges in the northern part of the playa [fig. 1, appendix 4]), respectively, likely represent shallow communication with adjacent surface-water drainage features. Nearly 50 percent of estimated surface water run-on to the playa occurs near these two sites (Interflow Hydrology, Inc., and Mahannah and Associates, LLC, 2013).

Energy-Balance Closure and Trends

Energy-balance closure and trends affected the magnitude and variability of computed ET estimates in this study. Energy-balance closure at the four eddy-covariance ET sites was evaluated using the energy-balance ratio and least squares regression of measured (non-gap-filled) turbulent fluxes compared to available energy for individual water years and during the period of record. Energy-balance ratios were computed using mean annual turbulent flux and available energy components during WYs 2010 and 2011, and ranged from 0.67 at the PL2 site for WY 2010 to 0.78 at the SV site for WY 2011 (table 8). Least-squares regressions were forced through a y-intercept of zero and were based on 30-minute turbulent fluxes and available energy averaged across a 24-hour period to reduce uncertainty associated with soil-heat flux measurements (Leuning and others, 2012). Regression slopes were slightly greater than (average of 2 percent) energy-balance ratios, and largely explained the variability in the relation between turbulent flux and available energy (daily coefficients of determination ranged from 0.86 to 0.96).

Because of limited knowledge regarding energy-balance closure, the decision of whether or not to force closure often is subjective. Many assumptions are necessary for Bowen-ratio-forced closure estimates to be accurate, including: (1) available energy estimates are error-free; (2) eddy-covariance measurements and the application of accepted (at the time this study) corrections and filters are accurate, and (3) discrepancy between available energy and the turbulent flux can be attributed to turbulent-flux measurements, possibly caused by advective flux divergence with similar scalar ratios to those measured by the eddy-covariance system; and (4) available energy estimates are representative of the same source area as eddy-covariance measurements. In this study, available-energy and turbulent-flux measurement errors were reduced using multiple corrections and filters (see section, "Data Correction, Filtering, and Gap-Filling Procedures"). This indicates that the remaining energy imbalance is a result of unidentified inaccuracies or systematic bias in the eddy-covariance turbulent-flux measurements (such as advective flux divergence) and (or) in net radiation measurements (such as unidentified instances of scaling on pyrgeometers used to measure longwave radiation and (or) calibration differences among net radiation sensors; see section, "Uncertainty"). Although also uncertain, soil-heat-flux measurement errors likely did not affect the energy imbalance when evaluated using the 24-hour average flux.

In this study, measured turbulent fluxes were considered a probable minimum. A probable maximum was computed by dividing 30-minute measured and gap-filled turbulent-fluxes by the energy-balance ratio for the respective water year to achieve energy-balance closure while maintaining consistency with the eddy-covariance measured Bowen ratio. Measurements made prior to WY 2010 represent a partial water year only (April 15–September 2009) and provide a biased EBR estimate. Therefore, partial water year values from 2009 were divided by the energy-balance ratio computed for the period of record. The best (most probable) estimate of the latent-heat (evaporative) flux in this study is the mean of the probable minimum and probable maximum estimates. The most probable estimate is hereinafter referred to as "corrected."

Daily energy-balance flux averages shown in figure 13 highlight the seasonal relations between energy components. Available energy is influenced primarily by net radiation. The soil-heat flux contributes minimally to the daily energy balance (average of less than 2 W/m^2 during the study period), but 30-minute daytime (net radiation greater than 5 W/m^2) contributions during the growing season (data not shown) were as much as 23 percent of net radiation on average, and proportions increased with increasing soil-water content. Although daily soil-heat flux estimates likely are

Table 8. Energy-balance ratio, slope, and coefficient of determination from ordinary least squares regressions comparing turbulent-flux and available-energy measurements, and percentage of good (non-gap-filled) 30-minute and daily data at four evapotranspiration sites, Dixie Valley, Nevada.

[**Site name:** DV, dense vegetation; SV, sparse vegetation; PL1, playa 1; PL2, playa 2. **EBR:** Energy-balance ratio of turbulent flux to available energy, computed using mean 30-minute turbulent flux and available energy measurements averaged over the water year. **Slope:** Determined using mean 30-minute turbulent flux and available energy measurements averaged over the day and evaluated over the water year, and a y-intercept of zero. **Coefficient of determination** and **Good data:** Indicative of 48 good 30-minute measurements over 24-hour period. **Abbreviations:** POR, period of record; –, not determined]

Site name	Water year	EBR	Slope	Coefficient of determination (r^2)		Good data, percent	
				Daily	30-minute	Daily	30-minute
DV	2010	0.77	0.78	0.96	0.95	59	75
	2011	0.75	0.77	0.92	0.92	46	71
	POR	0.75	0.76	0.95	–	58	–
SV	2010	0.74	0.76	0.87	0.87	71	91
	2011	0.78	0.81	0.90	0.88	67	87
	POR	0.74	0.76	0.88	–	70	–
PL1	2010	0.68	0.70	0.95	0.75	52	71
	2011	0.69	0.72	0.95	0.70	66	94
	POR	0.68	0.70	0.94	–	62	–
PL2	2010	0.67	0.70	0.86	0.54	58	84
	2011	0.73	0.75	0.93	0.45	42	80
	POR	0.68	0.7	0.88	–	53	–

accurate, 30-minute fluxes computed with the calorimetric method potentially were underestimated during the day and overestimated at night because of potential phase shifts in soil temperature between the soil surface and measurement depths of 2 and 6 cm bls.

Net radiation fluxes varied seasonally, with the highest fluxes occurring under clear skies during summer and the lowest fluxes occurring under cloudy skies during winter (fig. 13). Net radiation was greatest at the DV site, with a mean of about 113 W/m^2, when compared with other sites. Net radiation values at the SV and playa sites were, on average, within less than 3 W/m^2 of each other. Higher net radiation at the DV site likely results from lower outgoing short- and long-wave radiation measurements. Outgoing short-wave radiation typically decreases in magnitude with decreasing surface albedo and decreases with increasing vegetation cover. Summer measurements made with the NR01 net radiometer indicated that surface albedo ranged from about 0.15 to 0.2 at the DV site to about 0.25 to 0.4 at the SV and playa sites (data not shown). Net long-wave radiation generally was lowest for the DV site, indicating surface temperatures were lower there than at other sites.

Variations in net radiation across the turbulent-flux fetch area at playa sites were evaluated by deploying the NR01 net radiometer about 100 m from the stationary CNR2 radiometers (in the predominant wind direction) for a month during late summer and early autumn. Variations in net radiation were evaluated using the relation developed when the CNR2 and NR01 sensors were co-located at the stationary location. Comparisons indicate net radiation varied minimally within playa fetch areas, with 30-minute variations of less than 3 percent (less than 4 W/m^2 on average) at both sites.

Available energy, composed primarily of net radiation, mostly was partitioned to the sensible-heat component of the turbulent flux (fig. 13). The Bowen ratio, β, describing the ratio between H and λE (equation 16), was greatest at the playa sites and decreased from the SV to the DV site as λE increased. Daily Bowen ratios at playa sites ranged from 4 to 18 during spring through autumn and followed a seasonal pattern, increasing from spring to summer and decreasing from summer to autumn. Spring-to-autumn ratios typically ranged from about 0.5 to 6 at the DV site and 1 to 6 at the SV site. At the DV site, β increased with the start of spring as temperatures warmed, decreased between the onset (early April) and height (late June–early August) of the growing season as plants transpired at peak rates, and increased thereafter as soil dried out, plants became stressed, and eventually plants senesced. A similar pattern was measured at the SV site during the spring, but changing patterns during the summer and between summer and autumn were less notable as a result of a more water-limited environment. This small difference also could be a result of the confined aquifer beneath the SV site; the saturated zone remains at a constant depth at the SV site, but varies seasonally at the DV site and likely disassociates from the root zone during late summer. At all sites, β typically was low (between 1 and 2) during winter when net radiation was low and the ground surface was moist.

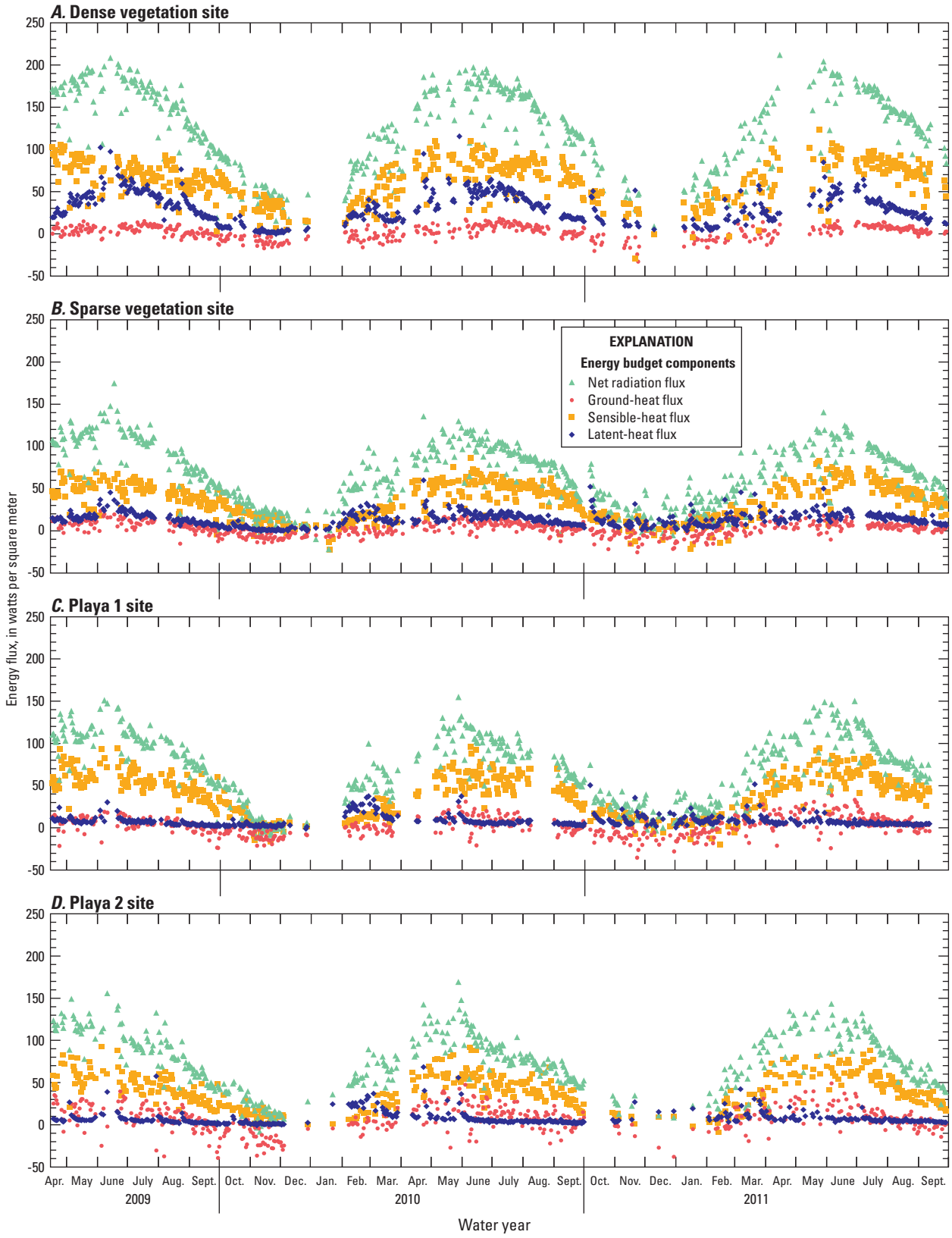

Figure 13. Measured 24-hour mean energy-budget components at evapotranspiration sites, Dixie Valley, Nevada, April 2009–September 2011. Only data where 48 good (non-gap-filled) measurements were made during a 24-hour period are shown.

Dew contributions to spikes in λ*E* at the PL2 site were evaluated during mid-July through September 2011 and were determined to be minimal. Measured spikes typically occurred during the early morning hours of mid-to-late summer. The cause of these spikes initially was thought to come from dew formation on the playa surface and, therefore, was tested using leaf-wetness sensors. Moisture on wetness sensors, which did not correspond to precipitation at the site, was measured only twice during the 2.5-month monitoring period (data not shown). The first spike in moisture occurred at 6:30 a.m. on September 8, 2011, and corresponded to a spike in λ*E*, yet the maximum relative humidity during the previous and following 24 hours was only 37 percent. Low relative humidity surrounding the moisture spike indicates that the sensors might have been affected by unrecorded precipitation (by tipping bucket gage). All other sites reported negligible precipitation between September 7 and 9, 2011. The second set of spikes in moisture also might have been a result of unrecorded precipitation. These spikes occurred at 8:00 p.m. on September 15, 2011, and 5:00 a.m. and 5:30 p.m. on September 16, 2011. The first and last of these spikes corresponded to spikes in λ*E* and relative humidity of 60 and 40 percent, respectively. The second spike corresponded to a minimal λ*E*, but the relative humidity reached 77 percent, indicating that dew formation on the sensor was probable. Although salt was not placed specifically on the sensors, wind-blown salt deposits could have reduced the saturation vapor pressure at the wetness sensor surface so that dew could form at 77 percent relative humidity; however, dew formation at 40 percent relative humidity is unlikely. Alternatively, the wetness sensor and λ*E* spikes could have resulted from unrecorded precipitation at the site because precipitation was measured at the nearby PL1 site. Overall, measurement results indicated that dew formation was small to negligible and might or might not have contributed to a small percentage of measured spikes in λ*E* that periodically occurred during summer morning hours.

Alternatively, the λ*E* spikes could be a result of topsoil rehydration at night. Playa topsoil can rehydrate at night through subsurface moisture redistribution and lead to a decrease in resistance of water vapor transfer during early morning hours (Malek, 2003). Regardless of the moisture source, these periodic, early-morning spikes in λ*E* were minimal when compared to the total random noise throughout the day during summer months.

Eddy-Covariance Evapotranspiration and Trends

Daily corrected ET (ET_c) totals generally followed a sinusoidal pattern at vegetated sites in response to available energy fluxes, with the highest ET occurring between early spring and midsummer, and the lowest ET occurring during the winter (fig. 14). Daily ET_c was computed by summing corrected 30-minute measurements during a 24-hour period. Corrected ET was computed as the mean of measured ET and the maximum ET as determined by adjusting annual turbulent fluxes upward to achieve full energy-balance closure. Evapotranspiration fluxes deviated slightly from this general sinusoidal pattern as water and energy availability fluctuated. Spikes in ET occurred in response to precipitation events. Similarly, short-term dips in ET also occurred during spring and summer months when cloud cover reduced net radiation. Although soil-water content typically was greatest during winter months, ET often was low and limited by low net radiation.

Evapotranspiration at vegetated sites was influenced by precipitation, air temperature, vapor pressure deficits, wind, and vegetation phenology in addition to available energy (figs. 13 and 14; tables 4–6 and 9). Corrected daily evapotranspiration ranged from 0 to 6.7 mm at the DV site and from 0 to 3.5 mm at the SV site. The sinusoidal pattern in daily ET generally followed a bimodal distribution with peak ET occurring during two separate time intervals. The first interval was during early spring of each year, and the second interval was during mid-spring through summer of each year. The early-spring peak, which was greatest in spring 2010 (although less so at the DV site), was influenced by high soil-moisture content from winter and early-spring precipitation and increasing net radiation. Following depletion of shallow soil moisture, daily ET decreased to a local minimum. The second peak began with the sprouting of leaves. Transpiration rates steadily increased until plants reached full shoot growth during midsummer, driving most of the daily ET. Following full shoot growth in midsummer, ET began to decrease slowly and reach minimum values as plants became stressed during late summer and leaves began to senesce. The second ET peak also corresponded with declining groundwater-level (fig. 12). Water levels in wells were shallowest at the start of the growing season, steadily decreased during late summer as plants became stressed, and slowly began to recover thereafter. Beyond late summer, ET at the vegetated sites was influenced primarily by bare soil evaporation in response to precipitation pulses and net radiation.

Reference crop ET (ET_{rc}) was computed for comparison with ET_c measurements from vegetated areas and for extrapolation of groundwater ET estimates to grassland and marshland areas (see section, "Groundwater Discharge by Evapotranspiration–Basin Scale"). In reference ET models, all energy available for evaporation is assumed to be accessible by the plant canopy (Shuttleworth, 1993). Reference ET was computed for grass using the standardized American Society of Civil Engineers equation (American Society of Civil Engineers, 2005) based on the Penmen-Monteith equation, and 30-minute data collected at the DV site (appendix 1). Annual ET_{rc} estimates were representative of actual crop ET estimates for alfalfa in Dixie Valley (Huntington and Allen, 2010).

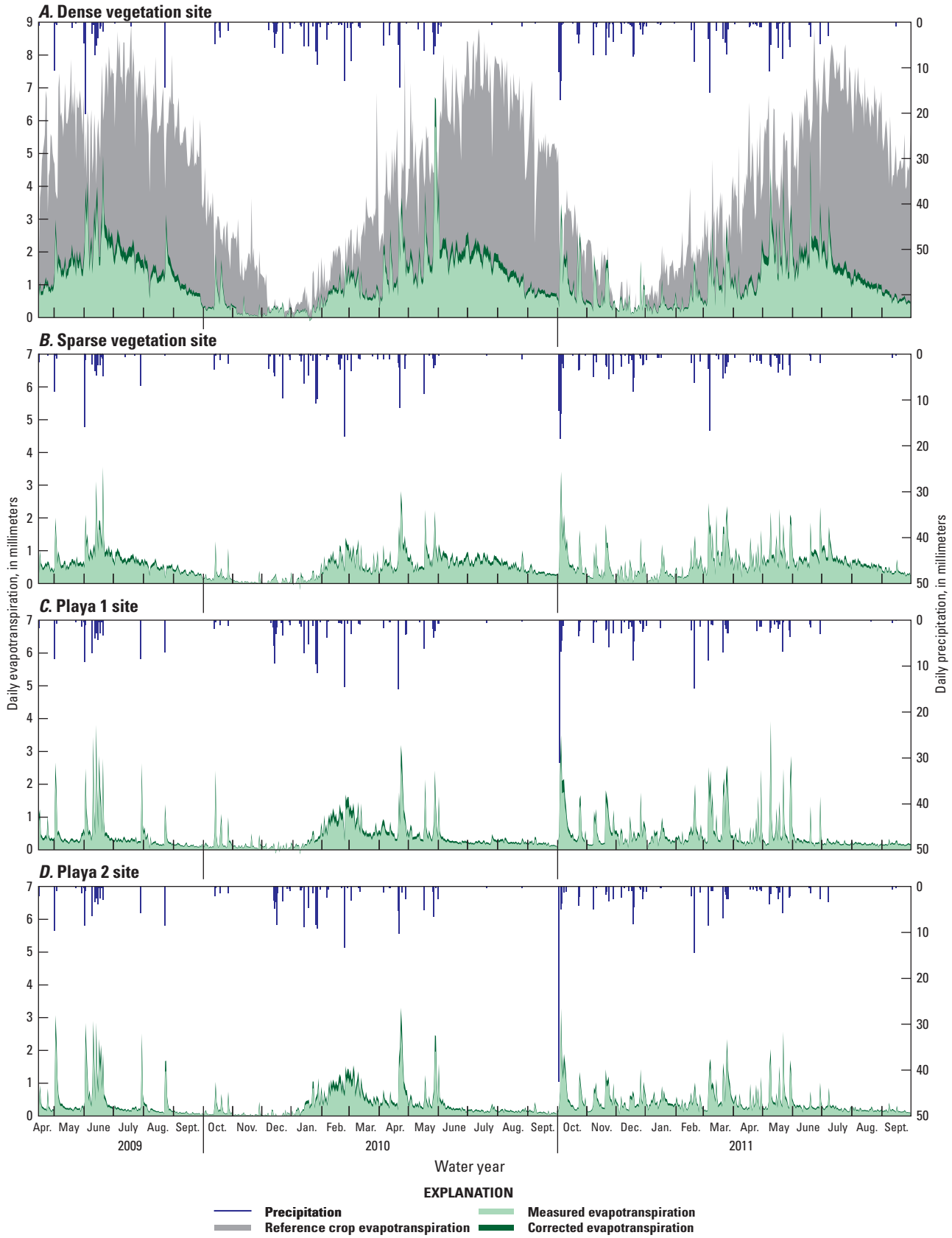

Figure 14. Measured and corrected daily evapotranspiration and daily precipitation at evapotranspiration sites, and daily reference crop evapotranspiration at the dense vegetation site, Dixie Valley, Nevada, April 2009–September 2011.

Table 9. Annual precipitation, energy-balance corrected evapotranspiration, groundwater evapotranspiration, mean annual groundwater evapotranspiration, and associated errors measured at evapotranspiration sites, Dixie Valley, Nevada, water years 2010–11.

[**Site name:** DV, dense vegetation; SV, sparse vegetation; PL1, playa 1; PL2, playa 2. **Precipitation:** Corrected for wind-related undercatch. **Precipitation error:** Summation of measurement error and maximum undercatch correction error. **ET_c**: Computed as the mean of annual measured ET and the maximum potential ET as determined by adjusting annual turbulent fluxes upward to achieve full energy balance closure. **ET_c probable error:** Square root of the sum of squared random and systematic errors. Random error determined using 24-hour differencing approach. Systematic error determined as the difference between ET_c and ET. **Estimated runoff:** Estimated from a combination of quarterly changes in soil water storage (0–75 centimeters below land surface at the PL1 site and 0–50 centimeters below land surface at the PL2 site.), differences between ET_c and precipitation, associated measurement errors, and field observations (appendix 5). **ET_g**: Groundwater evapotranspiration computed as ET_c minus precipitation plus runoff. All precipitation is assumed to be removed by ET before reaching the water table. **Abbreviations:** ET, evapotranspiration; ET_c, corrected evapotranspiration; ET_g, groundwater evapotranspiration; mm, millimeter]

Site name	Water year	Precipitation (mm)	Precipitation error (mm)	ET_c (mm)	ET_c probable error (mm)	Estimated runoff (mm)	ET_g (mm)	ET_g probable error (mm)	Mean annual ET_g (mm)	Mean annual ET_g probable error (mm)
DV	2010	156	1	403	53	0	247	53	225	40
	2011	218	1	421	59	0	203	59		
SV	2010	140	2	188	28	0	48	28	53	21
	2011	187	2	245	31	0	58	31		
PL1	2010	134	3	157	30	0	23	31	20	23
	2011	172	2	189	34	0	17	34		
PL2	2010	127	6	141	28	0	14	29	11	20
	2011	175	3	169	27	13	7	27		

Daily ET_{rc} followed a Gaussian distribution that seldom was matched by measurements at the DV site after precipitation events. During the growing season, daily ET measurements made at the DV site during dry periods (daily precipitation=0) averaged about one-third of concurrent ET_{rc} estimates.

At playa sites, daily ET followed trends similar to those measured at vegetated sites during autumn, winter, and spring, but trends deviated during the summer months (fig. 14). Evaporation on the playa was intermittent and occurred in response to precipitation-derived surface and soil moisture during autumn, winter, and spring of each year. During the summer in the absence of precipitation, playa evaporation was much less and represented evaporation of residual precipitation-derived soil moisture and playa groundwater. Daily ET_c ranged from 0 to 3.9 mm at the PL1 site, and from 0 to 3.3 mm at the PL2 site. Following precipitation pulses and spikes in playa evaporation, decreases in evaporation rates lasted for as much as 2 weeks.

Differences in evaporation rates and trends at the two playa ET sites likely represent differences in salt concentrations and the effect on vapor pressure and evaporation. For example, evaporation spikes appeared slightly smaller and subsequent decreases appeared slightly longer at the PL2 site than at the PL1 site (fig. 14). Site differences can be observed from electrical conductivity and salt concentration measurements. Electrical conductivity of near-surface soil water at the PL2 site was an average of 1.3 times that at the PL1 site (fig. 7). Similarly, salt concentrations measured in August 2009 were 1.8 to 2 times greater at the PL2 site than at the PL1 site. Increased salt concentrations at the PL2 site probably decreased evaporation rates by decreasing the saturation vapor pressure and increasing the surface tension of water molecules. Increasing albedo caused by high salt concentrations and crusts also probably decreased evaporation at the PL2 site compared to the PL1 site during the warmest time of year (Kinsman, 1976; Malek and others, 1990). Although the mean albedo was similar at the playa sites during the period of record, albedo typically was greater at the PL1 site during spring through early summer and was greater at the PL2 site during midsummer through early autumn (data not shown).

Formation of a surface salt crust following evaporative removal of precipitation from the playa surface probably limited evaporation of playa groundwater during summer and early autumn. In the absence of precipitation, daily ET during summer and autumn typically ranged from 0.01 to 0.2 mm and was at or approaching the measurement detection limit of the eddy-covariance method as determined from random uncertainty (see section, "Uncertainty"). Although water levels at the playa sites generally were shallowest (closest to the soil surface) during midsummer (fig. 12), corresponding water content and evaporation approached annual minimums (figs. 6 and 14). In addition to reduced saturation vapor pressure as a result of high salinity, drying of surface soils also led to formation of surface salt crusts that physically limited evaporation. Salt precipitation within pore spaces also likely occurred, further limiting soil permeability and evaporation rates (Nachshon and others, 2011).

Annual ET_c ranged from about 141 mm at the PL2 site in WY 2010 to 421 mm at the DV site in WY 2011 (table 9, fig. 15). Differences in annual ET_c at the two playa ET sites likely result from the increased salt concentration at the PL2 site.

Greater annual ET_c in WY 2011 than in WY 2010 represents a mean increase in precipitation of about 35 percent between the two water years. The greatest increase in annual ET_c was measured at the SV site (about 30 percent), followed by an approximate 20-percent increase at the PL1 and PL2 sites. At the DV site, however, annual ET_c increased by about 5 percent, compared to about a 40-percent increase in annual precipitation. A lack of direct compensation of annual precipitation by annual ET_c could represent measurement uncertainty as defined by error bounds in table 9 or could represent the phenological suppression of plant transpiration during relatively cool summer temperatures in WY 2011. Robinson and Waananen (1970) showed that the warmth of a growing season can greatly affect greasewood ET rates. Near Winnemucca, Nevada, Robinson and Waananen (1970) measured an increase in ET of about 46 mm from a dense (50-percent canopy cover) greasewood lysimeter from 1965 to 1966, despite a more-than-50-percent reduction in precipitation. This annual ET difference was attributed mainly to a warmer growing season (April–September) by about 230 degree days (Robinson and Waananen, 1970). In this study, the total warmth of the growing season (May–August) was only slightly greater for WY 2010 (by 4–12 degree days), but during the months of June and July, when consecutive daily ET rates were greatest, water year warmth differences were magnified (table 5). Degree-day differences during June and July indicate that WY 2010 was warmer than WY 2011 by 80 degree days at the DV site and by 83 degree days at the SV site. Although not as substantial as the degree-day differences reported by Robinson and Waananen (1970), warmer temperatures during June and July of WY 2010 could explain the lack of precipitation compensation by ET at the DV site. Nevertheless, the SV site did not show an ET_c intolerance to precipitation despite the cooler temperatures. This could be a result of greater canopy cover in 2011 than in 2010 (table 6), or less canopy cover at the SV site compared to the DV site, and hence, a lower transpiration contribution to total ET at the SV site (see section, "Groundwater Evapotranspiration Partitioning").

Local precipitation accounted for more than 70 percent of ET_c at all sites except the DV site, and precipitation contributions consistently increased from WY 2010 to 2011 at all sites. At the DV site, where phreatophyte cover is about 13 percent greater than at the SV site, precipitation contributions to annual ET_c were much lower than other sites and ranged from 39 percent during WY 2010 to 52 percent during WY 2011.

Annual runoff from playa ET sites was estimated by comparing seasonal changes in soil-water content and storage with differences between ET_c and precipitation, field observations, and errors associated with each measurement

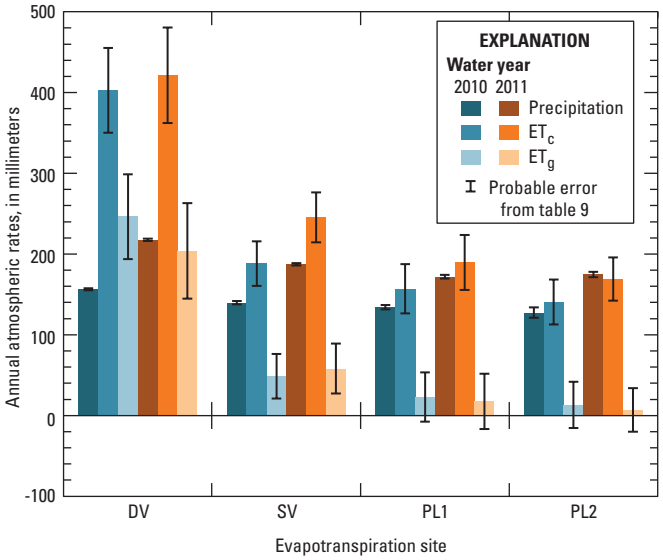

Figure 15. Annual measured precipitation, energy-balance corrected evapotranspiration (ET_c), and groundwater evapotranspiration (ET_g) at dense vegetation (DV), sparse vegetation (SV), playa 1 (PL1), and playa 2 (PL2) evapotranspiration sites, Dixie Valley, Nevada, water years 2010–11.

(table 9, appendix 5). Runoff at vegetated sites was assumed to be negligible. The land surface at the SV site is mostly flat and poorly drained (Soil Survey Staff, Natural Resources Conservation Service, 2011), and moisture from high-intensity precipitation and rapid snowmelt events typically lead to ponding within local topographic depressions. The land-surface soils at the DV site are well drained (Soil Survey Staff, Natural Resources Conservation Service, 2011) and the surface is mostly flat and densely vegetated; therefore, event-generated moisture was assumed to percolate into shallow soils rather than leave the measurement area as runoff. Playa runoff was computed seasonally using a simple approach where the measured change in water storage (product of water content and measurement depth interval) was subtracted from the difference between cumulative ET_c and precipitation. Water storage was evaluated across the upper 75 cm of soil at the PL1 site and within the upper 50 cm of soil at the PL2 site using seasonal volumetric water-content measurements from soil core samples. Event-generated runoff from the site that results from high-intensity rainfall or rapid snowmelt was assumed to occur in combination with run-on to the sites from upgradient playa locations, and water storage and ET_c measurements were assumed to compensate for differences between runoff and run-on. Therefore, runoff estimates are assumed to represent the net difference between runoff from and run-on to the site. Computed runoff estimates (that is, values exceeding the combined water content, ET_c, and precipitation measurement errors) were compared with monthly field notes and photographs to determine if estimates were realistic.

Seasonal evaluations reliably identified a single runoff event during the period of record at the PL2 site and negligible runoff at the PL1 site. About 13 mm of runoff at the PL2 site was estimated following 54 mm of precipitation that fell in early October 2010. This estimate was based on measurements made between July 6 and October 15, 2010 (appendix 5). The difference between ET_c, precipitation, and the change in water storage during this measurement period at the PL1 site was within the overall measurement error, and, therefore, was assumed to be negligible. Seasonal evaluations between November 3, 2009, and February 2, 2010, identified potential runoff of about 6 mm at the PL1 site, but comparisons with field evaluations negated this estimate (appendix 5). During the February 2010 field visit, several ponds established in local topographic depressions and distributed within and beyond the PL1 site measurement area were observed and likely represented snowmelt from the 10s of millimeters of snow that fell during the previous 2 months. Although not measured, the volume of water in these ponds was assumed to compensate for the difference between measured ET_c and precipitation. Pond-water accumulation and a lack of net runoff from snowmelt during this period also is supported by a seasonal peak in ET_c that occurred at both playa sites during February 2010 (fig. 14).

During shorter (monthly) periods when potential ET was low, runoff from and run-on to the playa ET sites undoubtedly occurred and could explain the discrepancy in precipitation compensation by ET_c among WY 2010 and 2011 measurements. However, a lack of continuous soil-water storage measurements to account for precipitation infiltration precludes reliable shorter-term runoff estimation. Runoff estimation methods in this study also do not account for seasonal temperature fluctuations that can largely affect water levels and water storage. Near-surface water content (2–6 cm bls) along with water-content profiles (15–60 cm bls) and water-level trends, indicate that the playa soil consistently is near saturation, and soil-water content trends could be influenced by water-level fluctuations (fig. 12) in addition to precipitation at the PL2 site (fig. 6). Overall, annual runoff estimates made using the simplified seasonal approach are assumed to be reasonable, and shorter-term inconsistencies are likely within the uncertainty of ET_c estimates.

Groundwater Discharge by Evapotranspiration

Groundwater ET (discharge) for each site was computed annually by subtracting locally measured precipitation from annual ET_c. Precipitation falling locally at all sites was assumed to be removed by ET. Annual runoff from the PL2 site was subtracted from precipitation before computing ET_g. Annual ET_g assessments made during WYs 2010 and 2011 indicate that annual ET_c consistently exceeded precipitation at all sites, but playa estimates were consistently within the probable measurement error (table 9, fig. 15). Water-year assessments of water content and unsaturated-zone water movement indicate that ET contributions from antecedent soil moisture, or moisture remaining from the previous water years, were negligible (see section, "Soil Physics"). Therefore, groundwater was assumed to be the primary source of ET_c demand not met by precipitation. At vegetated sites, groundwater contributions were attributed to root-water uptake of groundwater from the capillary fringe and shallow water table. At the playa sites, groundwater contributions were from direct evaporation of moisture within the upper capillary fringe, which extended to near-surface soils.

Annual ET_g estimates ranged from 7 to 247 mm among sites (table 9). The annual groundwater contribution to ET ranged from 24 to 61 percent of total ET at vegetated sites and 4 to 15 percent of total ET at playa sites. Groundwater ET at the PL1 and PL2 sites consistently was less than the estimated measurement error (table 9, fig. 15), highlighting the uncertainty of eddy-covariance measurements (see section, "Uncertainty") as water content measurements show no change between the start and end of the two water years (see section, "Soil Physics"). Despite these uncertainties, differences in ET_g between the two playa sites provide plausible evidence for increasing discharge with increasing distance outward from the playa center.

Mean annual ET_g for phreatophytic vegetation and playa sites (table 9) is similar to that reported for similar studies. The range in mean annual ET_g estimated for phreatophytic vegetation (53 and 225 mm for the SV and DV sites, respectively) was within the range of about 20–400 mm estimated for sparse-to-dense shrubland areas in Nevada (Berger and others, 2001; Moreo and others, 2007; Allander and others, 2009). Mean annual playa discharge estimates of 11 and 20 mm were within the lower end of estimates (0–230 mm) reported in previous studies from Nevada, Utah, and California (Malek and others, 1990; Maurer and others, 1994; Tyler and others, 1997).

Comparisons between WY 2010–11 and 30-year mean precipitation, and the measured variability within ET_g measured during WYs 2010 and 2011 indicate measured ET_g is representative of long-term discharge. Annual precipitation measurements in WY 2010 from nearby weather stations in Lovelock and Winnemucca (45 and 90 km from Dixie Valley, respectively) were similar to the 30-year mean estimate, whereas WY 2011 measurements were slightly greater than this value (Western Regional Climate Center, 2012). Assuming precipitation patterns in these areas are similar to those in Dixie Valley, similar conclusions can be made about water year precipitation totals measured in this study. Despite variations in water year precipitation from 2010 to 2011 in Dixie Valley, differences in ET_g estimates were within the bounds of estimated measurement error for all sites, indicating that ET_g is mostly insensitive to precipitation.

Uncertainty

Uncertainty in available energy, turbulent flux, evapotranspiration, and precipitation estimates was investigated in this study. Random, systematic, and gap-filling errors in variables used to estimate ET_g were investigated individually and used in combination to determine the probable error in mean annual estimates using standard error propagation techniques (Lee and Swancar, 1997).

Available Energy

The maximum probable uncertainty associated with available energy estimates was determined from net radiation measurements. The four CNR2 two-component net radiometers used to measure net radiation were calibrated to a higher-standard (NR01) four-component net radiation sensor. The accuracy of the NR01 is stated by the manufacturer as plus or minus 10 percent for daily measurements (Campbell Scientific, Inc., 2011). Soil-heat-flux errors in 30-minute measurements were reduced when evaluated during a 24-hour interval as the energy stored in the soil during the morning is released locally in the afternoon and evening. Moreover, energy is stored and released seasonally such that over an annual period, which is the basis of estimates reported for this study, soil-heat flux accounts only for a small part of available energy. In this study, the annual soil-heat flux accounted for less than 5 percent of available energy estimates at the SV, DV, and PL1 sites, and for less than 12 percent of available energy estimates at the PL2 site.

In addition to manufacturer-reported accuracy, manufacturer calibration differences between the NR01 and CNR2 instruments and field conditions during extended deployment periods also require consideration. As discussed in section, "Data Correction, Filtering, and Gap-Filling Procedures," the NR01 pyrgeometer, which measures longwave radiation, was calibrated using an indoor black body, whereas the CNR2 pyrgeometer was calibrated outdoors using the WISG standard. Although there is no internationally accepted longwave calibration standard, the WISG standard is internationally recognized. Therefore, to compare and calibrate CNR2 sensors to the NR01 standard in this study, the NR01 incoming longwave calibration was increased by 7.5 percent to account for calibration discrepancies. Potential bias associated with the different calibration techniques was assessed for all sites and water years by calibrating CNR2 sensors to the NR01 standard with and without the 7.5 percent calibration adjustment. The mean difference in cumulative net radiation among all sites and water years was about 5 percent with differences ranging from a minimum of 2 percent at the DV site in WY 2010 to a maximum of 10 percent at the PL1 site in WY 2010. Net radiation differences increased with decreasing canopy cover and surface roughness (data not shown). In all cases, net radiation measurements calibrated to the black body standard (NR01 without adjustment) were less than measurements calibrated to the WISG standard (NR01 with 7.5 percent adjustment). These results are supported by net radiometer comparisons done by Blonquist and others (2009), where NR01 longwave measurements were within 2 percent of measurements made with reference instruments and within 5 percent of measurements made using a four-component net radiometer manufactured by a separate company. These measurement differences were attributed to differences in calibration approaches. Overall, calibration-related accuracy errors in this study are just at or within the ±10-percent instrument accuracy reported by the instrument manufacturer.

Pyrgeometer scaling was shown to bias net radiation high by increasing the magnitude of net longwave radiation. This, in turn, caused a greater disparity between turbulent-flux and available-energy measurements during the identified scaling periods (summer 2009 at the SV site, and summer 2011 at the DV site). For example, during June–August 2011, the energy-balance ratio at the DV site improved from 0.73 to 0.92 when net longwave radiation estimates were corrected for pyrgeometer scaling. Although an attempt was made to identify and gap-fill periods when pyrgeometers were scaled, several periods were likely missed. This indicates that a small (likely less than 5 percent) positive bias in net radiation potentially persists. Therefore, the probable error in net radiation measurements, representing additive errors from manufacturer-reported accuracy and pyrgeometer scaling, is likely within ± 15 percent.

Turbulent Fluxes and Evapotranspiration

Errors in turbulent-flux measurements were evaluated and applied to ET measurements using a combination of random errors, systematic errors, and gap-filling errors. Random error in turbulent fluxes describes the precision of the measurements and was evaluated using the 24-hour differencing approach (Hollinger and Richardson, 2005; Richardson and others, 2012). With this method, two flux measurements ($X_{1,t}$, X_{1t+24}), at a single site, 24 hours apart, and under similar environmental conditions are considered analogs to the simultaneous paired two-tower approach (Finkelstein and Sims, 2001). Systematic error describes the accuracy of turbulent fluxes and was estimated by evaluating the imbalance between available energy and the turbulent flux. In addition to random and systematic error, turbulent flux gap-filling errors, as determined from RMS errors describing the calibration fit between measured and simulated λE fluxes, were applied to annual λE and ET estimates.

Random error in the turbulent-flux measurements (σ_{RE}) was estimated as the standard deviation (σ) of the difference between the two measurements divided by the square root of 2 ($\sqrt{2}$) (Richardson and others, 2012):

$$\sigma_{RE} = \frac{\sigma\left(x_{1,\,t} - x_{1,\,t+24}\right)}{\sqrt{2}} \qquad (19)$$

Data used for comparison were limited to good (non-gap-filled), summer, daytime (net radiation greater than 5 W/m^2) data where at least 2 weeks had passed since precipitation was measured. Additional criteria included when differences in air temperature were within 3 °C, wind speeds were within 1 m/s, and net radiation was within 10 W/m^2. More stringent filtering for wind directions within plus or minus 15 degrees had little effect on error estimates. Investigations beyond summer months produced similar results, but 2-week-long, precipitation-free measurement periods between November and May seldom occurred.

Random-error estimates were small and increased slightly with the absolute value of individual latent- and sensible-heat fluxes. Random error for each site was characterized by relating the 30-minute random uncertainty to the absolute value of latent- and sensible-heat fluxes using ordinary least squares regression (table 10). Total random error for sensible-heat fluxes was similar between all sites, whereas random error for latent heat fluxes varied between sites and increased with increasing Bowen ratios ($H/\lambda E$). Uncertainty in H increased from minimums of 2.15–6.10 W/m^2 to about 5 percent of the measured flux. Uncertainty in λE increased from minimum values of less than 1–2 W/m^2 to 4–9 percent of the measured flux at the vegetated sites and 17–23 percent of the flux at the playa sites. Low percent error at the DV and SV sites with respect to PL1 and PL2 sites (regression slope, table 10) corresponded with a greater range in λE magnitude. Latent-heat fluxes compared at the DV and SV sites ranged from 0 to more than 150 and 70 W/m^2, respectively. Notably higher percent λE errors for the playa sites, where flux magnitudes generally were less than 30 W/m^2, indicate random noise had a larger effect on the dataset and latent-heat flux measurements likely were approaching the detection limit of the eddy-covariance method.

Mean evapotranspiration errors computed from random error in 30-minute latent-heat fluxes were about 0.1 mm/d among all sites. Mean site errors ranged from 0.06 mm/d at the playa sites (with absolute errors of as much as 0.4 mm/d) to 0.12–0.17 mm/d at the vegetated sites (with absolute errors of about 0.3 mm/d). These errors in ET measurements are similar to the 0.1 mm/d uncertainty reported by Kampf and others (2005). They noted that eddy-covariance measurements on a playa could constrain evaporation rates only to within 0.1 mm/d.

Random error decreased with increased integration periods from 30-minute to seasonal and annual fluxes. Errors were propagated over integration periods by adding 30-minute ET errors as the square root of the sum of squared errors for measured values. Although application of linear relations to daytime fluxes was substantial with respect to ET estimates (table 10), propagation of random errors to compute the annual sum of ET greatly reduced the random error. At all sites, the propagation of random errors resulted in annual ET errors of less than 0.6 mm, which represent less than 1 percent of the ET_c error shown in table 9.

Systematic error was estimated by evaluating the range in energy-balance closure (table 8). Measured and gap-filled turbulent fluxes were assumed to represent the minimum probable systematic error, whereas fluxes corrected for full energy-balance closure within the water year represent the maximum potential systematic error. Corrected turbulent fluxes were computed as the mean of minimum and maximum potential fluxes; therefore, the maximum systematic uncertainty represents half of the difference between minimum and maximum turbulent fluxes. Evapotranspiration errors were computed from systematic error in annual λE, and represent an average of about 99 percent of the total ET_c error (table 9).

Turbulent-flux, gap-filling errors were determined from root-mean-square (RMS) errors describing the calibration fit between measured and simulated λE fluxes. The RMS errors between measured and simulated fluxes increased with the flux magnitude and ranged from 1.8 to 18.9 W/m^2, among all sites with a mean value of 10.4 W/m^2. Gap-filling errors were computed as the product of the gap interval and RMS error. These errors were summed over the water year and converted to a corresponding ET error. Gap-filling errors represent an average of less than 1 percent of the annual ET_c error (table 9).

Table 10. Random errors at evapotranspiration sites characterized by ordinary least squares regression of 30-minute random error compared with latent- and sensible-heat fluxes, Dixie Valley, Nevada.

[Thirty-minute random errors determined using the 24-hour differencing approach for all non-gap-filled turbulent fluxes measured at four evapotranspiration (ET) sites, Dixie Valley, Nevada. **Site name:** Number of measurement comparisons = 735, 1,119, 1,115, and 1,182 at DV, SV, PL1, and PL2 sites, respectively. DV, dense vegetation; SV, sparse vegetation; PL1, playa 1; PL2, playa 2. **Abbreviations:** mm/d, millimeter per day; W/m^2, watt per square meter; λE, latent-heat flux; H, sensible-heat flux; –, not applicable]

Site name	Random turbulent flux error (W/m^2)	Random evapotranspiration error (mm/d)	
		Mean absolute	Maximum absolute
DV	0.04 | λE | + 2.05	0.17	0.29
SV	0.09 | λE | + 0.89	0.12	0.3
PL1	0.17 | λE | + 0.37	0.06	0.24
PL2	0.23 | λE | + 0.44	0.06	0.4
DV	0.03 |H| + 6.10	–	–
SV	0.05 |H| + 3.62	–	–
PL1	0.05 |H| + 2.15	–	–
PL2	0.05 |H| + 2.72	–	–

The total ET_c probable error for WY 2011 ranged from 27 mm at the PL2 site to 59 mm at the DV site (table 9). Foken (2008) and Foken and others (2012) noted that despite the systematic energy imbalance, the sensor accuracy of eddy-covariance measurements typically is within about 5 percent for sensible-heat fluxes (CSAT 3 anemometer) and 10 percent for latent-heat fluxes (krypton hygrometer). Probable errors estimated in this study represent an average of about 16 percent of annual latent-heat fluxes and ET estimates, and are slightly greater than the range reported by Foken (2008) and Foken and others (2012).

Precipitation

Precipitation uncertainty was determined annually as the summation of the measurement error and the maximum undercatch correction error for each site and water year. Measurement error was evaluated using a combination of (1) comparisons between the stationary and temporarily co-located volumetric precipitation gages and (2) manufacturer-reported error. A replicate volumetric precipitation gage was installed for 2–6 months at each site to investigate random and systematic errors. Differences between gages typically ranged from 0 to 0.25 mm, except for a single measurement at the SV site (difference = 0.51 mm) following the October 2010 storm. This range is within the resolution of the bulk-precipitation measurement device (0.25 mm as reported by the manufacturer). No systematic bias was measured between replicate gages or measuring sticks; therefore, differences between measurements were assumed to represent only random errors. An error of 0.25 mm was assigned to all measurements made during the study and propagated as the square root of the sum of squared errors for measured values to compute cumulative water-year estimates. Random errors represent about 6 percent of the total precipitation error.

Errors associated with undercatch corrections were evaluated using the standard error describing the ordinary least-squares regression of wind speeds at the height of the precipitation gage and height of the continuously recording CSAT 3 anemometer for all sites. These errors are assumed to represent systematic errors. Standard errors were 0.12, 0.19, 0.28, and 0.54 m/s for the DV, SV, PL1, and PL2 sites, respectively. Estimated wind speeds at the height of the precipitation gage (during the period of record) were increased and decreased by the respective standard error at each site. Undercatch corrections then were applied to precipitation measurements, and the maximum increase or decrease in the water-year precipitation estimate (with respect to reported values in table 9) was selected as the undercatch correction error. An average of about 94 percent of the precipitation uncertainty was attributed to systematic error.

Total uncertainty in mean annual ET_g estimates represents the probable error shown in table 9. Total uncertainty typically increased with ET_g magnitude. Groundwater ET at the playa sites was less than the probable error. Probable error at the DV and SV sites was much less than the discharge estimates and accounted for about 20 and 40 percent of mean annual ET_g, respectively. A low error-to-estimate ratio at vegetated sites than playa sites increases confidence in the ET_g estimation approach in the areas contributing to most ET_g. Across the playa or areas with sparse vegetation cover, where ET_g is low to negligible, uncertainty analyses underscore the difficulty in determining accurate estimates.

Water Sourcing

Groundwater ET in arid, hydrologically closed, undeveloped basins occurs predominantly through evaporation from bare soil and transpiration from phreatophytes on the basin floor. In addition to quantifying total groundwater discharge, this study evaluated the relative proportions of groundwater being discharged from evaporation and transpiration-flux components. Depending on the soil type and depth to water, the source water of shallow soil moisture can be derived from groundwater, precipitation, or a combination of both. Although the primary source water for phreatophytes is groundwater and water within the capillary fringe above the water table (Ehleringer and others, 1991), phreatophytes are facultative and also can acquire water from shallow sources such as soil moisture and adjacent surface water features (Robinson, 1958; Dawson and Pate, 1996). By partitioning ET into evaporation and plant-transpiration components in vegetated areas, the groundwater contribution to each component can be apportioned with respect to the total groundwater flux to the atmosphere. In this study, source water contributions to evaporation and transpiration components were evaluated using measurements of eddy-covariance ET, bare-soil evaporation using a hemispherical chamber, canopy cover, and stable isotopes, and were supported with complementary soil physics data.

Chamber Evaporation

Periodic, portable chamber measurements of evaporation were made at vegetated eddy-covariance ET sites to investigate the relative contributions of bare soil evaporation and plant transpiration to continuous ET (appendix 6). Chamber measurements also were made periodically at the PL2 and PLW sites (fig. 1). Measurements at the PL2 site were used to relate chamber and eddy-covariance measurements, given that evaporation is the sole source of ET at this non-vegetated site. Paired measurements of eddy-covariance evaporation at the PL2 site and chamber evaporation (chamber E) at the PLW site (fig. 1) were used to evaluate evaporation variability between ET sites and the center of the playa, which typically is inundated with water more than 25 percent (3 months) of the year.

Portable chambers have been used to measure ET from cultivated alfalfa fields (Reicosky and others, 1983), bare soil, and sparsely vegetated plant communities (Stannard, 1988;

Stannard and Weltz, 2006; Garcia and others, 2008; Garcia and others, 2009). Chambers measure water vapor exchange between the surface of the Earth and the atmosphere from small areas (Dugas and others, 1997) by enclosing a known volume over a plant canopy, soil surface, or both, and then measuring the increase in vapor density in the chamber. The maximum rate of change in vapor density with time is proportional to the ET flux from the enclosed surface area (Stannard, 1988).

The chamber consists of a 2.4-mm thick, 1-m-diameter hemispherical dome made of Plexiglass® G (Stannard, 1988). A rigid, cylindrical skirt of similar diameter was added to the chamber base to ensure complete contact with the surface being measured. At vegetated sites, the skirt was embedded in the soil and surrounded with fine sand to seal and separate the internal chamber volume from the external atmosphere (fig. 16). On the playa, the seal was created by placing the combined chamber and skirt on the soil surface (without breaking the surface crust) and emplacing fine sand around the perimeter. A temperature and relative humidity probe (HMP45C) was used to measure vapor density, and internal fans were used to keep the air and water vapor well mixed within the chamber. Bare-soil evaporation was estimated using an equation from Stannard (1988):

$$E = 86.4\frac{MVC}{A} \tag{20}$$

where

E is the evaporation rate, in millimeters per day (mm/d),

M is the maximum slope of the vapor density time series, in grams per square meter per second [(g/m^2)/s],

V is the volume inside the chamber, in cubic meters,

C is the calibration factor of the chamber, unitless,

A is the land-surface area covered by the chamber, in square meters, and

86.4 is a factor used to convert units of water flux [(g/m^2)/s] to evaporation rate (mm/d).

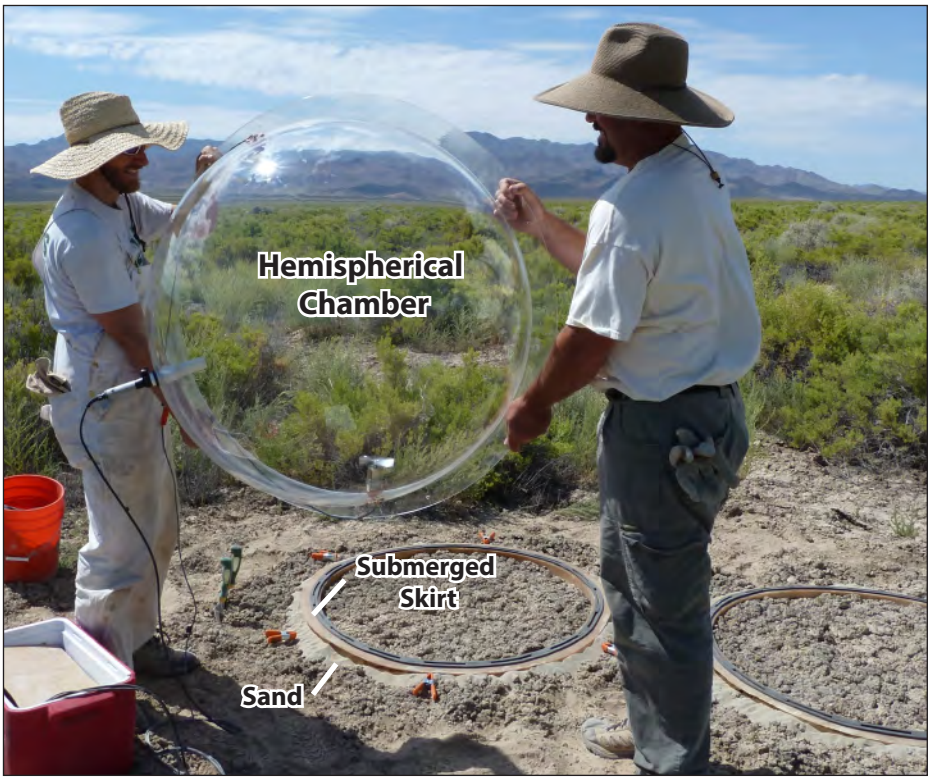

Figure 16. Chamber evaporation measurement location and setup at the dense vegetation site, Dixie Valley, Nevada. Photograph taken by C. Amanda Garcia, U.S. Geological Survey, July 7, 2010.

A one-layer, two-component model (Stannard, 1988; Stannard and Weltz, 2006) was used to estimate the relative contributions of evaporation (E) and transpiration (T) to continuously measured ET:

$$ET = Fc_s E + Fc_p T \quad (21)$$

where

F_c represents the fractional cover of soil (s) and plants (p) (shown as percent canopy cover in table 6) across the measurement area.

Evaporation contributions to total ET were computed as the product of bare-soil chamber E measurements and the fractional cover of soil determined from transect measurements. Equation 21 was rearranged to solve for transpiration contributions using measured eddy-covariance ET, chamber E, and fractional cover measurements.

Chamber evaporation measurements were made in the spring, summer, and autumn at the vegetated sites during water years 2009 through 2011 (appendix 6). Measurements during summer 2010 at both sites and summer 2011 at the DV site were not made because of cloud cover throughout the designated measurement day that could obscure comparisons between discrete chamber and continuous eddy-covariance measurements. Chamber measurements at the PL2 site were made in May, August, and November 2009, and in April 2010; measurements at the PLW site were made in August and November 2009, and in April 2010. Replicate chamber measurements (n=2 per 30 minutes) made at each site throughout the day were compared with paired half-hour eddy-covariance evaporation measurements.

Stable Isotopes

Stable isotopes of oxygen-18 and deuterium were used to quantify the relative proportions of source waters in plants, bare soil, and playa sediments adjacent to each ET station. These data then were combined with partitioned ET estimates at vegetated sites and eddy-covariance evaporation estimates at playa sites to periodically estimate ET_g. Stable isotopes of oxygen-18 and deuterium also were used to evaluate the source of groundwater at the PLW site.

Many studies have used stable isotopes to investigate seasonal patterns of plant water sources (Ehleringer and others, 1991; Chimner and Cooper, 2004; Scott and others, 2005). At vegetated sites, samples of greasewood-xylem water, groundwater, shallow soil water, and recent precipitation were collected during the spring, summer, autumn, and winter (groundwater and precipitation only) and were analyzed for oxygen-18 and deuterium. In playa areas, soil water, groundwater, and recent precipitation were sampled during the same seasons for isotopic composition to determine the relative mixture of source waters contributing to evaporation. The use of deuterium for water sourcing in halophytes such as greasewood can be problematic, however, because halophytes often discriminate against deuterium during root-water uptake. Because of this discrimination, substantial fractionation of the hydrogen isotope can occur (for example, root water is more negative than source waters; Lin and Sternberg, 1993). Therefore, only stable isotopes of oxygen-18 were used to evaluate plant water sources, similar to Chimner and Cooper (2004).

Samples were collected seasonally at ET sites from spring 2009 through summer 2011. Greasewood stem-water samples were collected by cutting woody stems below the green-leaf stems. Stem samples were cut from four plants at each site and combined in a single sample bottle to create a composite sample. Replicate composite samples were collected at each site. Groundwater samples were collected from site monitoring wells after three well-casing volumes of water were removed using a peristaltic pump. At the PL2 site, the well went dry within a few minutes of pumping; therefore, samples were collected after pumping the well dry three times, but without complete recovery. Precipitation was sampled from precipitation collectors quarterly and, as such, samples represented a weighted composite of rainfall and (or) snowfall from the previous season. Oil (0.5 in.) was consistently poured into collector cylinders after each sampling period to prevent evaporative enrichment of constituents within accumulated water. Soil samples were collected throughout the soil profile at each site during site installation and from near-surface (0–15 cm bls) and shallow (45–60 cm bls) depths during seasonal sampling events. Replicate (n=2) soil cores were taken at each depth on each sample date and samples were analyzed separately. All samples were packaged immediately in airtight bottles. Upon return to the office (typically 2–4 days), plant-stem samples were frozen and soil, groundwater, and precipitation samples were refrigerated until processed. Soil and plant-stem water were extracted using azeotropic distillation with toluene (Révész and Woods, 1990).

Samples also were collected from the PLW monitoring site from August 2009 through July 2010. Groundwater was sampled during September 2009, November 2009, April 2010, and July 2010. Samples were collected from standing water within and between the salt crust and land surface during August 2009 and from the precipitation-derived ephemeral pond during April 2010.

Soil and plant water, groundwater, and precipitation were analyzed for oxygen-18 and deuterium at the USGS Stable Isotope Laboratory in Reston, Virginia. Deuterium analyses were done using a hydrogen equilibration technique (Coplen and others, 1991; Révész and Coplen, 2008). This technique measures deuterium activity rather than concentration. Oxygen-18 analyses were done using the carbon dioxide equilibration technique (Epstein and Mayeda, 1953) and are reported as activity. Expression of brine isotopic data as an activity rather than concentration allows for direct evaluation of surface evaporation processes (Sofer and Gat, 1975).

At vegetated sites, binary mixing fractions were estimated using shallow root-zone soil water, plant-xylem water, and groundwater signatures of oxygen-18. Shallow root-zone soil water signatures were used instead of precipitation signatures at vegetated sites to account for evaporative fractionation of precipitation-derived soil moisture. Unsaturated-zone, liquid-water fluxes at vegetated sites (fig. 11) indicate that groundwater contributions to shallow and near-surface soil water signatures are negligible (see section, "Liquid-Water Fluxes"). Binary mixing of oxygen-18 ($\delta^{18}O$) signatures was evaluated using the following equation (Clark and Fritz, 1997):

$$\delta^{18}O_{Sample} = x\delta^{18}O_A + (1-x)\delta^{18}O_B \quad (22)$$

where

the sample signature (in per mil) represents that of xylem water at vegetated sites, and
x and $(1-x)$ represent the fractions of source waters A (groundwater) and B (precipitation-derived shallow soil moisture), respectively, within each sample water.

At playa ET sites, end-member mixing was evaluated using near-surface and shallow soil water, and precipitation signatures of oxygen-18 and deuterium. Shallow (45–60 cm bls), distilled soil water samples were used in place of groundwater in equations 23–25, and were assumed to represent signatures similar to groundwater. These samples were used because raw groundwater samples (collected with a peristaltic pump after purging three well-casing volumes) notably were more positive (greater than 6 per mil) in deuterium than groundwater samples that had been distilled using azeotropic distillation. Differences between distilled and undistilled playa groundwater samples likely highlight the "isotope salt effect" noted by Horita (2005), where dissolved salts in brines were shown to cause up to a 10 per mil discrepancy in the deuterium activity of distilled and undistilled water samples. In this study, deuterium signatures of distilled groundwater samples were similar (within 2 per mil analytical uncertainty) to signatures of distilled shallow soil water samples, whereas deuterium signatures of raw playa groundwater were consistently several units per mil (up to 6 per mil) more positive (enriched) than distilled shallow soil water samples. Oxygen-18 signatures were unaffected by this chemical interference. Horita (2005) also noted that isotopic exchange with hydrogen sulfide, hydrogen gas, hydrocarbons, or organic matter can increase deuterium values as a result of the large fractionation factors between water and these compounds. Although hydrogen sulfide typically is removed in the laboratory prior to sample analysis, additional confounding factors could be affecting deuterium signatures. End-member mixing models are described as (Mazor, 1991):

$$D_{p-g} = \left[\left(\delta^{18}O_p - \delta^{18}O_g\right)^2 + \left(\delta D_p - \delta D_g\right)^2\right] \quad (23)$$

$$D_{p-s} = \left[\left(\delta^{18}O_p - \delta^{18}O_s\right)^2 + \left(\delta D_p - \delta D_s\right)^2\right] \quad (24)$$

$$P_g = \frac{D_{p-s}}{D_{p-g}} \quad (25)$$

where

D_{p-g} is the difference between precipitation (p) and groundwater (g) signatures,
δD is the deuterium signature in per mil,
D_{p-s} is the difference between precipitation and near-surface soil water (s; 0–15 cm bls), and
P_g is the proportion of groundwater in near-surface soil water.

Groundwater Evapotranspiration Partitioning

Relative proportions of groundwater being discharged from evaporation and transpiration (where applicable) flux components were determined at each site. Source water contributions to evaporation and transpiration components were evaluated using seasonal trends in stable isotope composition.

Chamber Evaporation and Evapotranspiration Partitioning

Paired eddy-covariance (uncorrected) and chamber evaporation measurements at the PL2 site indicate that the chamber reasonably can predict eddy-covariance measurements and, therefore, can be used reliably to partition ET into E and T and to extrapolate measurements across the playa (fig. 17). Correlation analysis showed a highly significant, positive relation between the two measurement methods ($r=0.873$; $p>|r|<0.001$; where r is the correlation coefficient and p is the significance level). Based on 30-minute comparisons across all dates measured, mean chamber evaporation was about 7 percent less than eddy-covariance evaporation. These results are within the range of results from previous studies that reported similar correlation coefficients, but are contrary to results from previous studies that indicated chamber evaporation was slightly greater than eddy-covariance evaporation (Dugas and others, 1997; Stannard and Weltz, 2006; Garcia and others, 2009). Underestimation of eddy-covariance evaporation by the chamber likely resulted from higher external wind speeds relative to internal chamber fan speeds during measurements.

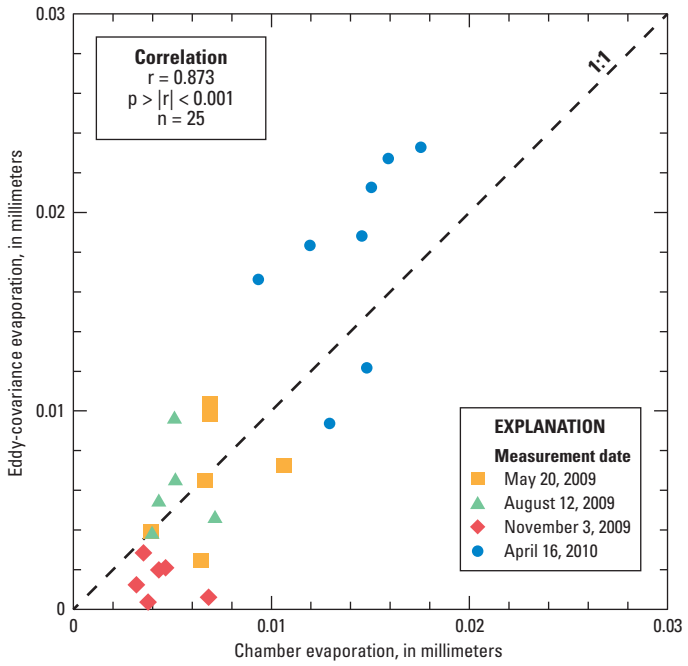

Figure 17. Comparison of 30-minute eddy-covariance and hemispherical chamber evaporation measurements at the playa 2 evapotranspiration site, Dixie Valley, Nevada, May 2009–April 2010. Relation described by the correlation coefficient (r), significance level (p), and sample size (n).

Wind speed measured at the PL2 site during May 2009, August 2009, and April 2010 comparisons was greater than 2 m/s on average and periodically exceeded 6 m/s. Eddy-covariance evaporation measurements typically were greater than (by an average of 27 percent) chamber measurements at wind speeds of more than 2 m/s, and similar to or less than (by an average of 14 percent) chamber measurements at wind speeds less than 2 m/s (paired measurements occurred when mean wind speed was either greater than or less than 2 m/s). Despite differences in instrumentation and in evaporation rates influenced by wind speed on the playa, these results validate the use of the chamber to partition eddy-covariance ET into evaporation and transpiration.

Evapotranspiration partitioning at vegetated sites using bare-soil chamber evaporation and canopy-cover measurements varied throughout the growing season and from site to site (table 11). Bare-soil evaporation at the vegetated sites is shielded partially-to-completely from wind by the plant canopy; therefore, chamber measurements were not adjusted for the 7-percent, wind-related bias measured on the playa. Bare-soil chamber evaporation and canopy cover-measurements were used in equation 21 to solve for the transpiration fraction of total ET. The evaporation fraction of ET decreased as soil dried during the growing season and typically was lowest during the late summer (table 11). Evaporation fractions of total ET at the DV site ranged from 0.13 to 0.89, and at the SV site ranged from 0.25 to 0.82 during this study. Varying greasewood leaf senescence patterns during the autumn influenced evaporation fractions of total ET; greasewood at the DV site typically senesced 1–2 weeks prior to greasewood at the SV site. For example, in mid-October 2010, about 60 percent of the leaves had dropped from DV shrubs and the remaining 40 percent were yellowish and stressed. At the SV site, roughly 70 percent of the leaves were still on the shrubs and most were still green. Differing senescence patterns likely are related to a fluctuating saturated zone at the DV site (unconfined aquifer), and a constant saturated zone (confined with varying pressure) at the SV site. At the DV site, roots likely become disconnected from their primary water source or capillary fringe (above the water table) when the water table declines to a minimum level during late summer, whereas at the SV site, roots remain in contact with the capillary fringe throughout the year.

Comparisons between chamber evaporation measurements near the PLW site and eddy-covariance measurements at the PL2 site are shown in figure 18. Similar precipitation rates were assumed between sites, but more than 0.3 m of accumulated precipitation and precipitation-derived run-on was measured at the PLW site during winter months and undoubtedly affected evaporation rates. Chamber measurements near the PLW site were made in August and November 2009 and April 2010. August 2009 and April 2010 measurements were made about 350 m west of the PLW site, whereas November measurements were made about 100 m west of the PLW site. During August 2009, saturated conditions beneath the thick salt crust at the PLW site precluded all-terrain vehicle access with chamber equipment; during April 2010, the ephemeral pond still was present at the PLW site so chamber measurements were made at the edge of the shrinking pond. Chamber evaporation near the PLW site was increased by 7 percent prior to comparison of measurements with eddy-covariance evaporation at the PL2 site. This adjustment was based on results from the PL2 site comparisons, which indicated that chamber evaporation was, on average, 7 percent lower than eddy-covariance evaporation. Mean chamber evaporation near the PLW site was about 13 percent greater than eddy-covariance evaporation at the PL2 site. Evaporation differences between the PL2 and PLW sites varied seasonally between dry and wet periods. In November 2009, the playa surface near the PLW site contained a concentric border of salt providing evidence of a recently evaporated surface water body. This ephemeral pond was derived from accumulation of local precipitation and precipitation-derived run-on from adjacent areas; about 5.3 mm of precipitation fell across the playa during the 3 weeks prior to evaporation measurements. Presence of the ephemeral pond only was observed following precipitation during winter and spring months and therefore was considered to be precipitation rather than groundwater derived.

Table 11. Periodic daily measurements of eddy-covariance evapotranspiration, evaporation and evaporation fractions of evapotranspiration, transpiration and transpiration fractions of evapotranspiration, groundwater fractions of plant-xylem water, and groundwater evapotranspiration at vegetated sites, Dixie Valley, Nevada, May 2009–September 2011.

[**Site name:** DV, dense vegetation; SV, sparse vegetation. **ET:** Values not corrected for energy-balance closure. **Evaporation:** Determined from bare-soil chamber measurements of evaporation and canopy-cover measurements using equation 23. **Transpiration:** Determined as difference between ET and evaporation. **Groundwater fraction of plant-xylem water:** Determined from stable isotope measurements of plant water extracted from greasewood using equation 22. **ET_g:** Product of transpiration and groundwater fraction of plant water. Groundwater evaporation is assumed to be negligible. **Abbreviations:** ET, evapotranspiration; mm, millimeter]

Site name	Date	ET (mm)	Evaporation fraction of ET	Evaporation (mm)	Transpiration fraction of ET	Transpiration (mm)	Groundwater fraction of plant-xylem water	ET_g (mm)
DV	05-19-09	1.92	0.34	0.65	0.66	1.27	0.92	1.17
	08-11-09	1.40	0.13	0.18	0.87	1.22	1.00	1.22
	11-05-09	0.11	0.83	0.09	0.17	0.02	0.63	0.01
	04-15-10	0.75	0.43	0.32	0.57	0.43	0.96	0.41
	10-14-10	0.73	0.89	0.65	0.11	0.08	0.85	0.07
	04-12-11	0.76	0.32	0.24	0.68	0.52	0.88	0.46
	09-27-11	0.43	0.26	0.11	0.74	0.32	1.00	0.32
SV	05-18-09	0.54	0.54	0.29	0.46	0.25	0.89	0.22
	08-10-09	0.51	0.47	0.24	0.53	0.27	0.97	0.26
	11-02-09	0.09	0.82	0.07	0.18	0.02	0.75	0.01
	04-14-10	0.42	0.72	0.30	0.28	0.12	0.78	0.09
	10-13-10	0.58	0.71	0.41	0.29	0.17	0.88	0.15
	04-13-11	0.43	0.25	0.11	0.75	0.32	0.75	0.24
	07-12-11	0.69	0.33	0.23	0.67	0.46	1.00	0.46
	09-26-11	0.23	0.41	0.09	0.59	0.14	1.00	0.14

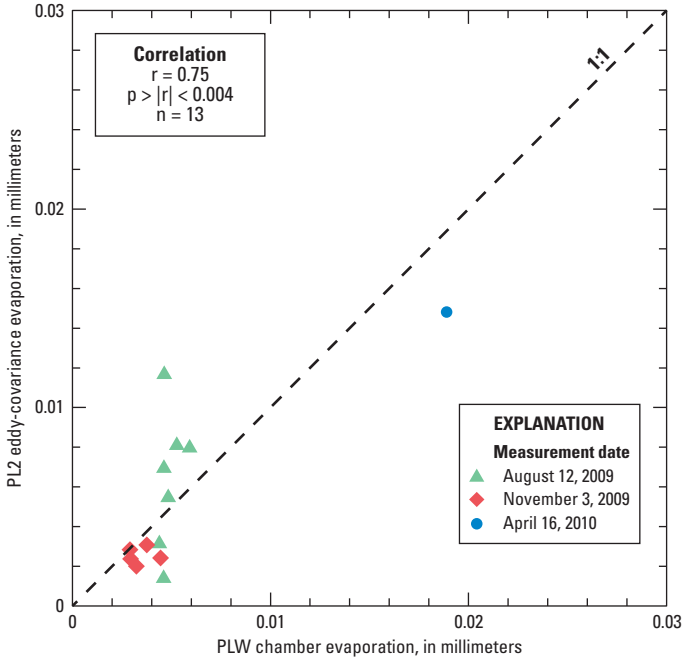

Figure 18. Comparison of 30-minute eddy-covariance evaporation at the playa 2 (PL2) evapotranspiration site and 30-minute hemispherical chamber evaporation near the playa-west (PLW) monitoring site, Dixie Valley, Nevada, August 2009–April 2010. Chamber measurements were adjusted upward by 7 percent. Relation described by the correlation coefficient (r), significance level (p), and sample size (n).

In November 2009 and April 2010, the playa surface near the PLW site was darker and surface salt crusts were thinner and less brittle than in August 2009. Comparisons between evaporation measurements following cool, wet periods in November 2009 and April 2010 indicate that evaporation near the PLW site was more than 30 percent greater than evaporation at the PL2 site. In August 2009, however, when the playa surface was lighter with a thicker (more than 1-cm thick) and more brittle salt crust, evaporation near the PLW site was about 25 percent lower than evaporation at the PL2 site. These results indicate that after evaporative removal of recent precipitation- and runoff-derived surface water, the salt crust that forms over the surface near the PLW site limits evaporation when compared to the PL2 site.

Source Water

Isotopic signatures of oxygen-18 and binary mixing models indicate that groundwater is the primary source water for phreatophytes at vegetated sites (fig. 19, table 11). At playa ET sites, oxygen-18 and deuterium signatures, along with end-member mixing models, indicate that groundwater is the primary source of near-surface soil water (fig. 19, table 12); however, groundwater contributions to ET are inconclusive because near-surface soil water measurements were collected from the depth interval of 0–15 cm bls rather than from the evaporative surface that likely penetrates only the upper few centimeters of soil. Like seasonal variations in oxygen-18 signatures of precipitation, near-surface (0–15 cm bls) soil water signatures varied seasonally at all sites, but the magnitude of the variation in oxygen-18 was smaller for the playa sites (fig. 19) because of the low permeability of playa sediments. Precipitation that falls on the playa from spring through autumn likely dissolves surface salt crusts and subsequently either ponds or penetrates only the near-surface soil (figs. 6–8) before evaporating. Mixing between fresh precipitation and surface salts likely reduces the potential evaporation of precipitation-derived soil moisture. With a topographic surface gradient of about 0.0002 m/m between the two playa sites and large evaporative demand, runoff of locally derived precipitation at these sites typically is small to negligible during late spring through early autumn (appendix 5), but might occur in response to intense, short-duration events. During winter, runoff of liquid precipitation or melting snow also typically is small to minimal, as precipitation dilution of near-surface signatures at the PL1 site (figs. 19 and 20) provides evidence of downward percolation of snowmelt.

Soil water oxygen-18 signatures within the depth interval of 45–60 cm bls were relatively constant during the period of record. Signatures varied within 3.5 per mil between seasons at vegetated sites and within 2 per mil at playa sites (fig. 19). Similar to water-content profiles (fig. 8), this lack of change indicates that evaporative extinction and notable precipitation percolation depths typically were above this depth interval. Based on trends in water content and matric potential, and liquid-water fluxes in the unsaturated zone, moisture within this zone was considered to be derived from precipitation at vegetated sites and predominantly groundwater at playa sites.

Isotopic groundwater signatures of oxygen-18 at ET sites were nearly constant at all but the PL1 site during the study period (fig. 19). Dilution of groundwater signatures at the PL1 site following heavy snowfall and subsequent melting during winter 2010 indicate that downward percolating snowmelt likely reached the water table as bypass flow along the observation well casing. In addition to the large change in water levels (fig. 12), support for bypass flow rather than downward percolation through the soil matrix is based on a large change in groundwater signatures relative to a small change in shallow soil water signatures. Shallow soil water (45–60 cm bls) signatures remained relatively constant (within 1 per mil during November 2009 and February 2010), whereas groundwater signatures decreased by nearly 6 per mil during the same period, indicating substantial dilution by more negative (depleted or lighter) water. Prior to this event, groundwater signatures varied seasonally by less than 0.25 per mil.

Table 12. Periodic daily measurements of eddy-covariance evaporation and groundwater fractions of near-surface soil water determined using end-member mixing with oxygen-18 and deuterium at playa 1 and playa 2 evapotranspiration sites, Dixie Valley, Nevada, May 2009–September 2011.

[**Evaporation:** Values not corrected for energy-balance closure. **Groundwater fraction of near-surface soil water:** Considered ambiguous if evaporative enrichment of near-surface soil water could be equally explained by enrichment of shallow soil water or precipitation signatures of oxygen-18 and deuterium. **Abbreviations:** mm, millimeter; PL1, playa 1; PL2, playa 2; –, no data]

Date	Evaporation (mm)		Groundwater fraction of near-surface soil water	
	PL1	PL2	PL1	PL2
May 20, 2009	0.27	0.14	0.73	Ambiguous
August 12, 2009	0.2	0.15	1	1
November 3, 2009	0.12	0.04	1	1
February 2, 2010	0.4	0.3	0.04	–
April 16, 2010	0.41	0.34	0.52	0.68
July 6–8, 2010	0.18	0.14	0.92	0.98
October 15, 2010	0.37	0.29	Ambiguous	Ambiguous
January 5, 2011	0.18	0.29	0.34	–
April 14, 2011	0.19	0.26	0.79	0.81
July 13, 2011	0.19	0.26	0.96	1
September 26–28, 2011	0.14	0.09	1	1

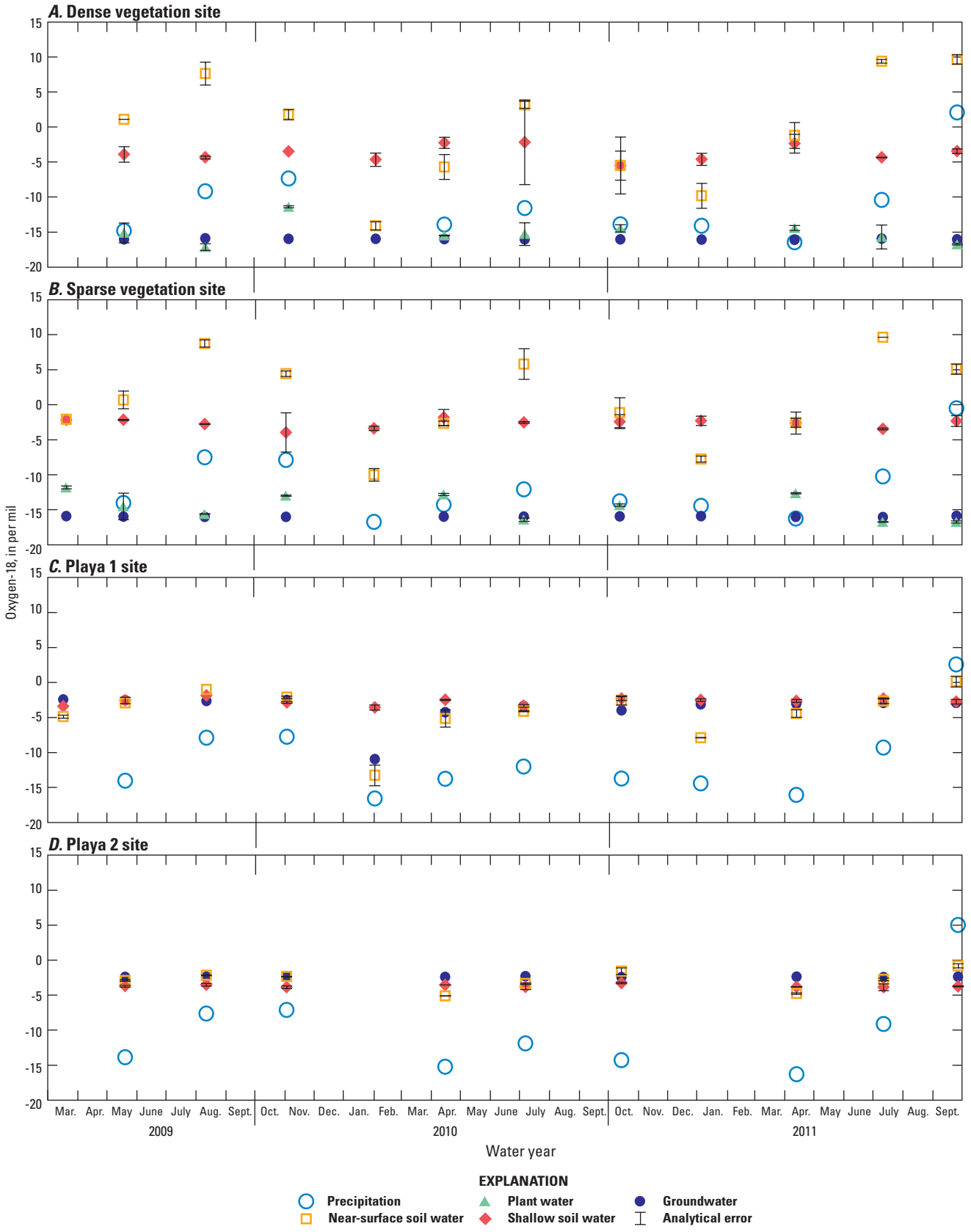

Figure 19. Periodic measurements of oxygen-18 in precipitation, near-surface (0–15 centimeters below land surface) and shallow (45–60 centimeters below land surface) soil water, plant stem water (greasewood), and groundwater at evapotranspiration sites, Dixie Valley, Nevada, March 2009–September 2011.

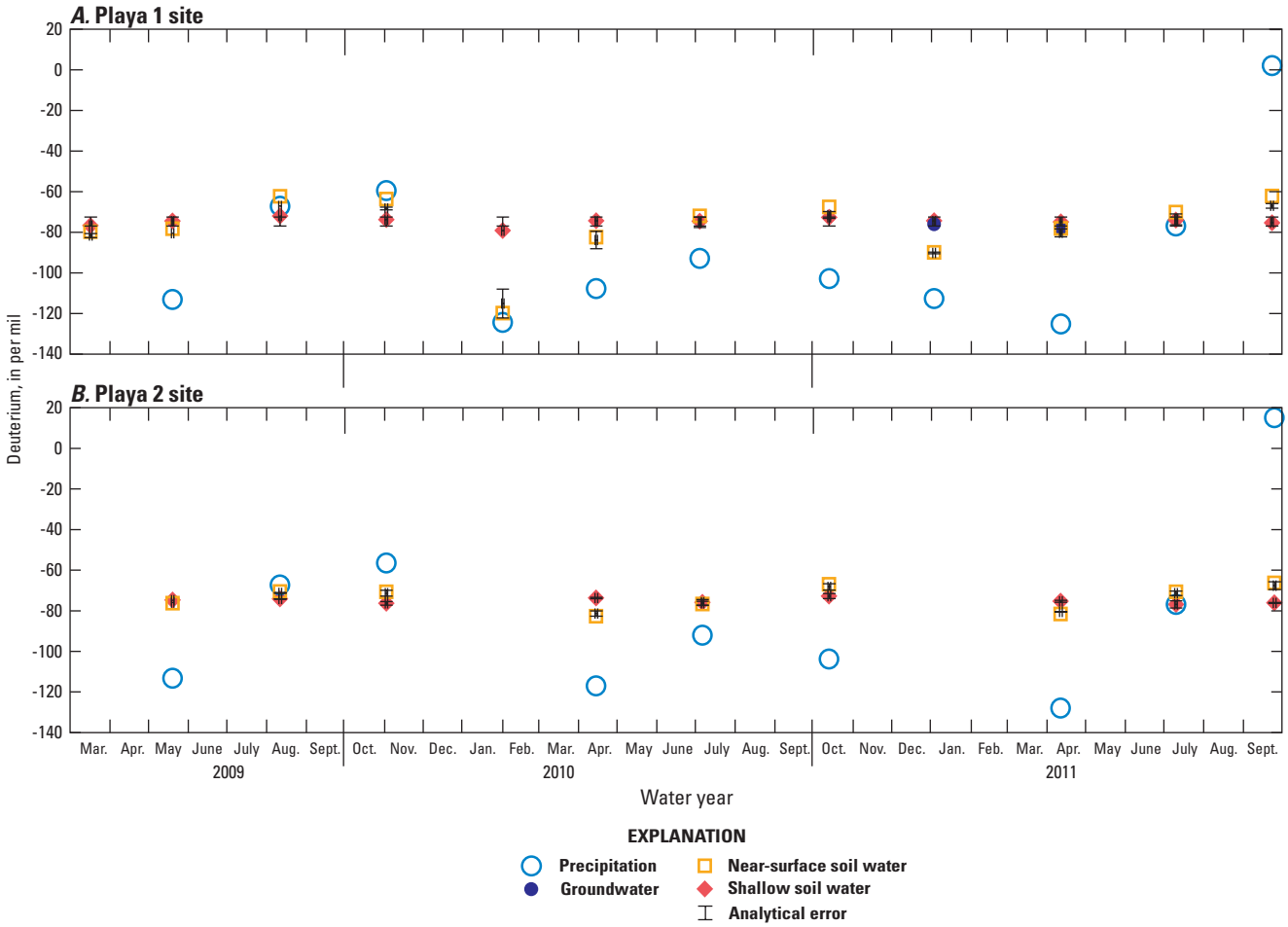

Figure 20. Periodic measurements of deuterium in precipitation, near-surface (0–15 centimeters below land surface) and shallow (45–60 centimeters below land surface) soil water, and groundwater at playa evapotranspiration sites, Dixie Valley, Nevada, March 2009–September 2011.

Following notable dilution at the PL1 site in February 2010, groundwater signatures gradually increased by 0.27 per mil from season to season (on average) over the next year (until about January 2011) as mixing with surrounding groundwater occurred. This slow recovery of groundwater signatures emphasizes the low conductivity of the playa material. Groundwater signatures at the PL2 site varied by less than 0.15 per mil during the study period and support a lack of downward percolation of precipitation to the saturated zone.

Playa deuterium signatures (fig. 20) followed trends similar to those of oxygen-18, with notable seasonal variations in precipitation and small variations in near-surface soil water. Groundwater signatures at the PL1 site are shown for the January and April 2011 sampling periods and were determined from distilled samples. A minimal difference between groundwater and shallow soil water samples supports the use of the shallow soil water as the groundwater end member in mixing models.

Binary mixing of groundwater and shallow soil water indicates that plants predominantly use groundwater throughout the year. Stem water signatures of greasewood varied slightly from season to season and typically were between shallow soil water (45–60 cm bls) and groundwater values (fig. 19). Signatures were most similar to groundwater during the summer months, and became slightly more positive (enriched) during the early spring, when ample shallow moisture was available, and during early autumn following precipitation. Groundwater fractions in greasewood plant-xylem water for the DV site ranged from 0.63 to 1.00, whereas those for the SV site ranged from 0.75 to 1.00 (table 11). Lower groundwater fractions typically corresponded with spring and autumn months, when precipitation-derived soil moisture content was greater than during other times of the year. These results indicate that greasewood consumption of groundwater is offset partially by consumption of readily available soil moisture when present.

Stem samples also were collected from big saltbush during July 2010 and 2011 to evaluate differences between phreatophytic shrub species at the DV site. Oxygen-18 signatures of big saltbush xylem water were about 1.4 per mil more positive (enriched) than those of greasewood, indicating that big saltbush used slightly less groundwater than greasewood at the time of measurement.

Groundwater fractions in big saltbush xylem water were within 2 percent of greasewood xylem water during July 2010 and within 10 percent in July 2011. Considering this slight variation and the dominance of greasewood in the study area, the groundwater fraction of transpiration was determined from greasewood.

The groundwater fractions of total ET (ratio of ET_g and ET, table 11) at the vegetated sites ranged from 0.09 to 0.87 for DV and from 0.14 to 0.67 for SV. These fractions were determined by (1) computing the transpiration fraction of total ET (equation 21) and (2) determining the relative proportion of transpiration attributed to groundwater (equation 22). Groundwater fractions of total ET were greatest during summer, followed by spring. During autumn, groundwater fractions typically were much lower because plants were nearly dormant and ET was influenced increasingly by evaporation of recent precipitation (fig. 14).

Groundwater fractions in near-surface (0–15 cm bls) soil water at the playa sites were determined from shallow soil water (used in place of groundwater because of the distillation effect on deuterium signatures) and precipitation source water end members using oxygen-18 and deuterium signatures (figs. 19–21, table 12). However, near-surface soil water signatures of both constituents often were more positive than shallow soil water (representing groundwater) and precipitation signatures. Greater near-surface soil water signatures often result from evaporative enrichment of precipitation- and groundwater-derived soil moisture. Therefore, the slope of the evaporative enrichment line (delineated from site-specific, near-surface soil water data) was used in combination with the end-member mixing to infer the more accurate source water (fig. 21). Slopes of evaporative enrichment lines were 3.7 at the PL1 site and 3.4 at the PL2 site (fig. 21), both of which are similar to corresponding slopes reported by Clark and Fritz (1997) for arid environments (3.9–4.2). During periods when evaporative enrichment of precipitation and deeper soil water (projected along the evaporative enrichment trend) equally could explain the near-surface soil water signature, groundwater fractions were considered ambiguous. For example, during October 2010, near-surface soil water signatures were more positive than shallow soil water signatures, and precipitation signatures fell along the soil water evaporative enrichment line; therefore, evaporative enrichment of precipitation and deeper soil water (projected along the evaporative enrichment trend) equally could explain the near-surface soil water signature. During summer (2009–11) and in November 2009, playa site precipitation signatures were much more positive than winter and spring precipitation signatures, but they did not plot along the evaporative enrichment line for soil water.

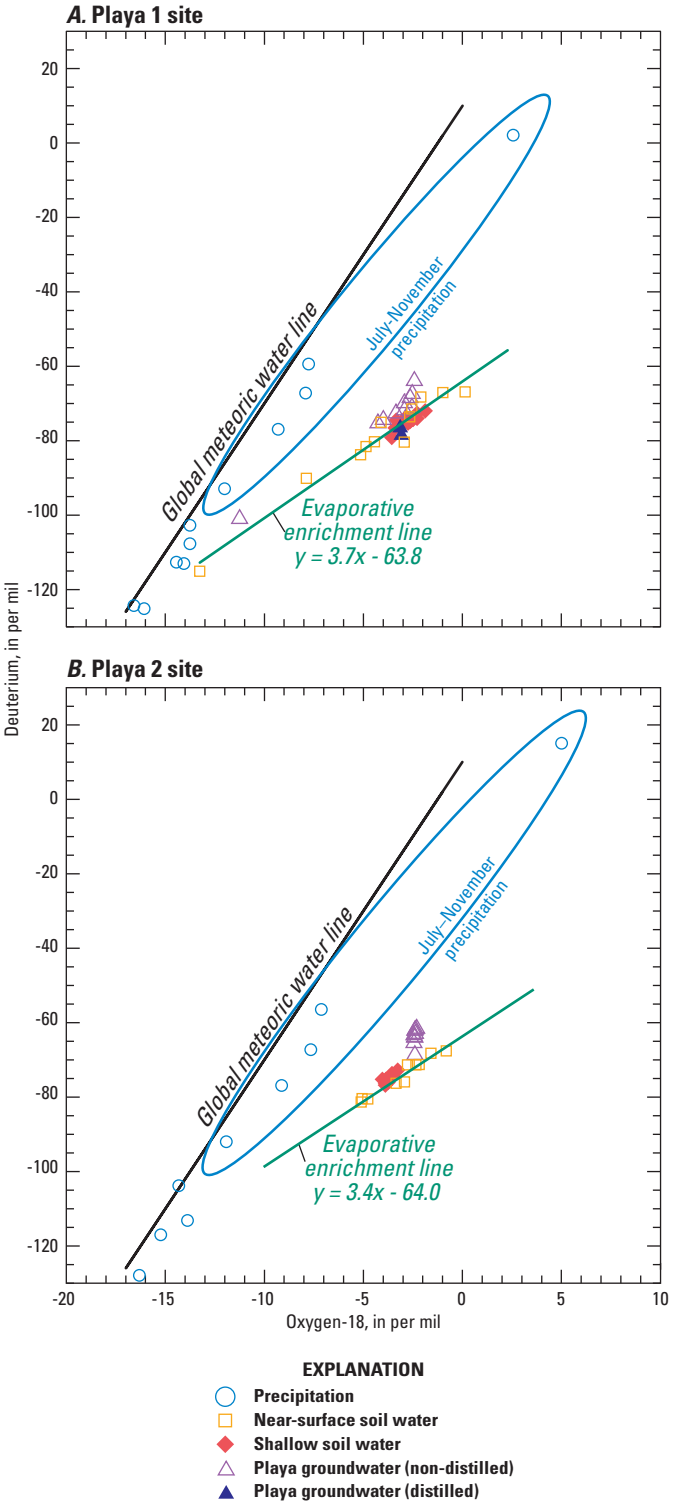

Figure 21. Comparison of deuterium and oxygen-18 measurements in precipitation, near-surface (0–15-centimeters below land surface) and shallow (45–60-centimeters below land surface) soil water, and groundwater at playa evapotranspiration sites, Dixie Valley, Nevada, March 2009–September 2011.

Near-surface soil water signatures during these periods were more positive than shallow soil water signatures, but continued to plot along the same evaporative enrichment line, indicating a groundwater source. Therefore, groundwater fractions during these periods were assigned a value of 1.

Periodic ET_g estimates were not made at playa sites because near-surface soil water signatures were likely biased toward groundwater. Isotopic signatures of near surface soil water represent the 15-cm bls integrated sample depth rather than the upper few centimeters of soil that likely contribute to evaporation. Near-surface water content (2–6 cm bls) along with water-content profiles (15–60 cm bls) and groundwater-level trends indicate that the playa soil is consistently near saturation and water content trends can be influenced by groundwater-level fluctuations (fig. 12). Small-to-negligible changes in near-surface soil-water content (2–6-cm bls) (fig. 6) indicate that precipitation percolation below this depth interval likely is small and evaporative penetration below this depth interval is minimal. Therefore, the integrated isotopic signature from the interval of 0–15 cm bls likely is skewed toward groundwater. The approach used in this study could be modified for future work on playas by limiting soil sampling to the upper 3–6 cm bls rather than the upper 15 cm bls.

Groundwater signatures at the PLW site were compared with ephemeral pond-water signatures and groundwater and soil water signatures at the playa ET sites to evaluate potential source waters (figs. 1 and 2, 22). All groundwater and standing water samples evaluated were grab samples (non-distilled); therefore, distillation effects on deuterium signatures were negligible between samples collected at the PLW site. Shallow and deeper groundwater signatures at the PLW site (sampled from depths of 30–60 and 180–240 cm bls, respectively) were similar at the time of measurement (September 2009), and temporal variability in shallow groundwater signatures was minimal (fig. 22).

Shallow groundwater signatures at the PLW site were nearly identical to ephemeral pond water sampled during April 2010 (fig. 22). Playa pond water is likely derived from precipitation as it only appears following winter precipitation events and the groundwater potentiometric surface typically is deepest during winter and spring and shallowest during summer months (fig. 12, appendix 1). Therefore, nearly identical isotopic signatures between PLW groundwater and pond water likely indicates that shallow groundwater near the PLW site is at least partially derived from ephemeral pond water. Samples of standing water beneath the salt crust and above land surface that were collected during August 2009 are more positive (enriched) than shallow PLW groundwater and pond water and help illustrate the local evaporative enrichment trend (fig. 22). Standing water that hydrates surface salt crusts and resides within and just below the crust during the summer months also is derived from pond water that likely became trapped beneath the crust following pond evaporation. Alternatively, this standing water could represent local groundwater discharge, where the groundwater reservoir was locally recharged by the pond earlier in the year.

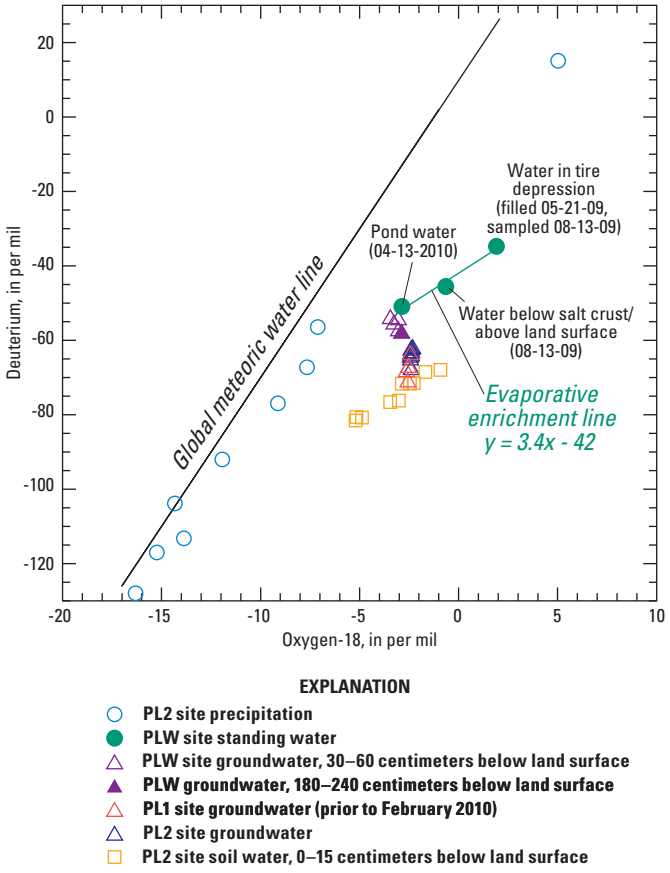

Figure 22. Comparison of deuterium and oxygen-18 measurements in groundwater and standing water at the playa-west (PLW) monitoring site; precipitation, near-surface (0–15 centimeters below land surface) soil water, and groundwater at the playa 2 (PL2) evapotranspiration site; and groundwater at the playa 1 (PL 1) evapotranspiration site, Dixie Valley, Nevada, March 2009–September 2011.

Shallow groundwater at the PLW site was an average of about 35 percent more negative (depleted) in oxygen-18 and 13 percent more positive (enriched) in deuterium than groundwater from PL1 and PL2 ET sites. In addition to salinity differences between sites and the "isotope salt effect" on deuterium signatures noted previously, Horita (2005) reported that evaporite dissolution could cause water to become progressively more negative (depleted) in oxygen-18 and more positive (enriched) in deuterium. Dissolution of the thick surface salt crust at the PLW site following pond inundation and (or) mixing with the sodium chloride deposit at the PLW site, which exists from 0.6 to 1.8 m bls (2 to 6 ft bls), could support the measured shift in isotopic signatures between the PLW site and playa ET sites.

Groundwater Discharge by Evapotranspiration—Basin Scale

Groundwater discharge in a basin most often occurs in low-lying topographic areas where groundwater is at or near land surface. Unlike regional recharge or subsurface flow, groundwater discharge (ET_g) is the only water-budget component that can be directly or indirectly measured. The discharge of groundwater to the land surface occurs by three natural processes: (1) spring and seep flow, (2) transpiration by local phreatophytic vegetation, and (3) evaporation from soil and open water. Many studies have shown that the amount and rate of water lost to the atmosphere by ET from groundwater discharge areas varies with vegetation type and cover, depth to water, and soil characteristics (Laczniak and others, 1999, 2001, 2006; Nichols, 2000). These and other recent studies have applied various remote-sensing techniques within groundwater discharge areas where satellite imagery, in combination with field mapping, was used to identify and group areas of similar vegetation and soil characteristics (Moreo and others, 2007; Smith and others, 2007; Laczniak and others, 2008). Evapotranspiration generally increases with increasing vegetation density and health, and soil wetness; therefore, these areal groupings are referred to as ET units because they are assumed to constitute areas with similar ET rates.

In this study, regional basin-scale groundwater discharge was estimated by (1) identifying and delineating the regional groundwater discharge area, (2) partitioning the discharge area into ET units using remotely-sensed imagery and field reconnaissance, and (3) relating ET units to site-scale ET_g estimates (see section, "Groundwater Discharge by Evapotranspiration—Site Scale"). Numerous studies have developed methods for direct ET and ET_g estimation from remotely sensed imagery and meteorological data (Bastiaanssen, 2000; Allen and others, 2007; Groeneveld and others, 2007). The approach used in this study differs from these methods; rather than directly predicting ET or ET_g rates from remotely sensed imagery, imagery in this study is used to characterize the distribution of vegetation and soil characteristics and to extrapolate local ET_g estimates (based on measured eddy-covariance and micrometeorological data) to the basin scale. Although improved significantly with modern instrumentation and methods, this basic approach has been used extensively by the USGS since the 1940s to estimate groundwater discharge from ET in Nevada.

Groundwater Discharge Area

The Dixie Valley groundwater discharge area (GDA; fig. 23) is characterized by phreatophytic vegetation along the boundaries and a non-vegetated playa in the center. The GDA boundary represents the transition from topographically upgradient xeric shrubs and a deeper unsaturated zone (typically 20 m bls or more), to a downgradient mix of xeric and phreatophytic shrubs and a shallower unsaturated zone. Vegetated areas in the GDA predominantly are composed of phreatophytic shrubs with smaller areas of grassland, xeric vegetation, bare soil, and agriculture where phreatophytic shrubs historically were present. The GDA was mapped using techniques similar to those used in studies throughout Nevada and eastern Utah (Nichols, 2000; Laczniak and others, 2001; Smith and others, 2007; Allander and others, 2009). National Agriculture Imagery Program (NAIP) imagery from 2006, a 10-m digital elevation model, water-level data, and a phreatophytic vegetation boundary established by Harrill and Hines (1995) were used in conjunction with field visits to delineate the GDA at a scale of about 1:24,000.

Harrill and Hines (1995) mapped the phreatophyte boundary and partitioned it into nine zones based on species composition and foliage-volume density as determined from 15 91-m line-transects measured across the valley. Partitioning was done by driving along established roads and mapping physical plant characteristics by visual inspection. In this study, David Groeneveld (HydroBio Advanced Remote Sensing, written commun., 2009) refined the Dixie Valley phreatophyte boundary mapped by Harrill and Hines (1995), and Groeneveld and Barz (2014) refined the transition between vegetated areas and the playa. The USGS used 2006 National Agriculture Imagery Program imagery to further refine the peripheral phreatophyte extent.

Using this initial refined GDA, 35 field reconnaissance locations were visited between June and August 2009 to verify the presence or absence of phreatophytic vegetation and to identify transition zones between phreatophytic and xeric vegetation. Dixie Valley is large and many areas are inaccessible to a standard vehicle because roads and trails are limited; therefore, field locations were selected based on accessibility. Each location was digitized into a geographic information system (GIS) dataset and road logs were kept using a Global Positioning System unit connected to a laptop computer running GIS software.

The final GDA was digitized into a GIS and was generalized and smoothed using ancillary datasets including 2006 NAIP imagery in areas where field reconnaissance was not conducted. The total GDA is composed of 65,007 ha (160,635 acres), which is similar to the area within the outer phreatophyte boundary delineated by Harrill and Hines (1995; 64,801 ha; 160,126 acres). Information regarding the GDA in digital format is available in appendix 7.

Evapotranspiration Units

Evapotranspiration units were characterized using a combination of vegetation indexes, brightness temperature, NAIP imagery, and field reconnaissance. Vegetation indexes and at-sensor brightness temperatures were calculated for

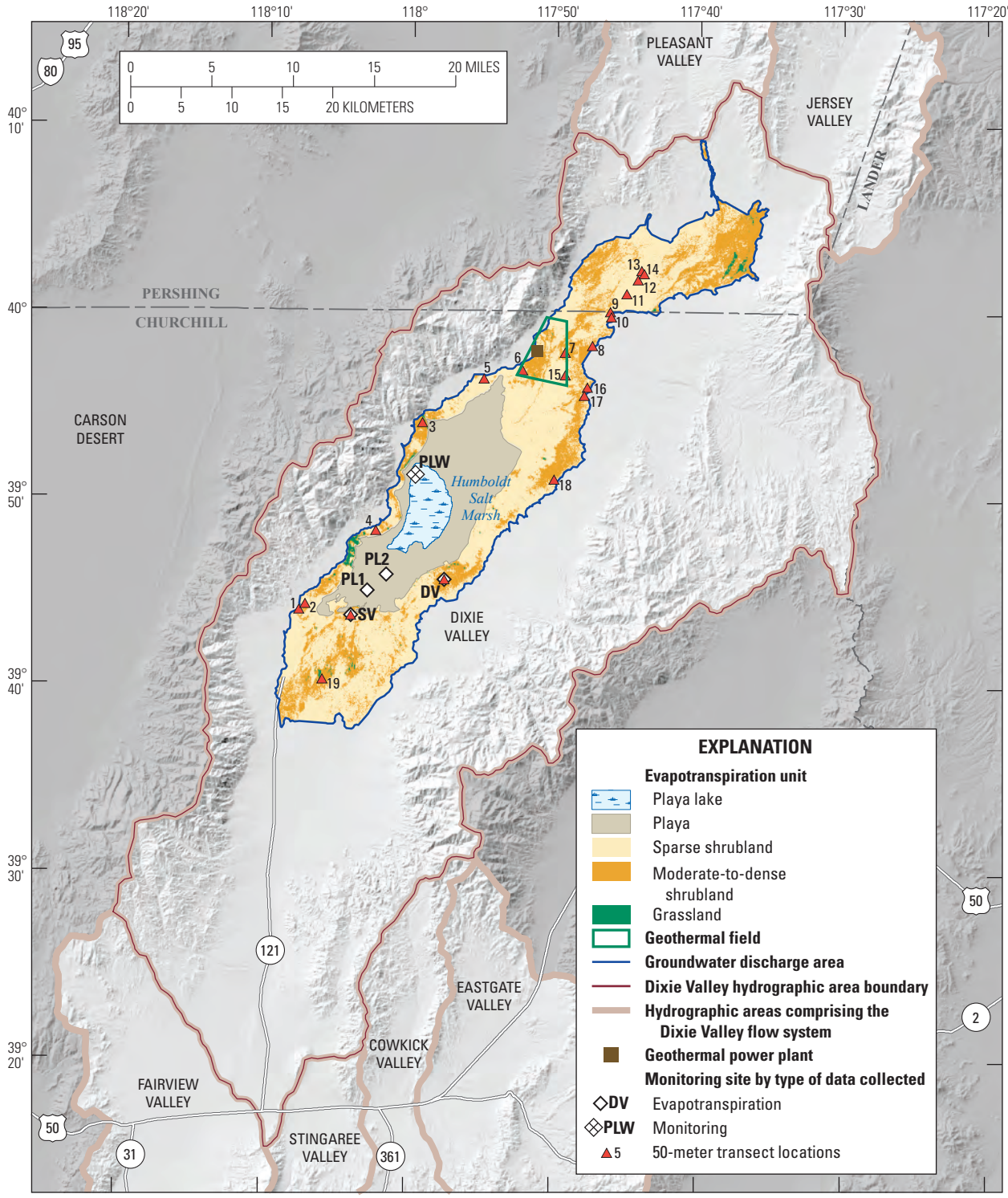

Base modified from 1:24,000-scale U.S. Geological Survey digital data, 2010. Shaded-relief base from 10-meter National Elevation Data, 2011. Universal Transverse Mercator, Zone 11, North American Datum of 1983

Figure 23. Evapotranspiration units for various vegetation and soil conditions and groundwater discharge area, Dixie Valley, Nevada.

Landsat scenes acquired across multiple dates prior to and during the study period. Vegetation indexes such as the NDVI are measures of leaf chlorophyll content, leaf area, canopy cover, and structure (Glenn and others, 2008). Brightness temperature measured at the satellite is a measure of the thermal emissions from the surface of the Earth and is directly related to actual surface temperature by the emissivity of the Earth. A combination of vegetation indexes and brightness temperature were assumed representative of vegetation type, cover, and volume within the GDA, and, therefore, were considered proportional to varying ET_g rates. Areas of anthropogenic disturbance (such as agriculture) were delineated and masked from computed images prior to ET unit delineation so that images were representative of pre-development surface conditions.

Landsat imagery has been used in several studies to characterize spatial and (or) temporal vegetation patterns, green leaf vegetation cover, and relations between vegetation and surface temperature (Goward and others, 1985; Price, 1990; Lambin and Ehrlich, 1996; Laczniak and others, 1999; Nichols, 2000; Berger and others, 2001; Groeneveld and others, 2007; Smith and others, 2007). Landsat is a group of Earth-observing satellites, the first of which was launched in 1972. Seven Landsat satellites have been successfully launched into orbit. Each Landsat satellite was equipped with one or more sensor instruments designed to collect imagery in several distinct spectral bands in reflective visible and infrared wavelengths, and in emitted thermal wavelengths (U.S. Geological Survey, 2012a). Between 2003 and the launch of Landsat 8 in 2013, Landsat 5 was the only fully functional satellite remaining in orbit. Therefore, imagery acquired by the Thematic Mapper (TM) instrument aboard Landsat 5 was used for this study. The TM instrument collects information in six spectral bands with wavelengths ranging from the visible blue (0.45 µm) to the short-wave infrared (2.35 µm), and in an additional seventh band with thermal infrared wavelengths between 10.4 and 12.5 µm. Continuous 180 km-wide swaths of TM imagery are broken into overlapping "scenes" of about 170 km in length. Each scene is imaged by the sensor every 16 days at 30-m spatial resolution (120 m for the thermal channel) and covers about 31,110 km^2. Landsat 5 TM scene locations are identified using a world reference system 2 path and row number. Dixie Valley is located within world reference system 2 path 42 row 32.

A combination of bands from TM scenes were used to identify and characterize natural and anthropogenic features within the image. For example, healthy vegetation absorbs light for use in photosynthesis in the red wavelengths collected in TM band 3 (TM3; 0.63–0.69 µm) and strongly reflects light in the near infrared wavelengths collected in TM band 4 (TM4; 0.76–0.90 µm). Vegetation indexes such as the Normalized Difference Vegetation Index (NDVI; Rouse and others, 1974), the Modified Soil-Adjusted Vegetation Index (MSAVI; Qi and others, 1994), and the Enhanced Vegetation Index (EVI; Huete and others, 1999) use the contrast between these distinct absorption and reflectance features to help identify vegetated areas and to characterize the health and spatial extent of vegetation communities. TM band 6 (TM6; 10.4–12.5 µm) records thermal infrared electromagnetic energy emitted from the earth's surface and can be used as an indicator of healthy vegetation. Surfaces with dense or healthy vegetation generally are cooler than surrounding surfaces covered with bare soil or sparse vegetation because of evaporative cooling from plant transpiration (Goward and others, 1985). Measured thermal emissions, therefore, often are inversely related to the amount of vegetation present in a scene.

Satellite Image Processing

Eight Landsat scenes collected during the study period (June 2009–August 2011) and one historical scene (August 2007) were acquired for ET unit delineation and ET_g estimation (table 13). These scenes represent a subset of available scenes where skies were free of clouds, vegetation canopies were green and active, and little to no antecedent precipitation was measured at nearby weather stations. All scenes were acquired by the TM sensor aboard Landsat 5 in the summer months to represent "growing-season" conditions when phreatophytic vegetation within the GDA is actively transpiring and shrubs have reached maximum growth.

Table 13. Coefficients of determination describing relations between phreatophytic shrub canopy cover and vegetation indexes, brightness temperature, and the ratio of the enhanced vegetation index to brightness temperature, Dixie Valley, Nevada, 2007–11.

[Phreatophytic shrub canopy cover values are shown in table 14. **NDVI:** normalized difference vegetation index. **MSAVI:** modified soil-adjusted vegetation index. **EVI:** enhanced vegetation index. T_B**:** brightness temperature. **EVI/**T_B**:** temperature normalized EVI]

Landsat scene dates	Regression statistic–coefficient of determination (r^2)				
	NDVI	MSAVI	EVI	T_B	EVI/T_B
08-08-07	0.71	0.75	0.76	0.70	0.83
06-26-09	0.62	0.59	0.65	0.61	0.78
07-28-09	0.65	0.59	0.60	0.68	0.71
07-15-10	0.53	0.49	0.57	0.60	0.71
07-31-10	0.57	0.51	0.63	0.62	0.74
08-16-10	0.53	0.48	0.60	0.64	0.75
07-02-11	0.47	0.46	0.53	0.58	0.71
08-03-11	0.49	0.47	0.56	0.62	0.72
08-19-11	0.34	0.35	0.50	0.55	0.75

Atmospheric Correction

The Landsat TM images were calibrated to top of atmosphere (TOA) reflectance (Chander and others, 2009) to remove the effects of varying sun angles, Earth-to-Sun distances, and TM sensor parameters. Sun elevation angles were calculated on a 1.5-km grid to avoid abrupt changes in sun angle at image borders. Although calibration to TOA reflectance eliminates image variation caused by astronomical and sensor calibration coefficients, it does not correct for atmospheric scattering and absorption. The effects of atmospheric scattering and absorption present in the TOA reflectance data were removed by applying date- and band-specific empirical calibration models to each band of the selected TM scenes. The models predicted apparent surface reflectance from TOA reflectance values for each scene and were defined using surface reflectance measurements of temporally stable calibration targets acquired from a low-flying aircraft and from ground measurements as described by David E. Eckhardt, Bureau of Reclamation, written commun., (2014). The resulting correction to apparent surface reflectance improves image correlation with surface biophysical parameters.

Calculation and Evaluation of Vegetation Indexes

NDVI, MSAVI, and EVI were calculated from each of the eight atmospherically corrected 2007–11 summer images. Calculation of these vegetation indexes results in a unitless single-band image with valid values between -1 and 1. Index values in vegetated areas nearly always are greater than 0 and, generally, the healthier and denser the vegetation, the higher the vegetation index value. Vegetation indexes that are based on a simple combination of the near-infrared and red wavelengths such as the NDVI are sensitive to the quantity of green leaf vegetation in a scene, but also are influenced by the composite background reflectance of the soil surface, plant litter, and woody plant material, particularly in areas of moderate-to-sparse vegetation cover. Huete and Jackson (1987) determined that vegetation indexes over discontinuous canopies such as those in this study area changed as a result of the reflectance factors of the underlying soil and the presence of senesced grasses, woody plant material, and leaf litter. Soil color, water content, and surface roughness can affect soil reflectance in all wavelengths from the blue to the shortwave infrared (Rondeaux and others, 1996), and these effects can create soil-induced influences on vegetation index values (Huete, 1988). The MSAVI is one of a group of vegetation indexes that use a canopy background adjustment factor to reduce the influence of soil and background reflectance on the index to increase the signal from healthy vegetation in the image. Qi and others (1994) proposed the MSAVI as a modification of the Soil Adjusted Vegetation Index (SAVI; Huete, 1988). The SAVI incorporated background adjustment factor, L, into the NDVI equation. In the SAVI, the optimal value of L can vary with vegetation cover but Huete (1988) determined that setting L equal to 0.5 reduced soil noise throughout a wide range of vegetation densities. The MSAVI introduced an inductive L function to the index and eliminated the need to specify a soil adjustment factor.

The EVI is a combination of the SAVI and the Atmospherically Resistant Vegetation Index (ARVI; Kaufman and Tanre, 1992). The combined indexes include an adjustment for canopy background effects derived from the SAVI and a correction for the effect of atmospheric aerosols from the ARVI. The atmospheric aerosol correction factor uses reflectance from the blue wavelengths measured in TM band 1 (TM1, 0.45–0.52 μm) and reduces the effect of smoke and haze in the atmosphere. The EVI does not reach maximum intensity or "saturate" as rapidly as the NDVI in dense vegetation and it has been shown to be well correlated with photosynthesis and plant transpiration in many studies (Glenn and others, 2008).

Each of the three vegetation indexes (NDVI, MSAVI, and EVI) was evaluated for its effectiveness in estimating phreatophytic shrub cover within the Dixie Valley GDA, which is assumed to be directly proportional to ET_g. Different vegetation species at 100 percent cover can have different vegetation index values as a result of varying chlorophyll content, internal leaf structure, and canopy structure (Glenn and others, 2008). In combination, these variations can reduce the significance of relations between the vegetation index and vegetation cover. NDVI, MSAVI, and EVI were calculated from each of the eight Landsat scenes and area-weighted means of vegetation index values were compared with field-based measurements of phreatophytic shrub cover across the GDA. Phreatophytic shrub cover was measured at 21 locations during mid-June 2010 using the line-transect method (table 14; Smith, 1974). At each location, vegetation type and canopy height measurements were made along four 50-m transects extending north, west, south, and east from a central point. The length of green (active) plant canopies overlying line transects also was measured and used to compute percent canopy cover. Bare soil cover included gaps between plants and within plant canopies. Percentages of canopy cover were computed as the ratio of the sum of individual measured canopy lengths across all four transects to the total transect length (200 m), and is assumed to apply to the entire plant community on an areal basis. Canopy cover of phreatophytes was computed using canopy lengths only from phreatophytes. Transect measurements made at the SV and DV ET sites were truncated from 100 m (table 6) to 50 m in each direction for comparison with the 19 other measurement locations (table 14) and with vegetation indexes. Measurement locations predominantly were positioned in sparse to moderately vegetated areas as are most characteristic of the GDA, with fewer locations characterizing dense vegetation cover. Although 19 of the 21 locations were measured only in June 2010, canopy cover-measurements for phreatophytic shrubs are assumed to remain fairly constant (within a few percentage points; table 6) from year to year. Mean vegetation

Table 14. Vegetation type, canopy cover, and height measured from 21 locations across the groundwater discharge area, Dixie Valley, Nevada, June 14–18, 2010.

[**Transect No./site:** Measurement locations shown in figure 23. DV, dense vegetation; SV, sparse vegetation. **Canopy cover:** Canopy cover for all four transects divided by the total transect length (200 m); canopy cover was estimated from additive measurements of the vertical projection of green (active) plant canopies overlying line transects. Total canopy cover includes phreatophytic and xerophytic shrubs and forbes. **Mean height:** Mean plant canopy height. **Abbreviations:** m, meter; –, no data]

Transect No./site	Canopy cover (percent)			Shrubs						Forb
				Greasewood		Rabbitbrush		Big Saltbush		Seepweed
	Total	Phreatophytic shrubs	Phreatophytic shrubs and forbs	Canopy cover (percent)	Mean height (m)	Canopy cover (percent)	Mean height (m)	Canopy cover (percent)	Mean height (m)	Canopy cover (percent)
1	7.8	5.7	7.8	5.4	1.0	0.3	–	0	–	2.1
2	8.5	5.2	8.2	4.9	0.6	0.3	–	0	–	3.0
3	21.8	16.7	21.8	15.0	0.7	0	–	1.6	0.9	5.1
4	9.1	3.0	4.6	3.1	0.4	0	–	0	–	1.6
5	12.1	6.8	9.5	4.4	0.7	1.6	0.7	0.8	0.5	2.7
6	8.1	6.4	7.8	6.4	0.9	0	–	0	–	1.4
7	39.9	38.4	39.9	31.6	1.0	4.2	1.0	2.6	0.8	1.5
8	14.4	5.3	12.7	5.3	0.7	0	–	0	–	7.4
9	3.2	1.5	2.5	1.5	0.8	0	–	0	–	1.0
10	9.2	2.0	6.6	2.1	0.7	0	–	0	–	4.6
11	18.7	7.1	7.1	7.1	0.6	0	–	0	–	0
12	6.6	0.5	1.3	0.5	0.5	0	–	0	–	0.8
13	11.1	2.7	7.1	2.7	0.6	0	–	0	–	4.4
14	0	0	0	0	–	0	–	0	–	0
15	8.2	4.6	6.1	3.2	0.7	1.5	0.7	0	–	1.5
16	12.3	5.5	10.8	5.5	0.6	0	–	0	–	5.3
17	6.5	3.6	6.0	3.7	0.6	0	–	0	–	2.4
18	7.5	2.4	7.5	2.4	0.4	0	–	0	–	5.1
19	23.9	17.1	21.0	9.2	0.8	3.5	0.7	3.2	0.8	3.9
DV[1]	31.7	23.3	31.7	20.4	0.8	0	–	2.9	1.0	8.4
SV[1]	8.4	7.9	8.4	7.9	0.6	0	–	0	–	0.4

[1]Measurements were truncated from 100 m (table 6) to 50 m for comparison with the 19 other measurement locations and with mean vegetation index values determined using a 45-m radial buffer around the central measurement point.

index values for each location were determined by creating a 45-m radial buffer around each point location in a GIS and calculating the area weighted mean of values within the buffered area. Ordinary least squares relations indicate that vegetation indexes were a better gage of phreatophytic shrub cover than total vegetation cover for all images evaluated, and that phreatophytes in Dixie Valley provide a stronger signal than xerophytes.

The EVI showed the best coefficient of determination (r^2) among the different vegetation indexes relating vegetation index value and phreatophytic shrub cover for all scenes (table 13). NDVI and MSAVI coefficient of determination (r^2) values were comparable, differing by less than 0.07 for all scenes. Between 2007 and 2010, EVI images showed r^2 values of greater than 0.55 (table 13). The 2011 EVI images had r^2 values ranging from 0.50 to 0.56. Based on the relation with transect data, EVI was selected as the preferred vegetation index for use in delineating ET units and upscaling ET_g estimates to the basin level.

Coefficients of determination describing the relation between vegetation indexes and phreatophytic shrub cover decreased from 2007 to 2011. This decrease in the ability of vegetation indexes to predict phreatophytic shrub cover likely was a result of *Bromus tectorum* (cheat grass), late season forbs, or other factors that can confound the vegetation index. The temporally degrading trend in r^2 among all indexes analyzed typically was caused by transect measurements from sparsely vegetated areas (less than 10 percent phreatophytic shrub cover), especially in areas located along the GDA periphery. David E. Eckhardt, Bureau of Reclamation, written commun., (2014) observed senesced annual grasses near the northern GDA boundary in September 2012, and noted that this area showed elevated NDVI values in the 2010 scenes relative to the other years evaluated. Field observations made in this study and between-year scene comparisons confirmed the presence of elevated vegetation index values and annual plants along most of the GDA periphery. The GDA periphery is characterized by sparse shrub cover where vegetation is

transitioning from phreatophytes to xerophytes. Vegetation indexes from each year were compared within and adjacent to the GDA by subtracting late July or early August images from the 2007 baseline image. August 2007 was selected as the baseline image because it consistently showed the best relation among vegetation indexes and phreatophytic shrub cover, and the 2006–07 water year was drier than average (Western Regional Climate Center, 2012), which minimized the presence of annual grasses and late season forbs. Overall, inter-annual comparisons indicated that pixels with vegetation index values greater than the 2007 baseline typically were located along the GDA periphery during 2009–11. These observations and comparisons emphasize the potential effects of senesced grasses (Huete and Jackson, 1987), increased leaf area on xerophytic shrubs, and actively photosynthesizing late season forbs on the vegetation indexes, particularly in 2010 and 2011. Variability within and beyond the GDA is assumed to result from similar phenomena.

Spatial and temporal variability in vegetation indexes also can result from biological soil crusts. Biological soil crusts were observed at 12 of the 21 transect locations, occurring in both sparsely and densely vegetated areas. Karnieli and others (1996) observed that biological soil crusts composed of mosses, lichens, algae, and cyanobacteria can show relatively high vegetation index values in sparsely vegetated areas where little to no photosynthetic activity by larger plants exists. They also noted that biological crusts are active when their substrate is wet and dormant when their substrate is dry. Crusts can become active for several days after precipitation or for several hours after dew formation during the night and early morning (Karnieli and others, 1996). Higher vegetation indexes resulting from intermittent photosynthesis in active biological crusts (when compared with dormant crusts) might partially explain the somewhat weaker relation (r^2) among phreatophytic shrub cover and vegetation indexes shown in table 13 ($\leq$0.76) and the variability between image years. However, because crusts remain active only for hours to days, their effects on vegetation indexes likely are related to spatial variability instead of temporal variability.

Brightness Temperature

Temperature information derived from Landsat 5 band TM6 was evaluated as a means to dampen variability in the calculated vegetation indexes owing to the effects of biologic soil crusts, forbs, and cheat grass on the calculated vegetation index, and to improve the relation with phreatophytic shrub cover. Objects on the surface of the Earth that have a temperature greater than absolute 0 (0 K) emit thermal electromagnetic radiation in the thermal or longwave (8.0–14 µm) part of the electromagnetic spectrum (Jensen, 2005). Most thermal sensing is done in the 8–14 µm part of the emitted electromagnetic spectrum because this is where peak energy emissions for most surface features occur (Lillesand and others, 2008). Past studies (Goward and others, 1985; Price, 1990; Lambin and Ehrlich, 1996; Sandholt and others, 2002) investigating biophysical controls on the surface temperature (T_S) of the Earth observed a negative correlation between vegetation indexes (such as NDVI) and T_S. These studies suggest that the relation generally is indicative of evaporative cooling resulting from plant transpiration or a cooler surface resulting from plant canopy shading. Vegetation, through the process of transpiration, considerably enhances evaporative fluxes to the atmosphere and greater vegetation cover should be associated with increased latent heat losses and a reduction in surface temperature (Goward and others, 1985). Similarly, shading caused by taller plant canopies can reduce surface temperatures relative to short canopies. These phenomena were measured at vegetated ET sites through net-longwave radiation measurements (data not shown), which are indicative of surface temperature. Net-longwave radiation measurements at the SV site (7.3 percent vegetation cover) averaged about 11 percent greater (more negative) than net-longwave radiation measurement at the DV site (24.8 percent vegetation cover), indicating that surface temperatures at the SV site also were greater than at the DV site. Surface temperature also might be a better indicator of plant stress than are vegetation indexes. Vegetation can remain green for some time after initial water stress, although surface temperature can increase rapidly under the same conditions (Sandholt and others, 2002). Phreatophytes in the study area GDA are not as water limited as surrounding sparsely distributed xerophytes, late season forbs, and biologic soil crusts. Therefore, phreatophytic vegetation should transpire more regularly than more water-stressed vegetation types growing in comparable soil regimes, even while potentially showing similar vegetation index values. Because of increased transpiration, T_S measured over phreatophytic vegetation in the study area is assumed to be cooler than T_S over non-phreatophytic land-cover types. Additionally, surface albedo in sparsely vegetated areas, which is affected by soil color, can greatly affect soil temperature. In sparsely vegetated areas with low albedo and dark soil cover, surface temperatures likely are greater than in areas with similar vegetation cover and lighter soil cover.

Top of atmosphere brightness temperature (T_B, degrees Celsius) data calculated from TM6 for the 10 Landsat scenes evaluated for this study were acquired from the Landsat Ecosystem Disturbance Adaptive Processing System (LEDAPS; U.S. Geological Survey 2012b). Brightness temperature from LEDAPS is calculated from standard equations presented in Chander and others (2009) (C. Jenkerson, U.S. Geological Survey Earth Resources Observation and Science Center (EROS), written commun., February 15, 2013). Radiant temperature in the form of T_B was considered a first-order approximation of the effects of plant transpiration on temperature. Brightness temperature measured at the satellite is a measure of the thermal emissions

from the surface of the Earth, but includes contributions from atmospheric absorption and emission in the thermal wavelengths. These atmospheric contributions were assumed to be insubstantial for the purposes of this study.

Brightness temperature is related to T_S by the emissivity (ε) of the object or body being measured:

$$T_S = \frac{T_B}{\varepsilon^{0.25}} \quad (26)$$

Emissivity is the ratio between the actual radiance emitted by a real-world selectively radiating body and a blackbody at the same thermodynamic temperature (Jensen, 2005). All selectively radiating bodies have emissivities ranging from 0 to 1 so that T_S is always equal to or greater than T_B. Although emissivity variation between different surface materials affects surface temperature values, remotely sensed radiative temperatures generally are good indicators of true surface temperatures (Goward and others, 1985). For the purpose of this analysis, T_B is considered adequate to convey relative differences between the surface temperatures of phreatophytes, annuals, forbs, and biologic soil crusts. Temperatures surrounding moderately dense stands of phreatophytes should be lower than those surrounding annuals, forbs, and biologic soil crusts because phreatophytes typically are taller and less water stressed. Similarly, temperatures surrounding darker crust- or gravel-covered soil in sparsely vegetated areas likely are higher than temperatures surrounding lighter soil.

Coefficients of determination describing the relation of phreatophytic shrub cover to T_B values were comparable to those determined for the multiple vegetation indexes, and ranged from a high of 0.70 for the August 8, 2007, scene to a low of 0.55 for the August 19, 2011 scene (table 13). Mean T_B values also were determined from a 45-m radial buffer operating on 30-m pixels resampled from the native 120-m pixels in the thermal band on the TM sensor.

Factors such as soil albedo and moisture (Friedl and Davis, 1994), emissivity of materials within a scene, and surface roughness can increase or decrease the actual T_S independently of transpiring green vegetation. For example, a decrease in green vegetation typically causes an increased surface albedo over bright soil, which, in turn, reduces surface heating. The effect of albedo on surface heating is small compared to latent heat exchanges associated with evapotranspiration in well-watered landscapes (Goward and others, 1985; Lambin and Ehrlich, 1996), but albedo effects are not fully understood in the more arid conditions of the study area. The magnitude of reduced surface heating from high-albedo soils relative to the energy of latent heat exchanges in moderate-to-dense phreatophytic vegetation is not well known but is assumed to be small. In areas with less than 10 percent plant cover, reduced surface heating from soil albedo could be much larger than in areas of moderate-to-dense plant cover. Spectral vegetation indexes also are adversely affected by soil background effects in low-density vegetation. Huete and others (1984) determined that soil noise in spectral indexes restricts reliable discrimination of green vegetation in areas with soil-type variations where plant cover is less than 25 percent. Soil moisture effects on brightness temperature were assumed to be small because near-surface soil -water content in vegetated areas generally was low during the summer (fig. 6) Surface roughness increases with vegetation height, resulting in greater turbulent exchange of water and sensible heat above the canopy. Vegetation height also increases surface shading, which can reduce surface temperature. Areas with taller (above 0.5 m) phreatophytic shrubs, therefore, likely are cooler than areas with short (below 0.25 m) non-phreatophytic vegetation cover because of greater surface roughness and turbulent or evaporative exchange with the atmosphere. Areas dominated by darker soils and biologic soil crusts are assumed to have higher brightness temperatures than areas with either lighter soils or vegetation cover.

Normalization of Vegetation Index with Brightness Temperature

The T_B data (degrees Celsius) were combined with EVI by dividing each EVI image by the TM6 T_B image calculated from the same scene, and multiplying the resulting image values by 1 million (to maintain data precision). Temperature-normalized EVI (EVI/T_B) images were evaluated against the transect data using a 45-m radial buffer and calculating the weighted mean of the EVI/T_B values as previously described in section, "Calculation and Evaluation of Vegetation Indexes."

The ordinary least squares relation with transect data improved using EVI/T_B as compared to either EVI or T_B alone so that all r^2 values were greater than 0.70 (table 13). The use of EVI/T_B also reduced the scatter in r^2 between the images analyzed because the EVI/T_B ratio likely lowered the vegetation index in "hotter" areas of forbs, cheat grass, bare soils, and (or) biological crusts with less effect in the relatively cooler phreatophytic vegetation or higher-albedo background soils. Despite this improvement, the capability of vegetation indexes, brightness temperature, or the combination of each to estimate variations in phreatophytic shrub cover was shown to degrade with decreasing cover for all image combinations analyzed.

Mean summer (late June–August) EVI/T_B images for each year were used to additionally reduce temporal and spatial variability in the imagery. The 2007 scene was left as a single image because it was the only cloud-free summer image available during that year. Relations between EVI/T_B and annual summer mean scenes are shown in figure 24 and highlight the weak relation at phreatophytic shrub canopy covers of less than 10 percent.

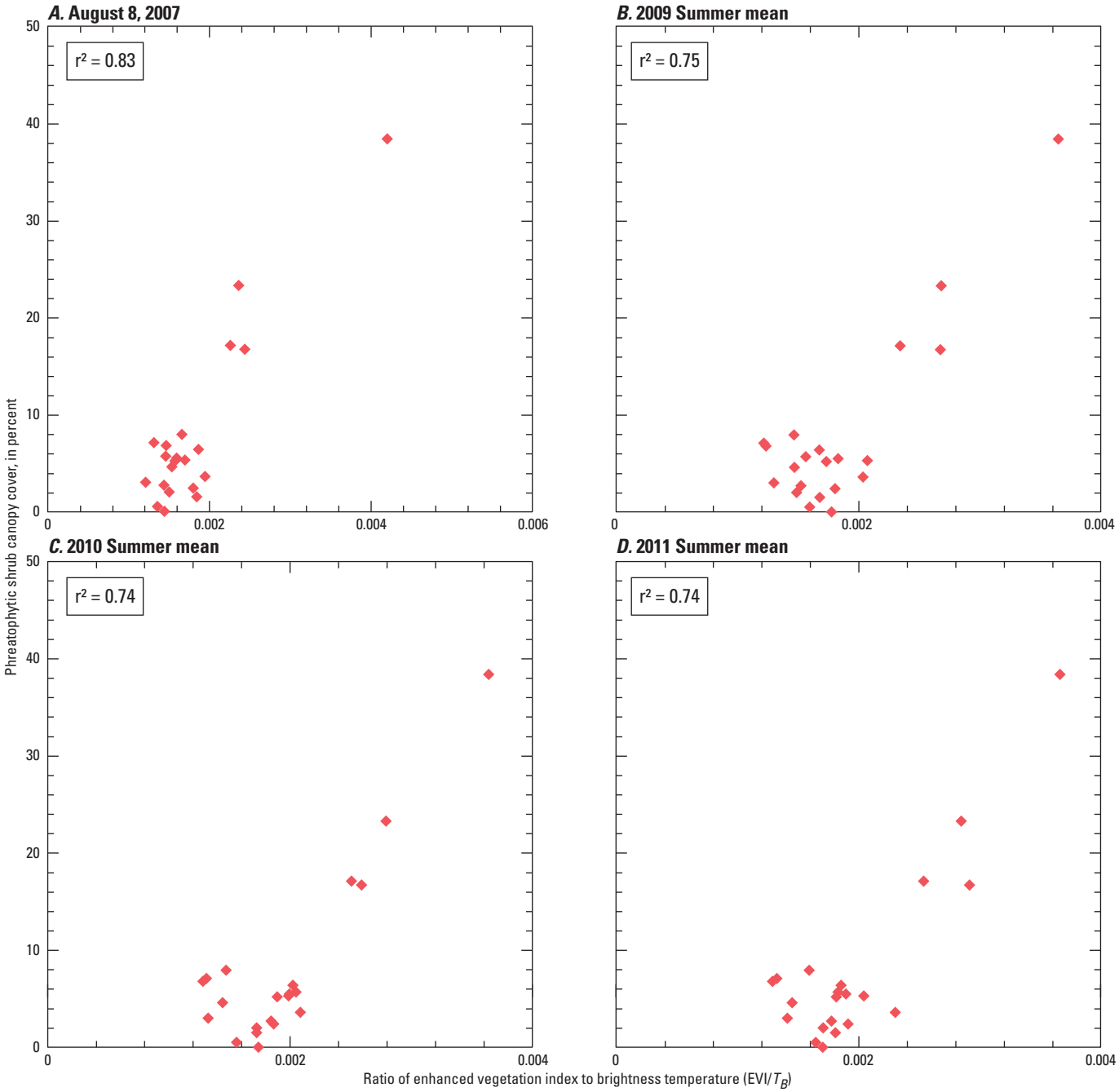

Figure 24. Relation between phreatophytic shrub canopy cover measured at 21 transect sites and the ratio of enhanced vegetation index to brightness temperature for (*A*) August 8, 2007, and (*B*) 2009, (*C*) 2010, and (*D*) 2011 summer mean images, Dixie Valley, Nevada. Transect sites are shown in figure 23. Relation is described by the coefficient of determination (r^2).

Characterization of Pre-Development Surface Conditions

Water managers typically rely on perennial yield determinations based on natural, pre-development, steady-state groundwater budgets. For a groundwater system in steady state, pre-development ET_g can represent long-term natural recharge to the system. For this reason, ET_g rates estimated in this study were computed so that they were representative of the pre-development, long-term ET_g rates occurring within the study area.

Characterization of pre-development surface conditions in the study area required that areas disturbed by agricultural activities (during this study and historically) or geothermal energy production within the GDA be delineated and masked from the EVI/T_B images. Masked areas were delineated using a combination of NAIP and Landsat TM imagery. Irrigated agriculture, meadows and riparian areas surrounding flowing wells in the agricultural settlement south of the playa, and potential historical agricultural areas characterized by rectilinear shapes that were markedly different from surrounding vegetation patterns were identified and delineated from uncalibrated Landsat scenes collected between 1972 and 2011. NAIP imagery from 2006 and 2010 was used to refine the Landsat-determined boundaries, to identify potential historical agricultural areas that were not apparent in Landsat scenes, and to delineate surface areas disturbed by geothermal activity or development. EVI/T_B values for the masked areas were computed from the surrounding undisturbed areas by filtering the EVI/$_B$ data using a sequence of averaging filters to progressively move smoothed valid data from the perimeter of the masked areas into the masked areas. Pre-development masks were considered sufficient to remove the effects of anthropogenic disturbance. These pre-development filtered scenes were used in conjunction with ancillary data to identify ET units within the GDA. The total anthropogenically disturbed area in the Dixie Valley GDA represents less than 3 percent of the GDA or 1,793 ha (4,430 acres). Recently (2009–11) irrigated cropland covers 490 ha (1,212 acres) within the GDA.

Groundwater discharge by artesian and irrigation wells was assumed to have little effect on phreatophyte cover at the land surface beyond areas influenced directly by surface discharge and discharge runoff from these wells. Near the historical agricultural settlement south of the playa, water levels measured between 1950 and 2010 show no clear increasing or decreasing trends among wells (Huntington and others, 2014). The local shallow basin-fill aquifer is interfingered with several clay layers that persist at general depths of 5–10, 15–30, and 45–70 m bls, creating localized confined systems and potential perched aquifers (Huntington and others, 2014). The shallow water table that supplies groundwater to local phreatophytic vegetation ranges in depth from about 1.5 to 6.1 m bls, whereas most of the nearby artesian wells are screened from 38 to 46 m bls. Therefore, water flowing from artesian wells likely originates from deeper, and in some cases, hydraulically separate water-bearing units and likely is not compensated for by a reduction in pressure heads within the shallow water-bearing units, above which ET_g is occurring. In areas where pressure heads might have been reduced, the depth to the saturated zone likely has remained unchanged as a result of the confined aquifer system. This is supported by field observations and nearby vegetation-cover measurements, which show no indication of a vegetation die-off that might be an expected result of a rapidly increasing saturated zone depth.

Near agricultural areas along the northern GDA boundary, greasewood was mapped at water-table depths of as much as 30.5 m bls (100 ft bls). This area is characterized by grassland adjacent to springs, and a transitioning landscape from sparse phreatophytes to xerophytes beyond. Historical (1950s–80s) water levels and those analyzed by Huntington and others (2014) indicate that depth to water has remained near or below the extent to which phreatophytes previously have been reported to exist (water table depth of as much as 19 m bls; Robinson, 1958). Water levels surrounding the irrigated cropland ranged historically from about 15.25–21.30 m bls (50–70 ft bls) during the 1960s–80s, to about 18.25–30.50 m bls (60–100 ft bls) during the 1980s–late 2000s (Huntington and others, 2014), which also is indicative of the vegetation transition apparent at the land surface. Investigation of drillers' logs indicates that some wells located within and along the northern GDA boundary penetrate multiple layers of clay between 15 and 34 m bls. These clay layers could create perched aquifers or could promote extensive capillary rise above the water table that has sustained the local, sparsely distributed greasewood community since agricultural pumping began to draw the water table down. In addition to precipitation, the sparsely distributed phreatophytic shrubs likely are sustained by the deep water table (more than 15.25 m bls [50 ft bls]) or deep soil water, the many springs along the northern and eastern GDA border, and (or) ephemeral surface-water discharging from Spring Creek (fig. 1). Considering the deep water table and apparent vegetation transition at the land surface, the effect of reported water table variations on the sparse vegetation community is assumed to be small to negligible.

In the vicinity of the geothermal plant, near the western edge of the GDA just north of the playa (figs. 1 and 23), water levels declined between the 1980s, when the plant was established, and 2010. This water-level decline likely is a direct response to geothermal pumping of basin-fill water (2.6×10^6 m^3/yr) that began in 1997. Water levels adjacent to the pumping well (within 0.4 km) have declined by nearly 8 m, whereas water levels in wells 5.5 and 6 km from the pumping well have declined by about 1–2 m (from initial static water-level depths of 17–18 m bls). Despite this notable decline in water levels, vegetation cover and vigor (as observed during field visits and measured at three transect

sites located within 2–4 km of the pumping well) appeared undisturbed. This indicates that the gradual water-level decline with distance from the pumping well was not rapid enough to notably affect the phreatophytic vegetation community during the period of record.

North of the geothermal plant, interferometric synthetic aperture radar data documented subsidence rates of as much as 10.5 cm/yr between 1992 and 1997 (Foxall and Vasco, 2003), and 4.5 cm/yr between 2006 and 2008 (John Bell, University of Nevada, Reno, written commun., 2010). If 10.5 cm/yr subsidence rates are applied from 1992 to 2001 and 4.5 cm/yr rates are applied from 2001 to 2011, subsidence could total nearly 150 cm in the affected area. Although field observations were not available to determine if subsidence effects on surface vegetation characteristics were substantial, areas affected by subsidence total less than 200 ha (500 acres) and represent less than 0.5 percent of the GDA. Therefore, the potential effects of subsidence on basin-scale predevelopment discharge estimates were considered minimal.

Evapotranspiration Unit Delineation

ET units were defined within the GDA in order to group areas characterized by similar phreatophytic vegetation type and cover and to extrapolate site-scale ET_g estimates across the basin (fig. 23; table 15). Using a combination of Landsat TM, EVI/T_B, and NAIP imagery, the GDA was partitioned into five evapotranspiration units: playa lake, playa, sparse shrubland, moderate-to-dense shrubland, and grassland. ET unit delineations represent generalizations of spatial vegetation and soil changes in the landscape and are not intended to be exact. Information regarding ET units in digital format is available in appendix 7.

The playa boundary that encompasses the playa and playa lake ET units covers about 17,705 ha (43,750 acres; fig. 23) and initially was delineated using 2008 Landsat data by identifying areas of high reflectance relative to adjacent vegetated areas. This playa boundary then was refined using the 2006 NAIP imagery at a 1:24,000 scale. The playa was devoid of vegetation during the study period except for a few sparsely distributed phreatophytes (less than 1 percent cover) around the periphery. About 60–70 percent of the playa edge was well defined by native shrubs, whereas the residual 30–40 percent was defined by a general boundary between the relatively flat playa surface and adjacent bare soil. Along the playa-bare soil interface, small surface drainages were used where available to determine the point at which the land surface gradient became constant and nearly zero, denoting the nearly flat playa land cover.

The playa lake ET unit represents playa areas that are wet or inundated with water more than 3 months (25 percent) of the year, whereas the playa ET unit represents playa areas that are dry (not covered with ponded surface water) more than 9 months (75 percent) of the year (table 15) (Briere, 2000). The playa lake ET unit occurs at the center and lowest elevation of the Dixie Valley basin. The playa lake is an ephemeral pond that typically is inundated with precipitation-derived surface water during winter and spring of each year when evaporative demand was at an annual minimum. For example, during February 2010, more than 0.3 m of standing water was measured at the western edge of the playa lake near the PLW monitoring site (fig. 1). This water was derived from snow and rain that began falling in early December 2009. The presence of standing pond water and floating salt crusts persisted into May 2010. Thereafter, the pond water evaporated to just above the land surface and was covered with a thick, saturated salt crust.

The playa lake boundary was determined from a bathymetric elevation model of the playa surface developed from a time series of Landsat images by Groeneveld and Barz (2014) and field observations. This boundary is about equal to the 1,030.5-m elevation contour, and is similar to the areal coverage of the Humboldt Salt Marsh (fig. 1). The playa ET unit was defined as the area between the playa lake and outer playa boundaries. Playa lake and playa ET units cover about 3,207 and 14,498 ha (7,925 and 35,825 acres), respectively (fig. 23).

Vegetation covers more than 70 percent of the GDA (47,321 ha [116,932 acres]). Vegetated areas were separated into three ET units: sparse shrubland, moderate-to-dense shrubland, and grassland (fig. 23, table 15). The units were derived by removing the playa boundary from the GDA boundary and interactively defining threshold EVI/T_B values to characterize first the transition from sparse to moderately dense shrubland and then the transition from dense shrubland to grassland. The vegetation thresholds were identified by evaluating multiple image distributions in combination with measured vegetation transects across the valley, NAIP imagery, and field observations.

The sparse shrubland ET unit covers 33,188 ha (82,009 acres or 51 percent of the total GDA; fig. 23) and predominantly was characterized by sparsely distributed phreatophytes (0–10 percent shrub cover with a mean of 4 percent cover), xerophytes, and annual forbs. Predominant phreatophytes include greasewood and seepweed, with lesser amounts of rabbitbrush, saltgrass, and pickleweed. The SV site is included in this unit. Near the playa, soil often is covered with salt; near the GDA periphery, soil often is covered with biological crusts (table 15). Canopy-cover measurements for shrubs totaled less than 10 percent for 17 of the 21 basinwide transects measured in this study (table 14, fig. 24). These 17 locations were assumed to be representative of sparse shrubland throughout the GDA and were used to guide the selection of a threshold describing the transition between sparse and moderate-to-dense shrubland ET units.

Table 15. Descriptions and photographs of evapotranspiration units identified, delineated, and mapped in the groundwater discharge area, Dixie Valley, Nevada, 2009–11.

[**Abbreviations:** ET, evapotranspiration; cm^3/cm^3, cubic centimeter per cubic centimeter; m, meter; bls, below land surface; mm, millimeter; mS/cm, milliSiemens per centimeter]

ET-unit name	ET-unit description	Photograph
Playa lake	Playa that is inundated with precipitation-derived water more than 3 months (25 percent) of the year. Near-surface soil water content ranges from about 0.45 to 0.70 cm^3/cm^3. Surface typically is covered with salt; crust thickness varies seasonally from less than 1 to more than 50 mm. Depth to the saturated zone ranges from land surface to about 0.2 m bls. Groundwater is considered a brine with electrical conductivity greater than 300 mS/cm.	
Playa	Playa that is inundated with precipitation-derived water less than 3 months (25 percent) of the year. Near-surface soil water content ranges from about 0.25 to 0.50 cm^3/cm^3. Depth to the saturated zone ranges from about 0.2 to 1.2 m bls. Groundwater is considered a brine with electrical conductivity ranging from 150 to more than 200 mS/cm.	
Sparse shrubland	Area dominated by bare soil with sparsely distributed perennial phreatophytes (shrubs and forbes), xerophytic shrubs, and annual forbes. Predominant phreatophytes include greasewood and seepweed, with lesser amounts of saltgrass and pickleweed. Predominant xerophytic shrubs include shadescale and Bailey's greasewood. Phreatophytic shrubs typically cover 0–10 percent of the landscape (4 percent on average). Soil is often covered with biological crusts near the groundwater discharge area periphery and with salt near the playa. Depth to the saturated zone typically varies spatially from about 1 to 20 m bls. Adjacent to agricultural pumping areas, depth to the saturated zone can reach 30 m bls.	
Moderate-to-dense shrubland	Area dominated by bare soil with moderately to densely distributed perennial phreatophytes including greasewood, rabbitbrush, and big saltbush. Shrub combinations vary from site to site, but are typically dominated by greasewood. Phreatophytic shrubs typically cover 4–40 percent of the landscape. Depth to the saturated zone typically varies spatially from about 1 to 6 m bls.	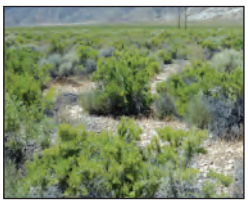
Grassland	Area dominated by short, dense perennial grasses. Grasses are primarily marsh and meadow grasses with lesser amounts of dense wetland vegetation and dense shrubland. Wetland vegetation is composed primarily of tall reeds and rushes. Unit includes occasional greasewood shrubs. Vegetation cover is greater than 40 percent of the landscape. This unit typically occurs near springs. Depth to the saturated zone ranges from about 0 to 20 m bls, but grasses typically are sustained by spring discharge where water tables are more than 3–5 m bls.	

The sparse shrubland ET unit was delineated using a step-wise procedure based on the mean EVI/T_B value characterizing the 17 transect locations. The mean pixel value of 1,571 from the 2007 image (mean of 17 transect locations showing less than 10 percent shrub cover) was used as a threshold to create an initial mask, where values selected were equal to or less than this threshold and characterized sparse shrub cover. Next, the mean pixel value of 1,617 for the 2009 summer mean image was used as a threshold to create a second mask characterizing areas with less than 10 percent phreatophytic shrub cover on average. The same approach was used for 2010 and 2011 summer mean images to create a total of four masks. These masks were combined into a single mask that represents the sparse shrubland ET unit, and the combined mask was applied to 2007 and 2009–11 summer mean images. Overall, 13 of the 17 transect sites showing less than 10 percent phreatophytic shrub cover intersected pixels in the combined mask. Of the four outliers, three sites intersected pixels immediately adjacent to the mask. Considering that pixel values were determined as the mean from a 45-m radial buffer surrounding the transect locations, the combined mask was considered a sufficient representation of sparse shrub cover.

Delineation of the sparse shrubland ET unit was further validated with transect data from Harrill and Hines (1995) who measured vegetation characteristics at 15 locations during April 1983 using the line-transect method. Each location was evaluated using a single direction transect extending to about 91 m (300 ft). Of the 13 transects within the GDA in this study (only 13 of 15 were within the discharge zones delineated in Harrill and Hines, 1995), nine showed less than 10 percent phreatophytic shrub cover. Seven of these nine transects were within the sparse shrubland ET unit delineated in this study, and one of the two outliers was located in a pixel immediately adjacent to the mask (data not shown). The remaining outlier was considered insignificant, as the accuracy of transect locations reported by Harrill and Hines (1995) was within 0.5 mi (0.8 km).

The moderate-to-dense shrubland ET unit covers 13,650 ha (33,730 acres, 21 percent of the total GDA) and is dominated by phreatophytic shrubs (about 4–40 percent cover) including greasewood, rabbitbrush, and big saltbush (fig. 23, table 15). Shrub combinations varied from site to site, but typically were dominated by greasewood. This ET unit is composed of image pixels that were excluded from the sparse shrubland and grassland ET unit masks. The DV site is in this ET unit.

The grassland ET unit was delineated by examining high values of EVI/T_B within 2007 and 2009–11 summer mean images in conjunction with field observations and NAIP imagery. Although transect locations and canopy-cover measurements excluded grassland areas, these data were used to guide the selection of a lower EVI/T_B grassland threshold. The maximum phreatophytic shrub cover from transect measurements was 38.4 percent (table 14). This value is similar to the upper range in plant cover reported by Nichols (2000), representing the transition from shrubland to grassland areas (25–40 percent plant cover).

The 2011 summer mean image was assumed to represent the mean extent of grassland within the GDA. A threshold value of 3,500 was selected interactively within the 2011 summer mean image by comparing transect measurements (table 14), field observations, and NAIP imagery. Pixels greater than the 3,500 threshold in the 2011 summer mean image were used to create a grassland mask that was then applied to 2007 and 2009–11 summer mean images. The grassland ET unit is composed of image pixels that were excluded from the sparse shrubland ET unit mask. The grassland unit is much smaller than the sparse shrubland unit and covers 464 ha (1,146 acres; 1 percent of the total vegetated area) (fig. 23, table 15). Short, dense perennial grasses with lesser amounts of dense wetland vegetation and dense shrubland dominate the grassland unit. Total vegetation cover is greater than 40 percent. Grassland areas primarily are adjacent to discharging springs near the playa periphery and in the northernmost part of the GDA (fig. 23).

Vegetated ET units might include small amounts of (1) irrigated cropland near the northern edge of the GDA, (2) historically active agricultural areas near the northern and southern edges of the GDA, (3) active geothermal areas, and (4) meadow and riparian areas surrounding flowing wells in the historical agricultural settlement area just south of the playa. These areas of anthropogenic influence were delineated and replaced with surface characteristics similar to the adjacent landscape in the summer mean EVI/T_B images in order to characterize pre-development conditions. However, depending on the image group analyzed, the effects of anthropogenically altered landscapes on the EVI/T_B images might have extended beyond the masked areas.

Groundwater Evapotranspiration Estimation

Groundwater ET for each ET unit was estimated volumetrically as the product of groundwater discharge estimates and the areas across which the discharge is occurring. Groundwater ET estimates applied were assumed to be representative of the pre-development, long-term rates (see section, "Groundwater Discharge by Evapotranspiration") occurring within the study area. Pre-development ET_g in anthropogenically disturbed areas was estimated by delineating these areas within the GDA and replacing vegetation indexes with values determined from the adjacent, native phreatophytic landscape (see section, "Characterization of Pre-Development Surface Conditions").

Playa

Groundwater ET for the playa lake and playa ET units was estimated using eddy-covariance-derived estimates from sites PL1 and PL2 and comparisons between evaporation measurements at the PL2 site and the PLW monitoring site on the edge of the playa lake ET unit. Stable isotope data collected at and near the PLW site and physical characteristics of the playa groundwater system were used to support estimates.

Groundwater ET from the playa lake ET unit, as shown in figure 2 and described in the section, "General Hydrology," predominantly represents local groundwater discharge rather than regional groundwater discharge. Local, cool season precipitation typically accumulates in the playa lake ET unit forming an ephemeral pond during the winter and spring of each year. This water is derived from precipitation that fell (1) onto the playa lake ET unit surface, (2) onto the playa ET unit and traveled as run-on to the playa lake ET unit, and (3) within the vegetated discharge area and traveled through surface drainages onto the playa where it accumulated within the playa lake ET unit (see section, "General Hydrology," which describes how less than 0.6 Mm^3 [500 acre-ft] of surface drainage was estimated to discharge onto the playa annually; Interflow Hydrology, Inc., and Mahannah and Associates, LLC, 2013). Soon after the pond forms, thick surface salts dissolve, forming a dense brine above the land surface. A combination of brine density and hydraulic head of the standing water undoubtedly lead to percolation of this water into subsurface soils, where it likely reaches the local water table (above 0.3 m bls [1 ft bls]) (fig. 2). This local recharge water probably mixes with shallow playa groundwater and subsequently is evaporated following evaporation of standing pond water to just above land surface. Although evaporative demand is greatest during summer and autumn, the presence of a thickening salt crust likely limits complete evaporation of the locally recharged brine water until late autumn of each year. Near the edge of the playa lake ET unit, isotopic signatures of oxygen-18 and deuterium indicate ephemeral pond water is the likely source of shallow groundwater and standing water that lies between the soil surface and salt crust during late summer (fig. 22; see section, "Groundwater Evapotranspiration Partitioning").

The discharge rate of locally derived shallow groundwater is unknown, but chemical and physical factors limiting evaporation such as soil salinity (sodium and chloride concentrations of about 420 and 690 mg/g), groundwater density (1.21 g/mL), and a thickening surface salt crust indicate summer and autumn groundwater discharge rates likely are similar to local winter and spring recharge (percolation) rates. A comparison between eddy-covariance evaporation measurements at the PL2 ET site and portable chamber evaporation measurements near the PLW monitoring site during August 2009 indicates that evaporation near the edge of the playa lake ET unit is about 25 percent lower than that measured at the PL2 site (see section, "Chamber Evaporation and Evapotranspiration Partitioning"). Evaporative discharge from the playa lake edge during late spring through autumn likely is derived from local ephemeral lake recharge water that could be mixed with a smaller proportion of shallow playa groundwater. Near the center of the playa lake ET unit standing water exists within and beneath salt crusts; however, salt concentrations also are likely greater than around the unit periphery, thus differences between evaporation rates along the edge and near the center of the unit are unknown. Regardless of the rate, the predominant source of this evaporative discharge water likely is ephemeral pond water during summer and autumn. Therefore, the water does not represent discharge from the regional groundwater flow system.

Mean annual ET_g from the playa lake ET unit was computed as the product of ET_g and the ET unit area (3,207 ha [7,925 acres]). A range in mean annual ET_g of 0–4 mm was estimated for this ET unit and represents regional groundwater discharge. An estimate of zero assumes that all evaporative discharge from the playa lake ET unit was derived from local ephemeral pond recharge water, as was interpreted from stable isotope analyses. The upper bound of 4 mm is based on the assumption that along the edge of the playa lake ET unit, some mixing likely occurs between local ephemeral pond recharge water and shallow playa groundwater. This upper bound was estimated by first reducing mean annual ET_g at the PL2 site (11 mm) by 25 percent to account for the evaporation discrepancy determined from August 2009 chamber evaporation comparisons. This estimate (8 mm) was reduced by another 50 percent to account for mixing between local recharge derived from ephemeral pond water, and playa groundwater. Although the mixing ratio between the two waters is unknown, the degree of mixing likely is greatest at the playa lake edge and negligible at the center. A ratio of 50:50, therefore, was assumed to adequately represent a potential upper bound.

Groundwater ET from the playa ET unit was estimated as the product of the ET unit area (14,498 ha [35,825 acres]) and the mean of annual ET_g measured at the two playa ET sites (16 mm [0.05 ft]). Estimated ET_g near the outer edge of the playa ET unit likely is greater than ET_g measured at the PL1 site, whereas ET_g between the two playa ET sites likely is somewhere between the two estimates. Likewise, ET_g between the PL2 site and the outer boundary of the playa lake ET unit (or inner boundary of the playa ET unit) likely is less than ET_g measured at the PL2 site. Playa material trends from interfingered playa and basin-fill sediments near the playa edge to predominantly finer grained silt and clay material toward the playa center. Therefore, in addition to salt accumulation, soil hydraulic properties also likely reduce playa ET_g from the playa edge toward the center. Recognizing

these differences, the mean of estimated ET_g at the two playa ET sites was considered a reasonable representation of the total discharge from this ET unit. This ET_g estimate can be considered an upper bound because some mixing might occur between playa groundwater and ephemeral pond water that locally recharges the playa lake ET unit, in addition to marginal mixing between playa and basin-fill groundwater (see section, "Groundwater Evapotranspiration Partitioning").

The plausibility of a mean ET_g estimate of about 16 mm/yr occurring across the playa ET unit was evaluated using analytical hydraulic calculations based on Darcy's law similar to calculations used by Jacobson and Jankowski (1989) and Hines (1992). Parameters used for this calculation include a hydraulic gradient of 0.00035 m/m between the SV and PL1 sites (representing the steepest gradient measured in April 2010), a playa perimeter of about 90 km, and a playa area of 14,498 ha (playa lake ET unit excluded). A range in transmissivity of 0.009–25 m^2/d (0.1–270 ft^2/d) was estimated using slug test results from Huntington and others (2014) for the lower bound, and saturated vertical hydraulic conductivities determined from playa soil cores (appendix 2) and an estimated playa thickness of 61 m (200 ft; Huntington and others, 2014) for the upper bound. Vertical hydraulic conductivity measurements from soil cores ranged from 8.8×10^{-8} to 4.7×10^{-6} m/s—within the range of textbook values for the horizontal hydraulic conductivity of clay to silt (1×10^{-11} to 2×10^{-5} m/s; Domenico and Schwartz, 1998); therefore, a vertical-to-horizontal anisotropy ratio of unity was considered reasonable. Using this range in transmissivity, computed annual playa groundwater discharge ranged from 0 to 2.5 mm. A mean annual playa ET_g of 1 mm was computed using the mean transmissivity determined from soil cores (11 m^2/d) (appendix 8).

Additional wells located within and just beyond the playa edge to the north, east, and west also were evaluated using Darcy's law. Using a transmissivity of 11 m^2/d, steeper hydraulic gradients to the east, west, and north yielded annual playa groundwater discharge estimates (29, 8, and 3 mm, respectively) that were greater than measured to the south (appendix 8). The mean of ET_g estimates from northern, southern, eastern, and western areas of the playa is about 10 mm/yr. These ET_g estimates were based on Darcy's law and provide strong support for eddy-covariance-derived ET_g estimates and the application of these values to the entire playa ET unit.

Vegetated Areas

Groundwater ET from the sparse shrubland ET unit was characterized by a single ET_g estimate determined from canopy-cover measurements at 16 locations and ET_g measured at the SV site. The ability of vegetation indexes to estimate variations in phreatophytic shrub canopy cover decreases as shrub cover decreases (fig. 24) because the vegetation index value generated by the soil background reflectance often overwhelms that of sparse vegetation. In addition to index obscurity by soil background reflectance, inter-annual comparisons of vegetation indexes (with and without normalization by brightness temperature) indicated large variations within the sparse shrubland ET unit and in areas adjacent to the GDA boundary. This variability was more representative of active or inactive biological soil crusts and the presence or absence of forbs and cheat grass than any real change in phreatophytic shrub cover or vigor that would support varying ET_g rates. At low percentages of canopy cover (less than 10 percent) characteristic of this ET unit, ET_g was assumed to vary linearly as a function of canopy cover. Only transect locations that were within or immediately adjacent to the sparse shrubland ET unit were used in this analysis (table 14, fig. 23). Groundwater ET was computed as the product of mean phreatophytic shrub canopy cover, determined from 16 basin-wide transect measurements (4.2 percent), and the ratio of ET_g-to-phreatophytic shrub cover measured at the SV site from four 50-m transects (53 mm / 7.9 percent cover) (tables 9 and 14). Mean phreatophytic shrub canopy cover measured at the 16 transect locations corresponded to a mean annual ET_g estimate of 28 mm (0.09 ft). Shrub cover measurements were considered representative of the ET unit at large.

The ET_g estimate of 28 mm is about 1.2 times the mean rate reported by Harrill and Hines (1995) for vegetation zones with less than 10 percent phreatophytic shrub cover (23 mm). The sparsest zone or ET unit defined by Harrill and Hines (1995) was assigned an annual ET_g estimate of 15 mm and was characterized by a mean phreatophytic shrub cover of 5 percent. This zone covered an area similar in size to that of the sparse shrubland ET unit in this study (within 3 percent). An additional three zones totaling about 8,500 ha (21,000 acres) were delineated by Harrill and Hines (1995) and assigned mean phreatophytic shrub covers of 6–8 percent and ET_g estimates of 18–64 mm.

Evapotranspiration from phreatophytic shrubland areas often is dictated by water limitations. Phreatophyte cover and groundwater use in the Great Basin typically are controlled by a combination of soil type, precipitation, and depth to groundwater. In contrast, ET from adjacent grassland areas often is controlled by energy limitations, as water often is readily available. Nichols (2000), Laczniak and others (2008), Moreo and others (2007), Allander and others (2009), and Devitt and others (2011) showed these characteristics by comparing actual and (or) groundwater ET with vegetation cover or vegetation indexes. Actual ET and ET_g relations with vegetation cover, type, or indexes for phreatophytic shrubland areas typically followed steep linear trends characteristic of water limited systems, whereas relations for grassland areas (where determined) followed more moderate linear trends characteristic of energy-limited systems.

Groundwater ET rates within the moderate-to-dense shrubland ET unit were determined using linear interpolation between estimated phreatophytic shrub canopy cover, the mean annual ET_g rate from the DV site, and the mean ET_g rate assigned to the sparse shrubland ET unit. In contrast to sparse areas, relations between phreatophytic shrub canopy cover and EVI/T_B were favorable for transect locations showing greater than 10 percent phreatophytic shrub cover (four locations) for all years evaluated. The relation between phreatophytic shrub cover and ET_g for the moderate-to-dense shrubland ET unit also was assumed to be linear; therefore, spatially continuous EVI/T_B distributions were used to estimate phreatophytic shrub cover across the ET unit. Phreatophytic shrub cover estimates were based on a five-point relation between EVI/T_B and phreatophytic shrub canopy cover (r^2 ranged from 0.91 in 2007 to 0.99 in 2010; fig. 25). Four data points represent transect locations showing greater than 10 percent shrub cover paired with EVI/T_B estimates from a 45-m radial buffer surrounding the point location. The fifth data point represents the mean phreatophytic shrub cover estimate for the sparse shrubland ET unit, paired with the minimum EVI/T_B pixel value within the moderate-to-dense shrubland ET unit for each summer image. The fifth point was included to characterize the sparse pixels remaining within the moderate-to-dense shrubland ET unit.

Estimated phreatophytic shrub cover distributions for each summer mean image were related to ET_g using linear interpolation between 2 points. The mean annual ET_g estimated at the DV site (225 mm) and a minimum ET_g of 28 mm (representing mean ET_g for the sparse shrubland ET unit) were paired with estimated shrub cover at the DV site and the minimum estimated shrub cover for the scene of interest, respectively. The estimated phreatophytic shrub cover-to-ET_g relation for these two points was applied to continuous distributions of estimated shrub cover within the ET unit to predict ET_g on a pixel-by-pixel basis. Use of the minimum shrub cover in the two-point relation ensured that this ET unit was bounded with a minimum ET_g corresponding with the sparse shrubland ET unit. Linear relations were developed for 2007 and 2009–11 summer mean images. Summer mean images incorporated 2–3 scenes during the summer growing season (table 13) and were used to generalize the variability in EVI/T_B distributions. A maximum threshold corresponding to a phreatophytic shrub cover of 40 percent was applied, where ET_g estimates corresponding to shrub cover values greater than this threshold were determined using the grassland relation.

Groundwater ET from the grassland ET unit also was determined using linear interpolation between two points. Transect locations and canopy-cover measurements excluded grassland areas; therefore, ET_g was assumed to vary linearly with EVI/T_B. The first point of the two-point relation represents ET_g and EVI/T_B values that correspond with 40 percent phreatophytic shrub cover (similar to maximum transect measurement) within the moderate-to-dense shrubland ET unit. The second point represents the maximum EVI/T_B image value and ET_g estimate of 1,167 mm (3.83 ft), computed as the difference between estimated reference crop ET for grass (American Society of Civil Engineers, 2005; fig. 14, appendix 4) and measured precipitation (table 9) at the DV site. This maximum ET_g estimate is slightly greater than the annual net irrigation water requirement for alfalfa in Dixie Valley (1,097 mm or 3.6 ft; Huntington and Allen, 2010), and, therefore, was assumed to reasonably characterize the maximum ET_g rate for the grassland ET unit encompassing both grass and marsh covered areas. The two-point relation was determined for 2007 and 2009–11 summer mean images and was applied to spatially continuous EVI/T_B distributions to estimate ET_g for all pixels within the grassland ET unit. As with the moderate-to-dense ET unit, a minimum EVI/T_B threshold corresponding to a phreatophytic shrub cover of 40 percent was applied, where ET_g estimates for EVI/T_B values less than or equal to this threshold were determined using the moderate-to-dense relation.

A multi-summer mean image was used to characterize mean annual ET_g across moderate-to-dense shrubland and grassland ET units. This multi-summer image was computed as the mean of 2009–11 summer mean images. Information regarding the multi-summer mean (2009–11) image in digital format is available in appendix 7. Although 2007 EVI/T_B image values adequately characterized phreatophytic shrub cover within the moderate-to-dense ET unit (coefficient of determination of 0.91), the two points used to spatially extrapolate ET_g across the ET unit (the minimum EVI/T_B value for the ET unit and that determined at the DV site location) appeared offset from the predicted relation compared to values within 2009–11 summer mean images (fig. 25). The lower index value at the DV site during 2007 is unknown because site visits began in 2009, but as a result, the slope of the linear relation between predicted phreatophytic shrub cover and ET_g for these two points was twice the slope determined for 2009–11 summer mean images. This steeper slope, in turn, inflated ET_g estimates compared to 2009–11 summer mean images when applied across the entire ET unit (table 16). Considering that field measurements and observations occurred between 2009 and 2011, a multi-summer mean image computed from 2009 to 2011 summer mean images was assumed to adequately characterize mean annual ET_g across moderate-to-dense shrubland and grassland ET units. Relations developed for 2007 and 2009–11 summer mean images for these ET units also were developed for the multi-summer (2009–11) mean image and applied to estimate mean annual ET_g.

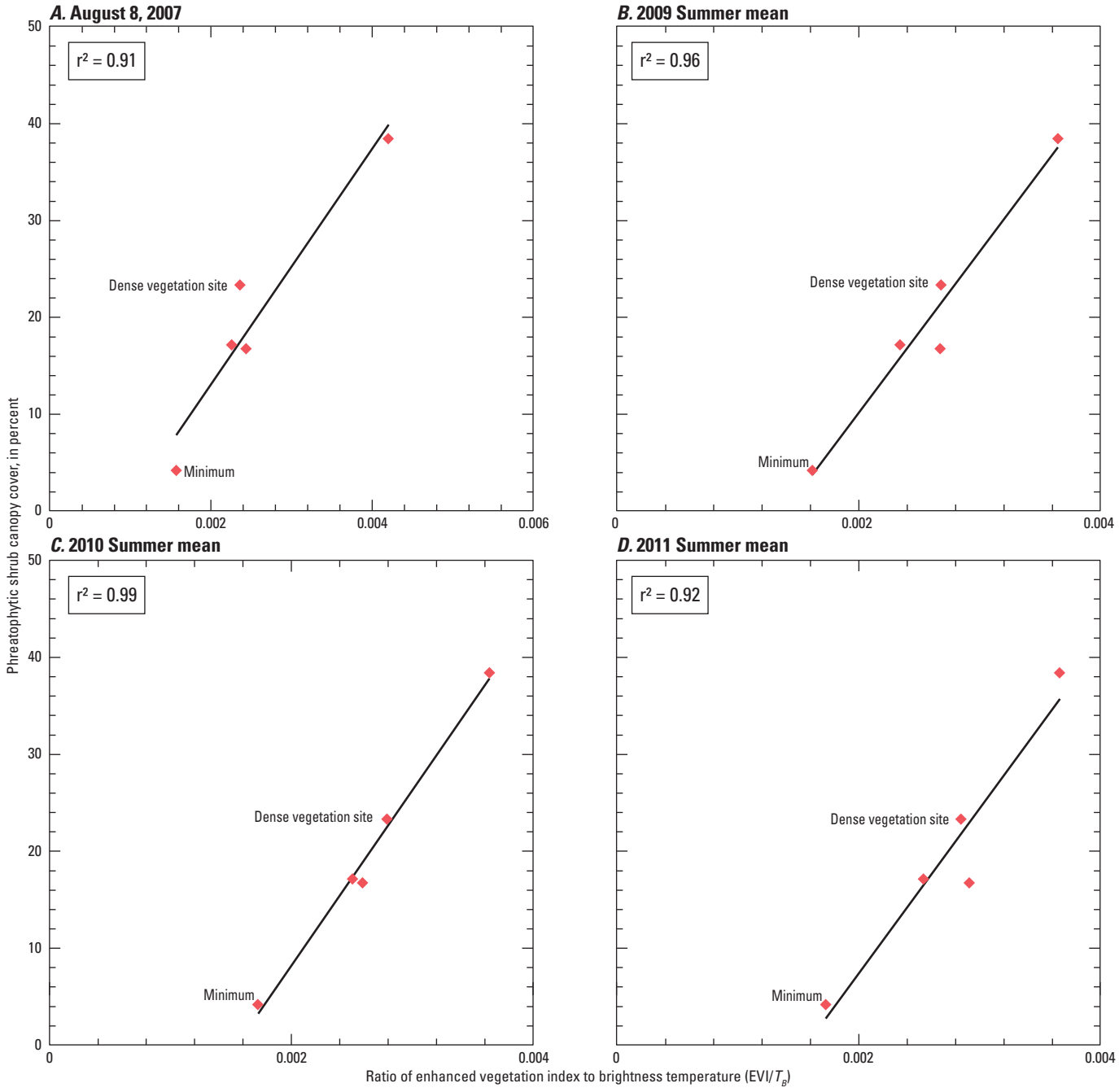

Figure 25. Relation between phreatophytic shrub canopy cover (typically greater than 10 percent) and the ratio of the enhanced vegetation index to brightness temperature for (*A*) August 8, 2007, and (*B*) 2009, (*C*) 2010, and (*D*) 2011 summer mean images, Dixie Valley, Nevada. Relation is described by the coefficient of determination (r^2).

Mean Annual Groundwater Discharge by Evapotranspiration

Estimated mean annual ET_g across the GDA totaled 28 Mm^3 (23,000 acre-ft) and was estimated using the multi-summer mean EVI/T_B image (table 16). The sum of ET_g from all ET units represents the mean annual ET_g for the basin. Groundwater ET from the playa ET unit was estimated at 2.2 Mm^3 (1,800 acre-ft), whereas groundwater ET from the playa lake ET unit was 0–0.1 Mm^3 (0–100 acre-ft) (table 16, fig. 26). Groundwater ET from vegetated areas totaled 25 Mm^3 (20,400 acre-ft). The moderate-to-dense shrubland ET unit contributed to about 54 percent of ET_g from vegetated areas; the sparse shrubland unit contributed to 37 percent of ET_g, and the grassland unit contributed to 9 percent of ET_g. The mean estimated basin-scale ET_g from moderate-to-dense shrubland was about 14 Mm^3 (11,000 acre-ft), whereas the mean basin-scale ET_g from sparse shrubland was 9.2 Mm^3 (7,500 acre-ft) and from grassland was 2.3 m^3 (1,900 acre-ft).

Table 16. Mean-annual basin-scale groundwater evapotranspiration and evapotranspiration unit area, including Landsat image dates, Dixie Valley, Nevada, 2009–11.

[**Area:** Values in parenthesis are in acres. **Mean annual ET_g from ET units:** Values in parenthesis are in acre-feet and have been rounded to two significant figures. **Multi-summer mean:** Determined for each pixel using 2009–11 summer mean images. The 2007 image was excluded. **Probable error:** The standard deviation for moderate-to-dense shrubland and grassland ET units from 2009–11 summer mean images. Total determined as the square root of the sum of squared errors. **Maximum probable error:** Determined for each ET unit by adding and subtracting the probable error from mean annual site-scale ET_g rates (table 9) used to scale measurements to the basin level. Total determined as the square root of the sum of squared errors. **Abbreviations:** ET, evapotranspiration; ET_g, groundwater evapotranspiration; EVI/T_B, temperature-normalized enhanced vegetation index; ha, hectare; Mm^3, millions of cubic meters; acre-ft, acre-foot; –, not estimated; GDA, groundwater discharge area]

ET unit	Area (ha)	Mean annual ET_g from ET units (Mm^3)						
		Landsat image dates				Multi-summer mean	Probable error	Maximum probable error
		08-08-07	Summer mean					
			2009	2010	2011			
Playa lake[1]	3,207	–	–	–	–	0–0.1	–	0.1
	(7,925)	–	–	–	–	(0–100)	–	(100)
Playa[2]	14,498	–	–	–	–	2.2	–	2.6
	(35,825)	–	–	–	–	(1,800)	–	(2,100)
Sparse phreatophytic shrubland[3]	33,188	–	–	–	–	9.2	–	3.7
	(82,009)	–	–	–	–	(7,500)	–	(3,000)
Moderate-to-dense phreatophytic shrubland[4]	13,650	17	15	14	14	14	0.6	3.0
	(33,730)	(14,000)	(12,000)	(11,000)	(11,000)	(11,000)	(500)	(2,400)
Grassland[5]	464	3.0	2.2	2.2	2.2	2.3	0.1	0.2
	(1,146)	(2,400)	(1,800)	(1,800)	(1,800)	(1,900)	(50)	(200)
Total	65,007	32	29	27	27	28	0.6	5.4
	(160,635)	(26,000)	(24,000)	(22,000)	(22,000)	(23,000)	(500)	(4,400)

[1]Groundwater ET determined as the product of ET unit area and about 0–0.125 of the mean ET_g from the PL2 ET site (table 9).

[2]Groundwater ET determined as product of ET unit area and mean ET_g from PL1 and PL2 ET sites (table 9).

[3]Groundwater ET determined as product of the average phreatophytic shrub cover within this unit (4.2 percent), and the ratio of ET_g-to-phreatophytic shrub cover measured at the SV site (tables 9 and 14).

[4]Groundwater ET determined from relation between ET_g and phreatophytic shrub canopy cover. Senesced grasses observed in the northernmost areas of the GDA likely confounded the vegetation index and led to an overestimate of ET_g for the moderate-to-dense ET unit. Therefore, mean annual ET_g for moderate-to-dense shrubland likely can be considered an upper bound.

[5]Groundwater ET determined from relation between ET_g and EVI/T_B.

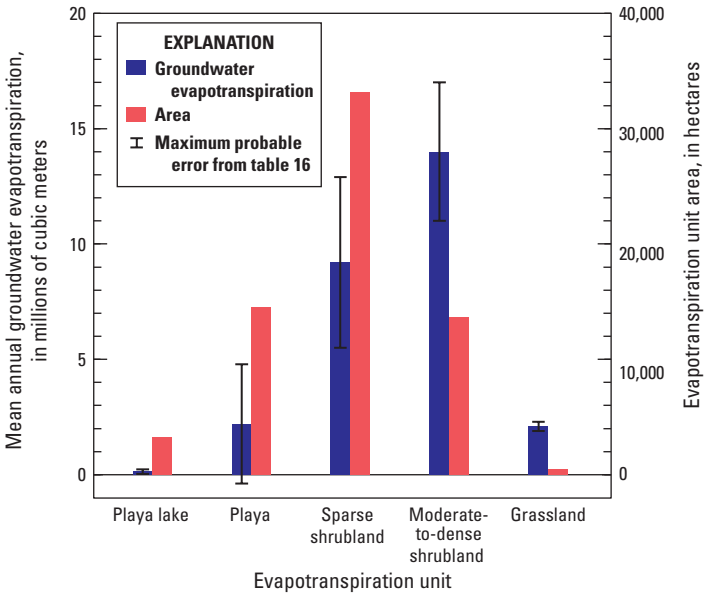

Figure 26. Graph showing mean annual basin-scale groundwater evapotranspiration from evapotranspiration units and evapotranspiration unit area, Dixie Valley, Nevada, water years 2010–11.

Annual groundwater ET within the moderate-to-dense shrubland ET unit ranged from about 28 to 499 mm (0.09 to 1.64 ft) with a mean of about 101 mm (0.33 ft) (fig. 27). About 96 percent of this ET unit area had ET_g values less than the DV site, and about 4 percent of the ET unit area had ET_g values greater than the DV site. Therefore, discharge from areas with ET_g values less than the DV site contributed to about 89 percent of the ET-unit total, whereas values greater than the DV site contributed to about 11 percent of the ET-unit total. These results indicate that site-scale ET_g determined for the sparse shrubland ET unit (through the SV site) and DV site was an acceptable approximation of the ET_g distribution within the moderate-to-dense shrubland ET unit. Differences in mean annual ET_g determined using the multi-summer mean and by directly averaging annual summer mean ET_g values from table 16 represent pixel-by-pixel averaging.

Mean annual ET_g from the moderate-to-dense ET unit is likely biased high owing to senesced annual grass effects on EVI/T_B index values. Senesced grasses observed in the northern most areas of the GDA likely confounded the vegetation index, which resulted in higher index values and estimated phreatophytic shrub cover than for similar areas in the remainder of the GDA. Limited field observations indicate that ET_g values for a large portion of the moderate-to-dense shrubland areas in the northern most GDA could be overestimated. Although this bias is likely within the maximum probable error of the estimate (discussed below), the mean annual ET_g for moderate-to-dense shrubland is likely an upper bound.

Annual groundwater ET within the grassland ET unit ranged from 140 to 1,167 mm (0.46 to 3.83 ft) with a mean of 503 mm (1.65 ft) (fig. 27). Although direct ET_g measurements were not made within this ET unit, this range is similar to measurements from other Great Basin studies in Nevada. Grassland ET_g ranged from an annual mean of 481 mm in Spring Valley (Moreo and others, 2007) to 630–670 mm in the Walker River Basin (Allander and others, 2009). In Ruby Valley, annual estimated ET_g ranged from 515 to 795 mm in grassland and meadow areas and from 1,067 to 1,100 mm in a bulrush marsh area (Berger and others, 2001). A similar range for grassland and marsh areas provides confidence in ET_g estimates and the linear upscaling approach applied in this study.

The maximum probable error associated with mean annual basin-scale ET_g was estimated at 5.4 Mm^3 (4,400 acre-ft), or about 20 percent of basin-scale ET_g. This value was determined by applying probable site-scale errors (table 9) to ET_g estimates used to scale site measurements to the basin level (table 16). Total maximum probable error was determined as the square root of the sum of squared maximum probable errors for each ET unit. Probable basin-scale error was determined as the standard deviation between annual summer ET_g estimates for sparse-to-dense shrubland and grassland ET units (table 16) and represented an average of about 4 percent of ET unit totals. Standard deviation of ET_g excluded the 2007 estimate. Although maximum probable error for the playa lake estimate is presented, physical constraints on groundwater flow within the playa indicate that the reported mean annual playa lake discharge is considered an upper bound.

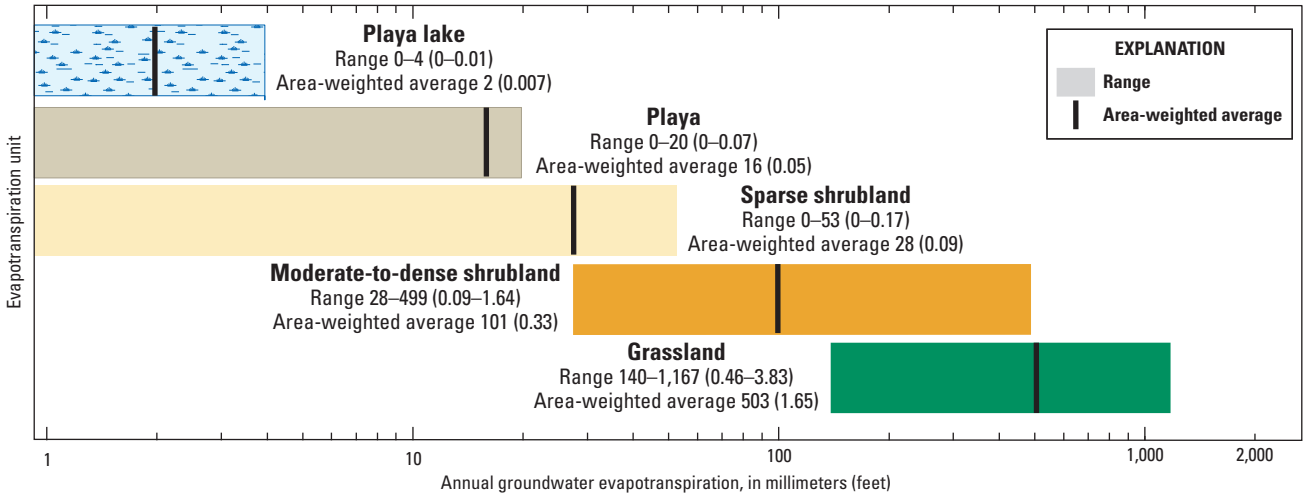

Figure 27. Graph showing mean annual groundwater evapotranspiration from evapotranspiration units, Dixie Valley, Nevada, water years 2010–11.

Comparisons with Previous Estimates

Previous estimates of ET_g in Dixie Valley were determined from limited data collected in this valley. In the mid-1900s, ET_g often was estimated by applying a constant rate to discharge areas where depth to water was within 15 m (about 50 ft) bls (Jim Harrill, U.S. Geological Survey, retired, written commun., 2010). In the 1970s, discharge estimates were improved with lysimeter measurements. Robinson and Waananen (1970) used lysimeters to measure ET_g and to develop relations between species-specific ET_g and volume foliage measurements (product of vegetation cover and height). In the 1990s, discharge estimates improved with the advancement of micrometeorological measurements and satellite imagery (Nichols, 1993, 2000), in combination with vegetation mapping. Mean annual ET_g estimates determined in this study were developed using advanced remote-sensing and micrometeorological measurements that were made in Dixie Valley. Advanced, in-place measurements provided more detailed delineations of ET_g areas, and more accurate measurements of local ET_g rates.

Groundwater ET estimates from this study are comparable overall to previous estimates made in Dixie Valley (table 17). Groundwater ET estimates from composite (sparse-to-dense) shrubland areas in this study are about 7–10 Mm^3 (6,000–8,500 acre-ft) greater than previous estimates in Dixie Valley for similarly classified vegetation groups. Previous studies applied annual ET_g per unit area values of 15–120 mm (0.05–0.41 ft) to areas with phreatophytic shrub cover of about 5–26 percent (Cohen and Everett, 1963; Harrill and Hines, 1995). In this study, ET_g estimated annually from the SV and DV sites (with mean phreatophytic shrub cover of 6.7 and 21.4 percent, respectively; table 6) ranged from 53 to 225 mm (0.17 to 0.74 ft), respectively (table 9). As a result, upscaling of ET_g estimates to a 46,857 ha shrubland area (115,785 acres) produced estimates that were as much as 70 percent greater than previous estimates.

Groundwater ET from the grassland ET unit was within the range of previous estimates from Dixie Valley, but associated acreages and ET_g estimates differed. Total grassland acreage measured during this study was about 1.5–3 times less than previous estimates (1,214 ha, Cohen and Everett, 1963; 1,942 ha, Harrill and Hines, 1995). In this study, the grassland ET unit incorporated saltgrass and marsh areas with dense coverage (greater than 40 percent) only, and ET_g values applied were similar to continuous micrometeorological measurements from other Great Basin studies in Nevada (see section, "Groundwater Evapotranspiration Estimation"). In contrast, previous Dixie Valley studies characterized grassland as a mix of bare soil and saltgrass, where saltgrass coverage ranged from 0 to 100 percent, and applied annual ET_g estimates of 60–244 mm (0.2–0.8 ft) that were collected predominantly from reconnaissance-level estimates made in other valleys prior to the 1950s (Everett and Rush, 1964).

Contrary to estimates made for shrubland and grassland ET units, ET_g estimates made for playa areas for this study are much lower than previous Dixie Valley estimates. Previous annual ET_g estimates applied per unit area of playa ranged from 30–90 mm (0.1–0.3 ft). These values were applied over 11,898–17,766 ha of playa to compute total playa ET_g of 3.6–16.3 Mm^3 (2,900–13,200 acre-ft) (Cohen and Everett, 1963; Harrill and Hines, 1995). In this study, mean annual playa ET_g estimates of 0 to 20 mm/yr were derived from in- place eddy-covariance ET, precipitation, chamber evaporation, stable isotope, and physical unsaturated-zone measurements. When applied across an area of 17,705 ha, ET_g estimates from this study are about 40–90 percent less than previous estimates. Differences between previous estimates and those made during this study indicate that actual playa discharge (from the regional groundwater flow system) is much lower than previously estimated.

Table 17. Comparisons of groundwater evapotranspiration estimates in Dixie Valley, Nevada.

[**Mean annual ET_g:** Values in parenthesis are in feet. **Mean annual basin-scale ET_g:** Values in parenthesis are in acre-feet and have been rounded to two significant figures. **Cohen and Everett (1963):** Estimate includes Jersey Valley to the northeast. **Abbreviations:** ET, evapotranspiration; ET_g, groundwater evapotranspiration; mm, millimeter; Mm^3, millions of cubic meters]

Composite ET unit	Mean annual ET_g (mm)			Mean annual basin-scale ET_g (Mm^3)		
	Current (water years 2010–11)	Cohen and Everett (1963)	Harrill and Hines (1995)	Current (water years 2010–11)	Cohen and Everett (1963)	Harrill and Hines (1995)
Playa (playa and playa lake)	0–20 (0–0.07)	30 (0.1)	30–90 (0.1–0.3)	2.3 (1,900)	3.6 (2,900)	5.4–16 (4,400–13,000)
Shrubland (sparse-to-dense)	0–499 (0–1.64)	30 (0.1)	15–120 (0.05–0.41)	23 (19,000)	16 (13,000)	13 (10,500)
Grassland	140–1,143 (0.46–3.83)	60–610 (0.2–2)	150–240 (0.5–0.8)	2.3 (1,900)	0.7 (600)	3.0–4.8 (2,400–3,900)
			Total	28 (23,000)	20 (16,000)	21–34 (17,000–28,000)

Limitations of Methodology

The accuracy of ET_g estimates presented here is limited by the eddy-covariance method, the limited spatial extent and temporal period of ET and precipitation data collection, and any potential errors in differentiating ET units and assigning ET_g estimates. The main assumptions that can affect and limit the accuracy of mean annual ET_g estimates in Dixie Valley are:

1. Measured site-scale ET, precipitation rates, and other meteorological variables are accurate and represent long-term means.
2. Sources contributing to ET other than regional groundwater can be removed accurately by subtracting direct precipitation and runoff from the ET estimate in playa and vegetated ET units.
3. Groundwater ET occurs only from areas delineated within the GDA.
4. ET_g from the moderate-to-dense shrubland and grassland ET units is adequately characterized using linear relations.
5. ET_g from the sparse shrubland ET unit is adequately characterized using mean phreatophytic shrub cover from 16 locations and the ET_g-to-shrub cover relation at the SV site.
6. ET_g from the playa lake ET unit is reasonably characterized using chamber and eddy-covariance evaporation comparisons along with stable isotope data and consideration of physical and chemical groundwater flow constraints.
7. Effects of soil reflectance and albedo on temperature-normalized EVI are negligible at phreatophytic shrub canopy covers of greater than 10 percent.
8. Estimates are representative of pre-development conditions, and pumping from the basin-fill aquifer system during this study and historically has not significantly reduced phreatophyte coverage or local spring and seep flow.

Annual measured ET documented in this report has maximum probable errors of 13–20 percent, where the relative error increases with decreasing flux magnitude from dense shrubland to playa areas. Annual ET estimates are considered to be of good quality because currently (during this study) accepted data processing and correction methods were applied to them. The mean energy-balance ratio calculated for all sites and water years (0.73) was just below the mean for other ET studies. However, resulting estimates of annual ET are reasonable compared to published values for sites and ET units with similar vegetation type and cover.

Assumptions that groundwater use by phreatophytes is consistent with phreatophytic shrub cover could lead to uncertainty when comparing areas with and without cohabitating xerophytes and areas with varying near-surface soil characteristics. Because greasewood is opportunistic and will use soil water in addition to groundwater, greasewood communities in competition with xerophytes might use more groundwater than an exclusively greasewood community. This uncertainty would be more pronounced early in the growing season following winter precipitation, corresponding with the early phenological stages of leaf-out. Comparisons of field-based estimates made in a valley and at sites containing similar phreatophytic shrub cover and depth to groundwater could be used to quantify this uncertainty; however, such comparisons were beyond the scope of this study.

Sparsely distributed greasewood located along the northern GDA boundary that follows Spring Creek to the basin divide might use ephemeral surface water, perched groundwater, or both. Limited nearby depth to groundwater data indicate that the water table typically is more than 18 m (59 ft) bls. Investigation of drillers' logs indicate that some wells located within and along the periphery of the northern GDA boundary penetrate multiple sections of clay material that occur between 15 and 34 m (49 and 112 ft) bls. These clay layers could create localized perched aquifers or promote extensive capillary rise above the water table that could sustain the local, sparsely distributed greasewood community. Nevertheless, contributions from the northernmost parts of the GDA, where the depth to water is greater than 15 m bls, represent less than 1 percent of the total ET_g estimate.

Moderate-to-dense shrubland ET_g values in the northern most GDA are likely biased high owing to senesced annual grass effects on EVI/T_B index values. Senesced annual grasses observed in this area often confounded EVI/T_B values, causing higher index values and estimated phreatophytic shrub cover than for similar areas across the GDA. Limited field observations indicate that ET_g values for a notable portion of the moderate-to-dense shrubland area in the northern most GDA is likely overestimated, but this bias is probably within the maximum probable error of the estimate.

Normalizing EVI by T_B does not take into account temperature differences caused by variations in soil albedo. Areas of dark soil with phreatophytic vegetation commonly are warmer than areas with similar vegetation and lighter soils. In the case of dark soils, the temperature-normalized EVI may be overcorrected and moderately dense stands of phreatophytes could be misclassified to the sparse shrubland ET unit. It is assumed that these misclassifications do not significantly affect the ET_g estimates. Soil background effects can alter calculated vegetation index values because of the reflectance of the soil and of leaf litter and senesced plant material on the soil surface. The EVI includes correction for soil background effects, but some soil reflectance remains in the vegetation index, particularly in areas of very sparse canopy cover. Assigning areas of sparse canopy cover to the sparse shrubland ET unit alleviates some of the error caused by residual soil background effects in sparse shrubland but, does not address the error completely.

The uncertainty of discharge estimated in the Dixie Valley study can be reduced by establishing additional ET sites to help reduce the uncertainty in the relation between ET rates and vegetation cover for a period sufficient to cover wet and dry years. Small changes in ET_g rates, when applied to large shrubland ET units, can greatly affect total discharge estimates. Long-term ET data collection is as important as long-term precipitation data collection because ET_g estimates rely on accurate and representative ET and precipitation measurements. Establishing additional long-term ET sites would (1) decrease the extent of interpolation and extrapolation; (2) provide greater temporal coverage to help confirm whether phreatophytic shrubs reduce groundwater usage during wet periods; and (3) improve the characterization of the relation between ET_g and Landsat data by providing a dataset for which the effects of differing precipitation, soil texture, depth to groundwater, and phreatophyte distributions can be evaluated.

Summary and Conclusions

A new estimate of groundwater discharge from Dixie Valley, Nevada, was computed from multiple years of measured groundwater evapotranspiration (ET_g) and remote sensing data. Pending applications for new groundwater appropriations in Dixie Valley necessitate an improved understanding of the groundwater resource including a revised groundwater discharge estimate based on detailed measurements in Dixie Valley. The U.S. Geological Survey, in cooperation with the Bureau of Reclamation and Churchill County, Nevada, estimated ET_g from Dixie Valley during water years (WY) 2010 and 2011.

Site-scale ET_g was estimated at four locations using the eddy-covariance method and micrometeorological measurements. Two sites, dense vegetation (DV) and sparse vegetation (SV), were located in shrubland areas, and two sites were located on the playa (playa 1 [PL1] and playa 2 [PL2]). Annual ET_g was computed as the difference between annual ET, local precipitation, and precipitation-derived runoff (where estimated). Groundwater ET estimates were supported with vegetation surveys, water-content profiles, unsaturated-zone liquid-water fluxes, and water levels. Water sourcing methods were used to quantify evaporation and transpiration contributions to total ET and to identify the primary source water contributing to each component throughout the study period. Water sourcing incorporated eddy-covariance ET measurements, chamber measurements of soil-water evaporation, and stable isotope measurements of precipitation, groundwater, and plant and soil water. Basin-scale ET_g was estimated by relating site-specific discharge estimates to Landsat imagery where applicable, and extrapolating this relationship across the basin.

Annual energy-balance corrected ET (ET_c) ranged from about 141 mm at the PL2 site in WY 2010 to 421 mm at the DV site in WY 2011. Annual ET_c at the DV site was nearly twice as high as that at the SV site, and represents a greater total vegetation cover (about 25 percent) at the DV site versus (about 7 percent) at the SV site. Low permeability clay sediments and surface and pore-scale salt crusts at playa sites restricted ET rates with respect to vegetated sites. Annual ET_c at all sites was slightly higher in WY 2011 than in WY 2010, and represents an increase in precipitation of about 30 percent. Measured annual site-scale ET documented by this report has a probable error averaging about 16 percent among all sites. Random error analyses indicate that the minimum detection limit of ET is about 0.1 millimeter per day.

Mean annual ET_g was 225, 52, 20, and 11 mm at the DV, SV, PL1, and PL2 sites, respectively. Annual ET_g at playa sites was consistently less than the probable error. This highlights the uncertainty of the discharge estimation method, where ET and precipitation rates are similar, as playa water content measurements show no change between water years.

Cumulative total liquid-water fluxes (isothermal+thermal liquid) measured in the unsaturated zone at vegetated sites indicated that ET_g through bare-soil evaporation did not occur during the study period. This was evident from a zero-flux plane at the DV site near the depth of 2.4 meters below land surface (m bls), and a consistently downward total liquid-water flux within the depth interval of 0.6–1.2 m bls at the SV site. Bare-soil evaporation at both sites likely removes only precipitation-derived shallow soil moisture.

Source water assessments from binary mixing of oxygen-18 isotopes in groundwater and shallow soil water indicate that plants predominantly use groundwater throughout the year. Groundwater fractions in greasewood stem water ranged from 0.6 to 1.0, and the groundwater fraction of total ET ranged from 0.09 to 0.87. End-member mixing of playa groundwater and precipitation indicates that groundwater is the predominant source of near-surface soil water as groundwater fractions ranged from 0.52 to 1.0 during spring and autumn. Stable isotope-derived discharge rates at the playa sites, however, were inconclusive because isotopic signatures represent the 15-centimeter below land surface integrated sample depth rather than the upper few centimeters of soil that likely represent the evaporating surface.

Near the playa center and the playa-west monitoring site, oxygen-18 and deuterium signatures and water-level trends indicated that a substantial source of shallow groundwater is the precipitation-derived ephemeral pond. Similarly, the source of standing water beneath the salt crust also appeared to be from ephemeral pond water.

Basin-scale ET_g predominantly occurred within a groundwater discharge area (GDA) covering 65,007 hectares (160,635 acres) of phreatophytic vegetation and playa. Within the GDA, five ET units characterizing areas of similar vegetation type and cover were delineated using enhanced vegetation index data normalized with brightness temperature, and phreatophytic shrub cover measurements from 21 locations. The five ET units include playa lake, playa, sparse shrubland, moderate-to-dense shrubland, and grassland.

The mean annual ET_g for each ET unit was estimated volumetrically as the product of ET_g and the ET unit area over which the discharge is occurring. The sum of ET_g from all ET units represents the mean annual ET_g of the basin. Mean annual ET_g from the playa ET unit was estimated at 2.2 Mm^3 (1,800 acre-ft) over a 14,498 hectare (35,825 acre) area. The playa lake ET unit was assigned a mean annual discharge value of 0–0.1 million cubic meters (Mm^3) (0–100 acre-feet [acre-ft]). Stable isotope data indicate that groundwater beneath the playa lake is predominantly derived from local recharge of ephemeral pond water; therefore, most if not all evaporation from this ET unit comes from sources other than regional groundwater discharge. Therefore, the playa lake ET unit estimate is considered an upper bound.

Mean annual ET_g from vegetated areas was about 26 Mm^3 (21,000 acre-ft) and was dominated by the moderate-to-dense shrubland ET unit, which constituted nearly 30 percent of vegetated areas. Discharge from the moderate-to-dense shrubland ET unit was estimated at 14 Mm^3 (11,000 acre-ft), whereas discharges from the sparse shrubland and grassland ET units were estimated at 9.2 Mm^3 (7,500 acre-ft) and 2.3 Mm^3 (1,900 acre-ft), respectively. Mean annual ET_g from the moderate-to-dense ET unit is likely biased high owing to senesced annual grass effects on EVI/T_B index values. Senesced grasses observed in the northern most areas of the GDA likely confounded the vegetation index such that phreatophytic shrub cover and ET_g were overestimated. Although this bias is likely within the maximum probable error of the estimate, the mean annual ET_g for moderate-to-dense shrubland presented here is likely an upper bound.

Total mean annual ET_g was estimated at 28 Mm^3 (23,000 acre-ft). The maximum probable error associated with mean-annual basin-scale ET_g was estimated at 5.4 Mm^3 (4,400 acre-ft), or about 20 percent of basin-scale ET_g. The probable error was estimated at 0.6 Mm^3 (500 acre-ft) and represents about 4 percent of mean annual basin-scale ET_g.

The total mean annual ET_g estimate in this study is comparable to previous Dixie Valley estimates, with much lower rates from playa ET units and greater rates from vegetated units. These differences likely stem from a lack of in-place measurements collected during previous studies and assumptions that discharge rates measured in other valleys can be applied to Dixie Valley. The use of advanced, in-place measurements in this study provided more refined delineations of groundwater discharge areas, and more accurate measurement and extrapolation of local ET_g rates than previous studies in Dixie Valley.

Acknowledgments

The authors gratefully acknowledge David I. Stannard (U.S. Geological Survey [USGS]), David M. Sumner (USGS), Amy Swancar (USGS emeritus), Kip K. Allander (USGS), Angela P. Paul (USGS), David E. Eckhardt (Bureau of Reclamation [Reclamation]), Justin H. Huntington, J. Mark Spears (Reclamation), Interflow Hydrology, Inc., and Mahannah and Associates, LLC, for helpful guidance and reviews; Michael A. Barrenchea (USGS), C. Justin Mayers (USGS), J. Mark Spears (Reclamation), Wesley Henson (University of Florida), Lindsay Burt (U.S. Army), Jonathan Arthur (USGS), Toby L. Welborn (USGS), Michael J. Johnson (USGS emeritus), and John Erik Shroeder (formerly USGS) for assisting with site instrumentation and data collection; Karen A. Thomas (USGS) for toluene extractions; David E. Eckhardt for remote sensing assistance;

David W. Smith (USGS) and Erin L. Orozco (USGS) for unsaturated-zone and evapotranspiration data processing; and Dean Tonenna (Bureau of Land Management) for plant species identification. Reclamation supported this work under Interagency Agreement R10PG80297.

References Cited

Agam, N., and Berliner, P.R., 2006, Dew formation and water vapor adsorption in semi-arid environments—A review: Journal of Arid Environments, v. 65, no. 4, p. 572–590.

Allander, K.K., Smith, J.L., and Johnson, M.J., 2009, Evapotranspiration from the lower Walker River Basin, west-central Nevada, water years 2005–07: U.S. Geological Survey Scientific Investigations Report 2009-5079, 62 p., http://pubs.usgs.gov/sir/2009/5079/.

Allen, R., Tasumi, M., and Trezza, R., 2007, Satellite-based energy balance for Mapping Evapotranspiration with Internalized Calibration (METRIC)—Model: Journal of Irrigation and Drainage Engineering v. 133, no. 4, p. 380–394.

Allison, G.B., and Barnes, C.J., 1985, Estimation of evaporation from the normally "dry" Lake Frome in South Australia: Journal of Hydrology, v. 78, nos. 3–4, p. 229–242.

American Society of Civil Engineers, 2005, The ASCE standardized reference evapotranspiration equation: Reston, Virginia, American Society of Civil Engineers, Environmental and Water Resources Institute, 59 p.

Barlow, P.M., 2003, Ground water in freshwater-saltwater environments of the Atlantic coast: U.S. Geological Survey Circular 1262, 113 p., http://pubs.usgs.gov/circ/2003/circ1262/.

Bastiaanssen, W.G.M., 2000, SEBAL-based sensible and latent heat fluxes in the irrigated Gediz Basin, Turkey: Journal of Hydrology, v. 229, nos. 1–2, p. 87–100.

Benoit, D., Johnson, S., and Kumataka, M., 2000, Development of an injection augmentation program at the Dixie Valley, Nevada geothermal field: Proceedings of the World Geothermal Congress, Kyushu-Tohoku, Japan, 2000, p. 819–824.

Berger, D.L., Johnson, M.J., and Tumbusch, M.L., 2001, Estimates of evapotranspiration from the Ruby Lake National Wildlife Refuge Area, Ruby Valley, northeastern Nevada, May 1999–October 2000: U.S. Geological Survey Water-resources Investigations Report 01-4234, 38 p., http://pubs.usgs.gov/wri/wri014234/.

Blaney, H.F., Taylor, C.A., Nickle, H.G., and Young, A.A., 1933, Water losses under natural conditions from wet areas in southern California: California Department of Public Works, Division of Water Resources Bulletin 44, 176 p.

Blonquist, J.M., Jr., Tanner, B.D., and Bugbee, B., 2009, Evaluation of measurement accuracy and comparison of two new and three traditional net radiometers: Agricultural and Forest Meteorology, v. 149, no. 10, p. 1,709–1,721.

Bossong, C.R., Caine, J.S., Stannard, D.I., Flynn, J.L., Stevens, M.R., and Heiny-Dash, J.S., 2003, Hydrologic conditions and assessment of water resources in the Turkey Creek watershed, Jefferson County, Colorado, 1998–2001: U.S. Geological Survey Water-Resources Investigations Report, 03-4034, 140 p., http://pubs.usgs.gov/wri/wri03-4034/.

Bowen, I.S., 1926, The ratio of heat losses by conduction and by evaporation from any water surface: Physical Review, v. 27, p. 779–787.

Briere, P.R., 2000, Playa, playa lake, sabkha—Proposed definitions for old terms: Journal of Arid Environments, v. 45, no. 1, p. 1–7.

Brotzge, J.A., and Duchon, C.E., 2000, A field comparison among a domeless net radiometer, two four-component net radiometers, and a domed net radiometer: Journal of Atmospheric and Oceanic Technology, v. 17, no. 12, p. 1,569–1,582.

Campbell, G.S., 1985, Soil physics with BASIC—transport models for soil-plant systems: Elsevier Science Publishing Company Inc., v. 14, 150 p.

Campbell, G.S., and Norman, J.M., 1998, An introduction to environmental biophysics (2d ed.): New York, Springer-Verlag, 286 p.

Campbell Scientific, Inc., 2011, Instruction manual for NR01 four-component net radiation sensor, revision 8/11, accessed March 23, 2013, at http://s.campbellsci.com/documents/us/manuals/nr01.pdf.

Chander, G., Markham, B.L., and Helder, D.L., 2009, Summary of current radiometric calibration coefficients for Landsat MSS, TM, ETM+, and EO-1 ALI sensors: Remote Sensing of Environment, v.113, no. 5, p. 893–903.

Chimner, R.A., and Cooper, D.J., 2004, Using stable oxygen isotopes to quantify the water source used for transpiration by native shrubs in the San Luis Valley, Colorado U.S.A.: Plant and Soil, v. 260, nos. 1–2, p. 225–236.

Clark, I., and Fritz, P., 1997, Environmental isotopes in hydrogeology: New York, Lewis publishers, 328 p.

Clement, R., 1999, EdiRe data software: University of Edinburgh, School of Geosciences, version 1.5.0.32, accessed October 28, 2013, at http://www.geos.ed.ac.uk/abs/research/micromet/EdiRe/.

Cohen, P., and Everett, D.E., 1963, A brief appraisal of the ground-water hydrology of the Dixie-Fairview Valley area, Nevada: U.S. Geological Survey Ground-Water Resources Reconnaissance Series Report 23, 40 p., accessed November 7, 2013, at http://images.water.nv.gov/images/publications/recon%20reports/rpt23-dixie_fairview_valley.pdf.

Coplen, T.B., Wildman, J.D., and Chen, J., 1991, Improvements in the gaseous hydrogen-water equilibration technique for hydrogen isotope-ratio analysis: Analytical Chemistry, v. 63, p. 910–912.

Dawson, T.E., and Pate, J.S., 1996, Seasonal water uptake and movement in root systems of Australian phreatophytic plants of dimorphic root morphology—A stable isotope investigation: Oecologia, v. 107, p. 13–20.

Devitt, D.A., Fenstermaker, L.F., Young, M.H., Conrad, B., Baghzouz, M., and Bird, B.M., 2011, Evapotranspiration of mixed shrub communities in phreatophytic zones of the Great Basin region of Nevada (USA): Ecohydrology, v. 4, no. 6, p. 807–822.

Doherty, J., 2010, PEST, Model-independent parameter estimation—User manual (5th ed., with slight additions): Brisbane, Australia, Watermark Numerical Computing, 279 p.

Domenico, P.A., and Schwartz, F.W., 1998, Physical and chemical hydrogeology (2d ed.): Wiley, 528 p.

Donovan, L.A., Richards, J.H., and Muller, M.W., 1996, Water relations and leaf chemistry of *Chrysothamnus nauseosus* ssp. *Consimilis* (Asteraceae) and *Sarcobatus vermiculatus* (Chenopodiaceae): American Journal of Botany, v. 83, no. 12, p. 1,637–1,646.

Dugas, W.A., Reicosky, D.C., and Kiniry, J.R., 1997, Chamber and micrometeorological measurements of CO_2 and H_2O fluxes for three C_4 grasses: Agricultural and Forest Meteorology, v. 83, nos. 1–2, p. 113–133.

Ehleringer, J.R., Phillips, S.L., Schuster, W.S.F., and Sandquist, D.R., 1991, Differential utilization of summer rains by desert plants: Oecologia, v. 88, no. 3, p. 430–434.

Epstein, S., and Mayeda, T., 1953. Variation of O^{18} content of waters from natural sources: Geochimica et Cosmochimica Acta, v. 4, no. 5, p. 213–224.

Everett, D.E., and Rush, F.E., 1964, Ground-water appraisal of Smith Creek and Ione Valleys, Lander and Nye Counties, Nevada: Carson City, Nevada Department of Conservation and Natural Resources, Ground Water Resources Reconnaissance Report 28, 21 p.

Evett, S.R., 2007, Soil water and monitoring technology, *in* Lascano, R.J., and Sojka, R.E., eds., 2007, Irrigation of agricultural crops, (2d ed.): American Society of Agronomy, no. 30, p. 25–82.

Finkelstein, P.L., and Sims, P.F., 2001, Sampling error in eddy correlation flux measurements: Journal of Geophysical Research Atmospheres, v. 106, no. D4, p. 3,503–3,509.

Finnigan, J.J., Clement, R., Malhi, Y., Leuning, R., and Cleugh, H.A., 2003, A re-evaluation of long-term flux measurement techniques, part 1—Averaging and coordinate rotation: Boundary-Layer Meteorology, v. 107, no. 1, p. 1–48.

Flint, A.L., Campbell, G.S., Ellet, K.M., and Calissendorff, C., 2002, Calibration and temperature correction of heat dissipation matric potential sensors: Soil Science Society of America Journal, v. 66, no. 5, p. 1,439–1,445.

Foken, T., 2008, The energy balance closure problem—An overview: Ecological Applications, v. 18, no. 6, p. 1,351–1,367.

Foken, T., Leuning, R., Oncley, S.R., Mauder, M., and Aubinet, M., 2012, Corrections and data quality control, *in* Aubinet, M., Vesala, T., and Papale, D., eds., Eddy covariance—A practical guide to measurement and data analysis: Springer Atmospheric Sciences, 38 p.

Foken, T., Wimmer, F., Mauder, M., Thomas, C., and Liebethal, C., 2006, Some aspects of the energy balance closure problem: Atmospheric Chemistry and Physics, v. 6, p. 4,395–4,402.

Foxall, B. and Vasco, D., 2003, Inversion of synthetic aperture radar interferograms for sources of production-related subsidence at the Dixie Valley geothermal field: Proceedings of the Workshop on Geothermal Reservoir Engineering, 28th, Stanford University, Stanford, California, 2003, p. 181–187.

Friedl, M.A., and Davis, F.W., 1994, Sources of variation in radiometric surface temperature over a tallgrass prairie: Remote Sensing of Environment, v. 48, no. 1, p. 1–17.

Fuchs, M., 1986, Heat flux, *in* Klute, A., ed., Methods of soil analysis part 1—physical and mineralogical methods (2d ed.): Madison, Wisconsin, American Society of Agronomy, p. 957–968.

Garcia, C.A., Andraski, B.J., Stonestrom, D.A., Cooper, C.A., Johnson, M.J., Michel, R.L., and Wheatcraft, S.W., 2009, Transport of tritium contamination to the atmosphere in an arid environment: Vadose Zone Journal, v. 8, no. 2, p. 450–461.

Garcia, C.A., Johnson, M.J., Andraski, B.J., Halford, K.J., and Mayers, C.J., 2008, Portable chamber measurements of evapotranspiration at the Amargosa Desert Research Site near Beatty, Nye County, Nevada, 2003–2006: U.S. Geological Survey Scientific Investigations Report 2008–5135, 10 p., http://pubs.usgs.gov/sir/2008/5135/.

Gash, J.H.C., and Dolman, A.J., 2003, Sonic anemometer (co)sine response and flux measurement— The potential for (co)sine error to affect sonic anemometer-based flux measurements: Agricultural and Forest Meteorology, v. 119, nos. 3–4, p. 195–207.

Gillham, R.W., 1984. The Capillary fringe and its effect on water-table response. Journal of Hydrology, 67, nos. 1-4, p. 307–324.

Glancy, P.A., and Rush, F.E., 1968, Water-resources appraisal of Smoke Creek-San Emidio Desert area, Nevada and California: Nevada Department of Conservation and Natural Resources, Water Resources–Reconnaissance Series Report 44, 57 p.

Glenn, E.P., Huete, A.R., Nagler, P.L., and Nelson, S.G., 2008, Relationship between remotely sensed vegetation indices, canopy attributes and plant physiological processes— What vegetation indices can and cannot tell us about the landscape: Sensors, v. 8, no. 4, p. 2,136–2,160.

Goward, S.N., Cruickshanks, G.D., and Hope, A.S., 1985, Observed relation between thermal emission and reflected spectral radiance of a complex vegetated landscape: Remote Sensing of Environment, v. 18, no. 2, p. 137–146.

Groenveld, D.P., and Barz, D.D., 2014, Dixie Valley, Nevada playa bathymetry constructed from Landsat TM data: Journal of Hydrology, v. 512, p. 435–441, accessed April 24, 2014, at http://dx.doi.org/10.1016/j.jhydrol.2014.02.046.

Groeneveld, D.P., Baugh, W.M., Sanderson, J.S., and Cooper, D.J, 2007, Annual groundwater evapotranspiration mapped from single satellite scenes: Journal of Hydrology, v. 344, nos. 1–2, p. 146–156.

Halford, K.J., Garcia, C.A., Fenelon, J.M., and Mirus, B.B., 2012, Advanced methods for modeling water-levels and estimating drawdowns with SeriesSEE, an Excel add-in: U.S. Geological Survey Techniques and Methods, book 4, chap. F4, 28 p., http://pubs.usgs.gov/tm/tm4-F4/.

Hanks, R.J., and Ashcroft, G.L., 1980, Applied soil physics— Soil water and temperature applications: New York, Springer-Verlag, 159 p.

Harrill, J.R. and Hines, L.B., 1995, Estimated natural ground-water recharge, discharge, and budget for the Dixie Valley area, west-central Nevada: U.S. Geological Survey Water-Resources Investigations Report 95-4052, 12 p., http://pubs.er.usgs.gov/publication/wri954052.

Heusinkveld, B.G., Jacobs, A.F.G., Holtslag, A.A.M., and Berkowicz, S.M., 2004, Surface energy balance closure in an arid region—Role of soil heat flux: Agricultural and Forest Meteorology, v. 122, nos. 1–2, p. 21–37.

Hines, L.B., 1992, Quantification of natural ground-water evapotranspiration in Smith Creek Valley, Lander County, Nevada, *in* Subitzsky, Seymour, ed., Selected papers in the hydrologic sciences, 1988–92: U.S. Geological Survey Water Supply Paper 2340, p. 9–20. http://pubs.usgs.gov/wsp/wsp2340/.

Hollinger, D.Y., and Richardson, A.D., 2005, Uncertainty in eddy covariance measurements and its application to physiological models: Tree Physiology, v. 25, p. 873–885.

Horita, J., 2005, Saline waters, *in* Aggarwal, P.K., Gat, J.R., and Froehlich, K.F., eds., Isotopes in the water cycle—Past, present, and future of a developing science: Springer., p. 271–287.

Huete, A.R., 1988, A soil-adjusted vegetation index (SAVI): Remote Sensing of Environment, v. 25, no. 3, p. 295–309.

Huete, A.R., and Jackson, R.D., 1987, Suitability of spectral indices for evaluating vegetation characteristics on arid rangelands: Remote Sensing of Environment, v. 23, no. 2, p. 213–232.

Huete, Alfredo, Justice, Chris, and van Leeuwen, Wim, 1999, MODIS Vegetation Index (MOD 13), version 3. Algorithm Theoretical Basis Document, accessed October 28, 2013, at http://modis.gsfc.nasa.gov/data/atbd/atbd_mod13.pdf.

Huete, A.R., Post, D.F., and Jackson, R.D., 1984, Soil spectral effects on 4-space vegetation discrimination: Remote Sensing of Environment, v. 15, p 155–165.

Huntington, J.L., and Allen, R.G., 2010, Evapotranspiration and net irrigation water requirements for Nevada: Nevada Division of Water Resources, 260 p., accessed March 13, 2014, at http://water.nv.gov/mapping/et/Docs/Evapotranspiration_and_Net_Irrigation_Requirements_for_Nevada_Compiled.pdf.

Huntington, J.M., Garcia, C.A., and Rosen, M.R., 2014, Hydrogeologic framework and occurrence, movement, and chemical characterization of groundwater in Dixie Valley, west-central Nevada: U.S. Geological Survey Scientific Investigations Report, 2014-5152, 58 p., http://pubs.usgs.gov/sir/2013/5152/.

Interflow Hydrology, Inc., and Mahannah and Associates, LLC, 2012, Dixie Valley spring reconnaissance and sampling report, 55 p., accessed March 13, 2014 at http://www.interflowhydro.com/pdf/Dixie-Valley-Spring-Report.pdf.

Interflow Hydrology, Inc., and Mahannah and Associates, LLC, 2013, Monitoring of stream flows and playa run-on in Dixie Valley for water years 2009, 2010, and 2011: Prepared for Churchill County, Nevada, 46 p., accessed March 13, 2014, at http://www.interflowhydro.com/pdf/Dixie_Valley_Streamflow_Report.pdf.

Jacobson, G., and Jankowski, J., 1989, Groundwater-discharge processes at a central Australian playa: Journal of Hydrology, v. 105, nos. 3–4, p. 275–295.

Jensen, J.R., 2005, Introductory digital image processing—A remote sensing perspective (3d ed.): Upper Saddle River, New Jersey, Prentice Hall, 592 p.

Jury, W.A., and Horton, R., 2004, Soil physics (6th ed.): New York, John Wiley and Sons, Inc., Hoboken, New Jersey, 370 p.

Kampf, S.K., Tyler, S.W., Ortiz, C.A., Muñoz, J.F., and Adkins, P.L., 2005, Evaporation and land surface energy budget at the Salar de Atacama, northern Chile: Journal of Hydrology, v. 310, nos. 1–4, p. 236–252.

Karnieli, A., Shachak, M., Tsoar, H., Zaddy, E., Kaufman, Y., Danin, A., and Porter, W., 1996, The effects of microphytes on the spectral reflectance of vegetation in semiarid regions: Remote Sensing of Environment, v. 57, no. 2, p. 88–96.

Kaufman, Y.J., and Tanre, D., 1992, Atmospherically resistant vegetation index (ARVI) for EOS-MODIS: IEEE Transactions on Geoscience and Remote Sensing, v. 30, no. 2, p. 261–270.

Kenny, J.F., Barber, N.L., Huston, S.S., Linsey, K.S., Lovelace, J.K., and Maupin, M.A., 2009, Estimated use of water in the United States in 2005: U.S. Geological Survey Circular 1344, 52 p., http://pubs.usgs.gov/circ/1344/.

Kinsman, D.J.J., 1976, Evaporites—Relative humidity control of primary mineral facies: Journal of Sedimentary Petrology, v. 46, no. 2, p. 273–279.

Kormann, R., and Meixner, F.X., 2001, An analytical footprint model for non-neutral stratification: Boundary-Layer Meteorology, v. 99, no. 2, p. 207–224.

Kutílek, M., and Nielsen, D.R., 1994, Soil Hydrology: Cremlingen-Destedt, Germany, CatenaVerlag, 370 p.

Laczniak, R.J., DeMeo, G.A., Reiner, S.R., Smith, J.L., and Nylund, W.E., 1999, Estimates of ground-water discharge as determined from measurements of evapotranspiration, Ash Meadows area, Nye County, Nevada: U.S. Geological Survey Water-Resources Investigations Report 99-4079, 70 p., http://pubs.usgs.gov/wri/wri994079/.

Laczniak, R.J., Flint, A.L., Moreo, M.T., Knochenmus, L.A., Lundmark, K.W., Pohll, G., Carroll, R.W.H., Smith, J.L., Welborn, T.L., Heilweil, V.M., Pavelko, M.T., Hershey, R.L., Thomas, J.M., Earman, S., and Lyles, B.F., 2008, Ground-water budgets, *in* Welch, A.H., Bright, D.J., and Knochenmus, L.A., eds., Water resources of the basin and range carbonate-rock aquifer system, White Pine County, Nevada, and adjacent areas in Nevada and Utah: U.S. Geological Survey Scientific Investigations Report 2007-5261, p. 43–68, http://pubs.usgs.gov/sir/2007/5261/section5.html.

Laczniak, R.J., Smith, J.L., and DeMeo, G.A., 2006, Annual ground-water discharge by evapotranspiration from areas of spring-fed riparian vegetation along the eastern margin of Death Valley, 2000–02: U.S. Geological Survey Scientific Investigations Report 2006-5145, 36 p., http://pubs.usgs.gov/sir/2006/5145/.

Laczniak, R.J., Smith, J.L., Elliot, P.E., DeMeo, G.A., and Chatigny, M.A., 2001, Ground-water discharge determined from estimates of evapotranspiration, Death Valley regional flow system, Nevada and California: U.S. Geological Survey Water-Resources Investigations Report 01-4195, 51 p., http://pubs.usgs.gov/wri/wri014195/.

Lambin, E.F., and Ehrlich, D, 1996, The surface temperature-vegetation index space for land cover and land-cover change analysis: International Journal of Remote Sensing, v. 17, no. 3, p. 463–487.

Larson, L.W., and E.L. Peck, 1974, Accuracy of precipitation measurements for hydrologic modeling: Water Resources Research, v. 10, no. 4, p. 857–863.

Law, B.E., Loescher, H.W., Boden, T.A., Hargrove, W.W., and Hoffman, F.M., 2005, AmeriFlux site evaluation and recommendations for network enhancement: Oakridge National Laboratory, accessed May 5, 2014, at: http://public.ornl.gov/ameriflux/AmeriFluxSiteEvaluationWEB.pdf.

Lee, T.M., and Swancar, A., 1997, Influence of evaporation, ground water, and uncertainty in the hydrologic budget of Lake Lucerne, a seepage lake in Polk County, Florida: U.S. Geological Survey Water Supply Paper 2439, 61 p., http://fl.water.usgs.gov/publications/Abstracts/wsp2439_lee.html.

Lee, X., Massman, W., and Law, B.E., eds., 2004, Handbook of micrometeorology— A guide for surface flux measurement and analysis: Dordrecht, the Netherlands, Kluwer Academic Publishers, 250 p.

Leuning, R., van Gorsel, E., Massman, W.J., and Isaac, P.R., 2012, Reflections on the surface energy imbalance problem: Agricultural and Forest Meteorology, v. 156, p. 65–74.

Lillesand, T., Kiefer, R.W., and Chipman, J., 2008, Remote sensing and image interpretation (6th ed.): New York, Wiley, 756 p.

Lin, G.L., and Sternberg, L.da.S.L., 1993, Hydrogen isotope fractionation by plant roots during water uptake in coastal wetland plants, *in* Saugier, Bernard, Ehleringer, J.R., Hall, A.E., and Farquhar, G.D., eds., Stable isotopes and plant carbon-water relations: San Diego, Academic Press, Inc., p. 497–510.

Malek, E., 2003, Microclimate of a desert playa—Evaluation of annual radiation, energy, and water budget components: International Journal of Climatology, v. 23, no. 3, p. 333–345.

Malek, E., Bingham, G.E., and McCurdy, G.D., 1990, Evapotranspiration from the margin and moist playa of a closed desert valley: Journal of Hydrology, v. 120, nos. 1–4, p. 15–34.

Malek, E., McCurdy, G., and Giles, B., 1999, Dew contribution to the annual water balances in semi-arid desert valleys: Journal of Arid Environments, v. 42, no. 2, p. 71–80.

Massman, W.J., 2000, A simple method for estimating frequency response corrections for eddy covariance systems: Agricultural and Forest Meteorology, v. 104, no. 3, p. 185–198.

Mauder, M., and Foken, T., 2006, Impact of post-field processing on eddy covariance flux estimates and energy balance closure: Meteorologische Zeitschrift, v. 15, p. 597–609.

Mauder, M., Oncley, S.P., Vogt, R., Weidinger, T., Ribeiro, L., Bernhofer, C., Foken, T., Kohsiek, W., De Bruin, H.A.R., and Liu, H., 2007, The energy balance experiment EBEX-2000—Part II— Intercomparison of eddy-covariance sensors and post-field data processing methods: Boundary-Layer Meteorology, v. 123, p. 29–54.

Maurer, D.K., Johnson, A.K., and Welch, A.H., 1994, Hydrogeology and potential effects of changes in water use, Carson Desert agricultural area, Churchill County, Nevada: U.S. Geological Survey Open-File Report 93-463, 101 p., http://pubs.er.usgs.gov/publication/ofr93463.

Mazor, E., 1991, Applied chemical and isotopic groundwater hydrology: London, Open University Press, 256 p.

Misrach, R., 1990, Bravo 20—The bombing of the American West: Baltimore, Md., The Johns Hopkins University Press, 152 p.

Moore, C.J., 1986, Frequency response corrections for eddy correlation systems: Boundary-Layer Meteorology, v. 37, nos. 1–2, p. 17–35.

Moreo, M.T., Laczniak, R.J., and Stannard, D.I., 2007, Evapotranspiration rate measurements of vegetation typical of ground-water discharge areas in the Basin and Range carbonate-rock aquifer system, Nevada and Utah, September 2005–August 2006: U.S. Geological Survey Scientific Investigations Report 2007–5078, 36 p., http://pubs.usgs.gov/sir/2007/5078/.

Moro, M.J., Were, A., Villagarcía, L., Cantón, Y., and Domingo, F., 2007, Dew measurement by eddy covariance and wetness sensor in a semiarid ecosystem of SE Spain: Journal of Hydrology, v. 335, nos. 3–4, p. 295–302.

Mualem, Y., 1976, A new model for predicting the hydraulic conductivity of unsaturated porous media: Water Resources Research, v. 12, no. 3, p. 513–522.

Nachshon, U., Weisbrod, N., Dragila, M.I., and Grader, A., 2011, Combined evaporation and salt precipitation in homogeneous and heterogeneous porous media: Water Resources Research, v. 47, no. 3, 16 p.

Nešpor, V., and Sevruk, B., 1999, Estimation of wind-induced error of rainfall gauge measurements using a numerical simulation: Journal of Atmospheric and Oceanic Technology, v. 16, no. 4, p. 450–464.

Nevada Division of Water Resources, 2012, Hydrographic regions and basins, Nevada's hydrographic regions, basins and sub-basins: Carson City, Nevada Division of Water Resources Web site (data on Churchill and Pershing Counties), accessed May 20, 2013, at http://water.nv.gov/programs/planning/counties.

Nichols, W.D, 1992, The uncertainty in water budget estimates in the Great Basin, *in* Herrmann, Raymond, ed., Managing water resources during global change: Proceedings of the American Water Resources Association Annual Conference and Symposium, 28th, Reno, Nevada, 1992, p. 309–317.

Nichols, W.D, 1993, Estimating discharge of shallow groundwater by transpiration from greasewood in the northern Great Basin: Water Resources Research, v. 29, no. 8, p. 2,771–2,778.

Nichols, W.D., 2000, Regional ground-water evapotranspiration and ground-water budgets, Great Basin, Nevada: U.S. Geological Survey Professional Paper 1628, http://pubs.er.usgs.gov/publication/pp1628.

Nimz, G., Janik, C., Goff, F., Dunlap, C., Huebner, M., Counce, D., and Johnson, S., 1999, Regional hydrology of the Dixie Valley geothermal field, Nevada— Preliminary interpretations of chemical and isotopic data: International Conference on Accelerator Mass Spectrometry, 8th, Vienna, Austria, September 6–10, 1999, 9 p.

Noborio, K., McInnes, K.J., and Heilman, J.L., 1996, Two-dimensional model for water, heat, and solute transport in furrow-irrigated soil— Theory: Soil Science Society of America Journal, v. 60, no. 4, p. 1,001–1,009.

Okaya, D.A., and Thompson, G.A., 1985, Geometry of Cenozoic extentional faulting— Dixie Valley, Nevada: Tectonics, v. 4, no. 1, p. 107–125.

O'Reilly, A.M., 2004, A method for simulating transient ground-water recharge in deep water-table settings in central Florida by using a simple water-balance/transfer function model: U.S. Geological Survey Scientific Investigations Report 2004-5195, 49 p., http://pubs.usgs.gov/sir/2004/5195/.

Papale, D., and Valentini, R., 2003, A new assessment of European forests carbon exchange by eddy fluxes and artificial neural network spatialization: Global Change Biology, v. 9, p. 525–535.

Philip, J.R., and de Vries, D.A., 1957, Moisture movement in porous materials under temperature gradient: Transactions of the American Geophysical Union, no. 38, p. 222–232.

Price, J.C., 1990, Using spatial context in satellite data to infer regional scale evapotranspiration: IEEE Transactions on Geoscience and Remote Sensing, v. 28, no. 5, p 940–948.

Priestley, C.H.B., and Taylor, R.J., 1972, On the assessment of surface heat flux and evaporation using large-scale parameters: Monthly Weather Review, v. 100, p. 81–92.

PRISM Climate Group, 2013, Parameter-elevation Regressions on Independent Slopes Model (PRISM) for 1981–2010: Corvallis, Oregon State University, PRISM database, accessed August 15, 2013, at http://prism.oregonstate.edu.

Qi, J., Chehbouni, A., Huete, A.R., Kerr, Y.H., and Sorooshian, S., 1994, A modified soil adjusted vegetation index: Remote Sensing of Environment, v. 48, no. 2, p. 119–126.

Reece, C.F., 1996, Evaluation of a line heat dissipation sensor for measuring soil matric potential: Soil Science Society of America Journal, v. 60, no. 4, p. 1,022–1,028.

Reicosky, D.C., Sharratt, B.S., Ljungkull, J.E., and Baker, D.G., 1983, Comparison of alfalfa evapotranspiration measured by a weighing lysimeter and a portable chamber: Agricultural Meteorology, v. 28, p. 205–211.

Révész, K., and Coplen, T.B., 2008, Determination of the delta (2H/1H) of water—RSIL lab code 1574, chap. C1 *of* Révész, K., and Coplen, T.B., eds., Methods of the Reston Stable Isotope Laboratory: U.S. Geological Survey Techniques and Methods, book 10, chap. C1, 27 p., http://pubs.usgs.gov/tm/2007/tm10c1/.

Révész, K., and Woods, P.H., 1990, A method to extract soil water for stable isotope analysis: Journal of Hydrology, v. 115, nos. 1–4, p. 397–406.

Richardson, A.D., Aubinet, M., Barr, A.G., Hollinger, D.Y., Ibrom, A., Lasslop, G., and Reichstein, M., 2012, Uncertainty quantification, *in* Aubinet, M., Vesala, T., and Papale, D., eds., Eddy covariance— Practical guide to measurement and data analysis: Springer Atmospheric Sciences, 37 p.

Robinson, T.W., 1958, Phreatophytes: U.S. Geological Survey Water Supply Paper 1423, 84 p., http://pubs.er.usgs.gov/publication/wsp1423.

Robinson, T.W., and Waananen, A.O., 1970, Evapotranspiration by woody phreatophytes in the Humboldt River valley near Winnemucca, Nevada, with a section on soil-moisture determinations: U.S. Geological Survey Professional Paper 491-D, 41 p., http://pubs.er.usgs.gov/publication/pp491D.

Rondeaux, G., Steven, M., and Baret, F., 1996, Optimization of soil-adjusted vegetation indices: Remote Sensing of Environment, v. 55, no. 2, p. 95–107.

Rouse, J.W., Haas, R.H., Schell, J.A., and Deering, D.W., 1974, Monitoring vegetation systems in the Great Plains with ERTS: Proceedings of the Earth Resources Technology Satellite-1 Symposium, 3d, National Aeronautics and Space Administration, Scientific and Technical Information Office, Washington, D.C., p. 309–317.

Sandholt, I., Rasmussen, K., and Andersen, J., 2002, A simple interpretation of the surface temperature/vegetation index space for assessment of surface moisture status: Remote Sensing of Environment, v. 79, nos. 2–3, p. 213–224.

SAS Institute, Inc., 2001, SAS/STAT® (software), version 8.2: Cary, N.C., SAS Institute, Inc. Web site, accessed October 30, 2013, at http://www.sas.com/technologies/analytics/statistics/stat/.

Schotanus, P., Nieuwstadt, F.T.M., and DeBruin, H.A.R., 1983, Temperature measurement with a sonic anemometer and its application to heat and moisture fluxes: Boundary-Layer Meteorology, v. 26, no. 1, p. 81–93.

Schuepp, P.H., Leclerc, M.Y., Macpherson, J.I., and Desjardins, R.L., 1990, Footprint prediction of scalar fluxes from analytical solutions of the diffusion equation: Boundary-Layer Meteorology, v. 50, nos. 1–4, p. 355–373.

Scott, R.L., Williams, D.G., Goodrich, D.C., Cable, W.L., Levick, L.R., McGuire, R., Gazal, R.M., Yepez, E.A., Ellsworth, P., and Huxman, T.E., 2005, Determining the riparian ground-water use within the San Pedro Riparian National Conservation Area and the Sierra Vista subwatershed, Arizona, chap. D *of* Leenhouts, J.M., Stromberg, J.C., and Scott, R.L., Hydrologic requirements of and consumptive ground-water use by riparian vegetation along the San Pedro River, Arizona: U.S. Geological Survey Scientific Investigations Report 2005–5163, 154 p., http://pubs.usgs.gov/sir/2005/5163/.

Shoemaker, W.B., Lopez, C.D., and Duever, M.J., 2011, Evapotranspiration over spatially extensive plant communities in the Big Cypress National Preserve, southern Florida, 2007–2010: U.S. Geological Survey Scientific Investigations Report 2011–5212, 46 p., http://pubs.usgs.gov/sir/2011/5212/.

Shuttleworth, J.W., 1993, Evaporation, *in* Maidment, D.R., ed., Handbook of hydrology: McGraw-Hill, Inc., p. 4.1–4.53.

Smith, J.L., Laczniak, R.J., Moreo, M.T., and Welborn, T.L., 2007, Mapping evapotranspiration units in the Basin and Range carbonate-rock aquifer system, White Pine County, Nevada, and adjacent areas in Nevada and Utah: U.S. Geological Survey Scientific Investigations Report 2007–5087, 20 p., http://pubs.usgs.gov/sir/2007/5087/.

Smith, R.L., 1974, Ecology and field biology (2d ed.): New York, Harper and Row, 850 p.

Sofer, Z., and Gat, J. R., 1975, The isotope composition of evaporating brines—Effect of the isotopic activity ratio in saline solutions: Earth and Planetary Science Letters, v. 26, no. 2, p. 179–186.

Soil Survey Staff, Natural Resources Conservation Service, 2011, Web soil survey: U.S. Department of Agriculture Web site, accessed August 10, 2011, at http://websoilsurvey.nrcs.usda.gov/.

Stannard, D.I., 1988, Use of a hemispherical chamber for measurement of evapotranspiration: U.S. Geological Survey Open-File Report 88-452, 18 p, http://pubs.er.usgs.gov/publication/ofr88452.

Stannard, D.I., Gannett, M.W., Polette, D.J., Cameron, J.M., Waibel, M.S., and Spears, J.M., 2013, Evapotranspiration from wetland and open-water sites at Upper Klamath Lake, Oregon, 2008–2010: U.S. Geological Survey Scientific Investigations Report 2013–5014, 66 p., http://pubs.usgs.gov/sir/2013/5014/.

Stannard, D.I., and Weltz, M.A., 2006, Partitioning evapotranspiration in sparsely vegetated rangeland using a portable chamber: Water Resources Research, v. 42, doi:10.1029/2005WR004251.

Steel, R.G., and Torrie, J.H., 1980, Principles and procedures of statistics: McGraw-Hill, New York, 633 p.

Stull, R.B., 1988, An introduction to boundary layer meteorology: Dordrecht, the Netherlands, Kluwer Academic Publishers, 666 p.

Swinbank, W.C., 1951, The measurement of vertical transfer of heat and water vapor by eddies in the lower atmosphere: Journal of Meteorology, v. 8, p. 135–145.

Tanner, B.D., and Greene, J.P., 1989, Estimate of sensible heat and water-vapor fluxes using eddy-correlation methods—Final report: Prepared for U.S. Army Dugway Proving Grounds: U.S. Army, Dugway, Utah, 17 p.

Thompson, G.A., and Burke, D.B., 1973, Rate and direction of spreading in Dixie Valley, Basin and Range Province, Nevada: Geological Society of America Bulletin, v. 84, p. 627–632.

Thorburn, P.J., Walker, G.R., and Woods, P.H., 1992, Comparison of diffuse discharge from shallow water tables in soil sand salt flats: Journal of Hydrology, v. 136, no. 1, p. 253–274.

Tsakiris, G., and Vangelis, H., 2005, Establishing a drought index incorporating evapotranspiration: European Water, v. 9–10, p. 3–11.

Turk, L.J., 1975, Diurnal fluctuations of water tables induced by atmospheric pressure changes: Journal of Hydrology, v. 26, nos. 1–2, p. 1–16.

Twine, T.E., Kustas, W.P., Norman, J.M., Cook, D.R., Houser, P.R., Meyers, T.P., Prueger, J.H., Starks, P.J., and Wesely, M.L., 2000, Correcting eddy-covariance flux underestimates over a grassland: Agricultural and Forest Meteorology, v. 103, p. 279–300.

Tyler, S.W., Kranz, S., Parlange, M.B., Albertson, J., Katul, G.G., Cochran, G.F., Lyles, B.A., and Holder, G., 1997, Estimation of groundwater evaporation and salt flux from Owens Lake, California, USA: Journal of Hydrology, v. 200, nos. 1–4, p. 110–135.

Tyler, S.W., Muñoz, J.F., and Wood, W.W., 2006, The response of playa and sabkha hydraulics and mineralogy to climate forcing: Ground Water, v. 44, no. 3, p. 329–338.

U.S. Salinity Laboratory Staff, 1954, Diagnosis and improvement of saline and alkali soils: U.S. Department of Agriculture, Agriculture Handbook No. 60, 159 p.

U.S. Geological Survey, 2012a, Landsat—A global land-imaging mission: U.S. Geological Survey Fact Sheet 2012-3072, 4 p., http://pubs.usgs.gov/fs/2012/3072/.

U.S. Geological Survey, 2012b, Landsat Ecosystem Disturbance Adaptive Processing System (LEDAPS)—Algorithm Description Document, version 1.3: U.S. Geological Survey, 20 p., accessed December 10, 2013, at http://landsat.usgs.gov/documents/ledaps_add.pdf.

U.S. Geological Survey, 2014, USGS water data for the Nation: U.S. Geological Survey database, accessed January 2, 2014, at http://waterdata.usgs.gov/nwis.

van Genuchten, M.Th., 1980, A closed-form equation for predicting the hydraulic conductivity of unsaturated soils: Soil Science Society of America Journal, v. 44, no. 5, p. 892–898, doi.10.2136/sssaj1980.03615995004400050002x.

Webb, E.K., Pearman, G.I., and Leuning, R., 1980, Correction of flux measurements for density effects due to heat and water vapour transfer: Quarterly Journal of the Royal Meteorological Society, v. 106, p. 85–100.

Western Regional Climate Center, 2012, Western U.S. Climate Historical Summaries: Desert Research Institute Web site, accessed May 5, 2014, at http://www.wrcc.dri.edu/Climsum.html.

White, W.N., 1932, A method of estimating ground-water supplies based on discharge by plants and evaporation from soil—results of investigations in Escalante Valley, Utah, *in* Contributions to the hydrology of the United States, 1932: U.S. Geological Survey Water Supply Paper 659, p. 1–105, http://pubs.er.usgs.gov/publication/wsp659A.

Willden, R., and Speed, R.C., 1974, Geology and mineral deposits of Churchill County, Nevada: Nevada Bureau of Mines and Geology Bulletin 83, 92 p.

Wilson, K., Goldstein, A., Falge, E., Aubinet, M., Baldocchi, D., Berbigier, P., Bernhofer, C., Ceulemans, R., Dolman, H., Field, C., Grelle, A., Ibrom, A., Law, B.E., Kowalski, A., Meyers, T., Moncrieff, J., Monson, R., Oechel, W., Tenhunen, J., Valentini, R., and Verma, S., 2002, Energy balance closure at FLUXNET sites: Agricultural and Forest Meteorology, v. 113, nos. 1–4, p. 223–243.

Yang, D., Goodison, B.E., Metcalfe, J.R., Golubev, V.S., Bates, R., Pangburn, T., and Hanson, C.L., 1996, Accuracy of NWS 8″ standard nonrecording precipitation gauge—Results and application of WMO intercomparison: Journal of Atmospheric and Oceanic Technology, v. 15, p. 54–68.

Young, A.A., and Blaney, H.F., 1942, Use of water by native vegetation: California Department of Public Works, Division of Water Resources Bulletin 50, 154 p.

Appendixes

For appendix 1, the spreadsheet distributed as part of this report is in Microsoft® Excel 2010 format. Column headers are described in the spreadsheet. Eddy covariance latent- and sensible-heat flux data are not corrected for energy imbalances. Spreadsheets are available for download at http://pubs.usgs.gov/pp/1805. Daily and sub-daily (30-minute) data are available for download at http://nevada.usgs.gov/water/et/index.htm; evapotranspiration, latent-, and sensible-heat flux data at this location are not corrected for energy imbalances

For appendixes 2–6 and 8, the spreadsheets distributed as part of this report are in Microsoft® Excel 2010 format. Column headers are described in the spreadsheet. Spreadsheets are available for download at http://pubs.usgs.gov/pp/1805.

Appendix 7 is available for download as a PDF at http://pubs.usgs.gov/pp/1805.

Appendix 1. Evapotranspiration and Micrometeorological Data for the Dixie Valley Study Area, Nevada, April 2009–September 2011

Appendix 2. Measured and Computed Soil Hydraulic Properties at Evapotranspiration Sites within the Dixie Valley Study Area, Nevada, and Unsaturated-Water Movement Equations

Appendix 3. Source Area Analysis for Evapotranspiration Sites within the Dixie Valley Study Area, Nevada, April 2009–September 2011

Appendix 4. Playa Groundwater-Level Data for the Dixie Valley Study Area, Nevada, April 2009–August 2011

Appendix 5. Playa Runoff Data for the Dixie Valley Study Area, Nevada

Appendix 6. Chamber Evaporation Data for the Dixie Valley Study Area, Nevada

Appendix 7. Description of Spatial Datasets Used to Calculate Basin-Scale Annual Groundwater Discharge Estimates by Evapotranspiration

Appendix 8. Playa Groundwater Discharge Determined from Analytical Hydraulic Calculations Based on Darcy's Law in the Dixie Valley Study Area, Nevada

Publishing support provided by the U.S. Geological Survey
Science Publishing Network, Tacoma Publishing Service Center

For more information concerning the research in this report, contact the
Nevada Water Science Center
U.S. Geological Survey
2730 N. Deer Run Rd.
Carson City, NV 89701
http://nevada.usgs.gov/water/

ISSN 2330-7102 (online)
http://dx.doi.org/10.3133/pp1805